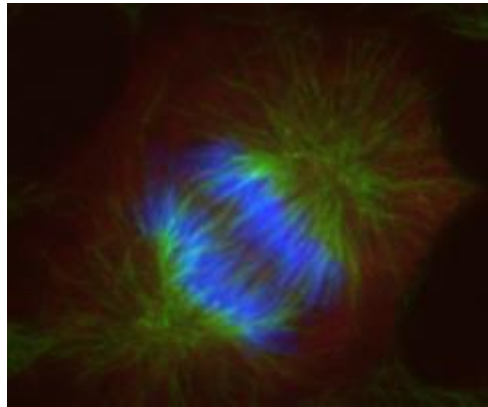UNIVERSITÀ DEGLI STUDI DI PAVIA

Dipartimento di Biologia e Biotecnologie "L. Spallanzani"

# Alternative strategies to overcome Cisplatin side effects and resistance



*Astesana Valentina*

PhD Program in Genetics, Molecular and Cellular Biology
XXXI cycle – 2015-2018

UNIVERSITÀ DEGLI STUDI DI PAVIA

Dipartimento di Biologia e Biotecnologie "L. Spallanzani"

# Alternative strategies to overcome Cisplatin side effects and resistance

**PhD Student**: Valentina Astesana

**Supervised by** Prof. Marco Biggiogera

Dott.ssa Maria Grazia Bottone

PhD Program in Genetics, Molecular and Cellular Biology
XXXI cycle – 2015-2018

# CONTENTS

# ABSTRACT

Cisplatin is one of the most effective chemotherapeutic agents used in the treatment of many type of tumours including non-small cell lung cancer, ovarian, testicular, glioblastoma, neuroblastoma and others. Cisplatin is able to form bonds with the N7 atom on guanine and adenine bases and when this damage is not repaired, DNA replication and transcription were stopped, inducing death of the cells. Despite the clinical benefit provided by Cisplatin many patients undergo phenomena of resistance and toxicity (especially ototoxicity, nephrotoxicity and neurotoxicity). Cisplatin resistance is generally multifactorial and arises through different mechanisms; one of this is correlated to high activity of PARP-1, an enzyme that modify proteins by poly-adenosine ribosylation (named PARylation). There are many targets of PARylation, one of these are histones. Moreover, high PAR levels correlate with weak infiltration by CD8$^+$ cytotoxic T lymphocytes (CTL) in human NSCLC. To overcome Cisplatin resistance and toxicity, alternative strategies were proposed: 1) the use of alternative platinum compounds, such as [Pt(O,O'-acac)(γ-acac)(DMS)], a platinum (II) complex containing acetylacetonate (acac) and a dimethylsulpide (DMS) in the coordination sphere of the metal and synthetized by the team of Prof. Fanizzi (University of Salento, Lecce), considering its activity and mechanism of action respect to Cisplatin and 2) the study of new mechanisms of resistance linked to a different immune response between Cisplatin sensitive and resistant tumour cells. For the first strategy we used human glioblastoma T98G cell line. Our results suggest that PtAcacDMS is

able to induce apoptosis and necrosis with a concentration five-fold lower respect to Cisplatin (10µM respect to 40µM). Furthermore, ultrastructural analysis of TEM revealed an intense process of autophagy takes place in the cells, confirmed by the analysis of autophagic markers. Different cell death can be regulated by calcium and by oxidative stress. We find that PtAcacDMS induce an acute increase in $[Ca^{2+}]_i$ respect to CDDP that was likely to be due to extracellular $Ca^{2+}$ entry and enhanced both cytosolic and endoplasmic reticulum $Ca^{2+}$ concentration after 48h of treatment. Increase of oxidative stress, especially the expression of ROS, can also represent a mechanism of cell death of PtAcacDMS and can modulate the modification of chromatin and thus gene expression. Further experiments are needed to confirm these data, in particular the analysis of specific mechanisms involved in the modulation of intracellular calcium and the analysis of apoptosis and autophagy when cells growing in absence of $Ca^{2+}$. For the second stage we used mouse LLC (Lewis lung cancer) non-small cell lung cancer cell line. After generating cell lines resistant to Cisplatin, followed by their characterization with respect to PARylation, cells were injected in immunocompetent C57BL/6 mouse to evaluate the immune infiltrate. *In vivo* results show differences in immune infiltrate, especially in TAMs and Treg, more expressed in resistant cells, but to confirm if PARP-1 is implicated in this modulation it will be necessary to manipulate the expression of PARP-1 in the clones CDDP-resistant, silencing its expression by siRNA, to evaluate whether these injected cells exhibit the same immune infiltrate as the WT cells.

# ACKNOWLEDGEMENTS

# ABBREVIATIONS

Δψm: mitochondrial transmembrane potential

$[Ca^{2+}]_i$: intracellular calcium concentration

$^1O_2$: sigle oxygen

Acac: acetylacetonate

AIF: apoptosis-inducing factor

Apaf-1: apoptotic peptidase activating factor 1

ASK1: apoptosis signal-regulated kinase 1

ATP: adenosine triphosphate

ATP7A: ATPase copper transporting alpha

ATP7B: ATPase copper transporting beta

ATP11B: ATPase phospholipid transporting 11B

BAK/BAK1: BCL-2 antagonist killer

BAPTA: 1,2-Bis(2-aminophenoxy)ethane-N,N,N′,N′-tetraacetic acid tetrakis (acetoxymethyl ester)

BAX: BCL-2 associated X

BCL-2: B-cell lymphoma 2

BCL2A1: BCL2 related protein A1

BCL2L2/BCL2-W: BCL2 like 2

BID: BH3 interacting domain death agonist

BSA: bovine serum albumin

c-FLIP: CASP8 and FADD like apoptosis regulate

$CaCl_2$: calcium chloride

CAMKs: $Ca^{2+}$/calmodulin (CaM)-dependent protein kinases

CAT: catalase

CD16/CD32: Fc fragment of IgG receptor IIIa/IIIb

CD45/PTPRC protein tyrosine phosphatase, receptor type C

CDDP: Cisplatin

CMA: chaperone-mediated autophagy

CNS: central nervous system

COX-2: cyclooxygenase-2

CPA: cyclopiazonic acid

CTL: cytotoxic T-lymphocytes

CTR1: copper influx transporter 1

cyt c: cytochrome c

DAMPs: damage-associated molecular pattern molecules

DAPK1: death-associated protein kinase 1
DCs: dendritic cells
DFFA/ICAD: DNA fragmentation factor subunit alpha
DFFB/CAD: DNA fragmentation factor subunit beta
DIABLO: diablo IAP-binding mitochondrial protein
DISC: death inducing signaling complex
DiOC6(3): 3,3'-dihexyloxacarbocyanine iodide
DMS: dimethylsulphide
DNA: deoxyribonucleic acid
DRs: death receptors
DRG: root ganglion neurons
ECL: Enhanced chemiluminescence
EDTA: ethylenediaminetetraacetic acid
EGTA: ethylene glycol-bis(β-aminoethyl ether)-N,N,N',N'-tetraacetic acid
EMT: epithelial-mesenchymal transition
ER: endoplasmic reticulum
ERCC1: excision repair cross-complementation group 1
ERK1/2: Extracellular signal-regulated kinase ½
FADD: Fas associated death domain
FAS/CD95/APO1: Fas cell surface death receptor
FASLG/CD95L/APO-1L: FAS ligand
FDA: Food and Drug Administration
FIS1: mitochondrial fission 1
FOXP3: forkhead box P3
GPx: glutathione peroxidase
GSH: glutathione S-transferase
$H_2O_2$: hydrogen peroxide
HAT: histone acetyltransferase
HCl: hydrochloric acid
HDAC: histones deacetylase
HDM: histones demethylase
HEPES: 2-[4-(2-hydroxyethyl)piperazin-1-yl]ethanesulfonic acid
HIF1: hypoxia-inducible factor 1
HMT: histones methyltransferase
HSP90: heat shock protein 90
IAP: inhibitor of apoptosis
ICOS: inducible T cell costimulator

IL-2: interleukin-2

IL-6: interleukin-6

INF-γ: interferon-gamma

InsP3Rs: inositol triphosphate receptors

IP3: inositol trisphosphate

JC-1 (5,5V,6,6V-tetrachloro-1,1V,3,3V-
        tetraethylbenzimidazolcarbocyanine iodide

JNK: c-Jun N-terminal kinase

KCl: potassium chlorate

Ly6: lymphocyte antigen 6 complex, locus C

Ly6G: lymphocyte antigen 6 complex, locus G

MAMs: mitochondrial-associated endoplasmic reticulum membranes

MAPK: mitogen-activated protein kinase

MAPK8/JNK: mitogen-activated protein kinase 8

MAPK14/p38: mitogen-activated protein kinase 14

MCU: mitochondria $Ca^{2+}$ uniporter

MDSC: myeloid derived suppressor cells

MFN2: mitofusin 2

$MgCl_2$: magnesium chloride

MHCII: histocompatibility-2, MHC

mHCX: mitochondrial $H^+/Ca^{2+}$ exchanger

mNCX: $Na^+/Ca^{2+}$ exchanger

MMPs: matrix metalloproteinases

MMP-3: matrix metalloproteinase 3

MMR: mismatch repair

MOMP: mitochondrial outer membrane permeabilization

MPTPs: mitochondrial permeability transitional pores

MRP2: multidrug resistance-associated protein 2

NAC: N-acetyl cysteine

NaCl: sodium chloride

NaF: sodium fluoride

NaOH: sodium hydroxide

NCCD: Nomenclature Committee on Cell Death

NER: nucleotide excision repair

NF-kB: nuclear factor-kappa B

NK: natural killer

NMDARs: N-methyl-D aspartate receptors

NO: nitric oxide

NOSs: nitric oxide synthases

NOX: NADPH (nicotinamide adenine dinucleotide phosphate) oxidase

NSCLC: non-small cell lung cancer

$O_2^-$: superoxide anion

$O_3$: ozone

OCT2: organic cation transporter-2

OD: optical density

$OH^-$: hydroxyl radical

OMM: outer mitochondrial membrane

OPA1: mitochondrial dynamic like GTPase

ORAI1: $Ca^{2+}$ release-activated calcium channel protein 1

$OsO_4$: osmium tetroxide

p62/SQSTM1: sequestosome 1

P2XRs: purinergic ionotropic receptor

PAR: poly-adenosine ribosyl

PARP-1: poly-adenosine ribosyl (PAR) polymerase-1

PARylation: poly-adenosine ribosylation

PBS: phosphate buffer saline

PD1: programmed cell death 1

PD-L1: programmed cell death 1 ligand 1

PI: iodide propidium

PI3K: phosphoinositide 3-kinase

PIP2: phosphatidylinositol 4, 5- bisphosphate

PIP3: phosphatidylinositol 3, 4, 5-triphosphate

PKC-α: Protein Kinase C- alpha

PMCA-1: Plasma Membrane Calcium ATPase 1

PMSF phenylmethylsulfonyl fluoride

PSS: physiological salt solution

PtAcacDMS: [Pt($O,O'$-acac)($\gamma$-acac)(DMS)]

PTEN: Phosphatase and tensin homolog

PTP: permeability potential pore

PTPC: permeability transition pore complex

PUMA: p53-upregulated modulator of apoptosis

RCS: reactive chloride species

RNS: reactive nitrogen species

ROI: regions of interest

ROS: reactive oxygen species

RSS: reactive sulfur species

RyRs: ryanodine receptors

SDS: sodium thiosulfate

SERCA: sarco/endoplasmic reticulum $Ca^{2+}$-ATPase

SMAC: second mitochondrial activator of caspases

SOCE: store-operated $Ca^{2+}$ entry

SOD: superoxide dismutase

STIM1: stromal interaction molecular 1

TAMs: tumor associated macrophages

TILs: tumor infiltrating lymphocytes

$T_H1$: type 1 helper

TLRs: toll-like receptors

TNF-α: tumor necrosis factor

TNFR1: TNF receptor superfamily member 1A

TNFRSF10A/TRAILR1/DR4: TNF receptor superfamily member 10a

TNFRSF10B/TRAILR2/DR5: TNF receptor superfamily member 10b

TRADD: TNFRSF1A associated via death domain

TRAIL: TNF superfamily member

Treg: regulatory T lymphocytes

Tris HCl: (hydroxymethyl)aminomethane hydrochloride

TRP: transient receptor potential

VDAC: voltage-dependent anion channel

VEGF: vascular-endothelial growth factor

VEGFR: vascular-endothelial growth factor receptor

VGCCs: voltage-gated calcium channels

XIAP: X-linked inhibitor of apoptosis

# 1. REVIEW OF THE LITERATURE

## 1.1 Cisplatin

Platinum compounds are largely used in clinical as tumor therapy. In particular, the cis-dichlorodiammine platinum (II) (also known as Cisplatin or CDDP) is the most effective based-platinum chemotherapeutic agent, synthesized for the first time by the Italian chemist Michele Peyrone in 1845, whose structure was clarified by Alfred Werner in 1893 (Dasari S and Tchounwou PB, 2014). However, the compound was not used as anticancer treatment until the 1960s when Rosemberg B et al. (1965) discovered its ability to induce the inhibition of cell division in *Escherichia coli*, lead the way of a possible use of Cisplatin as cancer chemotherapy. In 1978 the FDA (Food and Drug Administration) approved the clinical use of this compound (Apps S et al., 2015) and nowadays it has become a standard therapy for a wide range of malignancies including testicular, ovarian, bladder, head and neck, esophageal, small and non-small cell lung, breast, cervical, stomach and prostate cancers, Hodgkin's and non-Hodgkin's lymphomas, neuroblastoma, sarcomas, multiple myeloma, melanoma, and mesothelioma. (Florea AM and Büsselberg D, 2011, Ho GY et al., 2016).

Cisplatin and their analogous (Carboplatin, Oxaliplatin Nedaplatin, Lobaplatin, Heptaplatin) contain four ligands; the amine ligands and the chloride ligands or carboxylate compounds forming leaving groups allowing the platinum ion to form bonds with DNA bases (Goodsell DS, 2006 and Reed E 1998). To bind their target, platinum compounds act as prodrugs. Within cells, in which the concentration of $Cl^-$ is lower

than that in the extracellular environment (~2-10 mM *vs*. ~100 mM outside cells) (Galluzzi L et al., 2014), Cisplatin undergoes spontaneous aquation of their labile ligands so that they can form bonds with any nucleophile sites including the sulfhydryl groups of some proteins but in particular with the N7 atom on purines bases of mitochondrial and nuclear DNA (Dasari S and Tchounwou PB; 2014; Galluzzi L et al., 2014). When this damage is not repaired through the activation of mechanisms of DNA repair (such as NER (nucleotide excision repair) and MMR (mismatch repair)), DNA replication and transcription are stopped, inducing death of the cells (Roberts NB et al., 2016) (**Fig. 1**).
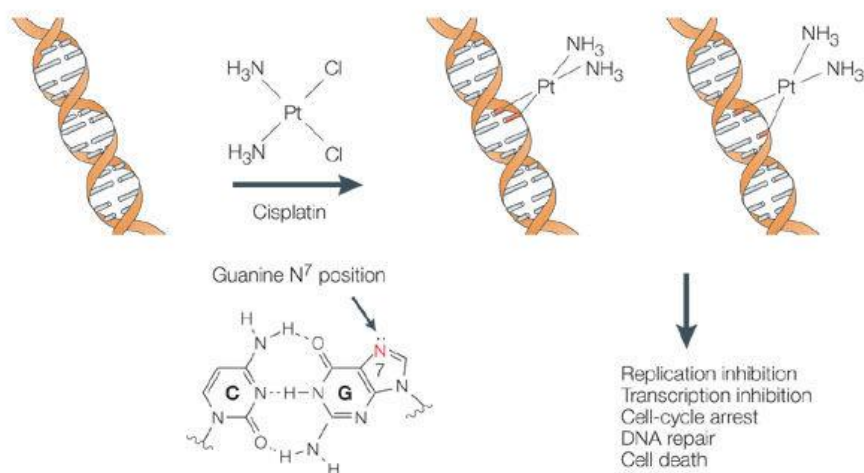


**Fig. 1** Formation of CDDP-DNA-adducts (Wang L and Lippard SJ, 2005).

Cisplatin cytotoxicity is directly dependent to its accumulation inside the cells. Copper influx transporter 1 (CTR1) is the major transporter of Cisplatin within cells (Holzer AK et al., 2006) while two copper efflux

transporters, ATP7A and ATP7B regulate platinum drug accumulation (Katano K et al., 2003; Samimi G et al., 2004) (**Fig. 2**).
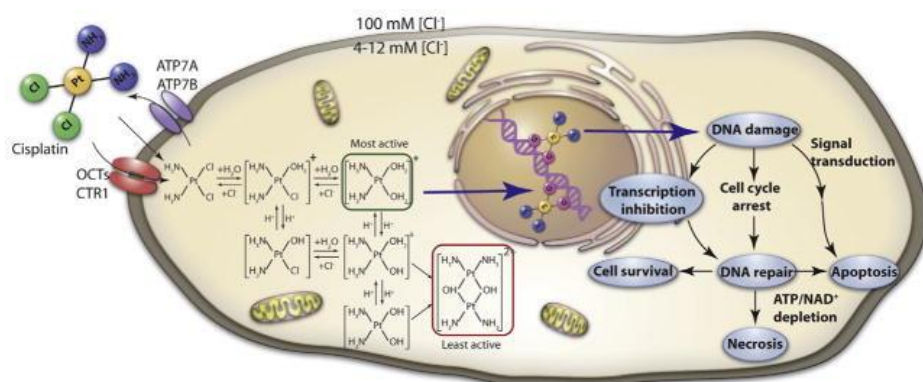


**Fig. 2** Representation of Cisplatin-efflux and influx outside and inside of a cell, mediated by its different transporters and its intracellular aquation (Oberoi HS et al., 2013).

Cisplatin is also able to interact with some proteins such as: GSH (glutathione S-transferase), which forms complexes GSH-CDDP subsequently removed from the cell, causing a reduction of the drug cytotoxic effect; metallothioneins involved in the detoxification of heavy metals that contribute to the mechanisms of Cisplatin resistance (Galluzzi L et al., 2014) or mitochondrial proteins like the VDAC (voltage-dependent anion channel); this results in the depletion of reducing equivalents and/or directly sustains the generation of reactive oxygen species (ROS). ROS can also directly induce DNA damage (Koberle B et al., 2010; Timerbaev AR et al., 2006). Moreover,

Cisplatin is able to interact with the protein tubulin, causing the depolymerization of microtubules and the alteration of cytoskeleton of tumor cells (Tulub AA and Stefanov VE, 2001). Also, binding the C-terminal domain of HSP90, Cisplatin inhibits the assembly and folding-protein activity of this chaperone (Ishida R et al., 2008).

## 1.2 Cisplatin-induced side effects

Despite the clinical benefit provided by Cisplatin since its clinical administration, many patients undergo phenomena of side effects, which restrict the dosage administrated. In addition to common side effects of almost all chemotherapeutic drugs (including nausea, vomiting, diarrhea and myelosuppression) due to indiscriminate dividing cells targets, Cisplatin induces also an elevated ototoxicity, nephrotoxicity and neurotoxicity (Ruggiero A et al., 2013).

### 1.2.1 Cisplatin ototoxicity

Cisplatin induces ototoxicity with high frequency and in particular in children ranging from 22% to 77% (Coradini PP et al., 2007; Knight KR et al., 2005; Kushner BH et al., 2006). In a recent study it was demonstrated that pediatric patients, after treatment with platinum compounds, shown sensorineural hearing loss which progress after long-term treatment especially in children with a central nervous system tumor (Waissbluth S et al., 2018) such as neuroblastoma.

Cisplatin induces ototoxicity trough different mechanisms; one of the most important concerns the increase of ROS generation: CDDP cause a depletion of GSH and a reduction of antioxidant enzymes in the rats'

cochleae (Rybak LP et al., 2000) promoting the apoptotic and necrotic cells death (Sheth S et al., 2017). The capacity of Cisplatin to generate ROS can be explained with its ability to interacts with sulfhydryl groups of antioxidant enzymes causing their inactivation. Furthermore, Cisplatin is able to induce the activation of NOX (NADPH oxidase) gene family that catalyze the formation of superoxide anion ($O_2^-$) (Banfi B et al., 2004); knockdown of this enzyme protects against hearing loss (Mukherjea D et al., 2010). Some antioxidant agents can be used to alleviate these side effects such as N-acetyl cysteine (NAC) and thiol compounds as the sodium thiosulfate (SDS), however they can reduce the amount of CDDP necessary for antitumor effect (Choe WT et al., 2004; Dickey DT et al., 2008; Wimmer C et al., 2004).

*1.2.2 Cisplatin nephrotoxicity*

Cisplatin nephrotoxicity affects 20-30% of patients, in particular the pediatric ones, in time and dose-dependent manner (Barton CD et al., 2018; Manohanar S and Leung N, 2018). Cisplatin is able to induce nephrotoxicity trough different mechanisms. The most common manifestation is represented by hypomagnesaemia, probably due to injury in the distal tubular that affects the reabsorption of the magnesium (Lajer H et al., 2005). Furthermore, in the proximal tubule, the overexpression of organic cation transporter-2 (OCT2) mediates the accumulation of drug in kidney cells (Filipski KK et al., 2008). Indeed, knockout mice for the OCT2 gene are protected for Cisplatin mediated-kidney injury (Filipski KK et al., 2009).

Another mechanism puts in place by kidney in response to Cisplatin is the increase of production of inflammatory elements such as interleukin-6 (IL-6), tumor necrosis factor (TNF-α), interferon-gamma (INF-γ) and T cells (Ramesh G and Reeves WB, 2002). In particular, Kang KP and colleagues (2009) demonstrated the implication of the nuclear factor-kappa B (NF-kB) pathway in the increase of TNF-α production after administration of Cisplatin. The inflammatory effect of Cisplatin is mediated also through the stimulation of production of damage-associated molecular pattern molecules (DAMPs) or "alarmins". DAMPs link the toll-like receptors (TLRs) on the surface of T-cells determining an increase in inflammation patterns (Gluba A et al., 2010). In order to reduce Cisplatin nephrotoxicity some strategies have been investigated: for example thiol agents, Acivicin and Ketoprofen act by reducing the activation of Cisplatin-glutathione conjugated; inhibitors of transporters reduce the entry of the drug in the cells; anti-inflammatory drugs, such as inhibitors of JNK (c-Jun N-terminal kinase) reduce the ROS generation or salicylates reduce the production of TNF-α (Manohanar S and Leung N, 2018).

### 1.2.3 Cisplatin neurotoxicity

After treatment with Cisplatin, about 50% of patients shown peripheral neuropathies that limit the possibility of a continuous therapy; furthermore, neurotoxic symptoms affect patients for long time (from 5 to 20 years) after the end of treatment (Sprauten M et al., 2012).
The worse damages take place in dorsal root ganglion neurons (DRG) in which the accumulation of Cisplatin is facilitated by the absence of

blood-brain barrier and the presence of fenestrated capillaries and facilitate the formation of DNA-adducts (Carozzi VA et al., 2015; McWhinney SR et al., 2009). As consequence, DNA transcription is stopped leading to neuron atrophy and interruption of axonal connection (Yan F et al., 2015). *In vivo* and *in vitro* studies have also demonstrated loss of DRG due to Cisplatin-induced apoptosis (Alaedini A et al., 2007; Gill JS and Windebank AJ., 1998; McDonald ES et al., 2005).

The overexpression of two types of transporters in neurones, CTR1 and OCT2, contribute to the uptake of Cisplatin into the cells and this aggravates the neurotoxicity (Cavaletti G et al., 2014).

Furthermore, mitochondrial DNA damage plays an important role in Cisplatin-related neurotoxicity: indeed, Cisplatin depletes the ATP and cellular calcium accumulation causing a reduction of mitochondrial movement in axons (Podratz JL et al., 2017). Moreover it alters the mitochondrial fission and fusion processes in peripheral nerves, probably due to down regulation of protein mitofusin 2 (MFN2) (Bobylev I et al., 2018).

## 1.3 Cisplatin-induced resistance

The efficacy of Cisplatin is limited by another negative characteristic, the resistance to treatment. Intrinsic or acquired resistance represents therefore the principal obstacle for the use of this compound (Galluzzi L et al., 2014). The primary or intrinsic resistance occurs when drugs are immediately ineffective for patients, while the acquired, or secondary resistance, is usually defined as progression of the disease

after an initial period of benefit from the clinical point of view and is refractory to further administration of the therapy. Resistance occurs in the majority of tumours, with the exception of testicular germ cells cancer in which >80% of patients shown a complete recovery (Winter C and Albers P, 2011).

Cisplatin resistance is generally multifactorial and arises through different mechanisms. Galluzzi L et al. (2014) proposed a classification into four categories of mechanisms of Cisplatin resistance summarized in **Fig. 3**.
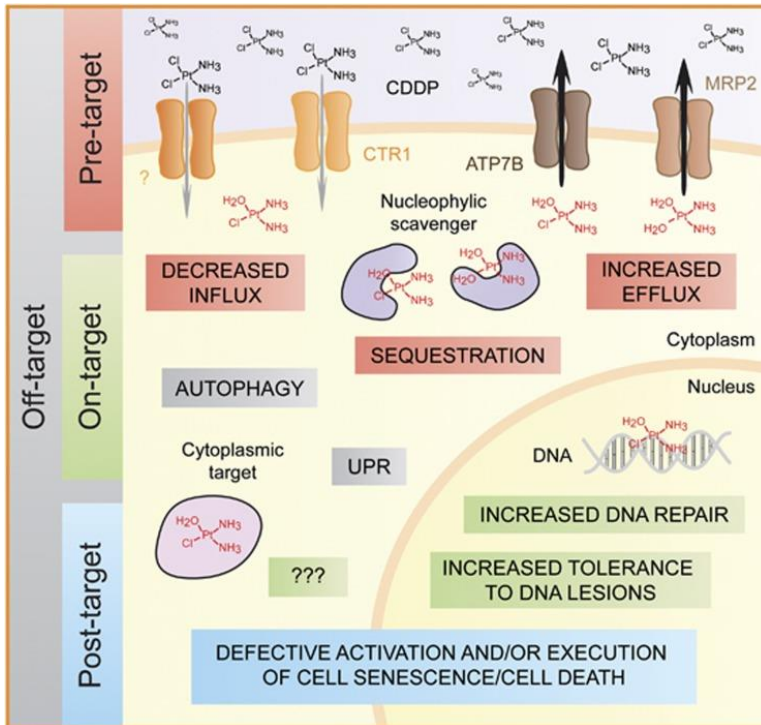


**Fig. 3** Representation of molecular mechanisms subdivided into different groups according to different type of cellular alterations (Galluzzi L et al., 2014).

The first category named *pre-target resistance* is independent of the damage caused by the drug and can occur due the alterations of the expression, subcellular localization and functionality of Cisplatin transporters; in particular, CTR1, which mediates the influx of drug and APT7A and ATP7B, which mediate the efflux outside the cell. A lot of evidences demonstrated that these transporters represent prognostic value in some tumours such ovarian, non-small-cell lung cancer and endometrial carcinoma (Aida T et al., 2005; Chen HH et al., 2012; Kalayda GV et al., 2008; Nakayama K et al., 2004). Other transporters contributing to the extrusion of Cisplatin can be implicated in resistance, for example the multidrug resistance-associated protein 2 (MRP2) (Korita PV et al., 2010; Yamasaki M et al., 2011) and the ATPase ATP11B (ATPase phospholipid transporting 11B) (Moreno-Smith M et al., 2013).

The second category called *on target resistance* includes the alterations in DNA-damage repair mechanisms that occur after Cisplatin action, in particular those concerning the NER system: an increase in expression level of the DNA-repair proteins has been associated with Cisplatin resistance in different type of tumours (Bellmunet J et al., 2007; Kim MK et al., 2008; Handra-Luca A et al., 2007; Olaussen KA et al., 2006). The principal protein implicated is ERCC1 (excision repair cross-complementation group 1), more expressed in resistant cells with respect to sensitive ones in many type of tumours and thus it can be regarded as a possible biomarker for Cisplatin resistance (Amable L, 2016).

The third category represents *the post target resistance* and arises in alterations of the machinery of cell death, in particular CDDP-induced apoptosis. In general, after administration of Cisplatin, cells suffer stress conditions and, to restore the cellular homeostasis, put in place processes such as the activation of some pro-apoptotic and anti-apoptotic signals, like BCL-2 associated X (BAX) and BCL-2 antagonist killer (BAK or BAK1), the accumulation of ROS and the opening of permeability transition pore complex (PTPC), the activation of ion channels subjected to redox regulation which alter the mitochondrial membrane permeability (Haouzi D et al., 2002; Kim JS et al., 2008; Tajeddine N et al., 2008); but also the expression of caspases and the members of BCL-2 family, which include BCL-2 (B-cell lymphoma 2) itself, BCL-X$_L$ (B-cell lymphoma-extra large) and others (Michaud WA et al., 2009; Sakamoto M et al., 2001; Williams J et al., 2005).

Finally, the *off target resistance* includes alterations in mechanisms not directly activated by Cisplatin such as the machinery of macroautophagy or the expression levels of the heat shock proteins which can induce a positive or negative response to Cisplatin action (Ren A et al., 2008; Yamamoto K et al., 2001; Yu H et al., 2011).

In conclusion, the multifaceted aspects of CDDP resistance make difficult the development of chemosensitization drugs. More recently clinical settings are taking place to study this problem directly on patients with different approaches such as genomic, metabolomic, methylomic, transcriptomic, proteomic to correlate Cisplatin resistance and gene expression, SNPs and the development of pharmacological

lines to overcome this problem. These approaches are important for advance medicine and the coming of personalized treatments.

## 1.4 Cancer cell metabolism and immune infiltration in Cisplatin resistant cancers

Within solid tumor, transformed cells are not alone and now understand the biology of these cells is no more sufficient for explain tumor formation (Kerkar SP and Restifo NP, 2012). Now a lot of evidences have shown the presence of nonneoplastic host elements such as components of immune system that contribute to carcinogenesis, tumor progression and metastasis formation (Mantovani A and Sica A, 2010; Schreiber RD et al., 2011; van Kempen LC et al., 2003). These cells are components of the stromal network that promote neovascularization and provide cytokines and inflammatory support to drive the proliferation of transformed cells (Murdoch C et al., 2008; Shojaei F et al., 2008). This interaction among the various cell types in the tumor microenvironment are now a new hallmark of cancer and therefore the study of these components could be the key to restore the cellular sensitivity to Cisplatin for a large type of tumors (**Fig. 4**).
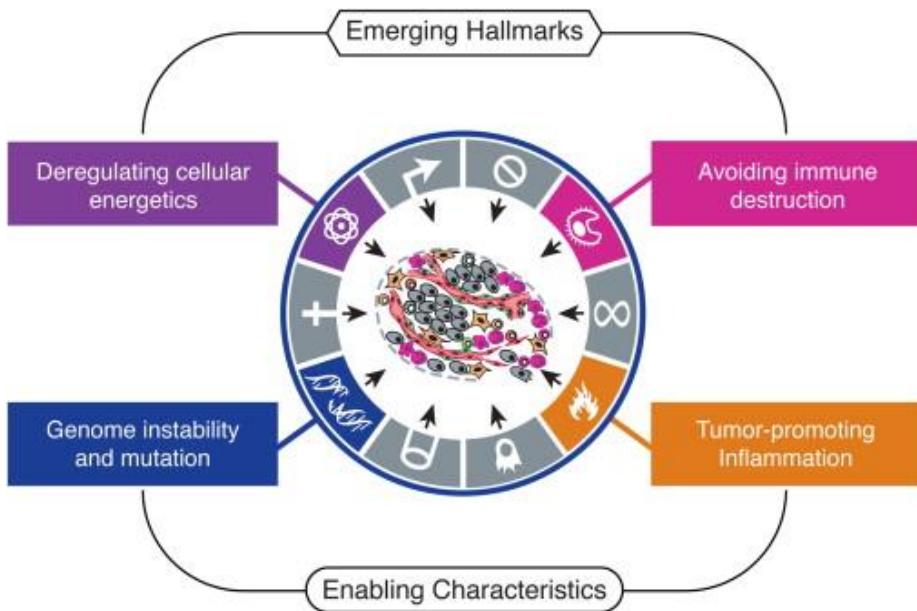
**Fig. 4** The new hallmarks of cancer (Hanahan D and Weinberg RA, 2011).

The composition of immune infiltrate includes CD3$^+$ T-lymphocytes, which generally are associated with good prognosis. Within this population, different subtypes can be recognised. The type 1 helper cells (T$_H$1 cells) expressing CD4$^+$ marker which produce IFNγ and IL-2 (interleukin-2). The cytotoxic CD8$^+$ T cells, (cytotoxic T-lymphocytes or CTL) are able to bring a potent anti-tumour immune response by inducing cancer cells apoptosis trough the pathway of perforins and granzymes: the presence of this lymphocytes defines the most-favourable prognosis (Fridman WH et al., 2017). However, the CD3$^+$ population includes a subset of cells called regulatory T cells (Treg) described as CD4$^+$/CD25$^+$/FOXP3$^+$ which possess the ability to suppress immune response also creating an immunosuppressive

environment that blunts antitumor effect response puts in place by $CD4^+$, $CD8^+$ and natural killer (NK) cells (Kerkar SP and Restifo NP, 2012). The presence of this population in the cancer immune infiltrating is associated with poor prognosis in most types of tumors.

Also myeloid cells, present in the immune infiltrate, are able to inhibit immune response using a variety of mechanisms, such as the creation of inflammatory environment. Furthermore, they mediate the phenomena of angiogenesis and metastasis formation (Ostrand-Rosemberg S and Sinha P, 2009; Sica A and Bronte V, 2007). Important myeloid cells subsets include myeloid derived suppressor cells (MDSC), macrophages and dendritic cells (DCs). Myeloid derived suppressor cells are described as a population $CD11b^+$ able to suppress $CD8^+$ T cells, but in fact they represent a heterogeneous population including cells of monocytic origin with high expression of the marker Ly6G and low levels of the marker Ly6C. They will differentiate into macrophages. Macrophages (MΦ) have the ability to present antigen to T lymphocytes but in the context of tumor microenvironment they play a role in the shutdown of T cells, promoting tumor growth (Qian BZ and Pollard JW, 2010). In particular TAMs (tumor associated macrophages), are M2-like MΦ able to inactivate the immunity response triggered by M1 macrophages, inhibiting like this the activation of natural killer cells, $T_H1$ and CTL (Gabrilovich DI et al., 2012).

DCs are professional antigen-presenting cells but in cancer their functionality decreases probably due to an abnormal myelopoiesis resulting in a reduced production of mature DCs and their accumulation

in tumor site (Gabrilovich DI, 2004). Also clinical studies have demonstrated a decreased presence of DCs in many types of tumors (Gabrilovich DI et al., 2012). Furthermore, in contact with malignant cells DCs develop functional impairments and are able to suppress T cells (Lin A et al., 2010). In **Fig. 5** is illustrated the composition of immune infiltrate in a generic solid tumor.
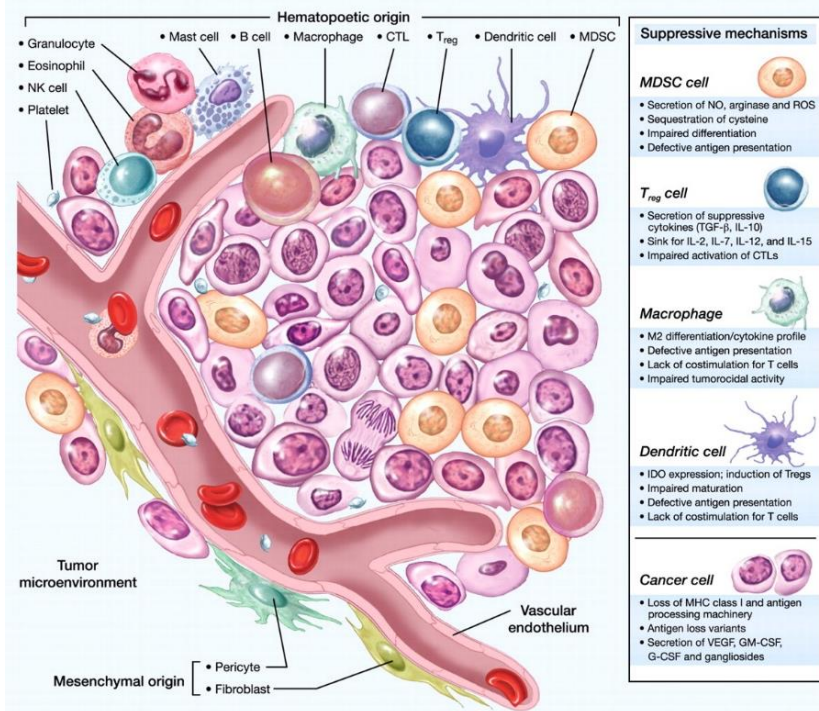


**Fig. 5** The different immune cells infiltrating solid tumours microenvironmental. In the right panel the mechanisms with which myeloid cells evade the immunity response (Kerkar SP and Restifo NP 2012).

It can be assumed there is a link between cancer cell metabolism and immune infiltration in Cisplatin resistant cancers. Indeed, Kroemer and colleagues have demonstrated that high activity of poly-adenosine ribosyl (PAR) polymerase-1 (PARP-1) correlates with weak infiltration by CD8^{+} cytotoxic T lymphocytes in patients with non-small cell lung cancer (NSCLC) (data not published).

PARP-1 is an enzyme which includes three subunits: a DNA-binding N-terminal domain with two zinc fingers motifs to detect the DNA damage, a C-terminal catalytic domain and an intermediate domain which contains an autoinhibitory PARP activity site (Ray Chaudhuri A and Nussenzweig A, 2017).

PARP-1 has a lot of functions; it regulates the life of cells preserving them by death or conversely induces apoptosis with a caspases-independent mechanism, preserves genome integrity and modulates transcription and DNA-damage repair (Schiewer MJ and Knudsen KE, 2014; Wang L et al., 2017). Furthermore, PARP-1 consumes nicotine adenine dinucleotide and ATP to covalently modify proteins by poly-adenosine ribosylation (named PARylation). There are many targets of PARylation, one of these are histones. Histones PARylation is very important because as consequence histones progressively acquire negative charges, causing their repulsion from interacting proteins and DNA. As a result, nuclear PARylation facilitates the relaxion of supercoiled DNA structures, including the accessibility of DNA to repair enzymes (Tallis M et al., 2014). The **Fig. 6** resumes the functions of PARP-1.
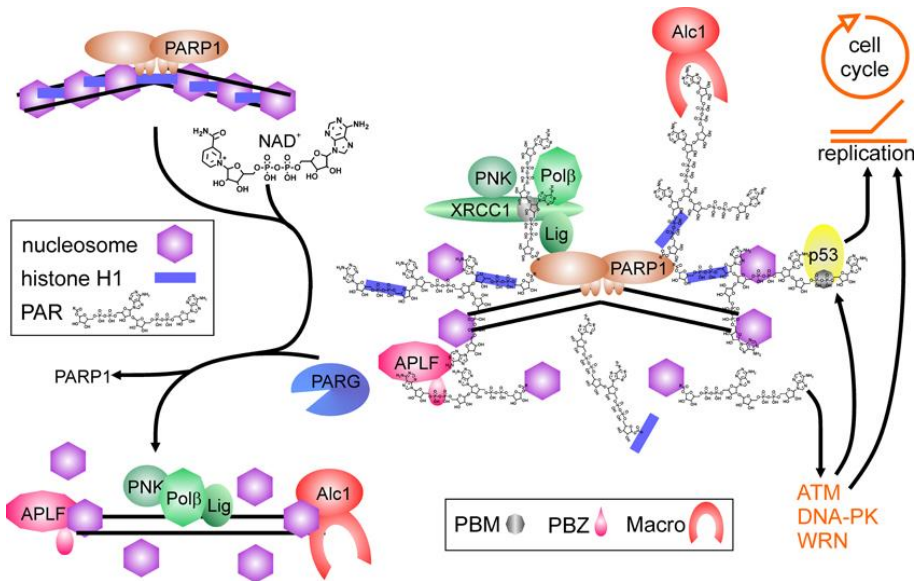
**Fig. 6** The role of PARP-1 in DNA damage repair. The blue bars represent histone H1, the purple hexagons represent the histones core (Beneke S, 2012).

Michels J et al. (2013) have demonstrated that clones of NSCLC A549 cells made Cisplatin-resistant shown elevated levels of PAR-containing proteins suggesting the existence of some genetic and epigenetic regulations that overexpress PARP-1 or increase its activity. Indeed, the specific mechanism which underpins this phenomenon is still unknown and other pathways can play an important role in this specific type of Cisplatin-resistance. Moreover, subsequent immunohistopathological analyses revealed that high PARP-1 activity constitutes negative prognostic features in patients with non-small cell lung cancer. This increase is not correlated with high expression of the enzyme (Michels et al., 2015) (**Fig. 7**).
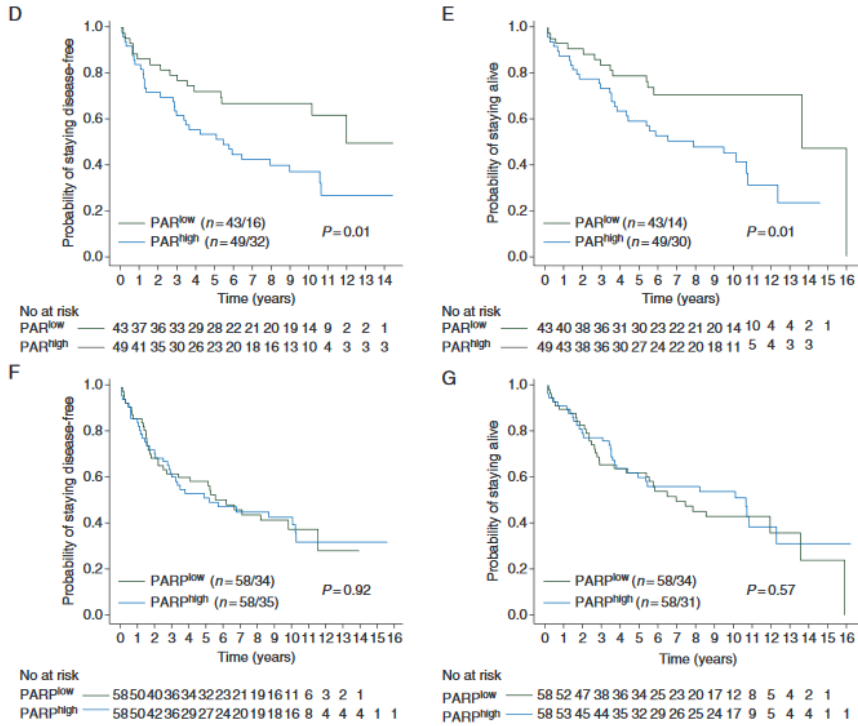
**Fig. 7** Prognostic value of PAR in patients with NSCLC. In line with literature data the activity of enzyme is not necessary correlate with its expression (Michels et al., 2015).

In summary it could be possible that intracellular PARP-1 activity influences the immune infiltrate by altering the concentrations of extracellular metabolites.

## 1.5 [Pt($O,O'$-acac)(γ-acac)(DMS)]: an alternative platinum (II) compound

To overcome Cisplatin drug resistance and toxicity, about forty years ago researchers all around the world started the development of analogous of Cisplatin. FDA approved clinically the use of two new platinum derivatives, Carboplatin and Oxaliplatin (Mandala M et al., 2004; Tattersall MN, 2002). Although Carboplatin shown a reduced neurotoxicity and nephrotoxicity, unfortunately both compounds have not provided advantages in clinical trials because they induce resistance mechanisms in the same tumours insensitive to Cisplatin (Galluzzi L et al., 2014).

Due to this negative aspect, in more recent years, new platinum drugs have been developed and designed to be either more cytotoxic to cancer cells compared with Cisplatin (Apps MG et al., 2015). One of these is the [Pt($O,O'$-acac)(γ-acac)(DMS)], a new platinum (II) complex containing acetylacetonate (acac) and a dimethylsulphide (DMS) in the coordination sphere of the metal, synthesized by the team of Prof. Fanizzi (University of Salento, Lecce, Italy). **Fig. 8** shows the different structure between CDDP and [Pt($O,O'$-acac)(γ-acac)(DMS)].
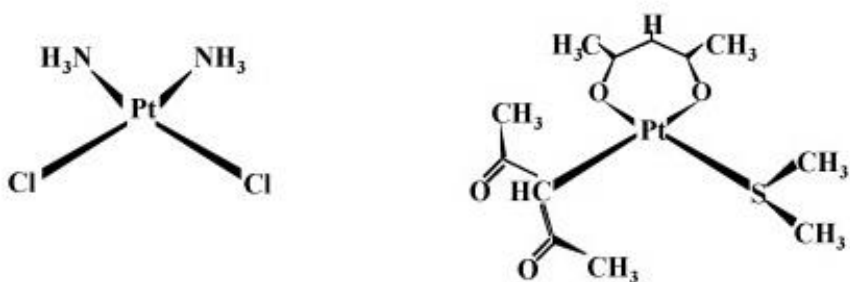
**Fig. 8** Chemical structure of CDDP (left) and [Pt(*O,O′*-acac)(γ-acac)(DMS)] (right) (Muscella A et al., 2007, modified).

This compound has been shown to induce apoptosis in Hela cells with a higher and more rapid cytotoxic activity *in vitro* respect to Cisplatin (Muscella A et al., 2007). In MCF-7 cells it was demonstrated that cytotoxicity of [Pt(*O,O′*-acac)(γ-acac)(DMS)] correlated with cellular accumulation but not with DNA damage (Muscella A et al., 2008). Indeed, the presence of DMS in the chemical structure of the molecule indicates its prevalence to link proteins containing thiol or thioester groups (Muscella A et al., 2007). Furthermore [Pt(*O,O′*-acac)(γ-acac)(DMS)] is able to induce cell death not only via apoptosis but also via anoikis at sublethal concentration and prevents events leading to cell migration and metastasis (Muscella  A et al., 2010).

In MCF-7 cells, [Pt(O,O'-acac)(γ-acac)(DMS)] increases the intracellular calcium concentration ($[Ca^{2+}]_i$) inhibiting PMCA-1 (Plasma Membrane Calcium ATPase 1)  and closing $Ca^{2+}$ channels opened by purinergic receptors; furthermore provokes the activation of PKC-α (Protein Kinase C- alpha) and the production of ROS that were responsible for the $Ca^{2+}$ permeability (Muscella A et al., 2011) (**Fig. 9**).
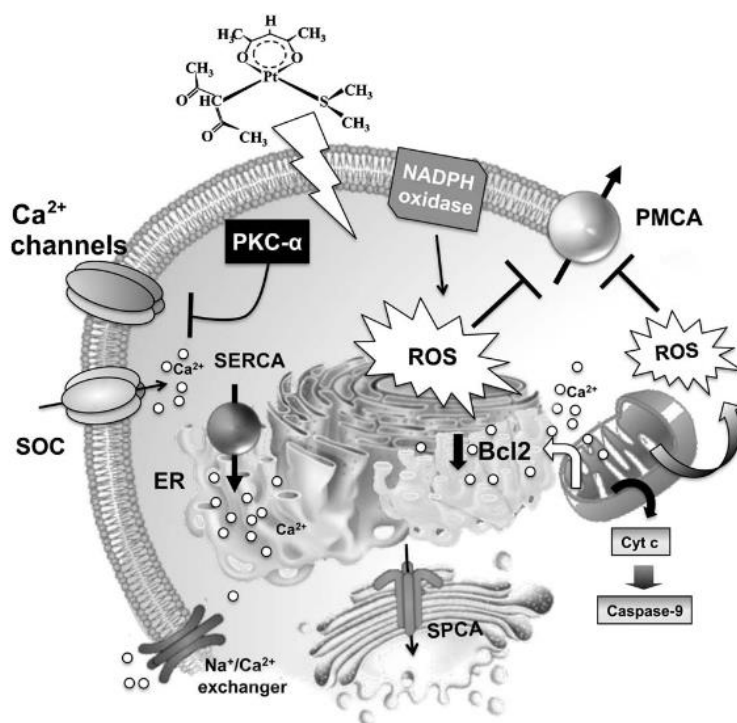
**Fig. 9** [Pt(O,O'-acac)(γ-acac)(DMS)] induces apoptosis by altering the homeostasis of intracellular calcium. This change is due primarily, to the decrease of PMCA activity, due to NADPH oxidase and mitochondrial ROS production, but also to the PKC-a-mediated closure of some channels.

Other studies demonstrated a more cytotoxic effect of [Pt(O,O'-acac)(γ-acac)(DMS)] in human epithelial breast cancer in primary culture than in normal healthy cells, and a faster depolarization of mitochondrial membrane potential in cancer cells respect to Cisplatin treatment (Vetrugno et al., 2014).

*In vivo*, the antitumor activity of [Pt(O,O'-acac)(γ-acac)(DMS)] was evaluated in two studies conducted by Prof. Fanizzi's team. In the first

it was used a mouse xenograft model of breast cancer (Muscella A et al., 2014): compared to Cisplatin, the new compound showed an increase of activity, a decrease of hepatotoxicity and nephrotoxicity and a major concentration of platinum in the blood vessels. In the second and more recent study, using a xenograft model of human renal cell carcinoma (Caki-1), the same authors demonstrated an inhibition of cell survival and angiogenesis of the [Pt(O,O'-acac)(γ-acac)(DMS)] fivefold greater than that of Cisplatin (Muscella A et al., 2016).

In mesothelioma tumour, *in vitro* and *in vivo* studies have shown an effective antitumor role of [Pt(O,O'-acac)(γ-acac)(DMS)] respect to Cisplatin inducing apoptosis in cell culture (ZL55) and reducing the tumour xenografts in mice, highlighting an important pro-apoptotic role of PKC-α. PKC-α is able to trigger a pathway which, activating the protein ERK1/2 (Extracellular signal-regulated kinase 1/2) can induce a cytotoxic effect. However [Pt(O,O'-acac)(γ-acac)(DMS)] appears to be able to inhibit the phosphorylation of ERK1/2, determining the occurrence of resistance (Muscella A et al., 2016; Muscella A et al., 2017).

Our laboratory investigated the different activity of the new compound in rat neuroblastoma B50 cell line: after exposure both to Cisplatin and [Pt(O,O'-acac)(γ-acac)(DMS)] for 48h, cells showed characteristic morphological alterations, more evident after treatment with the second compound, including fragmentation of organelles (such as lysosomes, such that they release their proteases in the cytoplasm), damage of Golgi apparatus, actin bundles of microtubules at the periphery and in the central region, fission and condensation of mitochondria, reduction

of the potential of the mitochondrial membrane, resulting in the activation of the intrinsic pathway of apoptosis (Grimaldi M et al., 2016). Other studies have shown that [Pt(O,O'-acac)(γ-acac)(DMS)] ensures the high platinum levels (4 times higher than those achieved with Cisplatin, with a greater ability to cross the blood brain barrier) in rat cerebellum in the perinatal period one week after administration of the drug, without altering the development of the central nervous system (CNS), preserving the normal dendritogenesis of Purkinje cells and in the absence of a particular impairment of migration of granule cells (Bernocchi G et al., 2011; Cerri S et al., 2011; Piccolini V et al., 2015). Furthermore, the effect of [Pt(O,O'-acac)(γ-acac)(DMS)] in calcium homeostasis also reflected in a reduction of neuronal damage respect to Cisplatin: in rat cerebellum development both compounds shown to be able to alter the Calbindin activity, determining an increase of $[Ca^{2+}]_i$, [Pt(O,O'-acac)(γ-acac)(DMS)] acts also on PMCA-1, bring back $[Ca^{2+}]_i$ at the normal level (Piccolini V et al., 2013). Also in the renal fibrogenesis of the rat, [Pt(O,O'-acac)(γ-acac)(DMS)] induced a minimal number of histopathological damages when compared with Cisplatin, and produced progressive cortical fibrotic lesions (Fenoglio C et al., 2015).

## 1.6 Cell death processing induced by platinum compounds in tumour cells

In multicellular organisms, cell death is an active and critical process that maintains tissue homeostasis and eliminates potentially harmful cells. The Nomenclature Committee on Cell Death (NCCD) proposed

using the adjective "programmed" to identify cases of cell death occurring in a completely physiological context such as post-embryonic development or preservation of tissue homeostasis. Conversely, the term "regulated" should be used to refer to cases of cell death that can be inhibited by specific pharmacological or genetic interventions, and they depend on defined molecular mechanisms (even if they are sometimes partially known). Thus, every case of programmed cell death is by definition regulated, but not *vice-versa*. Finally, the term "accidental cell death" indicates those cases of cell death that cannot be controlled (Galluzzi L et al., 2018). There are a lot of mechanisms of cell death resumed in **Fig. 10**. The three principals are: 1) type I or apoptosis, characterized by fragmentation of nuclear membrane, chromatin condensation, shrinkage of cytoplasm and formation of apoptotic bodies; 2) type II or autophagy showing the formation of cytoplasmic vacuolization followed by degradation of cellular component into lysosomes and 3) type III or necrosis trigging an inflammatory process (Galluzzi et al., 2007; Galluzzi L et al., 2017; Galluzzi L et al., 2018).
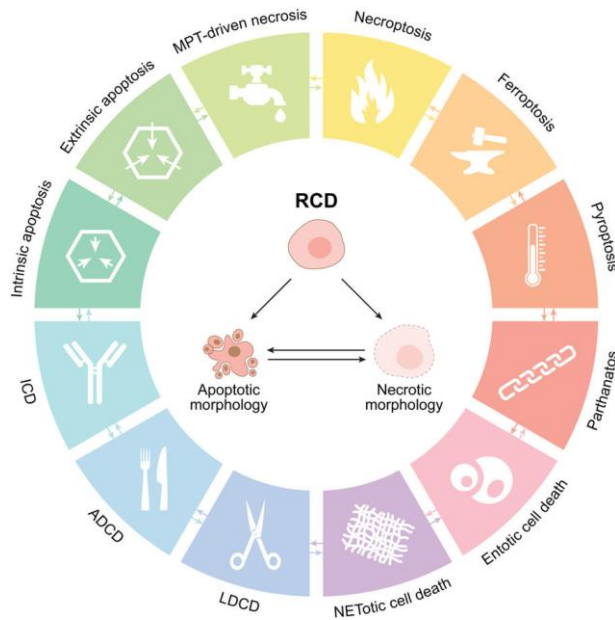
**Fig. 10** The principal cell death mechanisms known until today. Some mechanism starts wirh different molecular alterations an ADCD: autophagy-dependent cell death, ICD: immunogenic cell death, LDCD: lysosome-dependent cell death, MPT: mitochondrial permeability transition. (Galluzzi L et al., 2018).

## 1.6.1 Apoptosis

Two molecular pathways leading to apoptosis, can be recognized according to the origin of the stimulus: the intrinsic pathway and the extrinsic one. However, these pathways are not clearly separated, but they can influence each other through the participation of intracellular organelles such as mitochondria (Galluzzi L et al., 2018).

Intrinsic apoptosis is triggered by different stimuli such as DNA damage, endoplasmic reticulum stress, excessive production of ROS, hypoxic conditions, production of pro-apoptotic cytokines, lack of some growth factors (Czabotar PE et al., 2014; Pihàn P et al., 2017; Roos WP et al., 2016; Vitale I et al., 2017). These stimuli increase the mitochondrial outer membrane permeabilization (MOMP), and the loss of the electrical potential of the inner membrane (Galluzzi L et al., 2016; Tait SE and Green DR, 2010). These mechanisms hinder oxidative phosphorylation, generate uncoupling of the respiratory chain and excessive production of ROS. Furthermore, the opening of mitochondrial permeability transitional pores (MPTPs) located in the contact sites between the outer and inner membranes of the mitochondria, activates the protein OPA1 (mitochondrial dynamic like GTPase). This protein causes the consequent release in the cytosol of different proteins, normally located in the intermembrane space of these organelles (Frezza C et al., 2006; Tait SE and Green DR, 2010), including the cytochrome c (cyt c), a component of the electron transport chain and diablo IAP-binding mitochondrial protein (DIABLO) or SMAC (second mitochondrial activator of caspases) (Chai J et al., 2000; Du C e al. 2000; Verhagen AM et al., 2000).

In the cytosol, cytochrome c binds the apoptotic peptidase activating factor 1 (Apaf-1) and pro-caspase 9 (Caspase 9) and deoxyATP forming an apoptosome, a multiproteic complex inducing the activation of Caspase 9 (Li P et al., 1997) responsible in turn for the activation of executioner pro-caspases 3, 6 and 7 that trigger the cell demolition in both pathway of apoptosis. Caspases (cystinyl aspartate proteases) are

a class of proteases that recognize aspartate residues on intracellular proteins such as other caspases, which are cleaved along the proteolytic cascade; this recognition is made possible by the presence of a cysteine residue, together with one of glycine, in the conserved sequence QACXG (Gln-Ala-Cys-X-Gly, where X corresponds to a residue of arginine, glutamine or glycine) of such proteases, which contributes to the formation of the catalytic site. In summary intra- or extra-cellular apoptotic signals activate initiatory procaspases by proteolytic cutting; these in turn cut other procaspases, leading to a proteolytic cascade that is amplified thanks to the activation of the effector caspases and finally the latter of them activates a series of proteins responsible for the characteristic morphological changes of apoptotic cells (Julien O and Wells JA, 2017; Shalini S et al., 2015). XIAP (X-linked inhibitor of apoptosis) is a member of the IAP family (inhibitor of apoptosis) that blocks the apoptosis cascade by binding and inactivating caspases (Eckelman BP et al., 2006). One the most important caspases is Caspase 3. This caspase is responsible of fragmentation of DNA in oligonucleosomal fragments of 50-300 kb catalyzing the inactivation of DFFA (DNA fragmentation factor subunit alpha (also known as ICAD)) that triggers the catalytic activity of DFFB (DNA fragmentation factor subunit beta, also known as CAD) (Enari M et al., 1998). Indeed CAD, in proliferating cells, is linked to its ICAD inhibitor; in apoptotic cells, however, Caspase 3 cuts the inhibitor factor allowing the release of DNAses (Sakahira H et al., 2015). Caspase 3 is also capable to inactivating the enzyme PARP-1, (responsible of detection of DNA damage), by a proteolytic cleavage between the

residues of Asp214 and Gly215 of the restorative enzyme, generating two fragments, in order to separate the catalytic domain of 89 kDa from the DNA binding domain of 24 kDa (Los M et al., 2002). Another target of Caspase 3 is gelsolin, a protein that acts polymerizing the nucleus of actin and capable of binding phosphatidylinositol 4, 5- bisphosphate (PIP2), acting as a bridge between cytoskeletal organization and signal transduction; the fragmented gelsolin in turn cuts the actin (Kothakota S et al., 1997), thus explaining the structural alteration typical of apoptosis.

The intrinsic pathway is finely regulated by the pro- and anti-apoptotic components of the BCL-2 family of proteins, which control the permeability of the outer mitochondrial membrane (OMM): they can respectively favor or hinder the apoptotic process, as well as interact with each other thanks to the presence in these proteins of hydrophobic portions surrounded by others of amphipathic nature, inhibiting each other (Youle RJ and Strasser A, 2008). Based on the number and type of homology domains, the BCL-2 family contains four domains (BH1, BH2, BH3 and BH4) (Czabotar PE et al., 2014; Moldoveanu T et al., 2014; Shamas-Din A et al., 2013). In response to apoptotic stimuli BAX and BAK form pores in the outer mitochondrial membrane, permeabilize endoplasmic reticulum membranes and, activating the type 1 inositol triphosphate receptors (InsP3Rs), induce the leakage of $Ca^{2+}$ from ER to cytosol (Oakes et al., 2005). The two pro-apoptotic proteins containing a single BH3 domain, require the presence of some BH3-only proteins such as BIM (BCL2-interacting mediator of cell death), PUMA (p53-upregulated modulator of apoptosis) and BID

(BH3 interacting domain death agonist) to promote their activation by homo-oligomerization and, as consequent, the release of cytochrome c-mediated activation of caspases in the cytosol (Ren D et al., 2010).

The major anti-apoptotic members of BCL2 family are BCL2 itself, BCL2 like 1 (or BCL-$X_L$), BCL2 like 2 (BCL2L2 or BCL2-W) and BCL2 related protein A1 (or BCL2A1) (Galluzzi L et al., 2018). They contain all the four domains and act by binding the pro-apoptotic proteins inhibiting their activity (Barclay LA et al., 2015; Hardwick JM and Soane L, 2013; O'Neill KL et al., 2016). In **Fig. 11** is illustrated the complex intrinsic pathway of apoptosis.
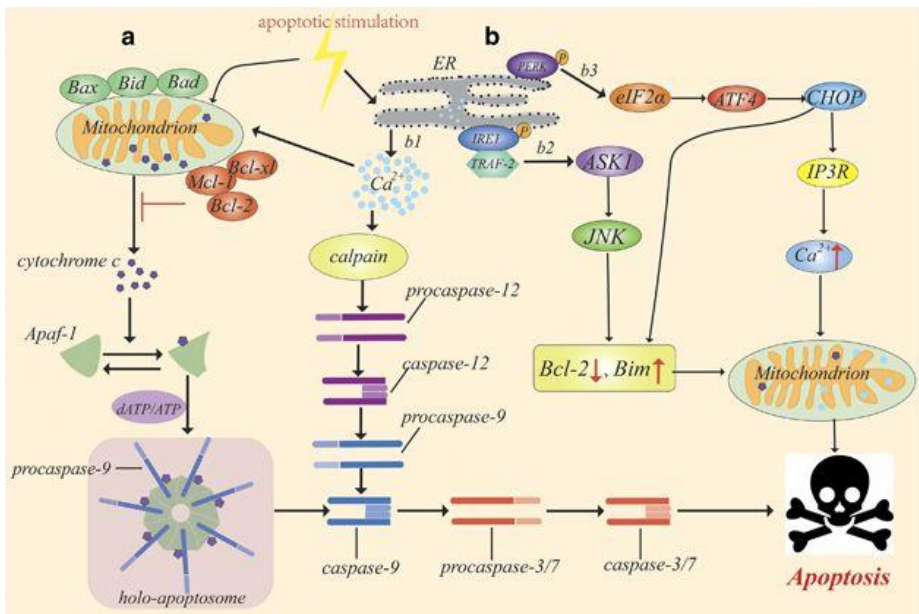


**Fig. 11** The intrinsic apoptosis pathway, Intracellular stimuli can upregulate the pro-apoptotic Bcl-2 family of proteins (a) or induce ER stress conditions (b) that increase intracellular calcium concentration (b1) or different upstream signalling proteins (b2), causing apoptosis (You Y et al., 2017).

The extrinsic pathway of apoptosis is put in place by perturbations of extracellular environment and it is triggered in particular by the so-called death receptors (DRs). Death receptors include: TNF receptor superfamily member 1A (TNFR1), 10a (TNFRSF10A or TRAILR1 or DR4), 10b (TNFRSF10B or TRAILR2 or DR5) and Fas cell surface death receptor (FAS or CD95 or APO1) (Aggarwal BB et al., 2012; von Karstedt S et al., 2017; Wajant H, 2002). After the binding with their ligands, respectively TNF superfamily member (or TRAIL) and FAS ligand (FASLG or CD95L or APO-1L), specific cytoplasmic adaptive proteins are recruited, which expose in turn a death domain (Fas associated death domain (FADD) and TNFRSF1A associated via death domain (TRADD)) that makes contact with the death receptor and allow the assembly with a multiprotein complexes: the most known is called bid capable to trigger the activation of Caspase 8 and Caspase 10 (Brenner D et al., 2015; Chan FK et al., 2000; Chinnaiyan AM et al., 1995; Fu Q et al., 2016; Kischkel FC et al., 2000; Scott FL et al., 2009). Caspase 8 can be inhibited by c-FLIP a pro-caspase protein, similar to the initiating procaspases, but lacking the proteolytic domain, thus capable of inactivate FADD and Caspase 8, competing with it for binding sites in the DISC complex (Hughes MA et al., 2016; Kavuri SM et al., 2011). Finally the execution of apoptotic process can be trigger by Caspase 3 and/or Caspase 7 which are activated by Caspase 8 (Barnhart BC et al., 2003), or in a second way (characteristic of tumor cells) Caspase 8 can activate the cytoplasmic BID protein, generating the t-BID form after proteolytic cut, which, on the mitochondria, binds and stabilizes BAX: this pro-apoptotic factor forms pores on the outer

mitochondrial membrane and allows cytoplasmic release of factors responsible for the intrinsic pathway (such as cytochrome c), in a "cross-talk" between the intrinsic and extrinsic pathways (Esposti MD, 2002, Huang K et al., 2016). In **Fig. 12** is illustrated the process of extrinsic apoptosis.
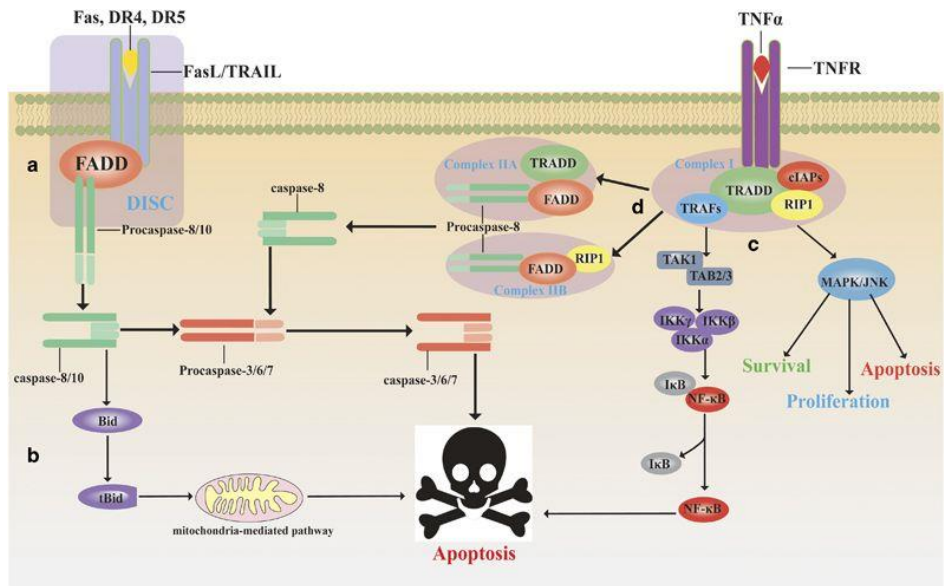


**Fig. 12** The extrinsic pathway of apoptosis. In this picture are illustrated the two major death receptors and the formation of multiprotein complexes able to activate caspases (You Y et al., 2017).

## 1.6.2 Autophagy

Autophagy is one of the main mechanisms of cell survival, with the aim of degrading damaged cytoplasmic components, which will be recycled by the cell (Boya P et al., 2013). While proteins can undergo a similar process through the ubiquitin-proteasome system, autophagy is the only

mechanism that also allows the destruction of entire defective organelles and the reuse of their simpler components to generate new and efficient ones (Elmore S, 2007). Furthermore, this process allows the elimination of damaged mitochondria and prevents the release of pro-apoptotic factors. Therefore, autophagy is a constitutively active process in eukaryotic organisms already in physiological conditions, essential for maintaining cellular homeostasis even in case of adaptation to adverse situations and it have been preserved during evolution (Mariño G et al., 2011). However, various factors can lead to an excessive degradation of the cytoplasmic components such as nutrient deficiency (especially the depletion of amino acids, also known as "nitrogen starvation" or "nitric restriction"), oxidative stress, excessive proteins misfolding, hypoxia, radiations, endogenous hormones or exogenous molecules (such as drugs) or pathogens. (Deretic V, 2009). Autophagy can be implicated not only in physiological conditions but also in diseases like tumors. In particular this process can act both as tumor growth suppression, and as survival mechanism for cancer cells (Chen N and Debnath J, 2010; Levy JMM et al., 2017; White E, 2015). The autophagic process, which requires the consumption of energy and therefore is ATP-dependent, can be effort in three different ways according to the mechanism of action: the micro- and macro-autophagy are not selective, while the chaperone-mediated autophagy (CMA) is restricted to proteins that exhibit a specific pentapeptide. The final degradation product is exactly the same.

*1.6.3 Necrosis*

Necrosis is an ATP-independent phenomenon, which is morphologically characterized by swelling of the cell, with the loss of cell homeostasis, as well as by the increase in the size of the various organelles, in particular of the mitochondria (which also condense and break, as well as the lysosomes), formation of cytoplasmic vacuoles and vesicles, distension of the endoplasmic reticulum, disaggregation and detachment of ribosomes, rupture of the membranes of the organelles and decondensation of the nuclei (Davidovich P et al., 2014; Kroemer G and Martin SJ, 2005). The loss of the integrity of the plasmatic membrane determines the inflammatory process associated with necrosis, due to the leakage of the intracellular material towards external environment: this efflux calls off leucocytes and others immunity cells capable of triggering an immune response and consequently an inflammatory process; this is the main difference compared to apoptosis (Kurosaka K et al., 2003; Savill J and Fadok V, 2000). Furthermore, while apoptosis affects single cells, necrosis can spread to contiguous cells, for this it is an uncontrolled and passive process.

In the last decade, several studies (Cho YS et al., 2009; Feng S et al., 2007; He S et al., 2009; Sun L et al., 2012; Vandenabeele P et al., 2010; Zhang DW et al., 2009) have demonstrated the existence of different pathways of regulated necrosis, showing the same features of non-regulated necrosis described above. All of these processes are characterized by different molecular mechanisms and define different types of regulated necrosis such as necroptosis, ferroptosis, oxytosis,

parthanatos, ETosis, NETosis, pyronecrosis and pyroptosis (Vanden Berghe T et al., 2014).

In particular, parthanatos cell mechanism involves the protein AIF (apoptosis-inducing factor), an oxidoreductase presents in the intermembrane space of mitochondria. AIF can be released from the intermembrane space without involving caspases. In particular, in case of alteration of the function of mitochondria, an excessive production of ROS activates PARP-1 and mediates the permeabilization of the membrane of the lysosomes, allowing the escape from these organelles of degradative enzymes such as cystin-protease cathepsins (in particular B) and calpains; all these proteins act on AIF, which undergoes a proteolytic cut essential for its release from the mitochondria to the cytosol and the nucleus, where acts provoking DNA damage and chromatin condensation (Polster BM et al., 2005; Susin SA et al., 1999; Yu SW et al., 2002).

## 1.7 The role of calcium in cell death and in tumours

The second messenger $Ca^{2+}$ is essential for normal biological functions such as proliferation, cell differentiation, fertilization, activation of transcription factors, ATP synthesis, neurotransmission, muscle contraction and apoptosis (Satheesh NJ and Büsselberg D, 2015). $[Ca^{2+}]_i$ is regulated and maintained at 100 nM while the extracellular concentration is around 1-2 mM (Clapham DE, 2007; Machaca K, 2011; Parkash J and Asotra K, 2010). When the homeostasis of $Ca^{2+}$ changes it can incur some diseases such as hypertension, cardiovascular diseases, diabetes, Alzheimer and cancers (Rizzuto R and Pozzan T,

2003). In particular, $Ca^{2+}$ can play an important role in progression and proliferation of cancer, migration, invasion and metastasis (Chen YF et al., 2013).

$[Ca^{2+}]_i$ homeostasis depends of both calcium entry from the extracellular environment and its release from the endoplasmic reticulum and mitochondria (Marchi S and Pinton P, 2016). The development of dyes detecting the presence of $Ca^{2+}$ (such as Fura-2 or Fluo-4) allows to quantify the amount of this ion in the cellular organelles and how its signal is altered in some diseases (Stewart TA et al., 2015). The homeostasis of $Ca^{2+}$ is ensured by an electro-chemical gradient across the plasma membrane. Calcium enters in the cytoplasm through different channels, for examples the voltage-gated calcium channels (VGCCs), which are activated after the depolarization of the membrane, or the non-voltage-gated channel such as the P2XRs (purinergic ionotropic receptor families) and the transient receptor potential (TRP) channels which mediate the influx of calcium in response to different stimuli (Burnstock G and Di Virgilio F, 2013; Marchi S and Pinton P, 2016; Montell C, 2005). TRPs play an important role also when the influx of calcium from the endoplasmic reticulum induces the opening of channels present in the plasma membrane taking an increase of this ion in the cytoplasm to restore the calcium concentration in the cellular stores. This mechanism is called SOCE (store-operated $Ca^{2+}$ entry) and it is regulated by TRP, ORAI1 ($Ca^{2+}$ release-activated calcium channel protein 1) and STIM1 (stromal interaction molecular 1) channels (Stathopulos PB et al., 2013).

Furthermore, the restoring of intracellular homeostasis of calcium is ensure by the PMCA-1 channel (Padányi R et al., 2016).

In the endoplasmic reticulum the release of calcium is subjected to the activation of receptors of the cell surface which activate the phospholipase C to produce inositol trisphosphate (IP3). This second messenger binds its receptors (IP3Rs) allow the release of calcium in the cytosol (Foskett JK et al., 2007). Others ER channels involved in calcium release are called ryanodine receptors (RyRs). Conversely, the sarco/endoplasmic reticulum $Ca^{2+}$-ATPase (SERCA), transports calcium into the ER trough an active process that requires ATP consumption (Marchi S and Pinton P, 2016). SERCA and its isoforms play an important role in the differentiation of cancer cells, in particular SERCA3, and its altered expression is correlated of various type of cancers (Brouland JP et al., 2005; Xu XY et al., 2012).

Also mitochondria are organelles associated to the regulation of calcium homeostasis. Important channels that mediated efflux and influx of $Ca^{2+}$ are placed along the outer and inner mitochondria membranes. Calcium can entry into this organelle through mitochondria $Ca^{2+}$ uniporter (MCU); their action is counteracted by mitochondrial $H^+/Ca^{2+}$ exchanger (mHCX) and $Na^+/Ca^{2+}$ exchanger (mNCX) both situated in the inner membrane, while the permeability of outer membrane is ensured by overexpression of the VDACs. (Rizzuto R et al., 2012). $Ca^{2+}$ can escape from the mitochondria also by the opening of the permeability potential pore (PTP). The presence or the absence of mitochondria uptake can regulate the release of calcium from ER. Indeed, in the absence of mitochondria uptake, the high

concentration of $Ca^{2+}$ in the cytosol favors the opening of IP3Rs and calcium is released from the ER. When the concentration in the cytosol increases further the same IP3Rs are inhibited. Conversely, in the presence of mitochondria uptake, the $[Ca^{2+}]_i$ decreases and the activation of IP3Rs is sustained (Bezprozvanny I et al., 1991).

Mitochondrial calcium concentration can regulate cell death and survival. An increase of calcium and ROS favors the opening of the PTP, trigger the change of mitochondrial membrane inner potential and release of pyridine nucleotides and cytochrome c (Di Lisa F and Bernardi P, 2009; O'Rourke B, 2000;). In neuronal exotoxicity, glutamate is able to induce the opening of N-methyl-D aspartate receptors (NMDARs) and consequently an increase in the cytosol calcium concentration (Nicholls DG, 2009; Pivovarova NB and Andrews SB, 2010). During this increase mitochondria retain calcium, so the necrotic process starts independently by mitochondria and dependent by the decrease of activity of cytoplasmic $Ca^{2+}$ clearing mechanism. The accumulation of calcium in mitochondria promotes the collapse of the electrochemical gradient, inducing cell death (Bano D et al., 2005). In apoptosis, the fragmentation of organelles starts with the PTP opening (Rasola A and Bernardi P, 2011, 2014). $Ca^{2+}$ induces also mitochondrial modifications: for example, the calcineurin-dependent translocation of mitochondrial fission 1 (FIS1) triggers mitochondrial fission and the release of cytochrome c (Cereghetti GM et al., 2008; Cribbs JT and Strack S, 2007: Frank S et al., 2001; Martinou JC and Youle RJ, 2006). Furthermore, some anti-apoptotic proteins, such as BCL-2, are able to reduce cytosolic and mitochondrial $Ca^{2+}$ response

inducing the ER calcium lack (Foyouzi-Youssefi R et al., 2000; Palmer AE et al., 2004; Pinton P et al., 2000; Pinton P et al., 2001). Pro-apoptotic factors (such as BAX and BAK) operate in the opposite way (Scorrano L et al., 2003). Alterations of this fine-tuning determine the onset of some disorders (such as tumors) (Rizzuto R et al., 2012).

Also the $Ca^{2+}$-binding proteins play an important role in the sequestration and in the surveillance of intracellular calcium concentration. Several hundred $Ca^{2+}$-binding proteins have been identified and most share a common motif (Lewit-Bentley A and Rety S, 2000). This pattern includes about 30 amino acids and consists of a helix-turn-helix motif, where the two helices are arranged like the thumb and index finger of a hand: it is commonly called also hand-EF motif. In almost all $Ca^{2+}$-binding proteins, two hand-EF motifs are in close proximity to form a bundle of four twisted helices (Vetter SW and Leclerc E, 2003). Some $Ca^{2+}$-binding proteins share this hand-EF pattern are: Calmodulin, Parvalbumin, Calretinin and Calbindin. Briefly, Calmodulin is one of the major calcium binding protein that interacts with several hundred different target proteins implicated in cell proliferation, programmed cell death and autophagy (Berchtold MW and Villalobo A, 2014). Parvalbumin contains a $Ca^{2+}/Mg^{2+}$ mixed site (Schwaller B, 2010) and its structure and function are very similar to Calmodulin. Calretinin (also called calbindin 2) represents one of the member of hexa-EF-hand protein family. Their first 5 EF-hand domains are able to bind calcium ions, while the sixth one is inactive. In mesothelioma and in colon cancer cells it leads to apoptosis through activation of Caspase 9-dependent pathway (Blum W and Schwaller B,

2013; Gander JC et al., 1996). High-level of Calretinin expression is detected in ductal carcinoma and is associated with poor overall survival (Taliano RJ et al., 2013). Finally, Calbindin is a calcium-binding protein involved in the modulation of $Ca^{2+}$ homeostasis that control a wide range of cell activities including apoptosis. Calbindin interacts with several proteins localized in cytoplasm, intracellular membranes and in the nucleus (Schwaller B, 2010). In **Fig. 13** are summarized the principal patterns involved in the control of calcium homeostasis.
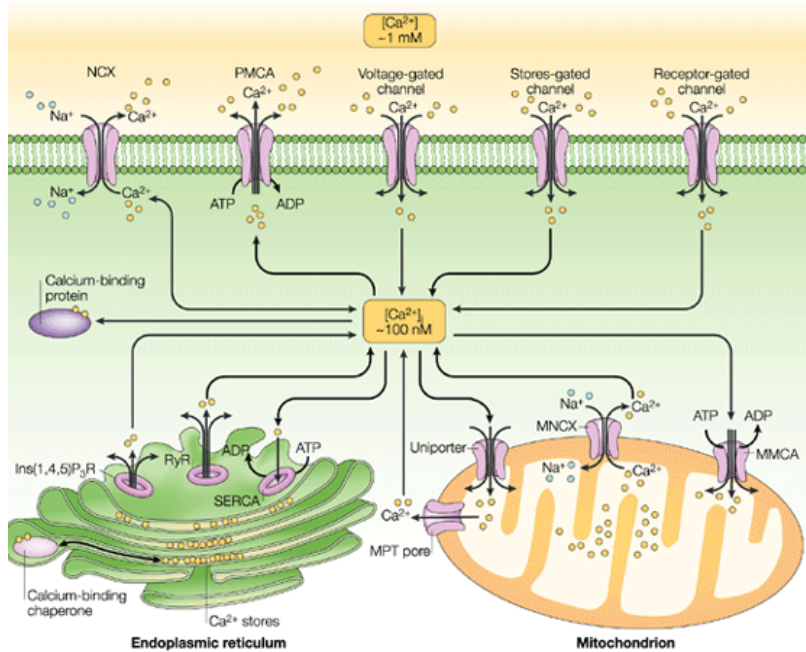


**Fig. 13** The regulation of $Ca^{2+}$ homeostasis through the different mechanisms. Picture shows the major receptors and channels implicated in the efflux and influx of $Ca^{2+}$ from extracellular space to cytosol and intracellular stores and *vice-versa* (Syntichaki P and Tavernarakis N, 2003).

An interesting aspect emerging in the more recent years is the role of mitochondrial-associated endoplasmic reticulum membranes (MAMs) in cancer. MAMs are sites between endoplasmic reticulum and mitochondria of about 10-25 nm in which the membranes of these two organelles make contact without the fusion and maintaining the biochemical distinction of ER and mitochondria (Csordas G et al., 2006; Morciano G et al., 2018). These sites have different roles: for example, they are implicated in the synthesis of lipid transporting the enzymes involved in this metabolic pathway (Vance JE, 2015), and in $Ca^{2+}$ transport signaling (Szabadkai G et al., 2006). In particular when $Ca^{2+}$ is released by the endoplasmic reticulum it is take-up by mitochondria through the VDACs presents in the outer mitochondria membrane near the ER-mitochondria contact sites (De Pinto VD and Palmieri F, 1992). The protein mitofusin 2, implicated in the mechanisms of fission and fusion of mitochondria, is associated with the formation of this contact sites, indeed is overexpressed in MAMs (de Brito OM and Scorrano L, 2008). The accumulation of calcium in mitochondria triggers mechanisms of cell death including apoptosis and autophagy (Bonora M et al., 2017; Morciano G et al., 2015). Many studies demonstrated the role of MAMs in cancer, in particular in the cell death processes and describing the role playing by the oncogene and oncosuppressors in the modulation of calcium signaling pathway (Booth DM et al., 2016; Gutierrez T and Simmen, T 2014; Gutierrez T and Simmen T, 2017; Ivanova H et al., 2017; Sassano ML et al., 2017). In **Fig. 14** are illustrated the MAMs.
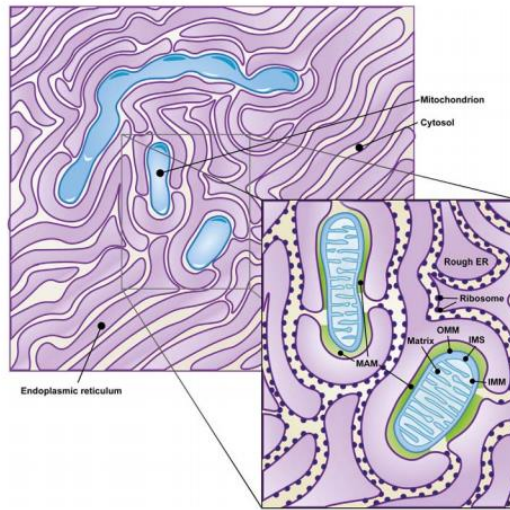
**Fig. 14** Mitochondria-associated ER membranes represented in this illustration in green in the right panel (Morciano G et al., 2018).

The use of chemotherapeutics, such as Cisplatin, causes changes in $[Ca^{2+}]_i$ in both cancer and non-tumor cells (Büsselberg D and Florea AM, 2017). The cytotoxicity of CDDP was studied on MCF-7 cells of breast carcinoma: increasing concentration of CDDP a larger number of cells undergo apoptosis, while the number of necrotic cells remains almost the same. Since the role of $Ca^{2+}$ in MCF-7 was not well understood, the effects of CDDP were investigated in both the parental line, MCF-7S, and in the CDDP-resistant MCF-7R line. After administration of drug, it was demonstrated a decrease in the $Ca^{2+}$ concentration in the resistant cells compared to the parental one. The conclusion was therefore that cell death is more related to an increase in $[Ca^{2+}]_i$ (Al-Taweel N et al., 2014).

## 1.8 The role of oxidative stress in cancer

The effect of oxidative stress in cells can be triggered on proteins and in DNA. In DNA it causes mutations, in particular the 8-hydroxy-2'-deoxyguanosine, and induces onset of cancers (Friedberg EC and Meira LB, 2006; Gupta RK et al., 2014). Oxidative stress can also alter the function of DNA mechanisms repair. In proteins, oxidative stress can be both reversible and irreversible; in particular this latter induces protein carbonylation and tyrosine nitration (Rao RS and Møller IM, 2011) and are used as biomarkers to evaluate the oxidative stress in some diseases (Prokai L et al., 2007; Stadtman ER, 2001). Reactive species implicated in the regulation of oxidative stress can be classified in four groups: ROS, RNS (reactive nitrogen species), RSS (reactive sulfur species) and RCS (reactive chloride species). In particular, ROS include superoxide anion ($O_2^-$), hydrogen peroxide ($H_2O_2$) hydroxil radical ($OH^-$) sigle oxygen ($^1O_2$) and ozone ($O_3$) (Sosa V et al., 2013). Damages that can be caused by ROS depend by the equilibrium between reactive species and antioxidant species. When this equilibrium is lost, some molecules as DNA, RNA, lipids and proteins alter their function (Veskoukis AS et al., 2012).

ROS mechanism is conserved in mammalians and promote different step of tumors: cellular proliferation, evasion of apoptosis, tissue invasion and metastasis and angiogenesis. The principal molecules implicated in induction and proliferation of tumors are the MAPK pathway and the PI3K pathway. In particular, among the member of MAPK, the protein ASK1 (apoptosis signal-regulated kinase 1, a MAPKKK) that regulated JNK (or MAPK8) and p38 (or MAPK14) can

be activated in response to stress conditions, including the increase of ROS (Tobiume K et al., 2001). PI3K catalyzes the phosphorylation of PIP3 (phosphatidylinositol 3, 4, 5-triphosphate) from PIP2 (phosphatidylinositol 4, 5- bisphosphate). The protein PTEN (phosphatase and tensin homolog) can inhibit this reaction when PTEN is oxidized by ROS (Seo JH et al., 2005). Also ROS can regulate the epithelial-mesenchymal transition (EMT), an important and reversible event in which cancer cells changed their epithelial phenotype and develop a more aggressive mesenchymal phenotype (Mani SA et al., 2008). ROS can interact with a lot of proteins implicated in this mechanism such as NF-kB, HIF1 (hypoxia-inducible factor 1) and cyclooxygenase-2 (COX-2) and the matrix metalloproteinase 3 (MMP-3) (Sosa et al., 2013). Finally, in the angiogenesis, the formation of new vessel important for the development of metastasis (Ushio-Fukai M and Nakamura Y, 2008), NADPH oxidases (for example Nox1-5) are the most important enzymes implicated in the formation of ROS: for example Nox1 is overexpressed in colon cancer and prostate cancer, inducing the production of $H_2O_2$, which increases the levels of VEGF (vascular-endothelial growth factor), VEGFR (vascular-endothelial growth factor receptor) and MMPs (matrix metalloproteinases) (Lim SD et al., 2005, Tojo T et al 2005).

In cells, the presence of antioxidant molecules assures the equilibrium between reactive species and antioxidant species. SOD (superoxide dismutase) is the principal enzyme involved in the neutralization of ROS: it catalyzes the dismutation of $O_2^-$ into $H_2O_2$ which, in turn, is

transformed in water by other enzymes, CAT (catalase) and GPx (glutathione peroxidase) (Halliwell B, 2007, Pacher P et al., 2007).

Nitric oxide (NO), synthetized by the family of nitric oxide synthases (NOSs), is implicated in various type of cancers as cervical, breast, central nervous system tumors and others. In particular, NO play an important role in genotoxic mechanisms, antiapoptotic effects, promotion of angiogenesis and metastasis and limit the effect of anti-cancer immune system (Choudhari SK et al. 2013). Nitrotyrosine is a biomarker of presence of NO in cells and it was correlated with lymph-nodes and metastasis formation in breast cancer (Nakamura Y et al., 2006). Furthermore, NO and Nitrotyrosine are increased in patients with lung cancer (Masri FA et al., 2005). In **Fig. 15** is summarized the signaling pathway of oxidative stress in cancer (Kudryavtseva AV et al., 2016).
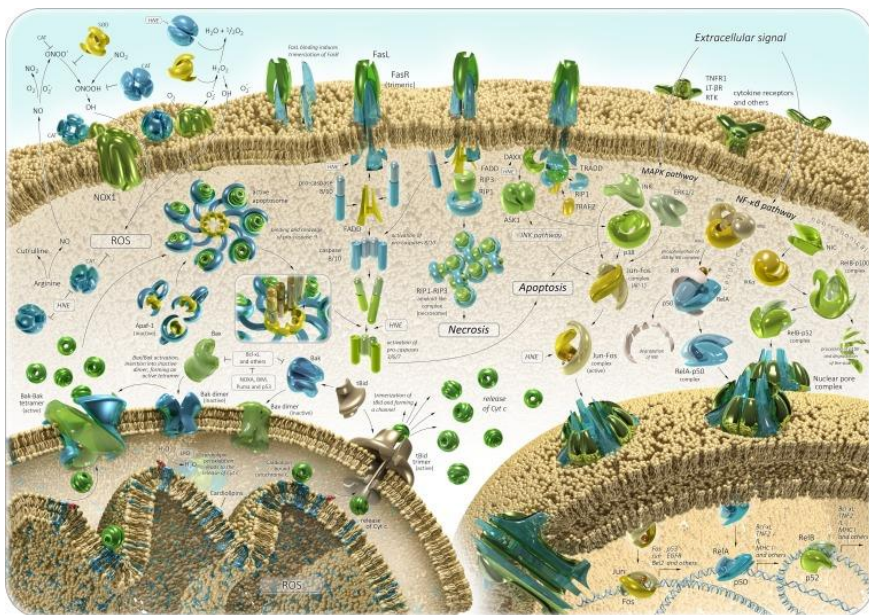


**Fig. 15** Signaling pathway of oxidative stress in cancer.

## 1.9 Role of histone methylation in cancer

Histone modifications play an important role in regulation of gene transcription and therefore in carcinogenesis (Cedar H and Bergman Y, 2009). Hitones modifications includes methylation, acetylation, phosphorylation, ubiquitination, sumoylation, proline isomerization and ADP ribosylation. These modifications are reversible and regulated by a series of enzymes such as histone acetyltransferase (HAT) and deacetylase (HDAC), methyltransferase (HMT) and demethylase (HDM) (Cohen I et al., 2011; Kouzarides T, 2007). In particular, methylation modifications are associated to heterochromatin which is densely compacted and transcriptionally inert (Kanwal R and Gupta S, 2012). Some of the most frequent histone methylations occurs on specific lysine are H3K9, H3K27 and H4K20 (Izzo A and Schneider R, 2010; Li B et al., 2007; Portela A and Esteller M, 2010). However, the degree of methylation can impact on gene transcription: in fact, tri-methylation (me3) of H3K27 and H3K9 is linked with gene silencing (Pan MR et al., 2018).

Some studies have associated the relation with histone methylation and cancer: for example, Yokoama Y et al. (2013) demonstrated that H3K9 trimethylation plays an important role in human colorectal cancer progression, possibly by promoting cell motility and invasion; Fraga MF et al. (2005) indicated that trimethylation of H4K20 is a common hallmark of human cancers; another study demonstrated that alterations in H3K9 and H3K27 methylation are associated with aberrant gene silencing in different types of tumors (Nguyen CT et al., 2002).

# 2. AIMS OF THE RESEARCH

The aim of the work addresses two main topics:

1. to determine whether the new platinum compound [Pt(O,O'-acac)(γ-acac)(DMS)] is more efficient than CDDP in treating glioblastoma. For this aim I performed cytofluorimetric analysis, molecular and immunocytochemical techniques on human glioblastoma T98G cell line to determine whether [Pt(O,O'-acac)(γ-acac)(DMS)] is able to induce cell death identifying differences in morphological features, protein localization and alteration in epigenetic modifications respect to Cisplatin. In particular, I focused my attention on the role of calcium and oxidative stress after administration of Cisplatin and [Pt(O,O'-acac)(γ-acac)(DMS)] on cells and their capability to induce differences in cellular homeostasis;

2. to explore the relationship between cell-intrinsic alterations in cancer metabolism and anti-cancer immune response. For this aim I have generated a series of mouse cell lines (Lewis lung cancer, LLC) that are resistant to Cisplatin, followed by their characterization with respect to PARylation. For this, cells were cultured in the continuous presence of increasing doses of Cisplatin, cloned by limiting dilution in the absence of Cisplatin and then cultured without any drug, followed by periodic monitoring of level of protein PARylation by immunoblot, and Cisplatin resistance by flow cytometry. Then I have generated tumors from parental and cisplatin resistant LLC cells in C57Bl/6

mice and I have analyzed the immune infiltrate using cytofluorimetry. These experiments were performed in the laboratory of Prof. Guido Kroemer (Centre de recherche des Cordeliers, Paris, France).

# 3. MATERIALS AND METHODS

## First part

### *Cell culture and treatment for T98G cell line*

Human glioblastoma T98G cells were cultured in 25 or 75 cm$^2$ flasks in Eagle's minimal essential medium supplemented with 10% fetal bovine serum, 1% glutamine, 100 U penicillin and streptomycin 1% sodium pyruvate and 1% of MEM non-essential amino acids solution in a 5% $CO_2$ humidified atmosphere.

Then, cells were submitted to continued exposure to Cisplatin 40 μM or Pt(O,O'-acac)(γ-acac)(DMS)] (hereafter PtAcacDMS) 10 μM for 48h. For the Cisplatin this concentration was chosen considering previous *in vivo* experimental design of the laboratory (i.e. a single injection of 5 μg/g b. w.). This dose corresponds to the most commonly used in chemotherapy (Bodenner DL et al., 1986; Dietrich J et al., 2006). For the PtAcacDMS the concentration used was chosen considering previous *in vitro* experiments of the laboratory (Grimaldi M, 2015, PhD thesis). For detection of apoptosis markers in calcium free-medium, BAPTA ((1,2-Bis(2-aminophenoxy)ethane-N,N,N′,N′-tetraacetic acid tetrakis(acetoxymethyl ester)) was used at concentration of 30 μM and treatment was carried out for 24h and 48h.

### *Identification of apoptotic cells*

For the identification of apoptotic cells via Annexin V/FITC versus PI, cells were detached by mild trypsinization, incubated with FITC-

conjugated Annexin V (3μl/$10^6$ cells) (Annexin V-FITC Apoptosis Detection Kit, Abcam, Italy) and were counterstained with 2 μg/ml of PI. After 10 min of incubation, dual-parameter flow cytometric analysis was performed with the flow cytometer Partec PAS III, equipped with argon laser excitation (power 200 mW) at 488 nm, 510–540 nm interference filter for the detection of FITC green fluorescence and a 610-nm long-pass filter for PI red fluorescence detection. Data were analyzed using FlowMax software Three independent experiments were carried out, and the average of the scores was used. Values are expressed as the mean ± SD, and differences were compared using Student's t test.

### *Measurement of mitochondrial membrane potential with JC-1*

Changes in mitochondrial membrane potential were monitored using JC-1 (5,5V,6,6V-tetrachloro-1,1V,3,3V- tetraethyl-benzimidazolcarbocyanine iodide, Molecular Probes, Invitrogen, Italy). JC-1 emits either green or red fluorescence, depending on the mitochondrial membrane potential; the green signal indicates depolarized mitochondria, and the red signal indicates polarized mitochondria (Reers M et al. 1995). Thus, the shift from red to green fluorescence is considered a reliable indication of a drop in mitochondrial membrane potential. Cells were harvested by mild trypsination and incubated in culture medium with 2 μM JC-1 for 20 min at 37 °C in the dark. After two washes with PBS at 37 °C, cells in suspension were analysed by flow cytometry using a Partec PAS III equipped with argon ion laser with 20 mW output power at 488 nm

excitation and with 530/30 and 585/42 nm band-pass emission filters. Data were analysed using FlowMax software. Values are expressed as the mean ± SD, and differences were compared using Student's t test.

### *Transmission electron microscopy*

The cells were collected in fresh 15 mL tubes by a gentle centrifugation and fixed with 2.5% glutaraldehyde (Gt) in PBS for 2 h at RT – Gt is preferred for good morphology preservation. After a centrifugation at 2000 rpm for 10 min at RT and several washes with PBS, the cells were post-fixed in 1% aqueous osmium tetroxide ($OsO_4$) for 2 h at RT for lipid fixation in order to preserve the membranous structures – several washes in $H_2O$ followed. Therefore, the cell pellets were pre-embedded in 2% Agar in $H_2O$, dehydrated in graded acetone and embedded in Epon resin. Finally, after 48 hours at 60°C to allow the resin polymerization, ultrathin sections of 70-80 nm were obtained with a Reichert OM3 ultramicrotome and collected on formvar-carbon-coated or naked nickel or gold grids (200 Mesh).

Grids were counterstained with uranyl acetate for 10 min and after numerous washes, lead citrate for 3 min. Sections were then observed and photographed with a TEM Zeiss EM 600, and the negatives scanned with Epson Perfection 4990 PHOTO at a 600 dpi resolution with EPSON scan software.

### *Semithin sections*

Samples were set up as previously described. Semi-thin sections of 0,5-1 µm were obtained with a Reichert OM3 ultramicrotome, collected on

slides and stained with toluidine blue. Then, sections were observed on an Olympus BX51microscope, and the images were recorded with an Optronics MagnaFire Camera equipped with the Cell^F program (Olympus Software Inc).

### *Immunofluorescence reactions*

After treatment, cells grown on coverslips were fixed with 4% formaldehyde for 20 min at room temperature and with 70% ethanol for 24 h at –20°C. Samples were incubated in a humidified chamber with the antibodies listed in **Table 1** prepared in PBS for 1h at room temperature. After three washes coverslips were incubated for 45 minutes with a solution of the secondary antibodies diluted 1:200 prepared in PBS. Nuclei were counterstained with 0.1 μg/mL of Hoechst 33258 for 6 min, then washed twice again and coverslips were mounted in a drop of Mowiol (Calbiochem) for fluorescence microscopy analysis.

| Antigen | Primary Ab | Dilution | Secondary Ab |
|---|---|---|---|
| Mitochondria (Sigma) | Human autoimmune serum recognizing the 70 kDa E2 subunit of the pyruvate dehydrogenase complex | 1:50 | Goat anti- human Alexa-Fluor 594 (Invitrogen) |
| Golgi apparatus | Human autoimmune serum recognizing proteins of Golgi apparatus | 1:250 | Goat anti- human Alexa-Fluor 594 (Invitrogen) |
| Lysosomes (Sigma) | Human autoimmune serum recognizing lysosomal proteins | 1:500 | Goat anti- human Alexa-Fluor 594 (Invitrogen) |
| Microtubules (Sigma) | α-tubulin | 1:1000 | Goat anti- mouse Alexa-Fluor 488 (Invitrogen) |
| Actin (Sigma) | Alexa-594 conjugated phalloidin | 1:500 | |

| Antigen | Primary Ab | Dilution | Secondary Ab |
|---|---|---|---|
| Caspase 9 (Cell signaling) | Polyclonal anti Caspase 9 antibody | 1:200 | Goat anti- mouse Alexa-Fluor 488 (Invitrogen) |
| Caspase 3 (Cell signaling) | Polyclonal anti Caspase 3 antibody | 1:200 | Goat anti- mouse Alexa-Fluor 488 (Invitrogen) |
| Caspase 8 (Cell signaling) | Polyclonal anti Caspase 8 antibody | 1:50 | Goat anti- mouse Alexa-Fluor 488 (Invitrogen) |
| PARP-1 (Cell signaling) | Monoclonal anti PARP-1 antibody | 1:200 | Goat anti- mouse Alexa-Fluor 488 (Invitrogen) |

**Table 1:** Primary and secondary antibodies for double immunofluorescence.

### *Protein extraction and quantification*

Upon treatments, the cells have been detached from the flasks with trypsin, put in test tubes and centrifuged (15 minutes at 1300 rpm). The pellet has been lysed in RIPA buffer (Tris HCl 1M pH 7.6, EDTA 0.5 M pH 8, NaCl 5 M, NP40 Nonidet), 100 µl over one million of cells, with the addition of: PMSF (protease inhibitors), 1 Mm, 10 µl phosphatase inhibitor (Sigma-Aldrich) for every ml of RIPA, and 20 µl of protease (Sigma-Aldrich) every ml of RIPA. The buffer has acted for 30 minutes at +4 ºC, then the test tubes have been centrifuged at 1300 rpm, for 15 minutes, at +4 ºC. The supernatant has been collected. The protein quantification has been realized by the Bradford method (Sigma-Aldrich).

## Western Blotting analysis of PARP-1 and p62/SQSTM1

Samples were electrophoresed in a 10% SDS-PAGE minigel and transferred onto a nitrocellulose membrane (BioRad, Hercules, CA) by a wet transfer for 3 h under a constant current of 400 mA. The membranes were saturated with PBS containing 0.2% Tween-20 and 5% skim milk and incubated with polyclonal rabbit anti-PARP-1 (Cell Signaling, Danvers, USA) diluted 1:1000 or polyclonal mouse anti-p62/SQSTM1 (Cell Signaling, Danvers, USA) overnight and monoclonal mouse anti-actin (Sigma-Aldrich, Italy) diluted 1:2000 for 30 minutes. After several washes, the membranes were incubated for 1 h with the proper secondary antibodies conjugated with horseradish peroxidase (Dako, Italy). Visualization of immunoreactive bands was performed by an ECL System and Hyperfilm Photografic Film (Amersham Life Sciences, Little Chalfont, UK) using the manufacturer's instructions.

## Immunocytochemical detection of histone methylation

After treatment cells grown on coverslips were fixed with 4% formaldehyde for 20 min at room temperature and with 70% ethanol for 24 h at –20 °C. Samples were incubated in a humidified chamber with polyclonal antibody anti H3K9me3 (GTX121677, GeneTex) diluited 1:50; or polyclonal antibody anti H3K27me3 (GTX121184, GeneTex) diluted 1:50 or polyclonal antibody anti H4K20me3 (GTX128960, GeneTex) diluted 1:200 in PBS + TritonX 0.5% for 2h. After five washes coverslips were incubated for 45 minutes with a solution of the secondary antibodies goat anti-rabbit Alexa-Fluor 488 (Molecular

Probes, Invitrogen) prepared in PBS and diluted 1:200. After five washes in PBS, nuclei were counterstained with 0.1 µg/mL of Hoechst 33258 for 6 minutes, then washed twice again and cells were mounted in a drop of Mowiol (Calbiochem) for fluorescence microscopy analysis.

## *Measurement of [Ca$^{2+}$]*

To evaluate the concentration of intracellular calcium we follow the procedure described by Lodola et al., 2012. T98G, grown on coverslips, were loaded with 4 mM fura-2 acetoxymethyl ester (fura2/AM; 1 mM stock in dimethyl sulfoxide) in PSS for 30 min at 37°C. After washing in PSS, the coverslip was fixed to the bottom of a Petri dish and the cells observed by an upright epifluorescence Axiolab microscope (Carl Zeiss, Oberkochen, Germany), usually equipped with a Zeiss 640 Achroplan objective (water-immersion, 2.0 mm working distance, 0.9 numerical aperture). T98G were excited alternately at 340 and 380 nm, and the emitted light was detected at 510 nm. A first neutral density filter (1 or 0.3 optical density) reduced the overall intensity of the excitation light and a second neutral density filter (optical density = 0.3) was coupled to the 380 nm filter to approach the intensity of the 340 nm light. A round diaphragm was used to increase the contrast. The excitation filters were mounted on a filter wheel (Lambda 10, Sutter Instrument, Novato, CA, USA). Custom software, working in the LINUX environment, was used to drive the camera (Extended-ISIS Camera, Photonic Science, Millham, UK) and the filter wheel, and to measure and plot online the fluorescence from 10–15 rectangular

''regions of interest'' (ROI) enclosing 10–15 single cells. Each ROI was identified by a number. Since cell borders were not clearly identifiable, a ROI may not include the whole T98G or may include part of an adjacent T98G. Adjacent ROIs never superimposed. $[Ca^{2+}]_i$ was monitored by measuring, for each ROI, the ratio of the mean fluorescence emitted at 510 nm when exciting alternatively at 340 and 380 nm (shortly termed ''ratio''). An increase in $[Ca^{2+}]_i$ causes an increase in the ratio. Ratio measurements were performed and plotted on-line every 3 seconds.

The resting $[Ca^{2+}]_i$ was calculated by using the Grynkiewicz equation, as described in Hartmann J and Verkhratsky A(1998):

$$[Ca^{2+}] = Kd * \left\{ \frac{F_{min380}}{F_{max380}} \right\} * \left\{ \frac{R - R_{min}}{R_{max} - R} \right\}$$

Where:

- Kd is Fura-2 effective dissociation constant (estimated at 135 at 22°C),

- Fmin380  is the fluorescence intensity following excitation at 380 nM in $Ca^{2+}$-free fura-2 (MIN solution)

- Fmax380 is the fluorescence intensity following excitation at 380 nM in $Ca^{2+}$-bound fura-2 (MAX solution)

- Rmin is the 340/380 ratio in MIN solution

- Rmax is the 340/380 ratio in MAX solution

Rmax was obtained by challenging the cells with the $Ca^{2+}$-ionophore ionomycin (10 µM) in the presence of extracellular 10 mM $CaCl_2$ (MAX solution), whereas Rmin was obtained by switching the

perfusate to a solution devoid of $Ca^{2+}$ and supplemented with EGTA (0.5 mM) (MIN solution).

ER $Ca^{2+}$ concentration and SOCE entry were evaluated by applying the $Ca^{2+}$-addback protocol in the presence of 30 µM CPA (Cyclopiazonic acid), as described in the Results. The amplitude of the peak $Ca^{2+}$ response to CPA was measured as the difference between the ratio at the peak and the mean ratio of 1 min baseline before the peak. The magnitude of SOCE evoked by CPA upon $Ca^{2+}$ restoration to the bath was measured as the difference between the ration at the peak of extracellular $Ca^{2+}$ entry and the mean ration of 1 min baseline before $Ca^{2+}$ readdition. Pooled data are given as mean±SE and statistical significance ($P < 0.05$) was evaluated by the Student's t-test for unpaired observation.

Physiological salt solution (PSS) had the following composition (in mM): 150 NaCl, 6 KCl, 1.5 $CaCl_2$, 1 $MgCl_2$, 10 Glucose, 10 Hepes. In $Ca^{2+}$-free solution (0 $Ca^{2+}$), $Ca^{2+}$ was substituted with 2 mM NaCl, and 0.5 mM EGTA was added. Solutions were titrated to pH 7.4 with NaOH. The osmolality of PSS as measured with an osmometer (Wescor 5500, Logan, UT) was 338 mmol/kg.


*Immunocytochemical staining for calcium markers*
After treatment cells grown on coverslips were fixed with 4% formaldehyde for 20 min at room temperature and with 70% ethanol for 24 h at –20 °C. Then cells were washed with PBS and incubated with blocking and permeabilization buffer (1% BSA, 0,3 M glycine in 0,1% PBS- tween). Samples were incubated in a humidified chamber with the

antibodies listed in **Table 2** prepared in PBS for 1h at room temperature. After three washes coverslips were incubated for 45 minutes with a solution of the secondary antibodies prepared in PBS and diluted 1:200. Nuclei were counterstained with 0.1 µg/mL of Hoechst 33258 for 6 min, then washed twice again and coverslips were mounted in a drop of Mowiol (Calbiochem) for fluorescence microscopy analysis.

| Antigen | Primary Ab | Dilution | Secondary Ab |
|---|---|---|---|
| Calmodulin (Abcam) | Monoclonal anti Calmodulin antibody | 1:200 | Goat anti- rabbit Alexa-Fluor 594 (Invitrogen) |
| Calretinin (Swant) | Polyclonal anti Calretinin antibody | 1:200 | Goat anti- rabbit Alexa-Fluor 594 (Invitrogen) |
| Parvalbumin (abcam) | Polyclonal anti Parvalbumin antibody | 1:100 | Goat anti- rabbit Alexa-Fluor 594 (Invitrogen) |
| Calbindin (Swant) | Monoclonal anti Calbindin antibody | 1:2000 | Goat anti- mouse Alexa-Fluor 594 (Invitrogen) |
| PMCA-1 (abcam) | Polyclonal anti PMCA-1 antibody | 1:300 | Goat anti- rabbit Alexa-Fluor 594 (Invitrogen) |
| Actin (Sigma) | Alexa-594 conjugated phalloidin | 1:500 | |
| Microtubules (Sigma) | α-tubulin | 1:1000 | Goat anti- mouse Alexa-Fluor 488 (Invitrogen) |

**Table 2** Primary and secondary antibody for detection of calcium markers.

*Immunochemical staining for oxidative stress markers*

For nitrotyrosine detection, after treatment cells grown on coverslips were fixed with ethanol:acetic acid (95:5) for 1 min. Then cells were washed with PBS and incubated with 200 µl of 5 mM peroxynitrite (Millipore) to the positive control or with 200 µl of mM degraded peroxynitrite to the negative control for 5 min. After wash with PBS the cells were incubated with 400 µl of 1% BSA in PBS for 30 min at room temperature. Then cells were washed and incubated with polyclonal rabbit anti-nitrotyrosine diluted 1:200 (Millipore) in 1% BSA in PBS overnight at 4°C. Cells were washed and incubated with Alexa 594-conjugated anti-rabbit antibody (Molecular Probes, Invitrogen, Milan, Italy) diluted 1:200 in PBS for 1.5 h at room temperature. After three washes in PBS, nuclei were counterstained with 0.1 µg/mL Hoechst 33258 for 6 minutes, then washed twice again and cells were mounted in a drop of Mowiol (Calbiochem) for fluorescence microscopy analysis.

For the other oxidative stress markers, after treatment cells grown on coverslips were fixed with 4% formaldehyde for 20 min at room temperature and with 70% ethanol for 24h at –20 °C. Cells were washed with PBS and incubated with blocking and permeabilization buffer (1% BSA, 0,3 M glycine in 0,1% PBS- tween). Then, cells were incubated with the following antibodies:

- polyclonal rabbit anti-SOD-1 diluted 1:200 in PBS (Santa Cruz Biotechnology, Dallas, Texas, USA) for 1 h. After three washes coverslips were incubated for 45 min with secondary antibody

Alexa-Fluor 594 goat anti-rabbit (Molecular Probes, Invitrogen) prepared in PBS and diluted 1:200;

- polyclonal rabbit anti-NOS2 diluted 1:200 in PBS (Santa Cruz Biotechnology, Dallas, Texas, USA) for 1 h. After three washes coverslips were incubated for 45 min with secondary antibody Alexa-Fluor 594 goat anti-rabbit (Molecular Probes, Invitrogen) prepared in PBS and diluted 1:200;

- polyclonal rabbit anti-ROS diluted 1:200 in PBS (Santa Cruz Biotechnology, Dallas, Texas, USA) for 1 h. After three washes coverslips were incubated for 45 min with secondary antibody Alexa-Fluor 594 goat anti-rabbit (Molecular Probes, Invitrogen) prepared in PBS and diluted 1:200.

After three washes in PBS, nuclei were counterstained with 0.1 µg/mL Hoechst 33258 for 6 minutes, then washed twice again and cells were mounted in a drop of Mowiol (Calbiochem) for fluorescence microscopy analysis.

*Fluorescence microscopy*

An Olympus BX51 microscope equipped with a 100W mercury lamp was used under the following conditions: 330-385 nm excitation filter (excf), 400 nm dichroic mirror (dm), and 420 nm barrier filter (bf) for Hoechst 33258; 450-480 nm excf, 500 nm dm and 515 nm bf for the fluorescence of Alexa 488; 540 nm excf, 580 nm dm, and 620 nm bf for Alexa 594. Images were recorded with an Olympus MagnaFire camera system and processed with the Olympus Cell F software.

*Statistical analysis of fluorescence intensity*

In order to detect the fluorescence intensity for quantitative analysis of protein expression the optical density (OD), i.e. pixel density, was measured using an automatic function of ImageJ Program. The statistical analysis was carried out calculating the OD average for the CTRL and each treatment. Three independent experiments were carried out, and the values are expressed as the mean ± SD, and differences were compared using Student's t test.

# Second part

*Cell lines, clones and culture conditions for non-small cell lung cancer LLC cell line*

For both wild-type (WT) cells and their CDDP-resistant counterparts (R) glutamax-containing Dulbecco's Modified Eagle's Medium medium has been used, supplemented with 10% fetal bovine serum, 100 U/mL penicillin G sodium salt, and 100 mg/mL streptomycin sulfate. Cell lines were routinely maintained at 37°C under 5% $CO_2$ and seeded in 12-well plates 24 hours before experimental determinations.

CDDP-resistant NSCLC cell clones were isolated from LLC cells (9 clones) that have been cultured in the continuous presence of CDDP (8 µmol/L) for 5 months. Cloning was performed by limiting dilution. Clones were maintained in CDDP-free conditions for 1 month before analysis of CDDP resistance and expression of PARylation.

## *Flow cytometry*

For the quantification of plasma membrane integrity and mitochondrial transmembrane potential (Δψm), WT and resistant clones LLC cells were collected, washed, and co-stained with 1 µg/mL propidium iodide (PI, which only incorporates into dead cells) and 40 nmol/L 3,3′-dihexyloxacarbocyanine iodide DiOC6(3), a mitochondrial transmembrane potential (Δψm)-sensitive dye for 40 min at 37°C. Flow cytometry analysis were conducted on a MacsQuant flow cytometer (Miltenyi Biotech). Data were analyzed by means of FlowJo v.X PC software (Treestar, OR, USA). Graphics and statistical analysis were performed with Microsoft Excel.

## *Immunoblotting*

For the detection of protein levels, cells were harvested, washed with PBS and lysed for 10 min on ice in a buffer prepared in 50 mM Tris (pH 7.4) and containing 250 mM NaCl, 0.1% NP-40, 0.1 mM phenylmethylsulfonyl fluoride (PMSF), aprotinine at 10 mg/mL, leupeptine at 10 mg/mL, and 100 mM NaF. After sonication, cell lysates were then centrifuged for 10 min at 13 000 rpm and the concentration of soluble proteins in supernatant was measured by a BCA assay method. Equal amount of proteins (50 µg) were resolved by precasted 4% to 12% SDS page gels, electrotransferred to polyvinylidene fluoride (PVDF) membranes and probed with primary antibodies specific for PAR. An antibody that recognizes actin was used to monitor equal lane loading. Finally, membranes were incubated with

appropriate horseradish peroxidase-conjugated secondary antibodies, followed by ECL chemiluminescence detection.

### *In vitro detection of PD-L1*

For the in vitro detection of the surface marker PD-L1, Cisplatin sensitive and resistant LLC cell lines were harvested, washed with PBS and seeded (one million for condition) into a 96-well plate. First cells were stained with LIVE/DEAD® Fixable Yellow Dead Cell dye (Invitrogen, Carlsbad, CA, USA) for 15 min at 4°C to discriminate viable cells from damaged cells. Then, tumor cells were incubated with antibodies against PD-L1 for 25°C at 4°C in the dark. Subsequently cells were washed with PBS+ BSA 0,5% and then fixed, permeabilized, washed two times and finally transferred into tubes for flow cytometry analysis. Data were analyzed by means of FlowJo v.X PC software (Treestar, OR, USA). Graphics and statistical analysis were performed with Microsoft Excel.

### *Isolation and phenotyping of tumor-infiltrating lymphocytes and myeloid cells by flow cytometry.*

For the quantification of immune infiltrate, mice tumor were collected and dissociated using Miltenyi Biotec mouse tumor dissociation kit (Miltenyi Biotec; Bergisch Gladbach, Germany) according to the manufacturer's protocol. The dissociated bulk tumor cell suspension was resuspended in RPMI-1640, sequentially passed through 70 μm and 30 μm nylon cell strainers (Miltenyi Biotec, Bergisch Gladbach, Germany) and washed twice in PBS. 200 μL of suspension were

transferred into a 96-well plate; centrifuged at 1200 rpm for 5 min and then stained with the following protocol. First cells were stained with LIVE/DEAD® Fixable Yellow Dead Cell dye (Invitrogen, Carlsbad, CA, USA) for 15 min at 4°C to discriminate viable cells from damaged cells. Then, tumor infiltrating cells were incubated with antibodies against CD16/CD32 (Fc blocker) before staining with fluorescent-labeled antibodies targeting T-cell surface markers for 25 min at 4°C in the dark: for the tumor infiltrating lymphocytes (TILs): anti-CD3, anti-CD8, anti-CD4, anti- CD25, anti-ICOS, anti PD1; for the tumor infiltrating myeloid cells: anti-CD45, anti-Ly6C, anti Ly6G; anti CD11b, anti CD11c, anti MHCII and anti-CD80. All the antibodies were diluted in PBS+ BSA 0,5%. Subsequently cells were washed with PBS+ BSA 0,5% and then fixed, permeabilized and washed two times. Then 6 followed the intracellular staining of TILs with the ab anti-Foxp3 for 25 min at 4°C in the dark, followed by two washes. Data were acquired using a BD LSRII flow cytometer (BD Biosciences,) and analyzed by means of FlowJo v.X PC software (Treestar, OR, USA). Graphics and statistical analysis were performed with Microsoft Excel and Prism software.

*Flow cytometry gating strategy.*

**Fig. 1** represents the gates apply to analyze the tumor infiltrating lymphocytes with FlowJo. In the first image, along the X-axis FSC-A (Forward Scatter) indicate a relative size for the cell. Along the Y-axis, the SSC (Side Scatter) parameter is a measurement of the granularity of the cell. Lymphocytes are characterized by low size and granularity

which allows to distinguish them from tumor cells. Alive CD3+ cells represent the T cells; this population can be divided into four categories: the major is CD4+/CD8- (identifying CD4+ T helper cells including T regulatory lymphocytes), then CD4-/CD8+ (identifying CD8+ T cells including cytotoxic T lymphocytes) and CD4-/CD8-. Within each cell subset, we can evaluate PD1/ICOS expression to estimate the activated status of T lymphocytes. Among the CD4+/CD8- T cells, we cab distinguished CD25+/Foxp3+ expressing cells, that typically represent the T regulatory lymphocytes (T-Reg), a generally immunosuppressive subpopulation of T-cells which modulate the immune system in many disorders like cancer.
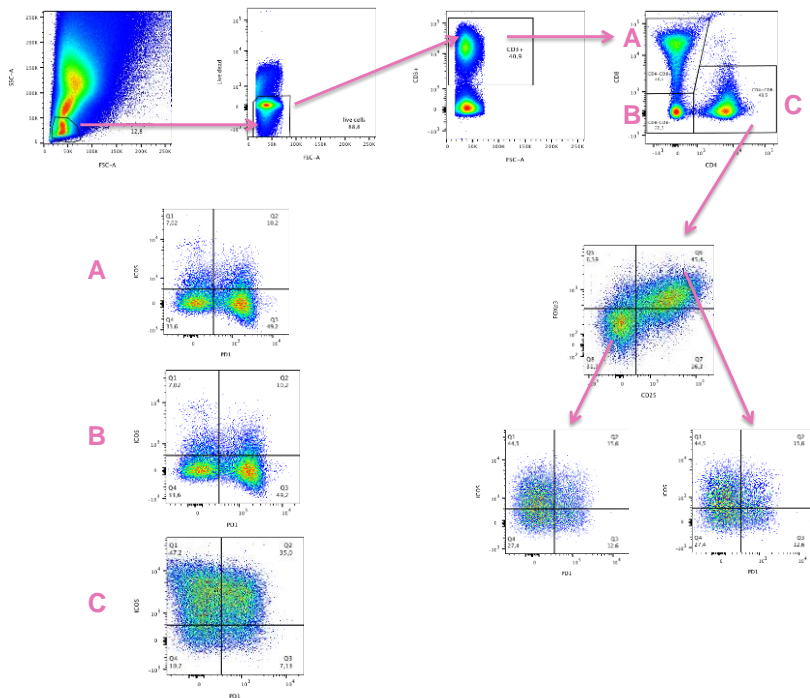


**Fig. 1** Flow cytometry gating strategy to analyze the tumor infiltrating lymphocytes with FlowJo.

**Fig. 2** represents the sequential gates apply to analyze the immune infiltrate of myeloid cells with FlowJo. In contrast to lymphocytes, myeloid cells are not characterized by different size and granularity. Among live cells, CD45+ represent the amount of leukocytes; this population can be divided into different categories expressing markers to distinguished lymphocytes B (and also the T ones), monocyte, granulocytes and dendritic cells: Ly6C is a marker for monocytes, as well as CD11b, Ly6G is able to select the granulocytes (in particular the eosinophil ones); CD11b and CD11c positive cells are classified as dendritic cells, while CD80 and MCHII are markers for activated B cells, monocytes and dendritic cells.
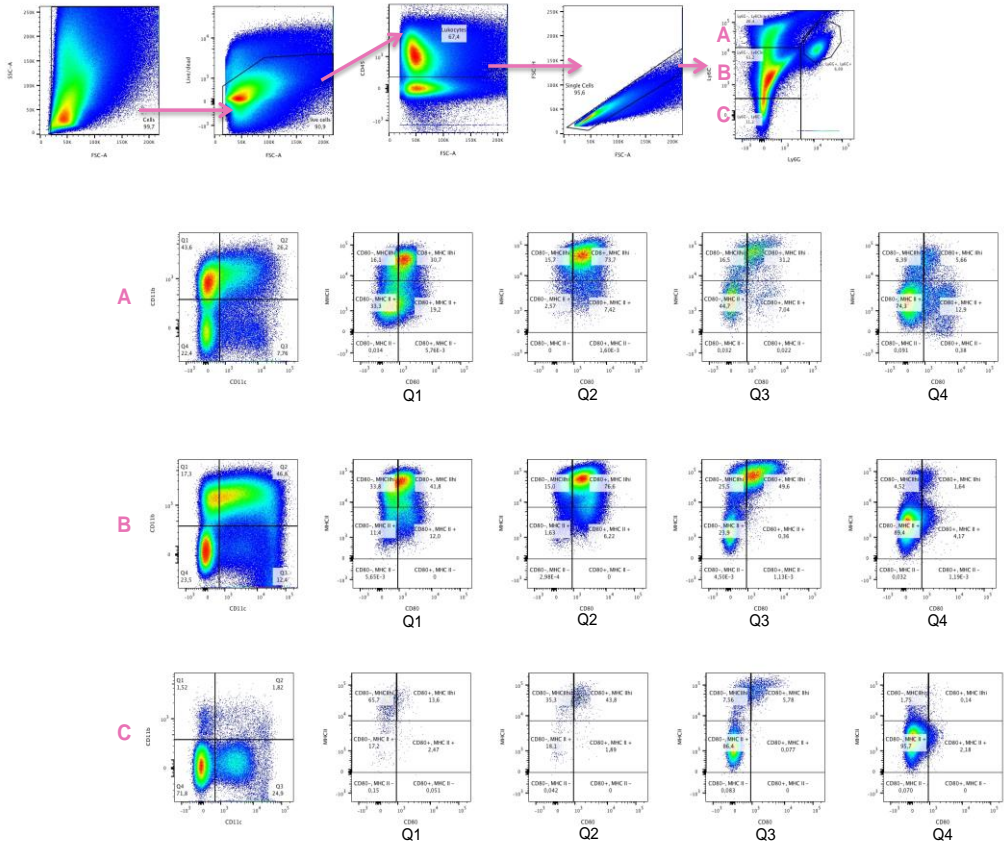
**Fig. 2** Flow cytometry gating strategy to analyze the tumor infiltrating myeloid cells with FlowJo.

# 4. RESULTS

## 4.1 First part

**Analysis of apoptotic cells after treatment**

To evaluate the amount of dead cells after treatment with CDDP and PtAcacDMS a biparametric analysis was performed with Annexin V and PI. In **Fig. 1A** representative cytograms are illustrated. In **Fig. 1B** an increase of death cells in treated *vs*. control cells is shown, in particular a significative difference in the mean of number of apoptotic cells in control (6.49%) and in treated cell with CDDP (14.29%) and PtAcacDMS (25.96%).
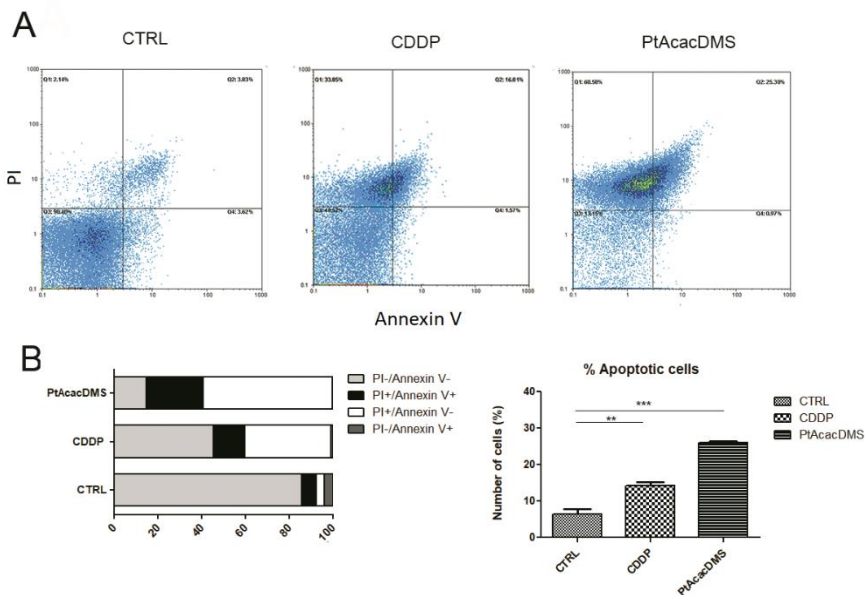


**Fig. 1 A** Representative cytograms of control and treated cells. **B** Histograms with the percentage distribution of different categories and in the right panel the percentage of apoptotic cells, data are represented as mean ± SEM (n = 3). * =P < 0.05; ** =P < 0.01 , ***= P < 0.001 (Student' t test).

*Cytofluorimetric analysis of the mitochondrial membrane potential changes*

Mitochondria play an important role on many aspect of cell life. Kroemer and collaborators were the first ones assuming the importance of permeabilization of mitochondria membrane during apoptosis (Kroemer G et al., 1995), that determine alterations in mitochondrial membrane potential (Green DR and Kroemer G, 2004). In T98G cell line the analysis of mitochondrial membrane potential ($\Psi$m) changes was performed using 5,5V,6,6V-tetrachloro-1,1V,3,3V-tetraethyl benzimidazolcarbocyanine iodide (JC-1). **Fig. 2** shows a greater depolarization of $\Psi$m in cells treated with both compounds (78.2% for CDDP and 89.1% for PtAcacDMS) respect to control (7.6 %).

**green (JC-1 monomer)**
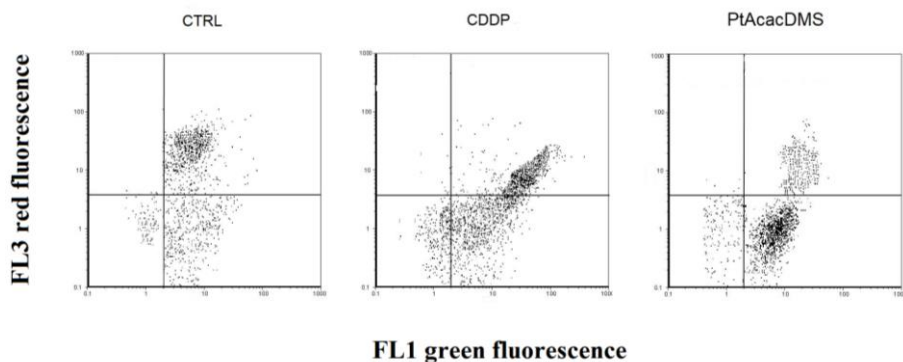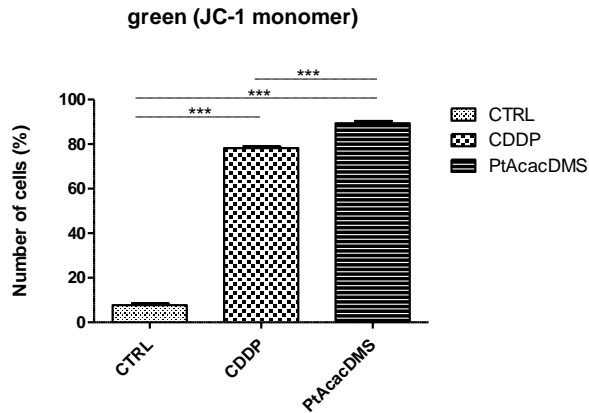


Fig. 2 Flow cytometric analysis of JC-1. Above, red and green fluorescence of mitochondria stained with JC-1 in control cells, treated with CDDP and PtAcacDMS. Below, the percentage of cells with reduced mitochondrial membrane potential. Statistical analysis was performed using Student's t: * = $p < 0.05$, ** = $p < 0.01$, *** = $p < 0.001$.

## Ultrastructural morphology of T98G cells in control condition and after treatment with platinum compounds

To confirm the morphology alterations induced by CDDP and PtAcacDMS, ultrathin sections were investigated with TEM. Control cells show a normal morphology with a large nucleus and a defined nucleolus, with typical mitochondrial and plasmatic membrane shape (**Fig. 3a**). After treatment with CDDP, cells show the typical morphology of different type of cell death, in **Fig. 3b** it is possible to notice the necrotic process, in which the plasmatic membrane is degraded, and the nuclear membrane is just distinguishable. Inside the nucleus the chromatin is condensed. The presence of a lot of vesicles with double membrane indicate the autophagic process; indeed, the

presence of material in some of these vesicles is well visible. In **Fig. 3c** is visible a cell in early apoptosis with the plasmatic membrane intact and the formation of "blebs" typical of this kind of cell death. In the cell in the upper right it is possible to notice elongated mitochondrial, characteristic of apoptosis. After treatment of PtAcacDMS in **Fig. 3d** two cells indicated two different way of cell death: in the lower left a necrotic cell with an extended condensed chromatin and loss of defined plasmatic membrane; in the upper right a cell in evident stage of early apoptosis. Finally, in **Fig. 3e** an autophagic cell with many vesicles and a nucleus still identifiable with condensed chromatin.
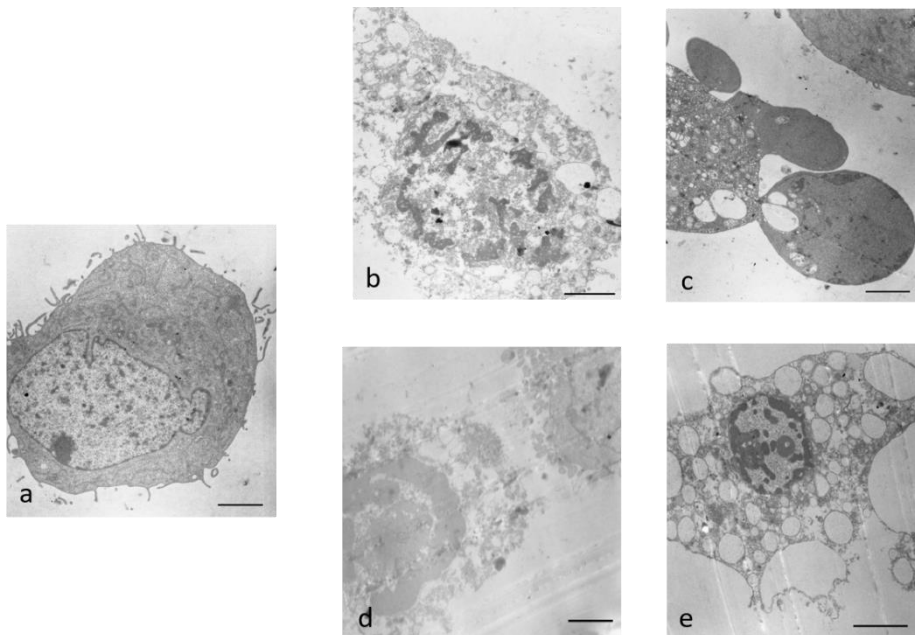


**Fig. 3** Ultrastructural morphology of control cells (**a**), CDDP 40 μM treated cells (**b** and **c**), PtAcacDMS 10 μM treated cells (**d** and **e**). Bars: 4 μm.

**Fig. 4** shows semithin sections stained with toluidine blue and observed with an optical microscope. The shape of control cells and treated cells with the two platinum compounds confirm the ultrastructural morphology of cells observed with TEM; in particular after administration of CDDP and PtAcacDMS it can possible detected cells in stage of apoptosis, necrosis and autophagy.
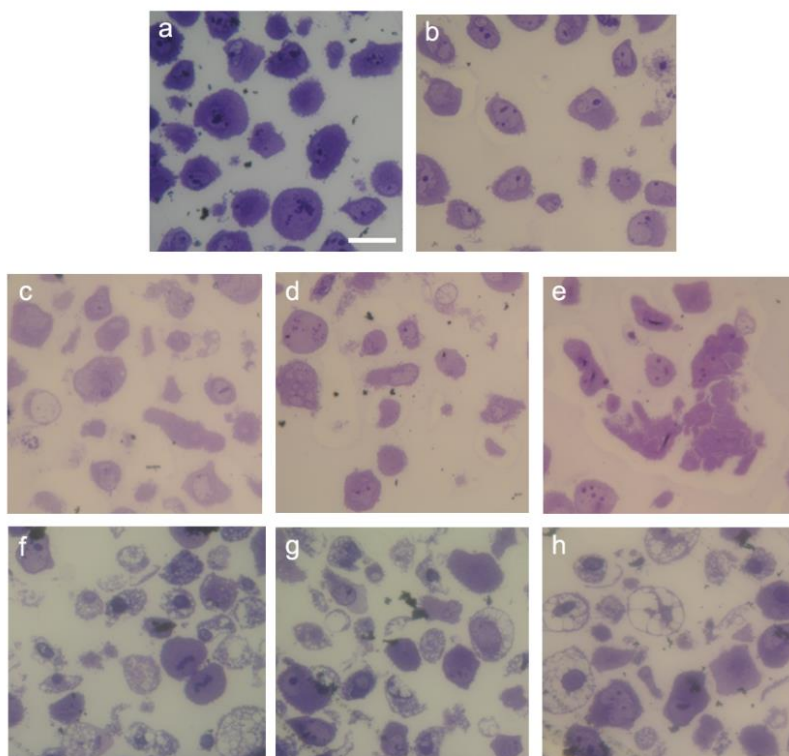


**Fig. 4** Semithin sections stained with toluidine blue. control cells (**a** and **b**), CDDP 40 μM treated cells (**c**, **d** and **e**), PtAcacDMS 10 μM treated cells (**f**, **g** and **h**). Bars: 40 μm.

*Immunocytochemical detection for mitochondria, Golgi apparatus and lysosomes*

Previous studies have demonstrated the effect of CDDP and PtAcacDMS on mitochondria, Golgi apparatus, actin cytoskeleton and tubulin on rat neuroblastoma B50 cell line (Grimaldi M et al., 2016). Thus, we wanted to evaluate the possible morphologic alterations of both compounds on human glioblastoma T98G cell line. First, we evaluated the morphology of mitochondria because they play an important role in many aspect of cell life. Compared with control cells, we see that after PtAcacDMS exposure, mitochondria show a homogenous distribution in the cytoplasm forming clusters. This event is maybe related to altered structure of tubulin, which is reorganized in bundles and loses its role as "anchoring" to cell organelles, probably because of the depolymerization of microtubules (**Fig. 5**).
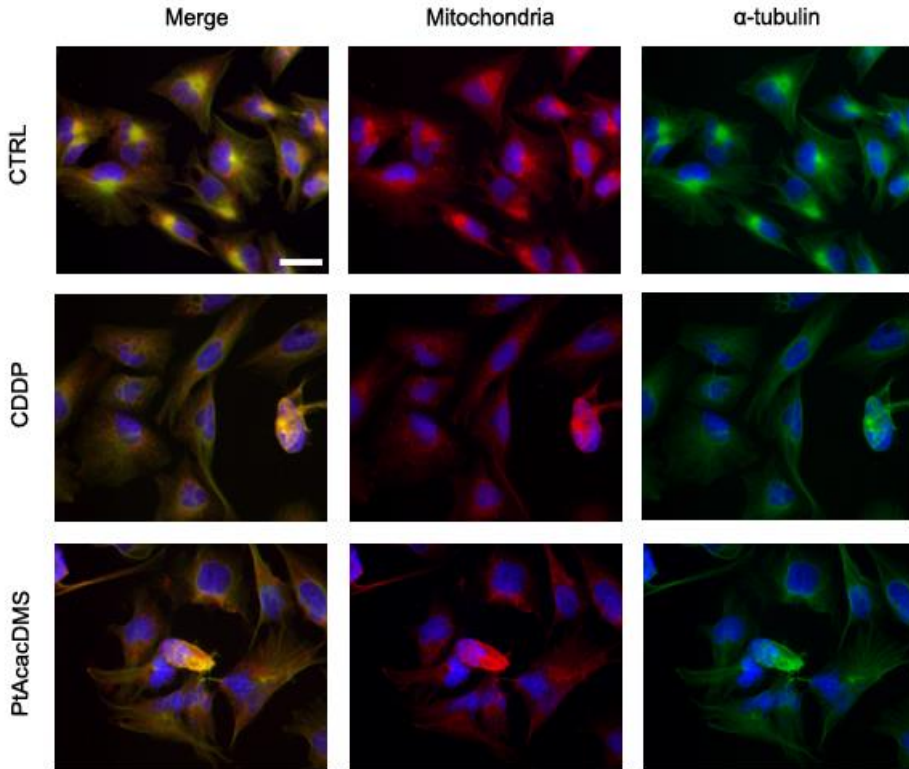
**Fig. 5** Immunocytochemical detection of mitochondria (red fluorescence) and α-tubulin (green fluorescence). DNA was counterstained with Hoechst 33258 (blue fluorescence). Bar: 40µm.

In comparison with control cells, after 48h of treatment, cells show alterations in Golgi apparatus morphology; in particular, after administration of PtAcacDMS, Golgi apparatus appears fragmented and dispersed in the cytoplasm with the loss of the particular semilunar shape, the cytoskeleton is collapsed and forming bundles determining alterations of the cell shape that lose their characteristic elongation. This alteration is less appreciable after stimulation of cells with CDDP in

which we can observe a partial reorganization in larger bundles (**Fig. 6**).
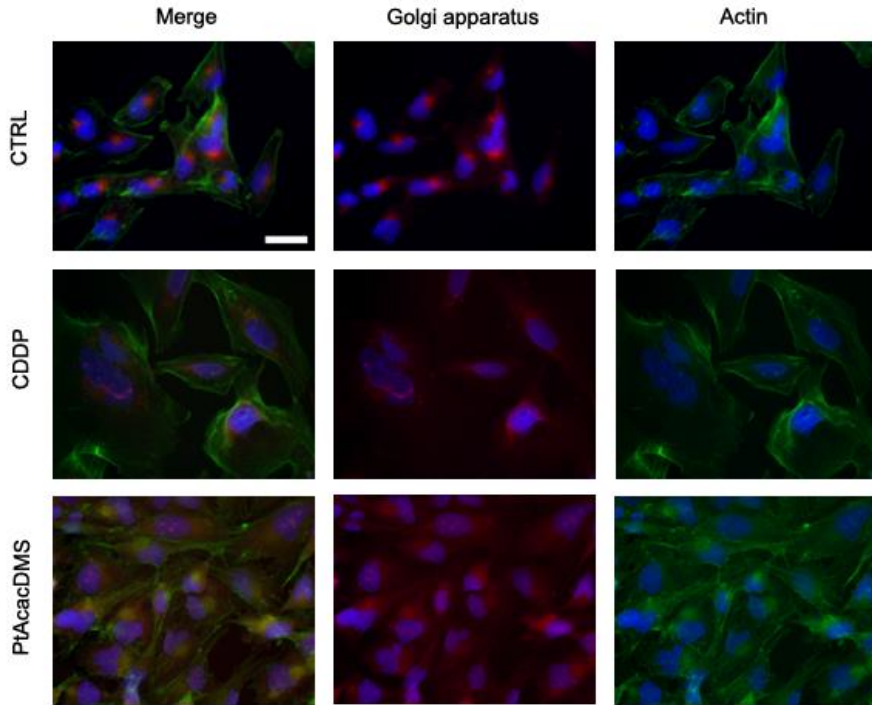


**Fig. 6** Immunocytochemical detection of Golgi apparatus (red fluorescence) and actinic cytoskeleton (green fluorescence). DNA was counterstained with Hoechst 33258 (blue fluorescence). Bar: 40µm.

Lysosomes are small membrane-enclosed organelles that contain a variety of enzymes (hydrolases) able to degrade different biological molecules, proteins, lipids nucleic acids, carbohydrates, but also other organelles. They represent the digestive system of the cell and play important role of different biological functions such as autophagy. In control cells lysosomes appear abundant and bigger with respect to drug treatment (**Fig. 7A**); in particular after administration of PtAcacDMS we can observe a halving of the amount of these organelles (**Fig. 7B**).

B
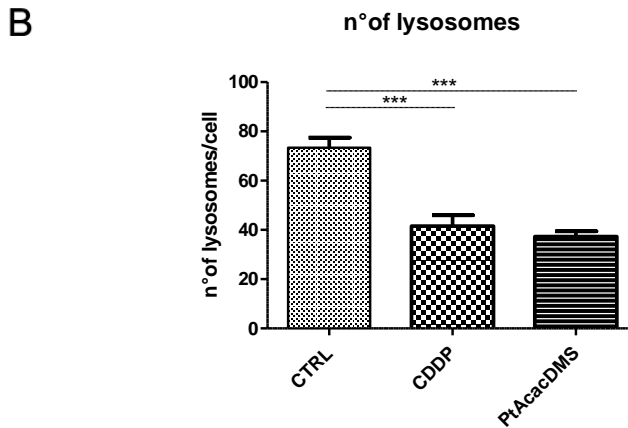
**n°of lysosomes**



**Fig. 7 A** Immunocytochemical detection of lysosomes (red fluorescence) and actinic cytoskeleton (green fluorescence). DNA was counterstained with Hoechst 33258 (blue fluorescence). Bar: 40µm. **B** Histogram with the number of lysosomes per cells.

## *Activation of intrinsic apoptotic pathway*

To evaluate if CDDP and PtAcacDMS are able to activate the intrinsic apoptotic pathway we evaluated the activation of Caspase 9 and Caspase 3. Caspase 9 is a major initiator of the apoptotic cascade and activates Caspase 3 through proteolytic cleavage. Compared to the control cells, after treatment for 48h with CDDP and PtAcacDMS, T98G cells show immunopositivity for both caspases; in particular, in cells where apoptosis is activated and morphologically visible, there is an increase of fluorescence (**Fig. 8A** and **9A**). Histograms in **Fig. 8B** and **9B** represent the percentage of fluorescence for control and treated cells for Caspase 9 and Caspase 3 respectively.

**Fig. 8 A** Immunocytochemical detection of Caspase 9 (red fluorescence) and actinic cytoskeleton (green fluorescence). DNA was counterstained with Hoechst 33258 (blue fluorescence). Bar: 40µm. **B** Hisogtam with the percentage of fluorescence in control and treated cells with CDDP and PtAcacDMS.
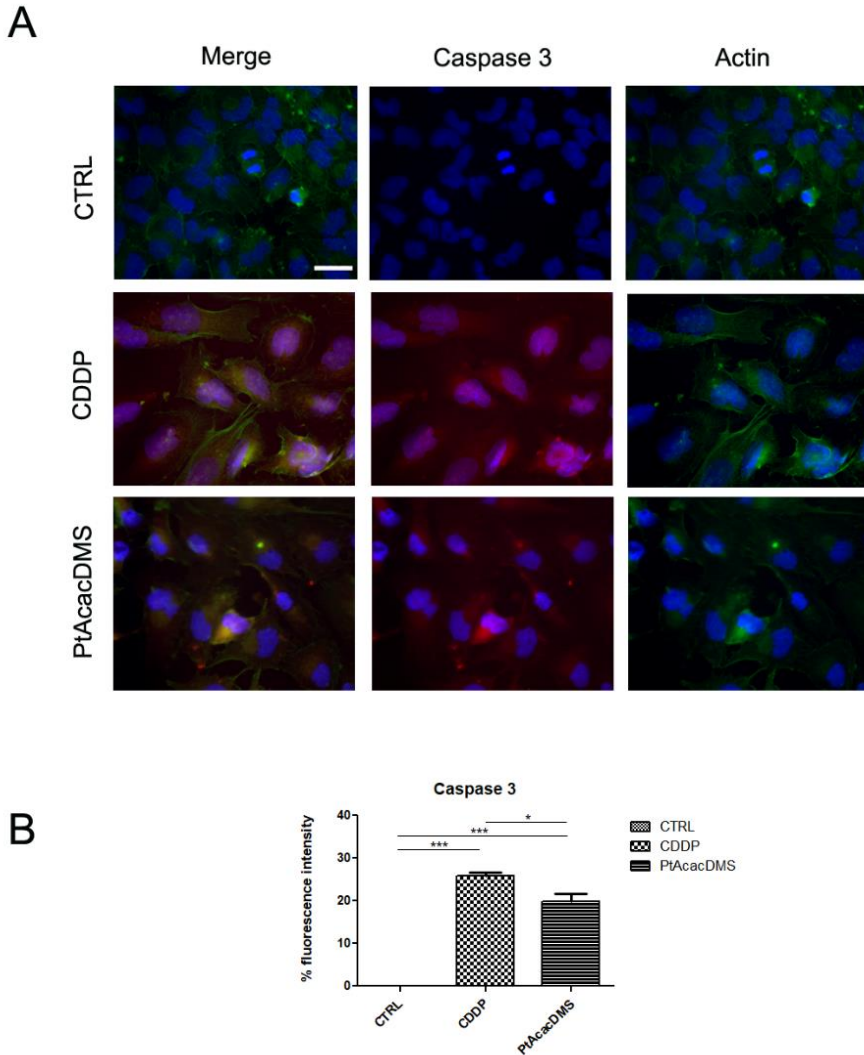
**Fig. 9 A** Immunocytochemical detection of Caspase 3 (red fluorescence) and actinic cytoskeleton (green fluorescence). DNA was counterstained with Hoechst 33258 (blue fluorescence). Bar: 40µm. **B** Histogram with the percentage of fluorescence in control and treated cells with CDDP and PtAcacDMS.

*Activation of extrinsic apoptosis pathway*

The trigger of extrinsic apoptosis pathway is puts in place by the death receptors and culminates with the activation of Caspase 8 by other caspases (such as Caspase 3 or Caspase 7), through proteolytic cleavage. After exposure to platinum compounds, T98G cells show high increase of activated Caspase 8, indicating that both CDDP and PtAcacDMS are able to trigger the two different pathways of apoptosis (**Fig. 10A** and **10B**), in particular PtAcacDMS seems to have a higher activation of extrinsic and intrinsic apoptosis pathway.

B
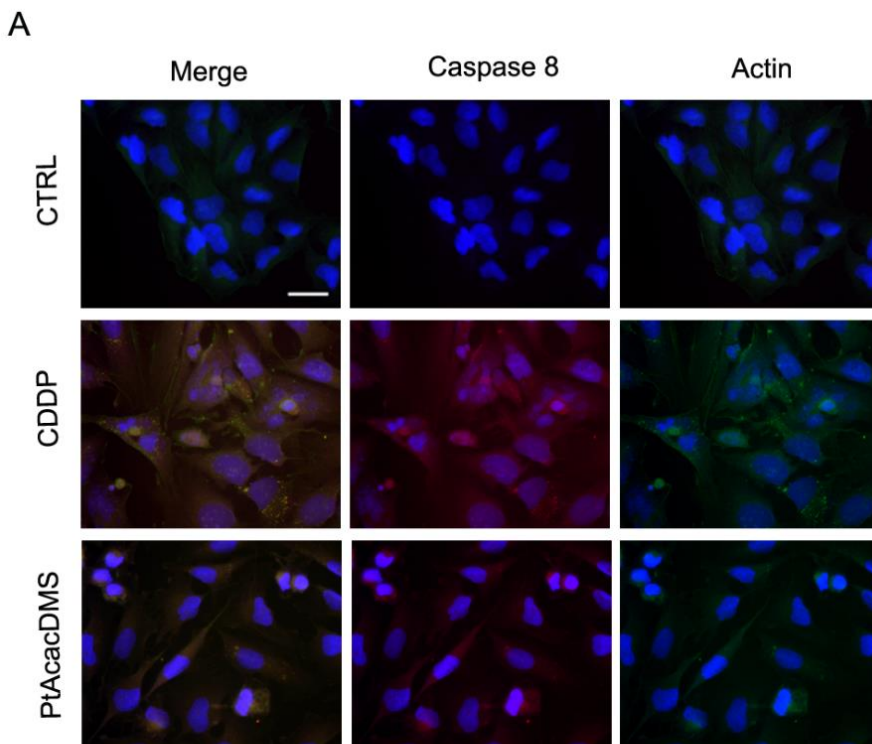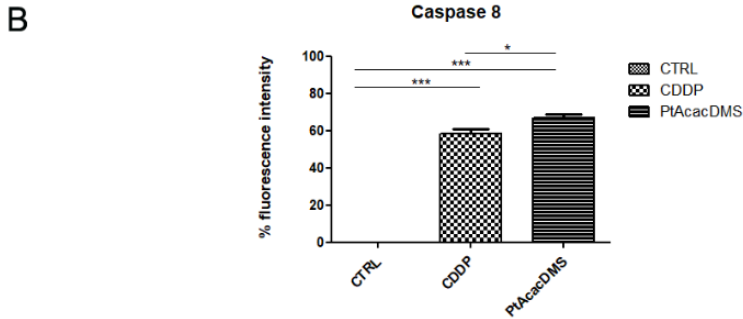


**Caspase 8**

**Fig. 10 A** Immunocytochemical detection of Caspase 8 (red fluorescence) and actinic cytoskeleton (green fluorescence). DNA was count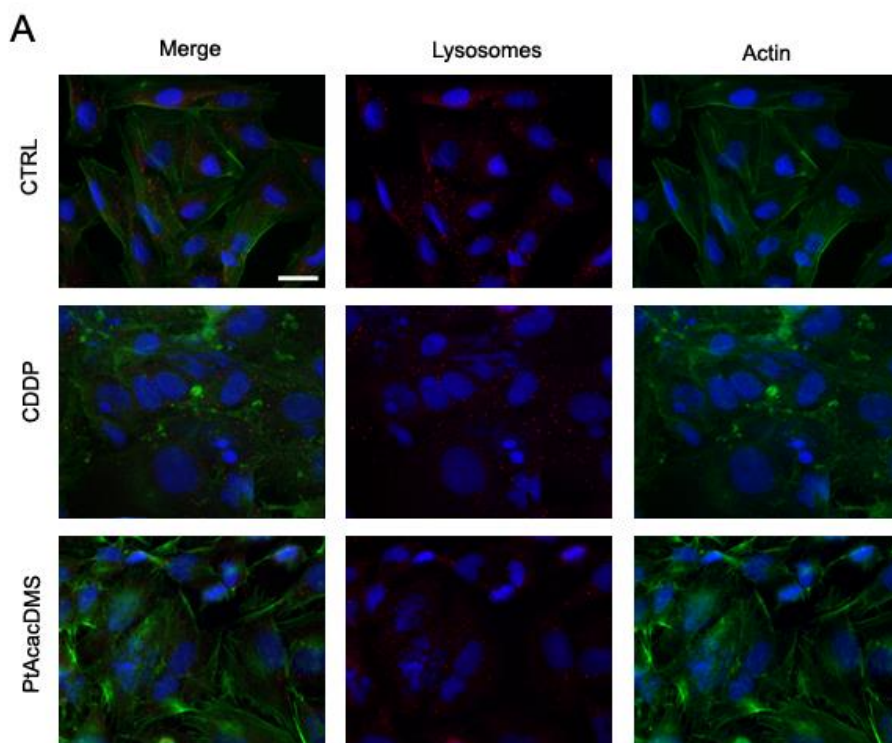erstained with Hoechst 33258 (blue fluorescence). Bar: 40µm. **B** Histogram with the percentage of fluorescence in control and treated cells with CDDP and PtAcacDMS.

## *Immunodetection of PARP-1*

Poly (ADP-ribose) polymerase-1 (PARP-1) is an enzyme involved in repair mechanisms of DNA damage, but also can directly induce apoptosis. In the cytosol PARP-1 is cleaved by Caspase 3 into two fragments: the 89 kDa fragment containing the catalytic site and the 24 kDa fragment containing the DNA binding site. In the nucleus, the 24 kDa fragment, missing the catalytic activity, is not able to trigger the DNA repair and cell undergoes death. The biggest fragment remains in the cytoplasm. In control cells, PARP-1 co-localizes with the nucleus. After 48h of treatment with CDDP and PtAcacDMS, PARP-1 is in the nucleus of early apoptotic cells while it is in the cytoplasm in late apoptosis: in this case it can possible to see the 89 kDa fragment, in the cytosol of cells showing a fragmented nucleus. Its presence is also

confirmed by analysis in Western Blotting in which only after treatment with CDDP and PtAcacDMS is present a second band (**Fig. 11**).
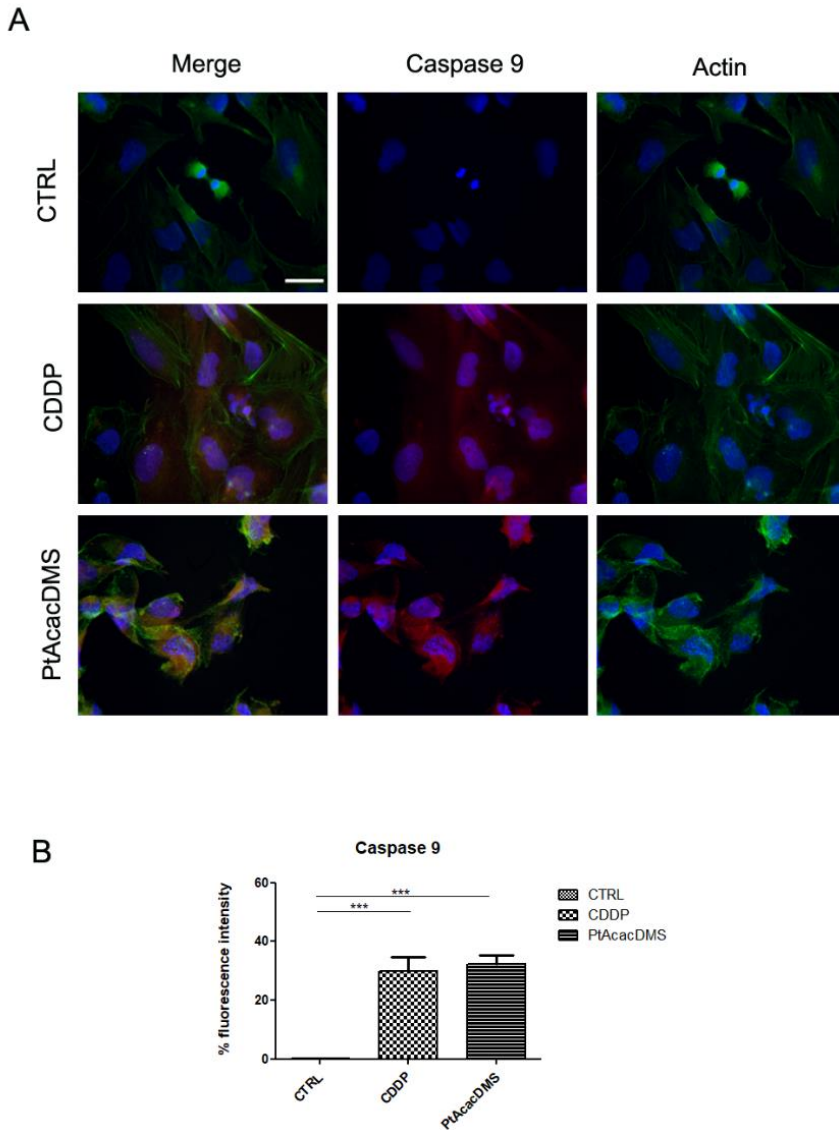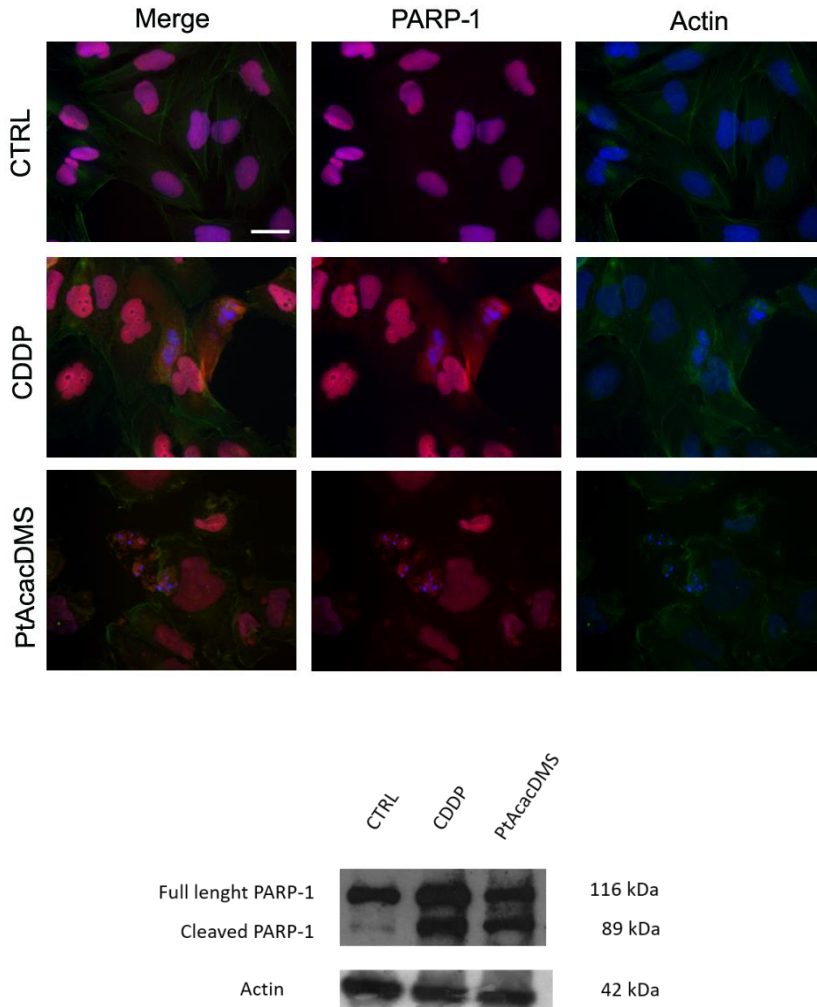


**Fig. 11** Immunocytochemical detection of PARP-1 (red fluorescence) and actinic cytoskeleton (green fluorescence). DNA was counterstained with Hoechst 33258 (blue fluorescence). Bar: 40µm. Below the Western Blotting reveals the presence of 89 kDa fragment.

*Immunoblotting of p62/SQSTM1*

p62/SQSTM1 is a marker of macroautophagy. As seen in **Fig. 3** the ultrastructural morphology has shown the presence of vacuoles in cells treated both with CDDP and PtAcacDMS, suggesting the possibility that cells put in place macroautophagy processes. Macroautophagy can be subdivided into different steps culminating in the formation of a double-membrane vesicle named autophagosome. Finally, autophagosome merges with the lysosomes, in which their acid hydrolases degrade the content of autophagosome, forming the so-called autophagolysosome. The cargo in the autophagosome is brought in by ubiquitination process and links by p62/SQSTM1 which contributes to transport of the cargo but it is also degraded with the cargo in the autophagolysosome (Glick D et al., 2010; Ohsumi Y, 2014).

Western Blot analysis shows a significative decrease of p62 in treated cells respect to control and in particular after administration of PtAcacDMS the decrease is higher respect to CDDP treatment (**Fig. 12**). These results agree with the ultrastructural morphology.
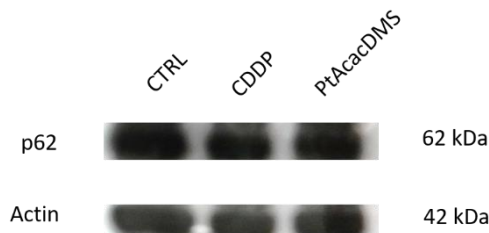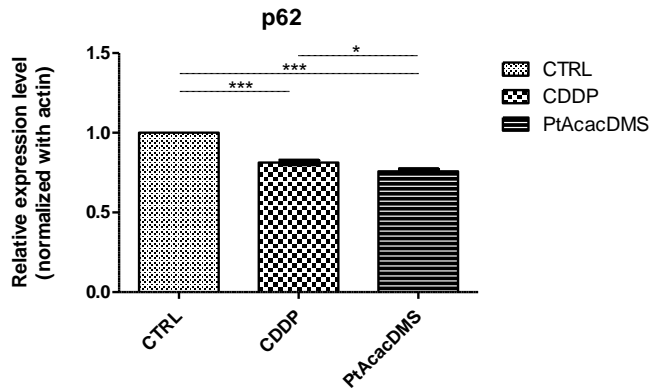
**Fig. 12** Western Blot analysis of p62.

*Immunocytochemical detection of histone methylation*

In this study three different histone modifications were analyzed in immunofluorescence to verify if CDDP and PtAcacDMS are able to alter the epigenetic of T98G. H4K20me3 is a marker of constitutive heterochromatin and its loss is associated to carcinogenesis (Bagnuykova TV et al., 2008), but it is also important for the development of tumors (Kwon MJ et al., 2010). H3K9me3 is an important epigenetic marker of heterochromatin and its modifications could become a predictable marker for different cancer injury (Füllgrabe J et al., 2011). Generally associated with constitutive heterochromatin, more recently it was demonstrated that H3K9me3 can collaborate with other histone modifications and trigger transcriptional repression (Zhang T et al., 2015). H3K27me3 is another marker of heterochromatin promoting the repression of transcription. It represents a prognostic factor in many type of tumors. In glioma it was

demonstrated that a decrease of H3K9me3 is associated with poor prognosis, while an increase in H3K27me3 is associated with a better prognosis (in terms of overall survival) (Maleszewska M and Kaminska B, 2015). Immunocytochemical reactions reveal an interesting presence of foci in cells stained with antibody anti H3K9me3 and H4K20me3, however the number of foci in tri-methylation of lysine 9 on histone 3 decrease in treated cells respect to control (**Fig. 13A** and **13B**), while it can be observed an increase of number of foci in tri-methylation of lysine 20 on histone 4 (**Fig. 14A** and **14B**). Furthermore for both the modifications, in particular for the H4K20me3, in cells treated with CDDP, but not with PtAcacDMS, an increase in fluorescence intensity is presents in nucleoli. Finally it can also be observed an increase of fluorescence for H3K27me3 and treated with both compounds respect to control, especially after administration of PtAcacDMS (**Fig. 15A** and **15B**).
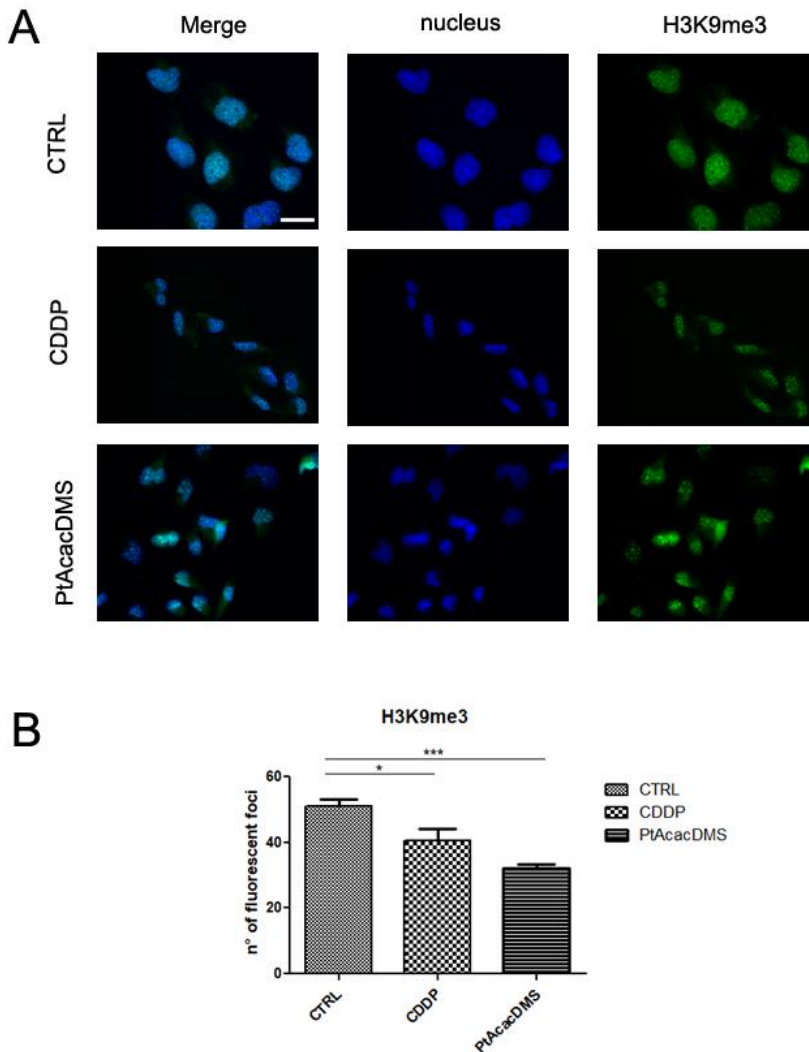
**Fig. 13 A** Immunocytochemical detection of H3K9me3 (green fluorescence) DNA was counterstained with Hoechst 33258 (blue fluorescence). Bar: 40µm. **B** Histogram with the number of fluorescence foci in control and treated cells with CDDP and PtAcacDMS.
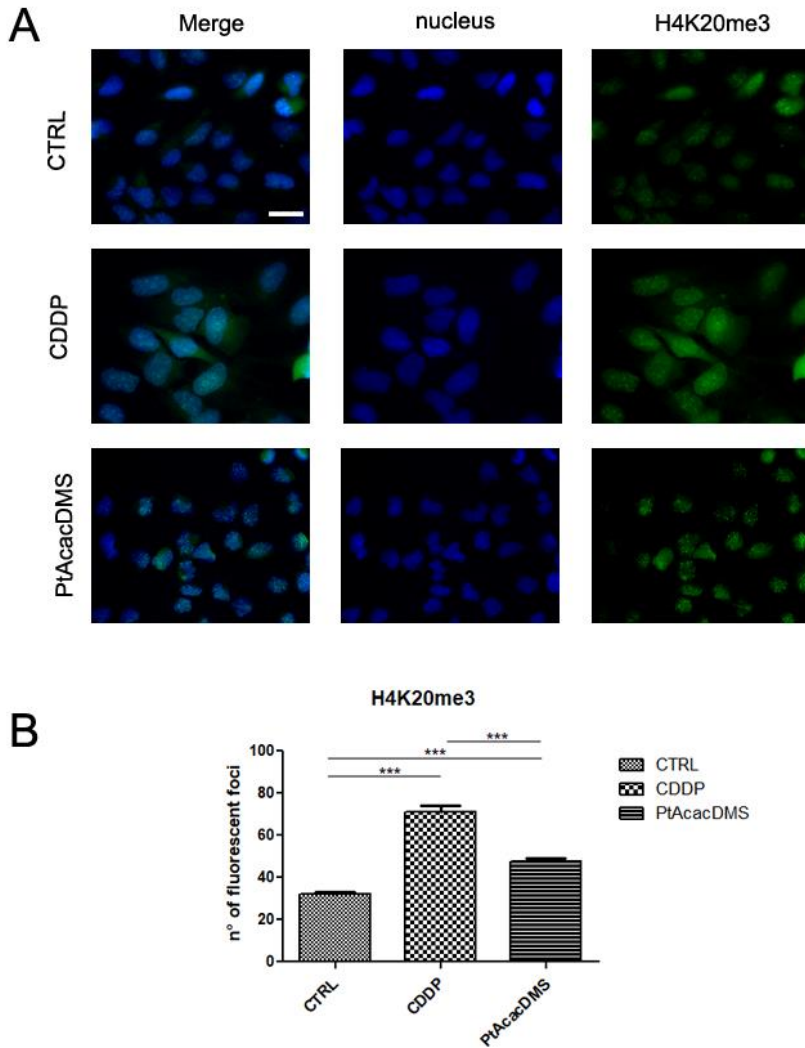
**Fig. 14 A** Immunocytochemical detection of H4K20me3 (green fluorescence) DNA was counterstained with Hoechst 33258 (blue fluorescence). Bar: 40μm. **B** Histogram with the number of fluorescence foci in control and treated cells with CDDP and PtAcacDMS.
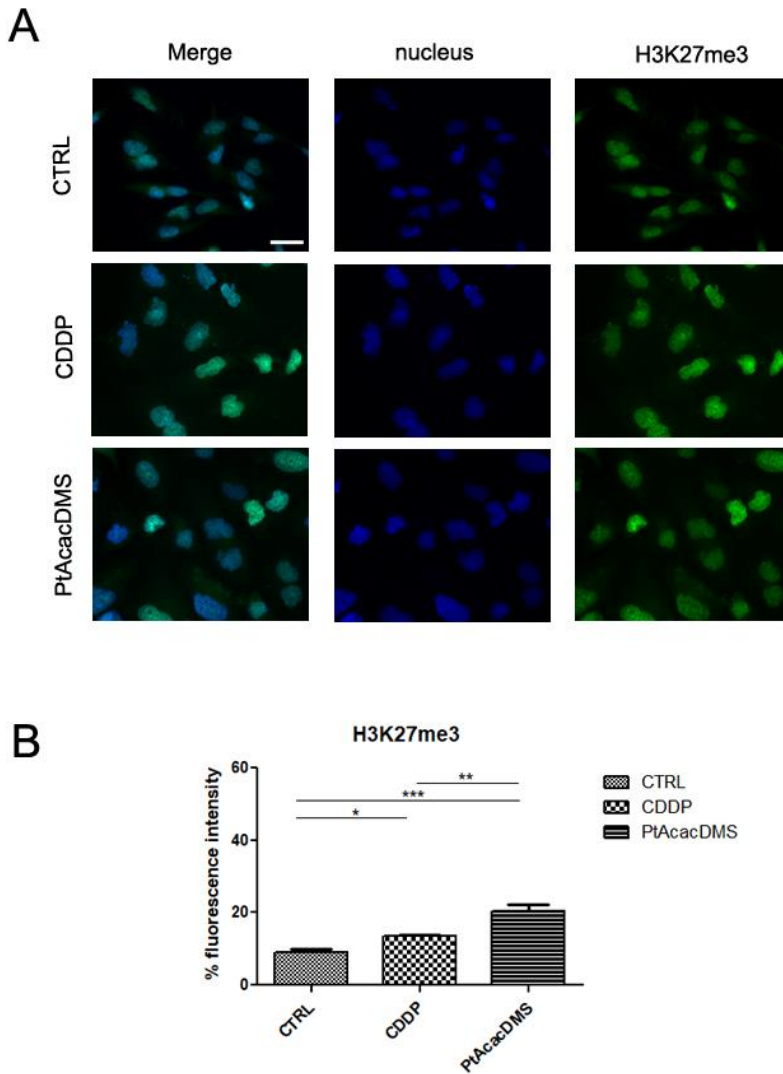
**Fig. 15 A** Immunocytochemical detection of H3K27me3 (green fluorescence)
DNA was counterstained with Hoechst 33258 (blue fluorescence). Bar: 40µm.
**B** Histogram with the number of fluorescence intensity in control and treated
cells with CDDP and PtAcacDMS.

*Calcium signaling in T98G cell line after treatment with platinum compounds*

The second messenger $Ca^{2+}$ plays important roles in biological system in physiology and pathological conditions, such as tumors. It is implicated in progression, proliferation, migration invasion and metastasis of the tumor cells, but also in death cells after exogenous perturbation, such as administration of antitumor drugs (Chen HH et al., 2013; Kerkhofs M et al., 2018; Morciano G et al., 2018). Intracellular $Ca^{2+}$ homeostasis depends of both calcium entry from the extracellular environment and its release from endogenous stores, such as the endoplasmic reticulum (Marchi S and Pinton P, 2016). To evaluate if CDDP and PtAcacDMS were able to induce cytotoxic calcium signals in T98G cells, we loaded the cells with the $Ca^{2+}$-sensitive fluorochrome, Fura-2, and then exposed them to CDDP or PtAcacDMS. As shown in **Fig. 16A** and **16B**, both compounds elicited a delayed, slow increase in $[Ca^{2+}]_i$ which reached a plateau at around 3000 sec after drug addition to the bath. Statistical analysis revealed that there was no difference in the percentage of cells responding to CDDP and PtAcacDMS (**Fig. 16C**), although PtAcacDMS elicited a significantly larger $Ca^{2+}$ signal compared to CDDP (**Fig. 16D**).
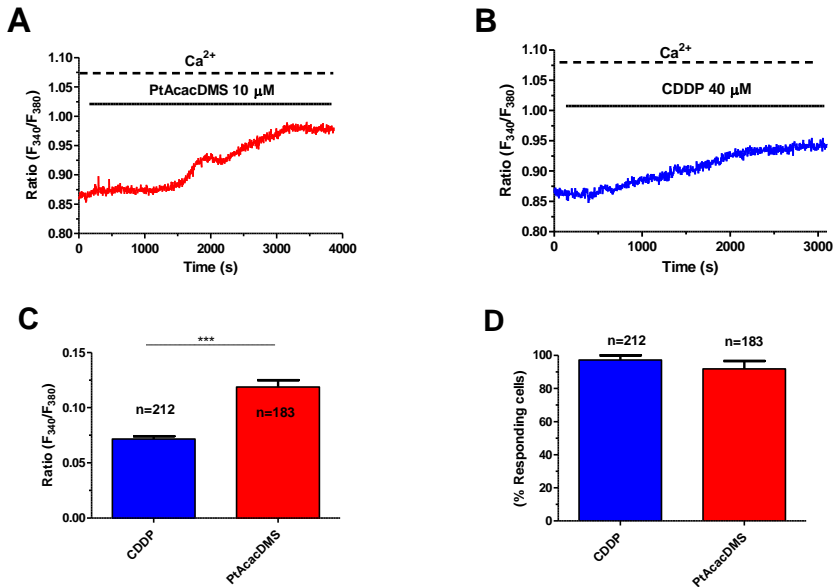
**Fig. 16** In **A** and **B** representative tracings of the $Ca^{2+}$ responses to PtAcacDMS and CDDP, respectively, showing that the acute addition of PtAcacDMS caused a larger increase in $[Ca^{2+}]_i$ as compared to CDDP. In **C** mean±SE of the percentage of T98G cells responding to PtAcacDMS and CDDP. In **D** mean±SE of the amplitude of the $Ca^{2+}$ signal induced by PtAcacDMS and CDDP in T98G cells.

In order to assess the source of the $Ca^{2+}$ response to platinum compounds, we challenged T98G cells with PtAcacDMS and CDDP in the absence of extracellular $Ca^{2+}$ ($0Ca^{2+}$). As shown in **Fig. 17A** and **17B**, neither of these drugs to increase the $[Ca^{2+}]_i$ under $0Ca^{2+}$ conditions, when only endogenous $Ca^{2+}$ release may occur. Conversely, restoration of extracellular $Ca^{2+}$ immediately resumed the $Ca^{2+}$ response to both PtAcacDMS and CDDP. As expected, PtAcacDMS-

induced $Ca^{2+}$ entry was significantly higher as compared to CDDP (Fig. **17C**). Taken together, these findings demonstrate that PtAcacDMS and CDDP increase the $[Ca^{2+}]_i$ in T89G cells by inducing extracellular $Ca^{2+}$ entry.
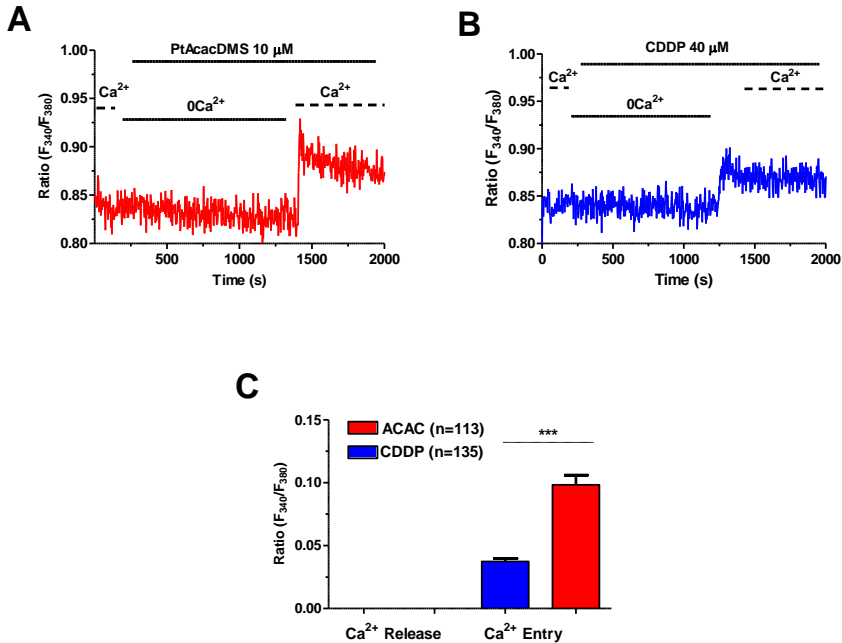


**Fig. 17** In **A** and **B** tracings of the $Ca^{2+}$ responses to PtAcacDMS and CDDP, respectively, in the absence (0 $Ca^{2+}$) and in the presence of extracellular $Ca^{2+}$. In **C** mean±SE of the amplitude of $Ca^{2+}$ release and $Ca^{2+}$ entry induced by PtAcacDMS and CDDP in T98G cells.

Extracellular $Ca^{2+}$ entry may dramatically interfere with intracellular $Ca^{2+}$ homeostasis by increasing resting $[Ca^{2+}]_i$ and loading the ER with $Ca^{2+}$ in a SERCA-dependent manner, thereby inducing apoptosis

(Pinton P et al., 2001; Xu Y et al., 2015). Therefore, we first evaluated basal $Ca^{2+}$ levels in T98G cells treated with PtAcacDMS and CDDP for 48 hours. As expected, resting $[Ca^{2+}]_i$ was significantly higher in T98G cells preincubated with PtAcacDMS compared to cells exposed to CDDP (**Fig. 18**).
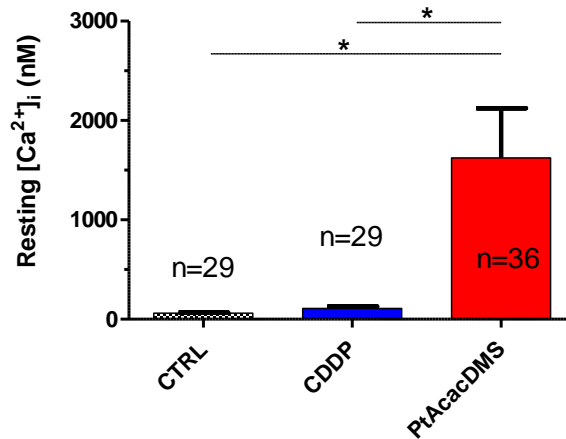


**Fig. 18** PtAcacDMS causes a larger increase in resting $[Ca^{2+}]_i$ as compared to CDDP in T98G cells after 48h of treatment.

To further evaluate whether platinum compounds affect ER $Ca^{2+}$ homeostasis after 48 hours of treatment, we exploited the so-called $Ca^{2+}$-addback protocol (Lodola F et al., 2012; Lodola F et al., 2017; Zuccolo E et al., 2016). Briefly, the cells were first bathed in the absence of extracellular $Ca^{2+}$ (0 $Ca^{2+}$) and then exposed to CPA (30 µM) to selectively block the SERCA activity. CPA prevents $Ca^{2+}$ sequestration into ER lumen and leads to a progressive $Ca^{2+}$ efflux through yet unidentified leakage channels, thereby depleting the ER

$Ca^{2+}$ pool. The ensuing increase in $[Ca^{2+}]_i$ is indicative of the amount of intraluminally stored $Ca^{2+}$ (Lodola et al., 2012; Lodola F et al., 2017, Zuccolo et al., 2016). After recovery of the initial elevation in $[Ca^{2+}]_i$ to the baseline, extracellular $Ca^{2+}$ was restituted to the perfusate to monitor SOCE amplitude. As shown in **Fig. 19**, CPA-induced ER $Ca^{2+}$ release and CPA-induced SOCE were significantly higher in T98G cells pre-incubated with PtAcacDMS and CDDP compared to control, i.e. not treated cells. However, there was no difference in the $Ca^{2+}$ response to CPA between PtAcacDMS and CDDP-treated cells. Taken together, these findings demonstrate that both resting $[Ca^{2+}]_i$ and ER $Ca^{2+}$ levels were significantly increased by platinum compounds, which is consistent with their cytotoxic effect. Moreover, the larger increase in resting $[Ca^{2+}]_i$ induced by PtAcacDMS could explain why this platinum derivative is more powerful than CDDP.
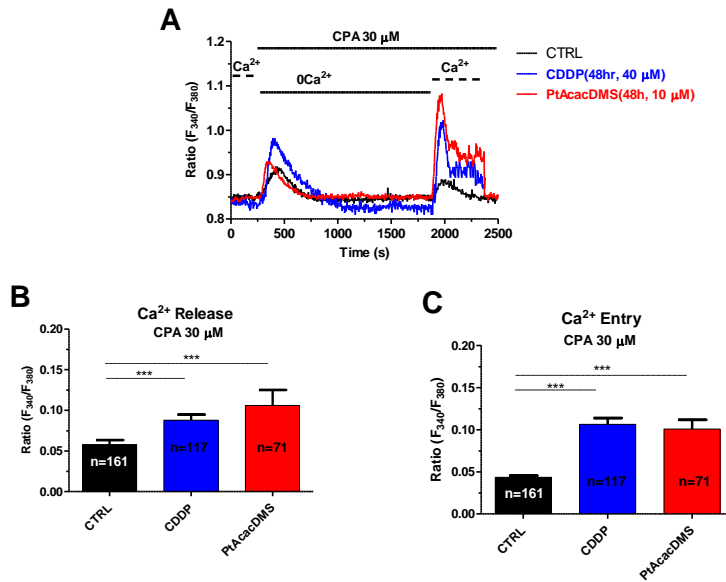
**Fig. 19 A** Representative tracing showing the $Ca^{2+}$ response to CPA after 48h treatment with CDDP and PtAcacDMS in absence (0 $Ca^{2+}$) and in presence of extracellular calcium. **B** mean±SE of CPA-induced ER $Ca^{2+}$ release under the designated treatments. **C** mean±SE of CPA-induced SOCE under the designated treatments.

***Regulation of calcium-binding proteins implicated in the modulation of $[Ca^{2+}]_i$***

*Calmodulin*

Calmodulin is a highly conserved, soluble intracellular protein and it is considered to be one of the major signal transducers of $Ca^{2+}$ signals in mammalian cells (Vetter SW and Leclerc E, 2003). Calmodulin is normally located in several cellular compartments including the cytosol, the membrane, the nucleus and several organelles. Recent studies in mammalian cells show that Calmodulin displays a dynamic localization during cell division, moving from the cytosol to the nucleus, attaching itself to the centrioles and the mitotic spindle during mitosis. Many proteins involved in $Ca^{2+}$ signal transduction alter their activity in response to changes in free $Ca^{2+}$ levels in the cell as they are able to bind calcium ions. $Ca^{2+}$ binds to the EF motif of Calmodulin and causes a conformational change allowing the $Ca^{2+}$/Calmodulin complex to bind specific "Calmodulin-binding" domains on target proteins some of which are implicated in the proliferation and migration of tumour cells (Berchtold MW and Villalobo A, 2014).

In T98G control cells Calmodulin is localized all around the nucleus and the morphology of cytoskeleton is well definite. After 48h of treatment with CDDP and PtAcacDMS we can observe changes in cell morphology, with presence of apoptotic nuclei and an increase of Calmodulin immunopositivity as highlighted in the box on the bottom left of the figure (**Fig**. **20**) Moreover cytoskeleton loses its structure and collapses.
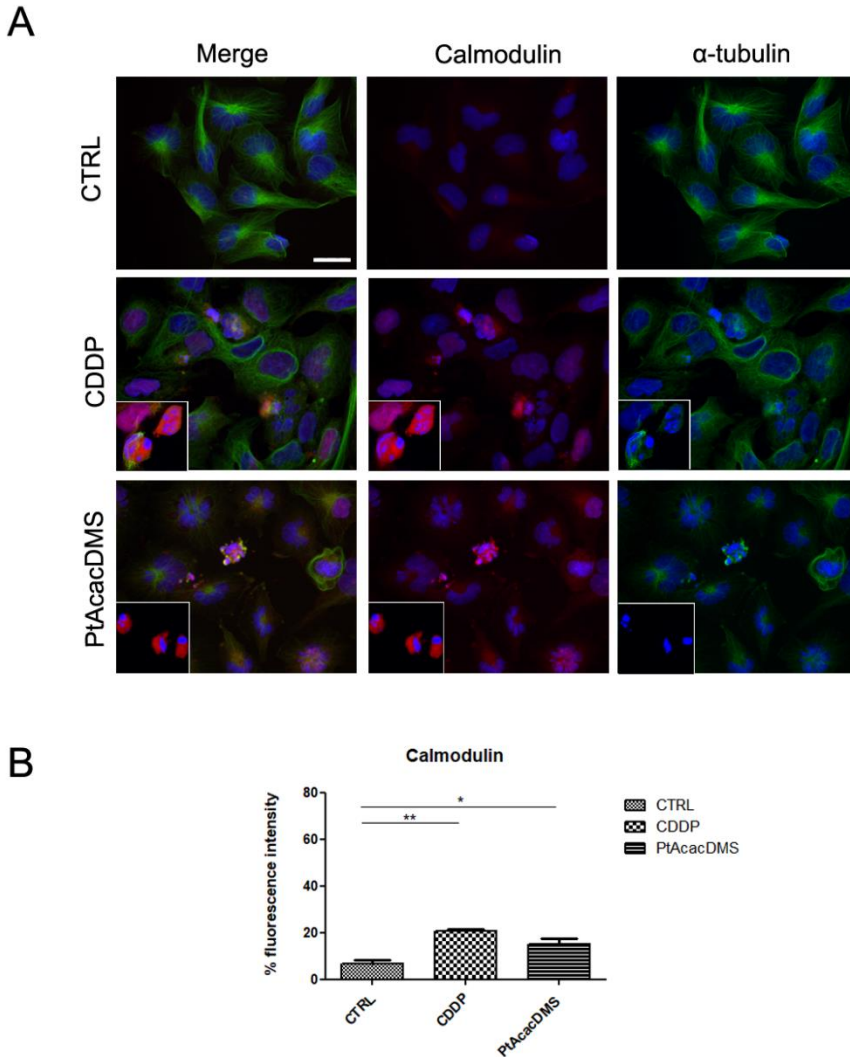
**Fig. 20 A** Immunocytochemical detection of Calmodulin (red fluorescence) and α-tubulin (green fluorescence). DNA was counterstained with Hoechst 33258 (blue fluorescence). Bar: 40µm. **B** Histogram with the percentage of fluorescence intensity in control and treated cells with CDDP and PtAcacDMS.

*Calretinin*

Calretinin (also called Calbindin 2) represents one of the members of hexa-EF-hand protein family. Their first 5 EF-hand domains are able to bind calcium ions, while the sixth one is inactive. In mesothelioma and in colon cancer cells Calretinin leads to apoptosis through activation of the Caspase 9-dependent pathway (Gander JC et al., 1996; Blum W and Schwaller B, 2013). High-level of Calretinin expression is detected in ductal carcinoma and is associated with poor overall survival (Taliano RJ et al., 2013). However, in other types of tumours, downregulation of the protein causes a $G_1$ arrest, this can trigger cell death (Shwaller B, 2013).

In T98G control cells Calretinin is distributed in all the cytoplasm. After 48h of CDDP, Calretinin remains localized in the perinuclear zone, but the actin cytoskeleton loses the morphology and collapses. After exposure to PtAcacDMS, Calretinin decreases its immunopositivity and appears less dispersed in the cytoplasm also in cells in evident phase of apoptosis (**Fig**. **21**).

**Fig. 21 A** Immunocytochemical detection of Calretinin (red fluorescence) and actin cytoskeleton (green fluorescence). DNA was counterstained with Hoechst 33258 (blue fluorescence). Bar: 40µm. **B** Graphic with the percentage of fluorescence intensity in control and treated cells with CDDP and PtAcacDMS.

*Calbindin*

Calbindin is a calcium-binding protein involved in the modulation of $Ca^{2+}$ homeostasis that control a wide range of cell activities including apoptosis. Calbindin interacts with several proteins localized in cytoplasm, intracellular membranes and in the nucleus (Schwaller B, 2010). In control condition, T98G cells present the standard shape, with actin organized in a regular morphology. Calbindin is localized in the cytoplasm. Cells treated with both compounds showed evident alterations: nuclei were fragmented, and the actin cytoskeleton collapsed. Calbindin increased immunopositivity in treated cells and after administration of PtAcacDMS seems to be localized also in the nuclei (**Fig. 22**).

*Parvalbumin*

Parvalbumin contains a $Ca^{2+}/Mg^{2+}$ mixed site (Schwaller B, 2010) and its structure and function are very similar to those of Calmodulin. In control cells Parvalbumin shows immunopositivity both in cytosol and in the nucleus. After treatment with both compounds, cells change their morphology, take on a rounded shape and protein decreases its fluorescence intensity only with PtAcacDMS. Furthermore, the protein localizes only in the cytoplasm of cells in evident stage of apoptosis (**Fig**. **23**).
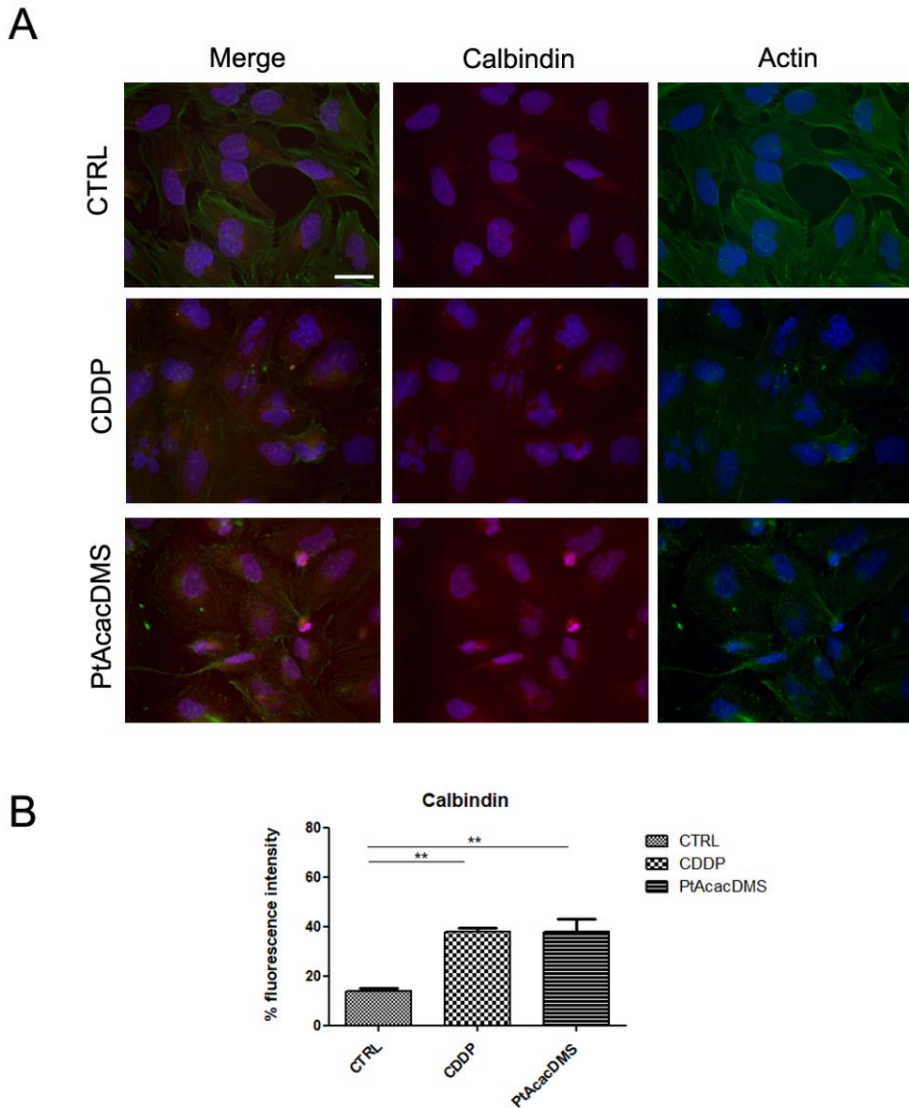
**Fig. 22 A** Immunocytochemical detection of Calbindin (red fluorescence) and α-tubulin (green fluorescence). DNA was counterstained with Hoechst 33258 (blue fluorescence). Bar: 40µm. **B** Histogram with the percentage of fluorescence intensity in control and treated cells with CDDP and PtAcacDMS.
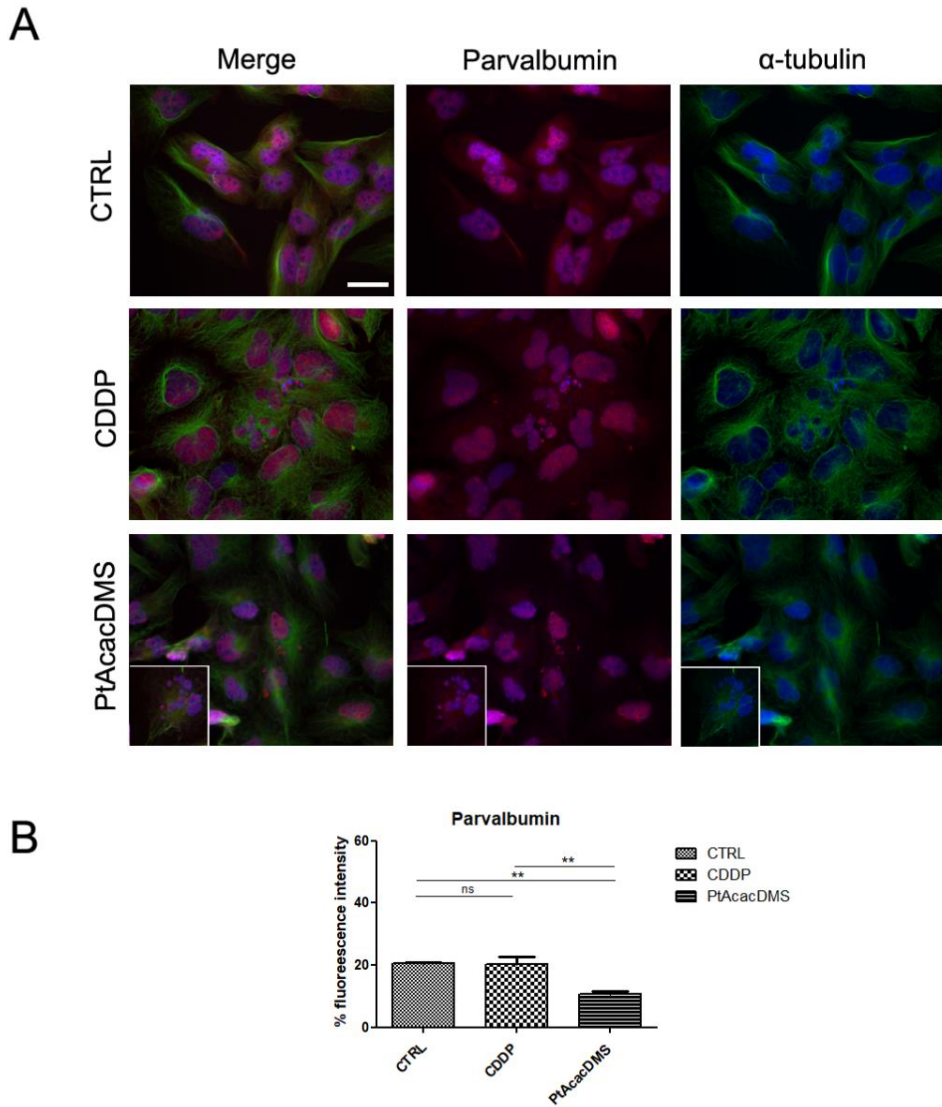
**Fig. 23 A** Immunocytochemical detection of Parvalbumin (red fluorescence) and α-tubulin (green fluorescence). DNA was counterstained with Hoechst 33258 (blue fluorescence). Bar: 40µm. **B** Histogram with the percentage of fluorescence intensity in control and treated cells with CDDP and PtAcacDMS.

## PMCA-1

PMCA-1 and its isoforms are important membrane proteins involved in maintaining the $Ca^{2+}$ gradient between the cytosol and the extracellular space (Di Leva F et al., 2008). PMCA-1 is a house-keeping gene expressed in almost of cells and its alteration is correlated to cancer lesions and to the differentiation stage of cancer cells (Padányi R et al., 2016). Indeed, in some type of cell lines transfected with SV-40 virus, it was demonstrated a down-regulation in protein expression and transcription of PMCA-1 and PMCA-4 (Reisner PD et al., 1997). Furthermore, PMCA-1 is downregulated in oral squamous cell carcinoma (Saito K et al., 2006).

In control T98G cells, PMCA-1 is localized in all the surface of the cells. Tubulin appears regular and cells show their characteristic shape. In cells treated with both platinum compounds, PMCA-1 seems to be lower expressed, especially in cells in evident stage of apoptosis with fragmented nuclei. Also in this case, as for the calcium buffering proteins, cytoskeleton collapses and cells loss their characteristic morphology. The statistical analysis of the percentage of fluorescent intensity confirms the significance of this down-regulation (**Fig. 24**).
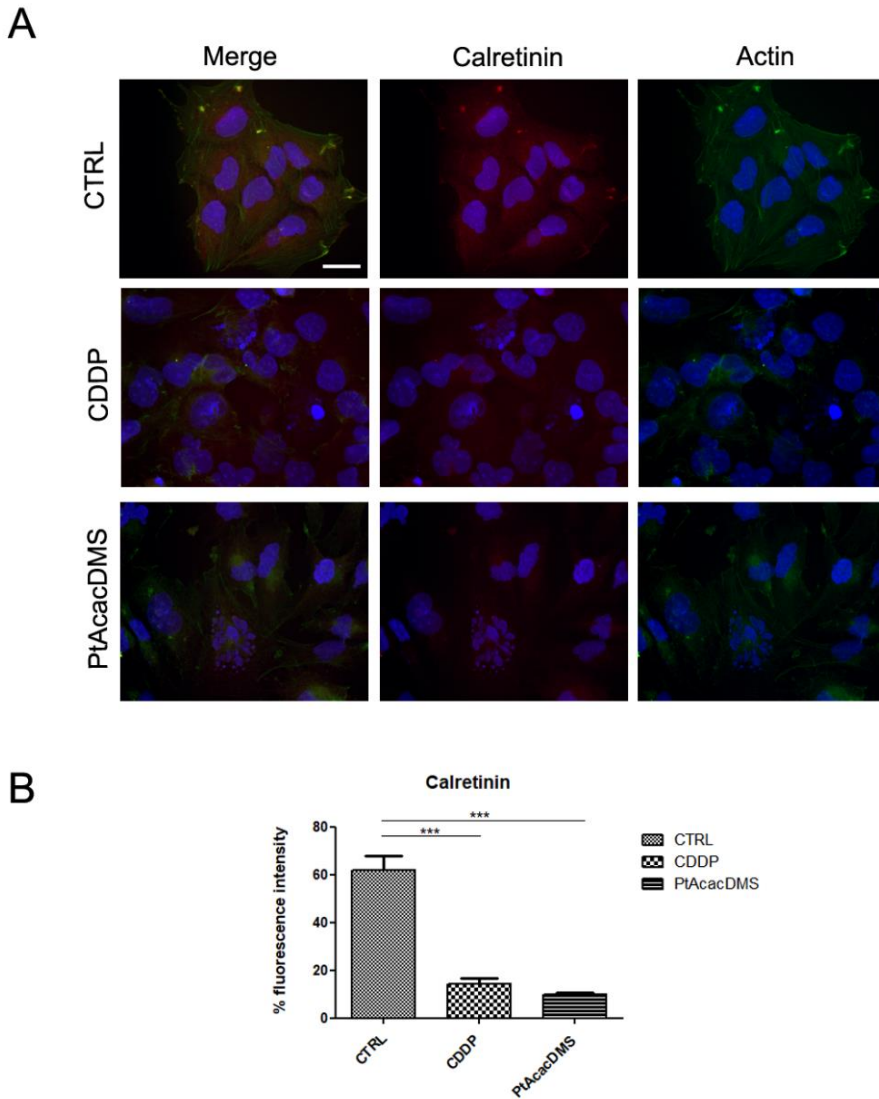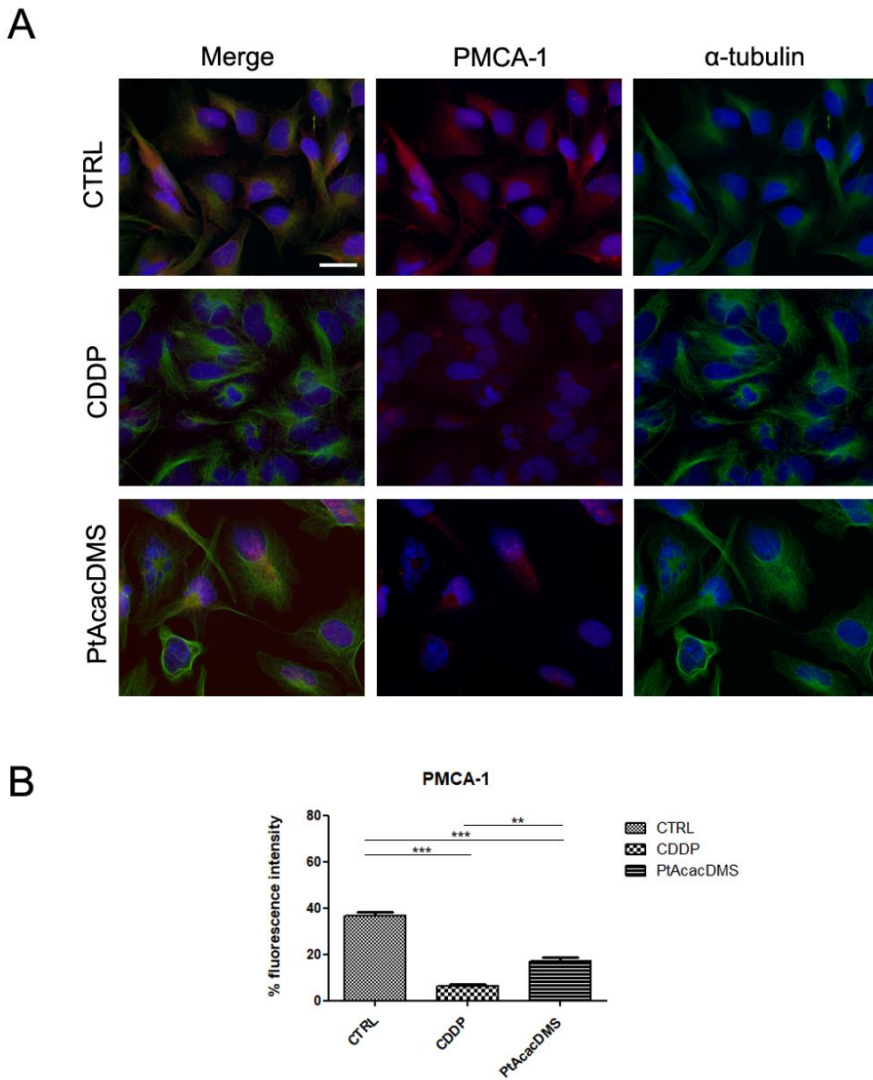
**Fig. 24 A** Immunocytochemical detection of PMCA-1 (red fluorescence) and α-tubulin (green fluorescence). DNA was counterstained with Hoechst 33258 (blue fluorescence). Bar: 40µm. **B** Histogram with the percentage of fluorescence intensity in control and treated cells with CDDP and PtAcacDMS.

## *Apoptotic markers in T98G cells grown in calcium-free medium*

To assess if the increase of $[Ca^{2+}]_i$ affects apoptosis, cells were grown in calcium-free medium; for this purpose BAPTA, a selective chelator of $Ca^{2+}$, was added to medium. Treatment with platinum compounds was performed after 24h and 48h; however, the combined action of BAPTA and platinum compounds after 48h of administration affects the analysis in immunofluorescence because a great amount of cells die and detach from the coverslip (data not shown). Thus, analysis of Caspase 3, involved in both pathway of apoptosis, was performed after 24h of treatment. In **Fig. 25A** and **B** immunofluorescence detection is shown.
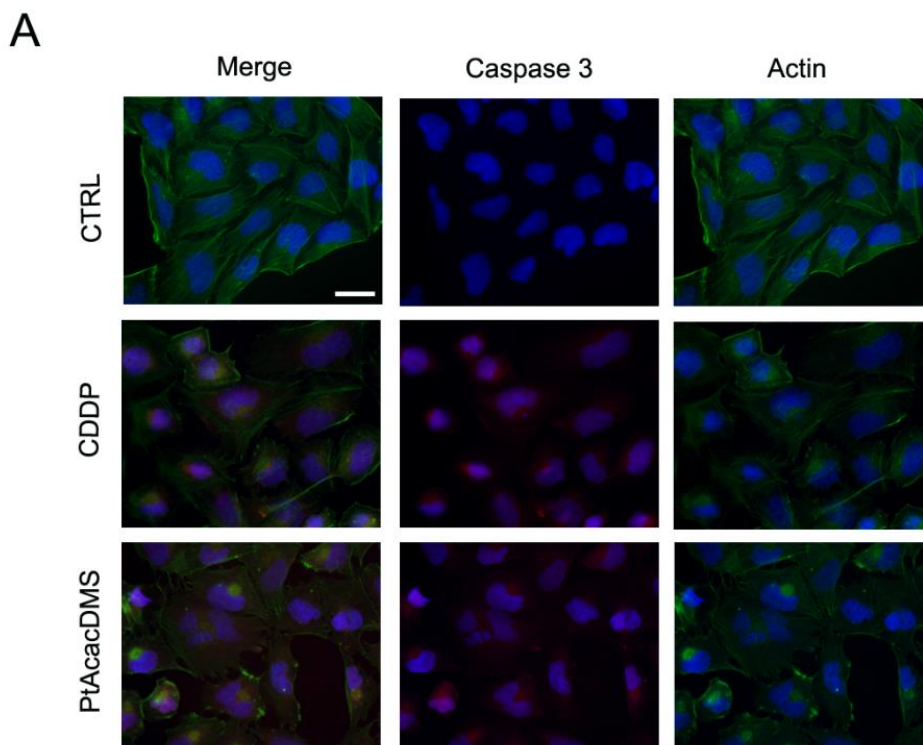
B
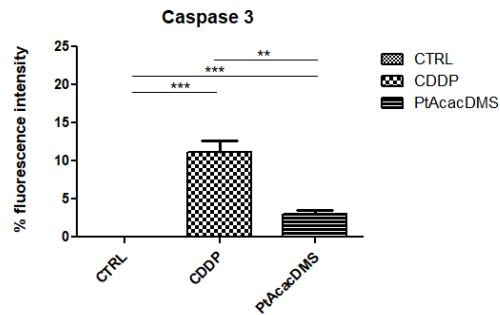


**Fig. 25 A** Immunocytochemical detection of Caspase 3 (red fluorescence) and actinic cytoskeleton (green fluorescence) in cells grown in calcium-free medium. DNA was counterstained with Hoechst 33258 (blue fluorescence). Bar: 40µm. **B** Histogram with the percentage of fluorescence in control and treated cells with CDDP and PtAcacDMS.

Then, to evaluate the effect of calcium in activation of Caspase 3 we analyzed the immunopositivity of the protein in T98G grown in presence and in absence of calcium. Interestingly, we can observe a significative decrease in immunopositivity in cells grown in calcium-free medium, especially after treatment with PtAcacDMS (**Fig. 26**). This very preliminary result can indicate an important role of $[Ca^{2+}]_i$ in the regulation of apoptosis.
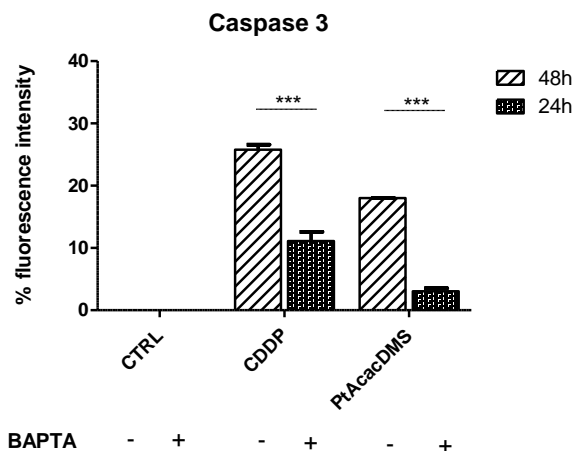
**Fig. 26** Histograms with the percentage of fluorescence in control and treated cells with CDDP and PtAcacDMS grown in presence or absence of calcium.

## *The role of oxidative stress in T98G*

The role of oxidative stress is strictly correlated with the increase of calcium because when the $[Ca^{2+}]_i$ increases, some proteases, such as caspases, are activated, leading to inhibition of PMCA-1 and induction of apoptosis (Pàszty K et al., 2007; Schwab BL et al., 2002). Furthermore, some evidences have shown that the production of ROS increases the cytotoxicity after administration of both CDDP and PtAcacDMS (Muscella A et al., 2011). Based on these premises, we decide to investigate if PtAcacDMS can induce changes to some markers of oxidative stress respect to CDDP.

*Nitrotyrosine*

Nitrotyrosine is an indicator of cell damage and inflammation and produce NO that can regulate some physiological functions, but it is also associated with pathological conditions such as rheumatoid arthritis and coeliac disease. Recently NO has been associated with epigenetic regulation altering the histones and DNA modifications and inhibiting the epigenetic enzymes (Socco S et al., 2017).

As aspect in the negative control degraded peroxynitrite prevent the formation of nitrotyrosine, while in the positive control peroxynitrite oxidizes sulfhydryls and modifies tyrosines to form 3-nitrotyrosine. In comparison with both control, after treatment with both compounds there is an increase of nitrotyrosine expression but not significative difference between CDDP and PtAcacDMS (**Fig. 27**).
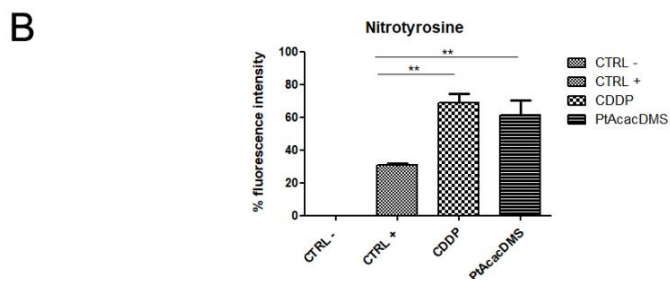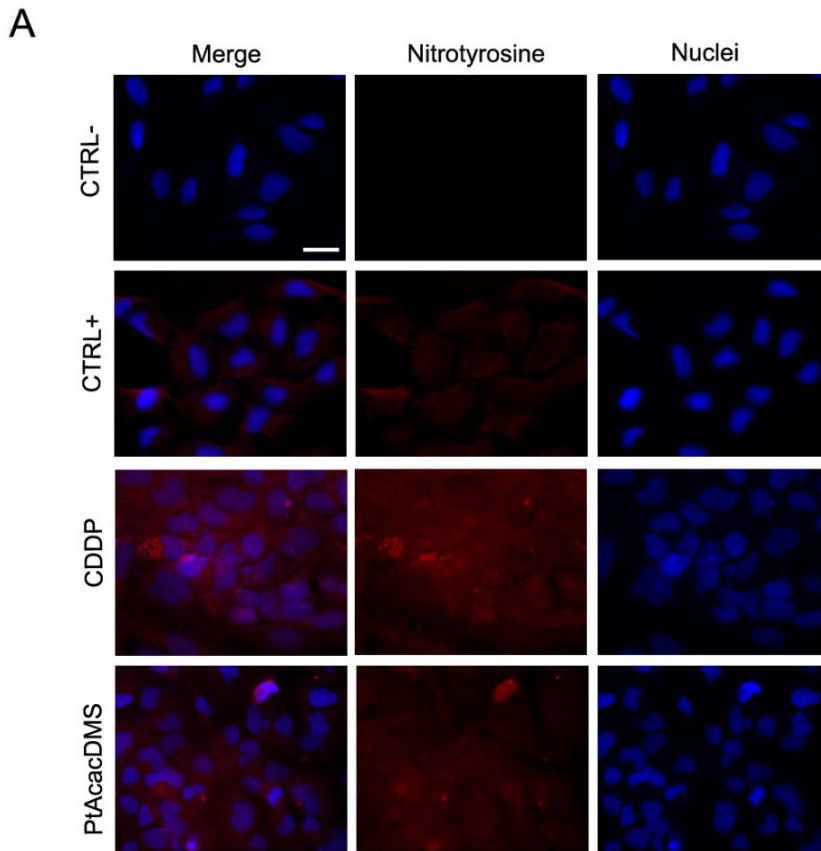
**Fig. 27 A** Immunocytochemical detection of nitrotyrosine (red fluorescence). DNA was counterstained with Hoechst 33258 (blue fluorescence). Bar: 40µm. **B** Histogram with the percentage of fluorescence intensity in control and treated cells with CDDP and PtAcacDMS.

*ROS*

In the cells, the equilibrium of reactive oxygen species must be guaranteed because ROS are very important for some function as signaling and protein regulation. The principal source of ROS production are mitochondria; therefore, if the function of mitochondria is altered, also the equilibrium of ROS is compromised. Also, in cancer ROS can alter the cancer phenotype, generate genetic instability with possible mutation at DNA level and alter the signaling network (Okon IS and Zou MH, 2016). ROS are also correlated with drug resistance. ROS are high reactivity increasing level of oxidative stress and therefore damage of the cells. ROS include superoxide anion ($O_2^-$), hydrogen peroxide ($H_2O_2$), hydroxil radical ($OH^-$), single oxygen ($^1O_2$) and ozone ($O_3$) (Sosa V et al., 2013) and these different isoforms can be interconverted from one form to another. Furthermore, also superoxide anion can form the reactive nitrogen species (RNS) and peroxynitrite ($ONOO^-$) following reaction with nitric oxide. (Okon IS and Zou MH, 2016).

As seen in **Fig. 28** in T98G control cells ROS are less expressed respect to control cells, in particular after administration of PtAcacDMS there is a significative increase in ROS expression respect to CDDP. PtAcacDMS seems to increase the oxidative stress as well as the level of calcium after 48h of treatment.
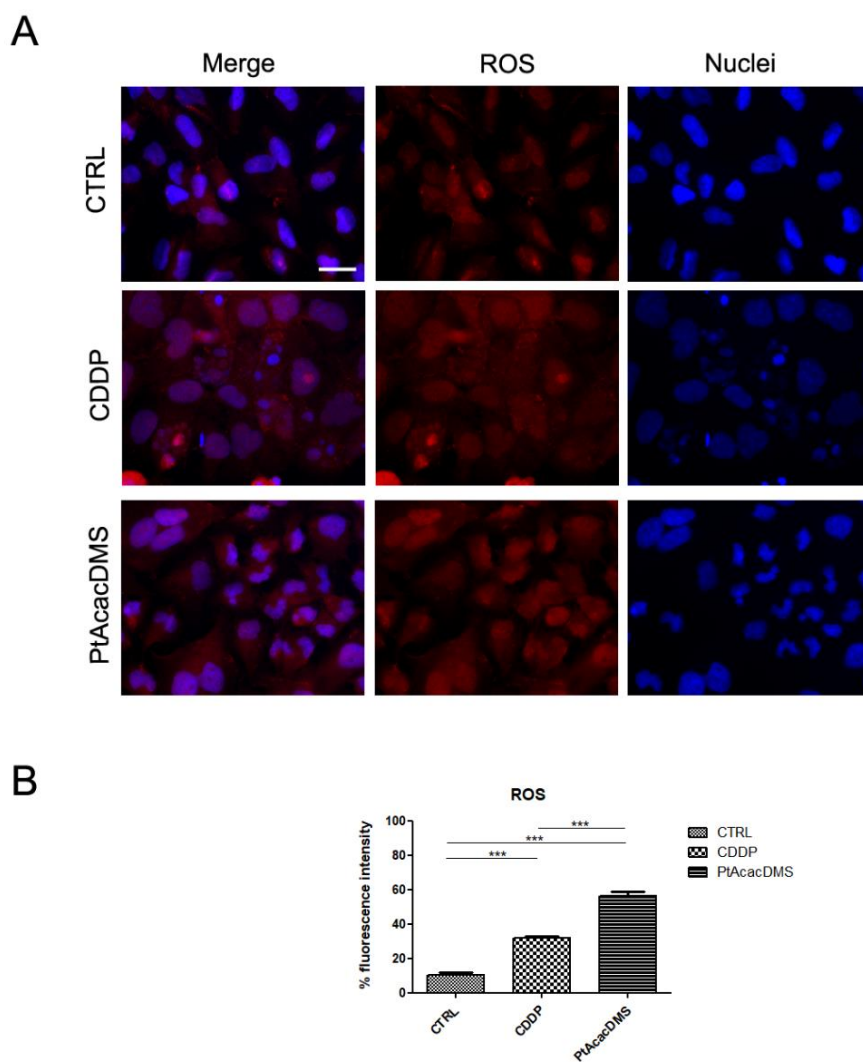
**Fig. 28 A** Immunocytochemical detection of ROS (red fluorescence). DNA was counterstained with Hoechst 33258 (blue fluorescence). Bar: 40µm. **B** Histogram with the percentage of fluorescence intensity in control and treated cells with CDDP and PtAcacDMS.

*NOS2*

NOS2 (also known as iNOS, inducible NOS), is one of the members of NOS family and the only one capable to produce NO in elevate quantity, determining a high cytotoxic effect on cells and tissues. Transcription of NOS2 is highly regulated: leukocytes, cytokines and other elements of the immune system participate to the regulation of expression of this protein (Thomas DD et al., 2016). In tumor cells NOS2 has a double effect: trough the production of NO, overexpression of NOS2 stimulates growth and proliferation of tumor and formation of metastasis, but in the microenvironment context is able to enhanced the immune system to defeat cancer (Vannini F et al., 2015). **Fig. 29** shows that NOS is localized both in nucleus and in cytoplasm and there is an increase in immunopositivity of NOS in treated cells respect to control, especially after PtAcacDMS administration, in which NOS is more expressed respect to Cisplatin.
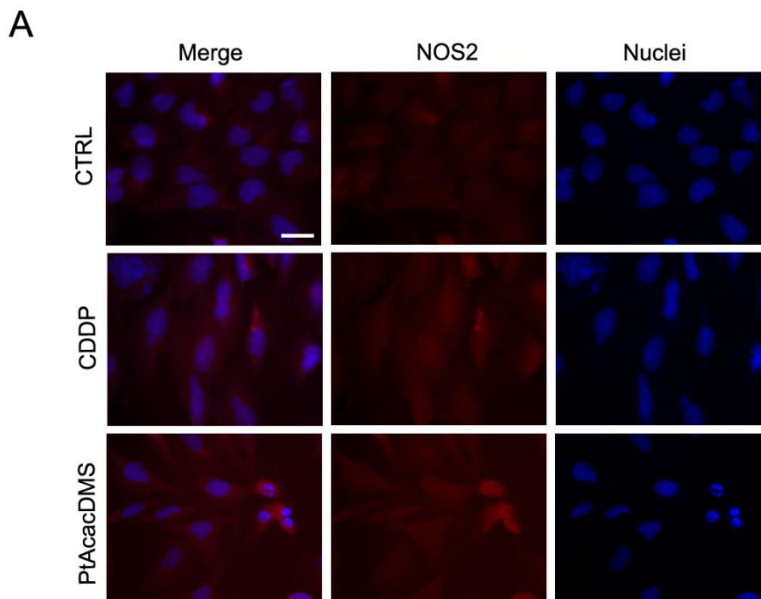
B
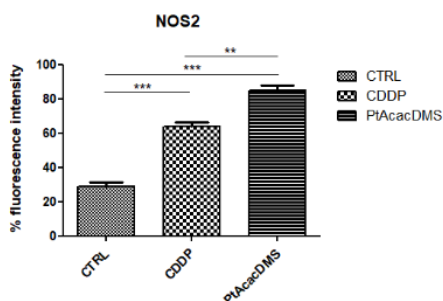


**Fig. 29 A** Immunocytochemical detection of NOS2 (red fluorescence). DNA was counterstained with Hoechst 33258 (blue fluorescence). Bar: 40µm. **B** Histogram with the percentage of fluorescence intensity in control and treated cells with CDDP and PtAcacDMS.

*SOD-1*

Compared to aforementioned markers of oxidative stress, SOD-1 acts as antioxidant, indeed it catalyzes the dismutation of $O_2^-$ into $H_2O_2$ which, in turn, is transformed in water by other enzymes, CAT (catalase) and GPx (glutathione peroxidase) (Halliwell, 2007; Pacher et al., 2007). Several evidences show that levels of SOD are generally low in tumor cells, therefore radiotherapy and chemotherapy aren't affected by the action of this protein (Yamaguchi S et al., 1994). In the cells SOD-1 is localized in cytosol. In T98G, SOD-1 shows a great immunopositivity in control cells, while in cells treated with the two platinum compounds the expression decrease greatly, without any differences between CDDP and PtAcacDMS as see in **Fig. 30**.
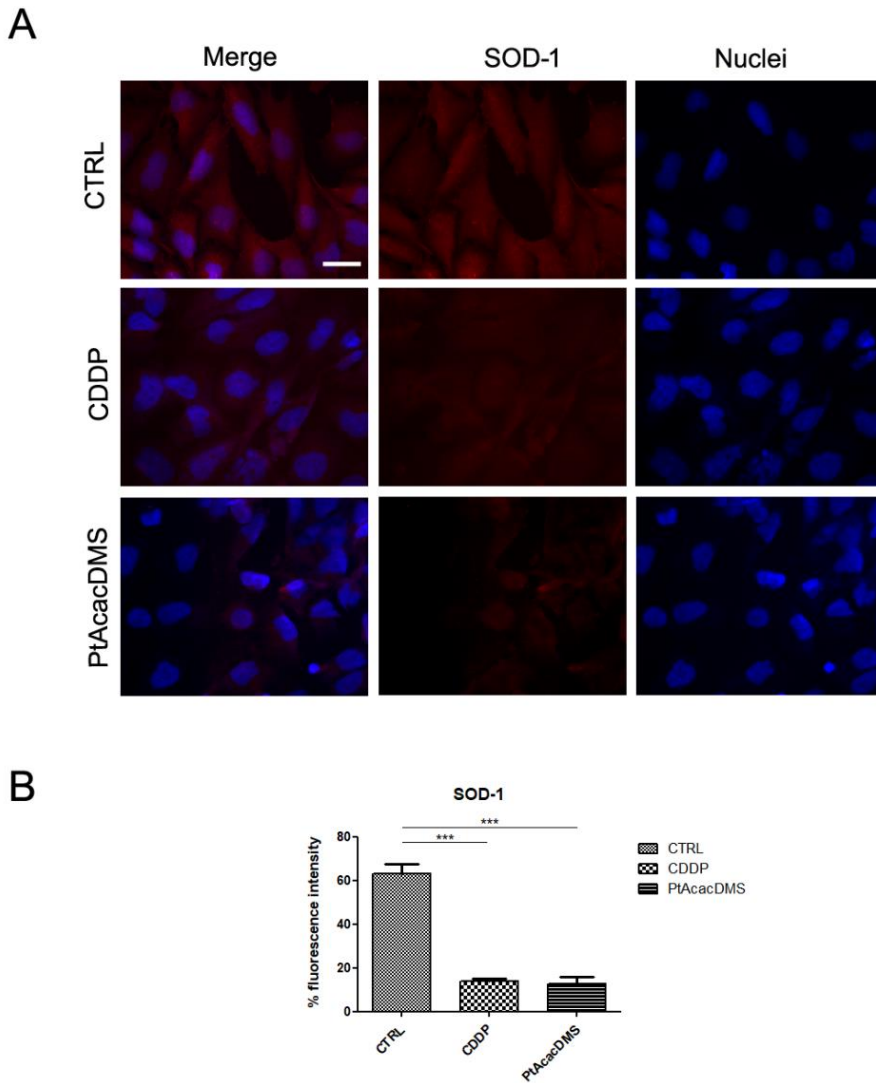
**Fig. 30 A** Immunocytochemical detection of SOD-1 (red fluorescence). DNA was counterstained with Hoechst 33258 (blue fluorescence). Bar: 40µm. **B** Histogram with the percentage of fluorescence intensity in control and treated cells with CDDP and PtAcacDMS.

# 4.2 Second part

***Flow cytometry to detect Cisplatin resistance***

Compared with parental, WT LLC cells, all resistant clones exhibited a reduced frequency of dying ($DiOC_6(3)^{low}PI^-$) and dead ($PI^+$) cells upon exposure to CDDP concentrations ranging from 5 to 50 μmol/L. All experiments were conducted in triplicates and independently repeated at least 3 times, yielding comparable results. Data were analyzed with Microsoft Excel and statistical significance was assessed by means of one-tailed Student t tests. *P*-values were considered significant when lower than 0.05 (**Fig. 1**).
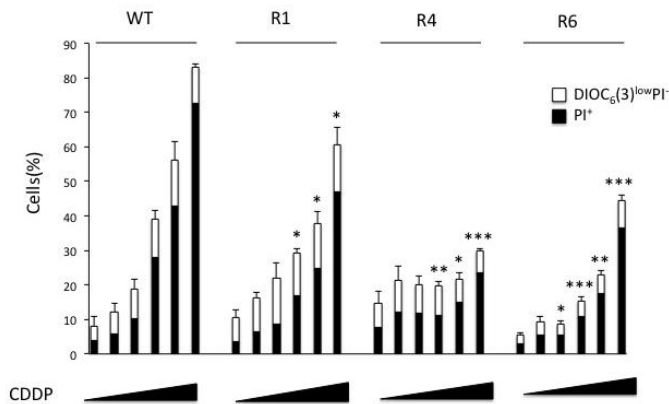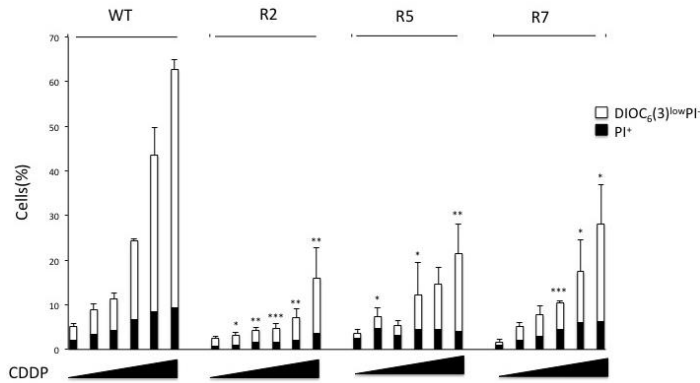
**Fig. 1** WT mouse NSCLC LLC cells and 6 CDDP-resistant derivatives (R) were maintained in control conditions or treated with increasing concentrations of CDDP (5, 10, 20, 30, and 50 μmol/L) for 48 hours. White and black columns illustrate the percentage of dying [DiOC$_6$(3)l$^{ow}$PI$^-$] and dead (PI$^+$) cells, respectively (means ± SEM, $n = 3$). *, P < 0.05; **, P < 0.01; ***, P < 0.001 (Student t test), compared with equally treated WT cells.

### *Immunodetection of PARylation*

For immunoblot analysis I have chosen 3 clones more CDDP-resistant: R2, R5 and R7. Each clone reveals an increase of PAR-containing proteins respect to WT: this result correlates with cytofluorimetric analysis (**Fig. 2**). Statistical significance was assessed by means of one-tailed Student's tests.
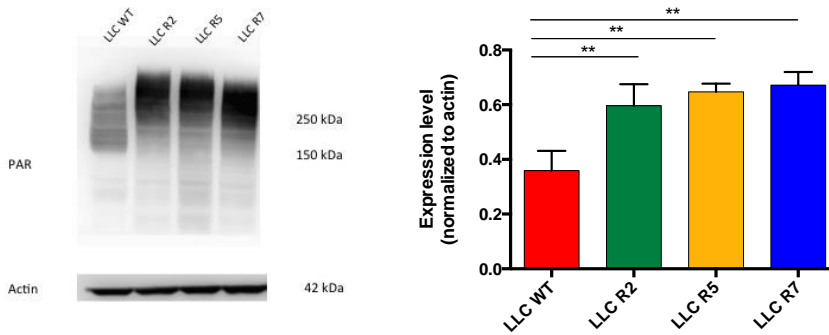
**Fig. 2** Representative immunoblot reveals PAR upregulation in CDDP resistant clones R2, R5 and R7 as compared to WT cells. Actin levels were monitored to ensure equal loading of lanes. $P < 0.05$; **, $P < 0.01$; ***, $P < 0.001$ (Student t test), compared with equally treated WT cells.

## Mice

Immunocompetent C57BL/6 female mice were maintained in pathogen-free conditions. In a first experiment, mice were subcutaneously grafted with 500000 parental LLC cell line (WT) or CDDP-resistant clones LLC cells (suspended in 200 µL PBS). Tumor growth was routinely monitored with a common caliper and tumor surface (A) was calculated according to the formula A= maximal diameter x minimal diameter. When tumors reached 10 mm$^2$ mice were sacrificed. As shown in **Fig. 3**, we found a significant heterogeneity of tumor growth as a function of the clones.
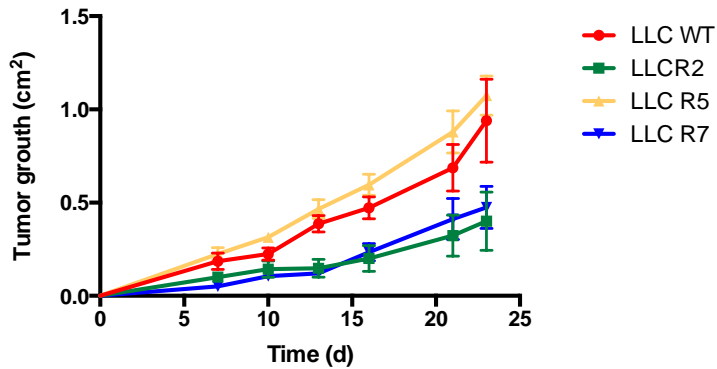
**Fig. 3**. Growth tumor in the first experiment, with injection of 500000 cells/mouse.

In order to obtain a more homogeneous growth allowing the simultaneous analysis of the immune infiltrate in all the tumors, we injected different amounts of cells based on the slopes of the tumor growth curves of the first experiment (**Table 1**). Finally, mice were sacrificed when tumors reached 1 cm$^2$. **Fig. 4** shows the growth curve of tumors at different days.

| Cell type | n° of cells injected |
|-----------|----------------------|
| LLC WT | 1080147 |
| LLC R2 | 2643004 |
| LLC R5 | 860081 |
| LLC R7 | 2366378 |

**Table 1** Amount of cells injected for WT murine LLC cells and their CDDP-resistant derivatives. The number of cells was calculated from slope ratio of growth curve of precedent experiments.
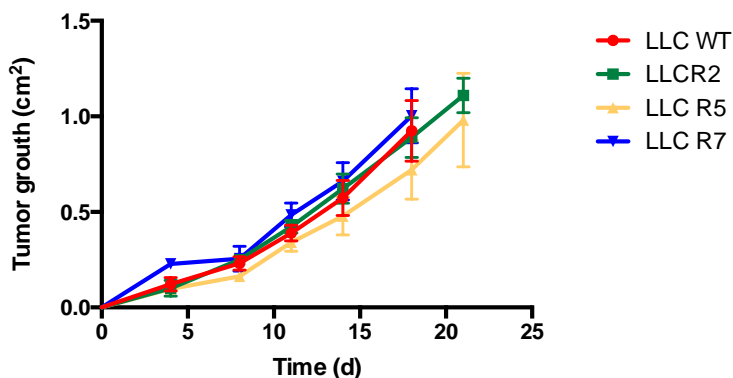


**Fig. 4** WT murine LLC cells and their CDDP-resistant derivatives were subcutaneously grafted in Immunocompetent C57BL/6 female mice (5 per group) and the tumor growth was routinely monitored with a standard caliper and is reported as means ± SEM.

*Analysis of different population of tumor infiltrate lymphocytes*

After mice were sacrificed, the tumor infiltrates were isolated as described in Material and methods and the different population separated by cytofluorimetry. Data are analyzed by the program Flow Jo and the following images (**Fig. 5** – **Fig. 9**) represent the results and statistical analysis to established if there are differences in tumor infiltrate lymphocytes populations between Cisplatin sensitive and resistant LLC cell line.
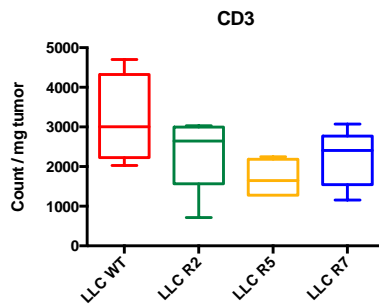


**Fig. 5** Amount of CD3+ lymphocytes normalized to tumor weight.
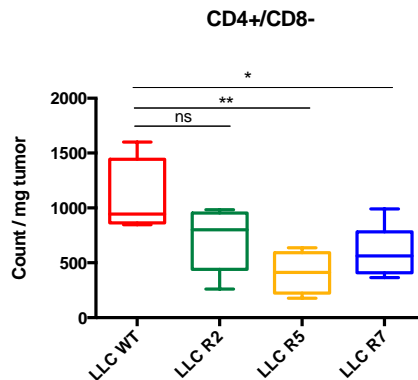


**Fig. 6** Amount of CD4+/CD8- lymphocytes into the CD3+ population normalized to tumor weight and the expression of transmembrane markers.
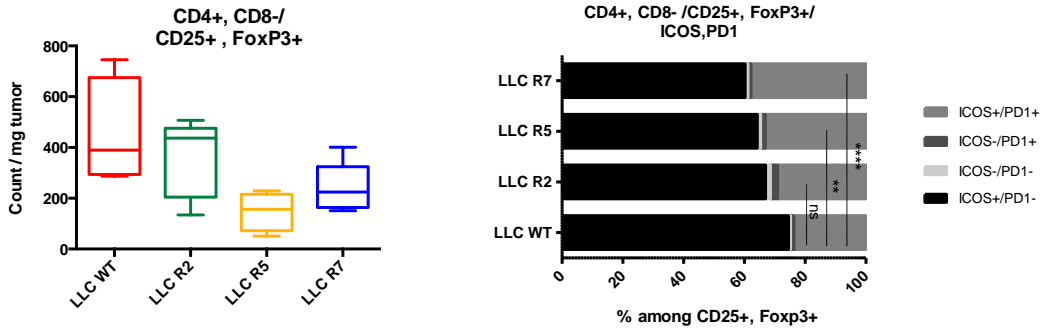
**Fig. 7** Amount of CD25+/FoxP3+ lymphocytes into the CD4+/CD8-population normalized to tumor weight and the expression of transmembrane marker ICOS and PD1. This population represents the lymphocytes T-reg.
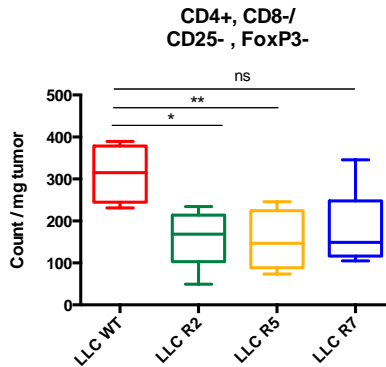


**Fig. 8** Amount of CD25-/FoxP3- lymphocytes into the CD4+/CD8-population normalized to tumor weight.
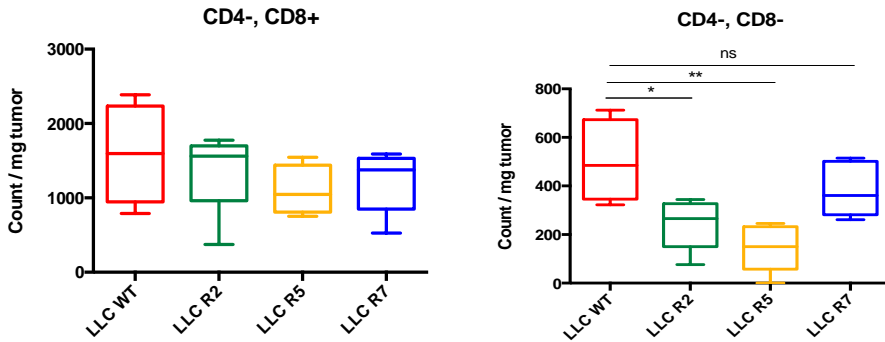
**Fig. 9** Amount of CD4-/CD8+ and CD4-/CD8- lymphocytes into the CD3+ population normalized to tumor weight.

## *Expression of PD-L1 in sensitive and resistant LLC cell lines*

Cytofluorimetric analysis revealed no differences between WT and CDDP-resistant LLC cell lines for PD-L1 transmembrane expression. All experiments were conducted in triplicates and independently repeated at least 3 times, yielding comparable results. Data were analyzed with Microsoft Excel considering the mean of fluorescence **(Fig. 10).**
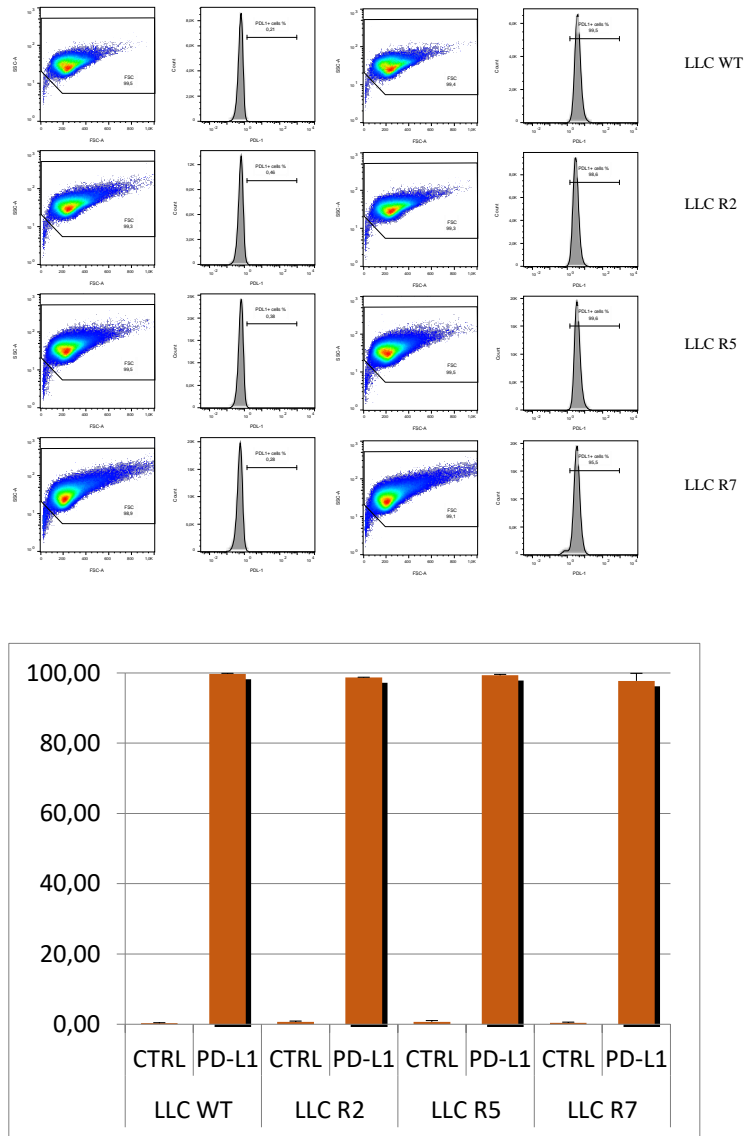
**Fig. 10** PD-L1 expression inn WT and CDDP resistant cell lines. Above a representative dot plot of gating strategy and below the quantitative data are shown.

## *Analysis of different population of tumor infiltrate myeloid cells*

After mice were sacrificed the tumor infiltrate were isolated as described in the chapter material and methods and the different population separated by cytofluorimetry. Data are analyzed by the program Flow Jo and the following images (**Fig. 11** – **Fig. 14)** represent the results and statistical analysis to established if there are differences in tumor infiltrate myeloid cells populations between Cisplatin sensitive and resistant LLC cell line.
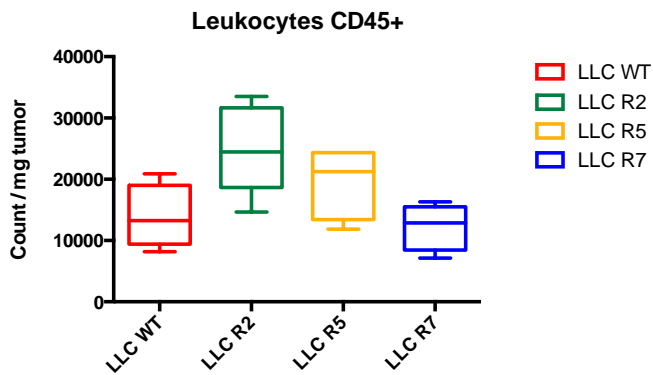


**Fig. 11** Amount of CD45+ leukocytes normalized to tumor weight.
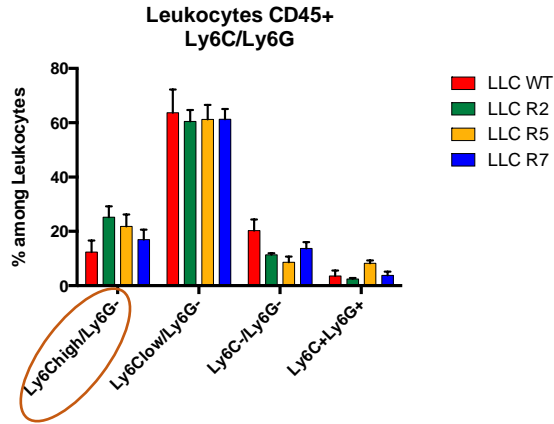
**Fig. 12** Amount of Ly6C/Ly6G leukocytes into the CD45+ population normalized to tumor weight. An interesting difference it shows for the Ly6Chigh/Ly6G- population.
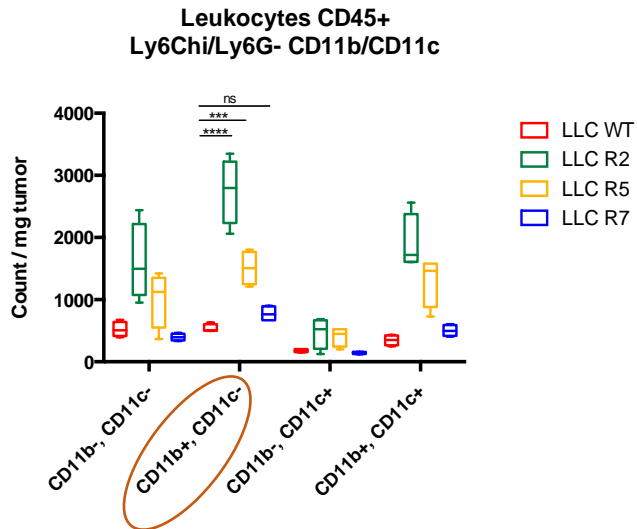


**Fig. 13** Amount of CD11b/CD11c leukocytes into the CD45+, Ly6Chigh/Ly6G- population normalized to tumor weight.
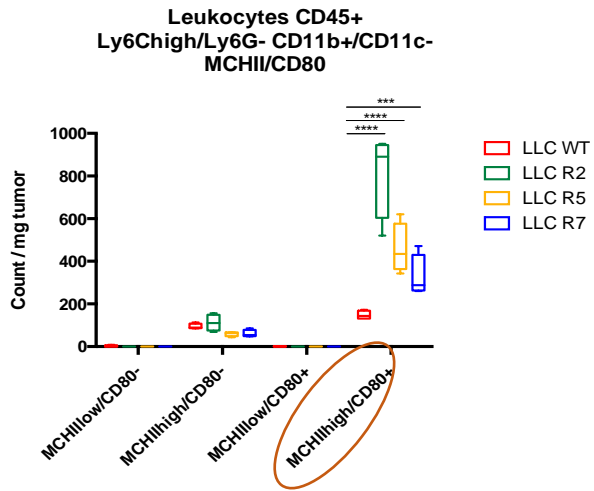
**Fig. 14** Amount of MHCII/CD80 leukocytes into the CD45+, Ly6Chigh/Ly6G-, CD11b+/CD11c- population normalized to tumor weight. An interesting difference it shows for the CD11b+/CD11c- population.

# 5. DISCUSSION

The aim of this research was to study alternative strategies to overcome the phenomena of toxicity and resistance trigger by tumour cells after administration of Cisplatin, that affects its use in clinical settings. In particular, in this work, two strategies were investigated: 1) the use of an alternative platinum compound, named Pt(O,O'-acac)(γ-acac)(DMS)], considering its activity and mechanism of action versus Cisplatin and 2) the study of new mechanisms of resistance linked to a different immune response between Cisplatin sensitive and resistant tumour cells.

For the first strategy we used human glioblastoma T98G tumour cells. In agreement with data previously obtained from our laboratory, (Grimaldi M, 2015, PhD thesis), after administration of two platinum compounds, we can observe an increase in apoptotic and necrotic cells, in particular after administration of PtAcacDMS. The new compound acts at a concentration four-fold lower respect to CDDP; this indicate an increased toxicity in human tumour cells and a possible lower systemic toxicity. Apoptotic events were analysed through different parameters. First of all, the analysis of mitochondrial membrane potential with JC-1, an important indicator of mitochondria function and cell health. The analysis reveals a higher presence of green fluorescent monomer after administration of PtAcacDMS, indicating a greater depolarization of mitochondrial membrane, probably due to the opening of MPTP and release of ions and molecules that affect the respiratory chain and other factor implicated in the molecular mechanisms of apoptosis. The increase of MOMP indeed is a crucial

event of the apoptosis intrinsic pathway. The release of pro-apoptotic factors and the inhibition of anti-apoptotic factors culminating in the activation of Caspase 9 that, in turn, activates Caspase 3, the principal effector of apoptosis. In T98G there is an evident increase of these caspases after treatment with both compounds, in particular after administration of PtAcacDMS, Caspase 3 is more expressed with than after CDDP treatment, reflecting the higher increase in mitochondrial membrane depolarisation. To confirm the activation of the intrinsic pathway we analysed the expression of PARP-1, one of the principal target of Caspase 3. In control cells, PARP-1 is normally localized in the nucleus. After activation of Caspase 3, PARP-1 is translocated in the cytoplasm where is cleaved in two fragments: the 89 kDa fragment, which contain the catalytic domain, remains in the cytosol, the 24 kDa fragment, in the nucleus, is not able to trigger the DNA repair. Inactivation of PARP-1 is important for activation of apoptosis: indeed, its inactivation prevents an excessive loss of energy, necessary for DNA repair mechanisms. This energy is important to trigger the apoptotic process: indeed, the over-expression of PARP-1 favours the depletion of ATP, and tumour cells dead *via* necrosis rather than apoptosis. PARP-1 represents therefore a molecular switch between different type of cell death (Fischer U et al., 2003). Cisplatin and other chemotherapeutic agents can trigger also the extrinsic pathway of apoptosis which is promoted by the activation of Caspase 8 and then Caspase 3 or Caspase 7. Indeed, evidences show that Cisplatin can activate the CD95 receptor/ligand system, upregulate both receptor and ligand CD95L, through transcriptional factors (such as Nf-kB) able to

link to the promoter of genes and trigger the transcription. Also p53 has a similar role promoting the overexpression of CD95 by linking on the first intron of the gene after chemotherapeutical treatment. Furthermore, the antibody antagonist of CD95L inhibit the apoptosis pathway. In some type of tumours, Cisplatin was able to induce overexpression of FADD and procaspase 8 (Fulda S and Debatin KM, 2006). T98G cells treated with PtAcacDMS and CDDP show up-regulation of Caspase 8. Taken together these results confirm the activation of both apoptosis pathway after treatment of platinum compounds, in particular after administration of PtAcacDMS.

Apoptosis seems to be the principal type of cell death for human T98G tumour cells. Ultrathin section at TEM and semithin section at optical microscopy confirmed the presence of apoptotic cells and necrotic cells, but have highlighted that also autophagy is triggered by both platinum compounds as shown by the presence of big vacuoles disseminate in the cytosol. The presence of autophagic process was confirmed by the down-regulation of the protein p62/SQSMT1, also implicated in neurodegenerative disease (Hara T et al., 2006), after treatment with platinum compounds. This decrease of p62 is very important: indeed the high expression level of this protein indicates a basal autophagic process leading resistance to apoptosis induced, for example, by chemical stimuli such as drugs. This mechanism is the bases of Cisplatin resistance in ovarian epithelial carcinoma (Yu H et al., 2011). This preliminary result does not appear to indicate any difference in induction of autophagy between CDDP and PtAcacDMS, but further

experiments are necessary to investigate the involvement of other markers of autophagy (such as ATG proteins).

Lysosomes are important organelles in the process of autophagy. Their membrane fuse with that of autophagosomes forming autophagolysosome, in which cargo and p62 are degraded. Interestingly, after treatment with CDDP and PtAcacDMS the number of lysosomes decreases. This peculiarity can be explained considering the stress condition and the increase of oxidative stress in treated cells, in particular the low concentration of $H_2O_2$ that favours the lysosome membrane permeabilization and the disruption of lysosomes. The loss of structure and function of these organelles can also occur after the impairment of mitochondrial function and consequently increase of ROS (see below): these conditions favour the activation of Caspase 9 and Caspase 8 and thus intrinsic and extrinsic apoptosis (Dielschneider RF et al., 2017; Eno CO et al., 2013). In conclusion, apoptosis seems to be the form of cell death to prevail after the induction of autophagy when the number of lysosomes decrease. Apoptosis was also investigated by immunostaining of organelles. After administration of both platinum compounds, Golgi apparatus and mitochondria loss their localization and structure: especially after treatment with PtAcacDMS mitochondria are homogeneous distributed in all the cytoplasm and the Golgi apparatus results to be fragmented and disperse in the cytoplasm with the loss of the particular semilunar shape. This is due to disruption of the cytoskeleton of actin and microtubules, that induce morphological changes to the form of the cells, nevertheless maintain the integrity of plasmatic membrane, typical characteristic of apoptosis

process respect to necrosis, according to our previous work (Grimaldi M, 2015, PhD thesis; Grimaldi M et al., 2016).

Modulation of intracellular calcium signalling is an important way of regulation for different cellular process, since calcium acting as a second messenger, in tumour and non tumour cells. Also apoptosis, autophagy and necrosis can be induced by high and uncontrolled levels of intracellular calcium as largely demonstrate by literature data (Zhivotovsky B and Orrenius S, 2011). In the intracellular environment calcium is sequestered or exchanged between different compartment by pumps and during this flux calcium can bind regulatory protein for regulatory functions or buffering proteins. Furthermore, more evidences show that both CDDP and PtAcacDMS are able to induce an increase of intracellular calcium in some type of cancers (Florea AM et al., 2005; Florea AM et al., 2009). In T98G cells, in presence of extracellular calcium, we can observe an increase in $[Ca^{2+}]_i$, more evident after acute effect of PtAcacDMS respect to CDDP: both compounds are able to trigger an influx from the extracellular space. This mechanism continues also after 48h of treatment but only in cells exposed to PtAcacDMS: indeed after stimulation of ionomycin, that affects the influx of calcium from the stores, CDDP seems to not influence the $[Ca^{2+}]_i$, in agreement with literature data (Al-Taweel N et al., 2014). Therefore, the two compounds seem to show a different mode of action and to better understand their modulation of intracellular calcium we evaluated the platinum compounds-induced $[Ca^{2+}]_i$ regulation on ER, one of the principal calcium store, with mitochondria, in the cells. The analysis demonstrates an increase of $[Ca^{2+}]_i$ for both

platinum compounds respect to control cells, in presence of CPA which inhibit the influx of calcium ions in ER. In summary, after 48h of treatment, while CDDP influence the $[Ca^{2+}]_i$ acting preferentially on intracellular stores, PtAcacDMS seems to modulate intracellular calcium both from influx through plasmatic membrane and efflux through ER. Further experiments are necessary to evaluate if platinum compounds influence the release of calcium by mitochondria. In these mechanisms an important role may be played by PMCA-1: its lower concentration after treatment of both platinum compounds might inhibit the efflux of calcium in the extracellular space, ensuring high levels of this ion in the cells, in agreement with data literature (Muscella A et al., 2011). Others pumps and channels such as IP$_3$R, and RyR could be modulated by CDDP and PtAcacDMS. Buffer calcium-binding protein confirm a modulation in $[Ca^{2+}]_i$ between control and treated T98G. Calretinin and Parvalbumin (highly expressed in CNS), show a decrease in fluorescence intensity in cells exposed to platinum compounds, in particular after treatment with PtAcacDMS, this could cause a higher free-calcium in the cytoplasm; while Calmodulin show an increase in fluorescence intensity. When Calmodulin links calcium activates the CAMKs (Ca$^{2+}$/calmodulin (CaM)-dependent protein kinases). These kinases have an important role in many aspects of tumors including cell proliferation, invasion, metastasis and also apoptosis (Wang YY et al., 2015), because their ability to regulate many proteins. One of this serine/threonine kinases is DAPK1 (death-associated protein kinase 1) activated by binding of Ca$^{2+}$-activated Calmodulin which can regulate the formation of autophagosome, or

activate the apoptotic pathway by the trigger of the Fas receptor signaling (Singh P et al., 2016). Immunofluorescence shown increase of fluorescence intensity also for the protein Calbindin: this could be explained with the presence of some mechanisms of resistance put in place by the cells to try to restore the calcium homeostasis. Indeed, literature data indicate that Calbindin is able to protect cells against apoptosis and oxidative stress (Christakos S and Liu Y, 2004; Guo Q et al., 1998; Sun S et al., 2011). Further experiments will be necessary to better understand this interesting result and to investigate differences in modulation of Calbindin by CDDP and PtAcacDMS, in particular the effects of the compounds on the long-term treatment will be evaluated. Furthermore, preliminary results on cells grown without extracellular calcium seems to reinforce the hypothesis of the role of calcium in affecting apoptosis in T98G cell line. Additional experiments are needed to confirm these findings, as analyzing the others apoptotic markers and performing cell proliferation assay to quantify the decrease in apoptotic death mechanisms in T98G after treatment with CDDP and PtAcacDMS. In conclusion, the ability of $Ca^{2+}$ to induce cell death after treatment with platinum compounds opens the way to new therapeutic targets.

Many evidences have shown that oxidative stress is an important modulator in carcinogenesis and tumor survival. Since 1956 is known that the lack of mitochondrial membrane potential induces a variety of oxidative species especially ROS, able to induce the release of cyt-c and trigger the extrinsic and intrinsic apoptosis pathway. Furthermore, ROS can contribute to regulate intracellular calcium levels because PMCA-

1, in presence of elevated oxidant species, is inactivated, internalized from the plasma membrane and degraded (Zaidi A, 2010). Another oxidative pathway implicated in tumor cell death is that of NO/peroxynitrite with superoxide anion implicated in the lipid peroxidation and apoptosis. The complex can interact with SOD and inhibit apoptosis (Kudryavtseva AV et al., 2016). Furthermore, nitrotyrosine, derived from the reaction between peroxynitrite and tyrosine residues of proteins, is used as a biomarker for quantifying oxidative stress level in the cells (Garcia-Garcia A et al., 2012). Literature data confirm that both CDDP and PtAcacDMS can induce oxidative stress and subsequently death of tumor cells (Chirino YI and Pedraza-Chaverri J, 2009; Muscella A et al., 2011; Vetrugno C et al., 2014). As expected in our experiments we found high expression of ROS and nitrotyrosine in treated cells respect to control cells; however only in the case of ROS its fluorescence intensity is higher after administration of PtAcacDMS respect to Cisplatin. The production of NO was evaluated analyzing the immunopositivity of iNOS, the major enzyme implicated in its production. iNOS appears more expressed in both platinum compounds treated cells, but with prevalence after PtAcacDMS administration. Finally, we also analyzed the expression of SOD: immunocytochemistry confirms a great intensity of fluorescence in T98G control cells, while in the treated cells the level of this enzyme decreases.

Oxidative stress can influence chromatin structure through different way, such as post-translation modifications of histones; this influences gene expression, regulation of cell survival or cell death and

mutagenesis (Kreuz S and Fischle W, 2016). For this, we evaluated some of principal histone modifications in immunocytochemistry and we found a different regulation in control and treated cells. Our preliminary results show that H3K9me3 is more expressed in T98G control cells, while H3K27me3 is more expressed in treated cells, especially after administration of PtAcacDMS: this is in accord with literature data in which more evidences have shown that these two different histones modifications are mutually exclusive (Zhang T et al., 2015). H4K20me3 is more expressed in treated cells but with prevalence after CDDP administration. These results can suggest a possible role of oxidative stress on histone lysine methylation, but some questions remain still open, and further experiments are necessary to better understand what are the specific mechanisms involved in oxidative stress-induced chromatin changes, the cellular effects of these changes, how this can influence the physiological setting of the cells (Kreuz S and Fischle W, 2016) and if platinum compounds or other chemotherapeutic treatments are involved in this mechanism.

For the second strategy we used mouse LLC (Lewis lung cancer) non-small cell lung cancer cell line. We have generated a series of mouse cell lines resistant to Cisplatin, followed by their characterization with respect to PARylation: between 9 resistant clones generated we have chosen 3 of these showing more Cisplatin resistance and a higher level of PARylation. Then, immunocompetent C57BL/6 female mice were subcutaneously engrafted with parental LLC cell line (WT) or CDDP-resistant clones LLC cells to analyze the tumor infiltrate by cytofluorimetry. The immune system, in particular the tumor

infiltrating lymphocytes (TILs), macrophages; dendritic cells and granulocytes play an important role in the control in a wide range of tumors (Eggermont A et al., 2014).

The analysis of FlowJo data seems to show a lower infiltration of lymphocytes (CD3$^+$) in Cisplatin-resistant tumors as compared to sensitive WT ones. This decrease is also observed when we divided the lymphocytes population into different groups expressing either the CD4 marker which identifies the subpopulations of lymphocytes T helper and T regulatory cells (T-reg) or the CD8 marker that identifies the subpopulation of cytotoxic T lymphocytes. The subpopulation that does not express the two markers is made up of other types of immune cells such as natural killer cells and other types of lymphocytes like γδ T-cells. Several studies demonstrated that CD8$^+$ cytotoxic T-cells (CTL) are essential for tumor destruction, while Forkhead box P3 (FoxP3$^+$) CD4$^+$ regulatory T-cells, inhibit CTL function, support proliferation of B-lymphocytes, and may promote an anti-inflammatory immune response that could enhance tumor growth (Zitvogel L et al., 2015).

In our preliminary *in vivo* experiments, we observed a lower infiltration in particular of CD4$^+$ population in Cisplatin-resistant tumors as compared to parental WT tumors, so we can speculate that cancer cells expressing PARhigh have a lower capacity to provoke an anti-cancer immune response. Furthermore, murine studies have demonstrated that CD4$^+$/CD25$^+$ T cells (Treg) are able to abolish T-cell mediated immunity, while the depletion of CD25$^+$ can enhance tumor immunity and rejection. Murine and human natural CD4$^+$/CD25$^+$ cells express high levels of FoxP3. In our data, activated (ICOS$^+$/PD1$^+$) T-reg cells

are more expressed in the Cisplatin-resistant tumors as compared to WT, suggesting a reduced immune response against Cisplatin-resistant cancer cells. Moreover, there are no differences for what concerns the expression of PD-L1 on the surface of tumor cells, therefore it can be hypothesize that this mechanism is not implicated in a different tumor aggressiveness that can lead alterations in the response of immune system between sensitive and resistant tumors.

Macrophages and granulocytes contribute to tumor pathogenesis, promote angiogenesis, cell invasion and tumor progression. They accumulate in the tumor macroenvironment and become immunosuppressive. (Gambrilovich DI et al., 2013). My preliminary results revealed no differences in CD45$^+$ cells between WT and CDDP-resistant tumors, but when we analyzed the amount of leukocytes in the three major subpopulation (like monocytes-derived macrophages, dendritic cells and granulocytes) we observed an interesting difference in CD11b$^+$ and CD11c$^-$ cells: this subpopulation may correspond to monocyte-like cells with cross-presentation ability, as demonstrated by the co-expression of MHCII and CD80 markers. Monocytes are precursor of macrophages; the literature data demonstrated that in both human and mice these cells facilitate the tumor growth and their presence is associated with poor clinical outcome (Mantovani A and Sica A, 2010; Qian BZ and Pollard JW, 2010).

# 6. CONCLUSIONS AND PERSPECTIVES

This research focused on two aspects of Cisplatin that unfortunately can limit its use in clinical settings. To overcome the side effect on patients caused by the administration of CDDP we evaluated the cytotoxic potential of a different platinum compound, the PtAcacDMS, on human glioblastoma T98G cell line and we analyzed a series of molecular pathway to better understand the specific mechanism of action. Our results show that PtAcacDMS seems to be able to induce apoptosis, necrosis and autophagy, but especially for autophagy pathway, more experiments are necessary to confirm the data obtained. The role of intracellular calcium in tumor is an emerging field of study because the variation of $[Ca^{2+}]_i$ can modulate the tumor progression and the response to chemotherapeutical drug. Our results show an important $[Ca^{2+}]_i$–regulation mediated by CDDP and especially PtAcacDMS. To confirm these results it will be necessary evaluate the expression of molecular mechanisms involved in the flux of calcium from intracellular stores or extracellular space to cytoplasm and confirm if, in cells growing in absence of calcium, there is a decrease of apoptotic processes.

Furthermore, the presence of DMS in the chemical structure of the molecule indicates its possible linking of proteins containing thiol or thioester groups. Data in the literature have shown that the ability of the relatively heavy platinum atoms to disperse electrons make them useful for electron microscopy, producing densely stained areas where platinum atoms are accumulated in tumor cells and tissue; in particular in the glial cells Cisplatin is accumulated in mitochondria and

ribosomes. It could be interesting identify which organelles contain elevated levels of accumulated platinum using a "platinum staining" for electron microscopy in different types of tumors to obtain a more detailed understanding the mechanisms by which PtAcacDMS and Cisplatin-induced death of cells through interaction of different cytosolic and nuclear targets. This could lead to the discovery of new molecular target therapy for the treatment of Cisplatin resistant tumors. Furthermore, the low concentration to which PtAcacDMS acts (four-fold lower than that of CDDP), might be a candidate to decrease side effect of CDDP and other chemotherapeutic agents.

Secondly, we have analyzed a particular type of Cisplatin resistance: indeed, by prolonged exposure to Cisplatin, we have obtained Cisplatin-resistant LLC clones that accumulate elevated levels of PAR-containing proteins, probably by upregulation of PARP-1 activity. Analysis of tumor infiltrating lymphocytes in preliminary *in vivo* experiments suggests differences in the immune infiltrate content and phenotype between Cisplatin-sensitive and resistant LLC cells. It seems that immune-suppressive mechanisms are generated by Cisplatin-resistant LLC cells as compared to control parental cancer cell, but further experiments are necessary to confirm these results. Furthermore, to confirm that PARP-1 influences the immune infiltrate it will be necessary to manipulate the expression of PARP-1 in the clones CDDP-resistant to evaluate whether these injected cells exhibit the same immune infiltrate as the WT cells.

# REFERENCES

**Aggarwal BB, Gupta SC, Kim JH.** Historical perspectives on tumor necrosis factor and its superfamily: 25 years later, a golden journey. Blood. 2012; 119:651-665

**Aida T, Takebayashi Y, Shimizu T, Okamura C, Higasimoto M, Kanzaki A, Nakayama K, Terada K, Sugiyama T, Miyazaki K, Ito K, Takenoshita S, Yaegashi N.** Expression of copper-transporting P-type adenosine triphosphatase (ATP7B) as a prognostic factor in human endometrial carcinoma. Gynecol Oncol. 2005; 97(1):41-45

**Al-Taweel N, Varghese E, Florea AM, Büsselberg D.** Cisplatin (CDDP) triggers cell death of MCF-7 cells following disruption of intracellular calcium ([Ca(2+)]i) homeostasis. J Toxicol Sci. 2014; 39:765-774

**Alaedini A, Xiang Z, Kim H, Sung YJ, Latov N.** Up-regulation of apoptosis and regeneration genes in the dorsal root ganglia during cisplatin treatment. Exp Neurol. 2008; 210:368-374

**Amable L.** Cisplatin resistance and opportunities for precision medicine. Pharmacol Res. 2016; 106:27-36

**Apps MG, Choi EH, Wheate NJ.** The state-of-play and future of platinum drugs. Endocr Relat Cancer. 2015; 22:219-233

**Bagnyukova TV, Tryndyak VP, Montgomery B, Churchwell MI, Karpf AR, James SR, Muskhelishvili L, Beland FA, Pogribny IP.** Genetic and epigenetic changes in rat preneoplastic liver tissue induced by 2-acetylaminofluorene. Carcinogenesis. 2008; 29:638-646

**Banfi B, Malgrange B, Knisz J, Steger K, Dubois-Dauphin M, Krause KH.** NOX3, a superoxide-generating NADPH oxidase of the inner ear. J. Biol. Chem. 2004; 279:46065–46072

**Bano D, Young KW, Guerin CJ, Lefeuvre R, Rothwell NJ, Naldini L, Rizzuto R, Carafoli E, Nicotera P.** Cleavage of the plasma membrane Na+/Ca2+ exchanger in excitotoxicity. Cell. 2005; 120:275-285

**Barclay LA, Wales TE, Garner TP, Wachter F, Lee S, Guerra RM, Stewart ML, Braun CR, Bird GH, Gavathiotis E, Engen JR, Walensky LD.** Inhibition of Pro-apoptotic BAX by a noncanonical interaction mechanism. Mol Cell. 2015; 57:873-886

**Barnhart BC, Alappat EC, Peter ME.** The CD95 type I/type II model. Semin Immunol. 2003; 15:185-193

**Barton CD, Pizer B, Jones C, Oni L, Pirmohamed M, Hawcutt DB.** Identifying cisplatin-induced kidney damage in pediatric oncology patients. Pediatr Nephrol. 2018; 33:1467-1474

**Bellmunt J, Paz-Ares L, Cuello M, Cecere FL, Albiol S, Guillem V, Gallardo E, Carles J, Mendez P, de la Cruz JJ, Taron M, Rosell R, Baselga J; Spanish Oncology Genitourinary Group.** Gene expression of ERCC1 as a novel prognostic marker in advanced bladder cancer patients receiving cisplatin-based chemotherapy. Ann Oncol. 2007; 18:522-528

**Beneke S.** Regulation of chromatin structure by poly(ADP-ribosyl)ation. Front Genet. 2012; 3:169

**Berchtold MW, Villalobo A**. The many faces of calmodulin in cell proliferation, programmed cell death, autophagy, and cancer. Biochim Biophys Acta. 2014; 1843:398-435

**Bernocchi G, Bottone MG, Piccolini VM, Dal Bo V, Santin G, De Pascali SA, Migoni D, Fanizzi FP**. Developing central nervous system and vulnerability to platinum compounds. Chemother Res Pract. 2011; 2011:315418

**Bezprozvanny I, Watras J, Ehrlich BE.** Bell-shaped calcium-response curves of Ins(1,4,5)P3- and calcium-gated channels from endoplasmic reticulum of cerebellum. Nature. 1991; 351:751-754

**Blum W, Schwaller B.** Calretinin is essential for mesothelioma cell growth/survival in vitro: a potential new target for malignant mesothelioma therapy? Int J Cancer. 2013; 133:2077-2088

**Bobylev I, Joshi AR, Barham M, Neiss WF, Lehmann HC.** Depletion of mitofusin-2 causes mitochondrial damage in cisplatin-induced neuropathy. Mol Neurobiol. 2018; 55:1227-1235

**Bodenner DL, Dedon PC, Keng PC, Borch RF.** Effect of diethyldithiocarbamate on cis-diamminedichloroplatinum(II)-induced cytotoxicity, DNA cross-linking, and gamma-glutamyl transpeptidase inhibition. Cancer Res. 1986; 46:2745-2450

**Bonora M, Morganti C, Morciano G, Pedriali G, Lebiedzinska-Arciszewska M, Aquila G, Giorgi C, Rizzo P, Campo G, Ferrari R, Kroemer G, Wieckowski MR, Galluzzi L, Pinton P.** Mitochondrial permeability transition involves dissociation of F(1)F(O) ATP synthase dimers and C-ring conformation. EMBO Rep. 2017; 18:1077-1089

**Booth DM, Enyedi B, Geiszt M, Varnai P, and Hajnoczky G.** Redox nanodomains are induced by and control calcium signaling at the ER mitochondrial interface. Mol Cell 2016; 63:240-248

**Boya P, Reggiori F, Codogno P.** Emerging regulation and functions of autophagy. Nat Cell Biol. 2013; 15(7):713-720

**Brenner D, Blaser H, Mak TW.** Regulation of tumour necrosis factor signalling: live or let die. Nat Rev Immunol. 2015; 15:362-37

**Brouland JP, Gélébart P, Kovàcs T, Enouf J, Grossmann J, Papp B.** The loss of sarco/endoplasmic reticulum calcium transport ATPase 3 expression is an early event during the multistep process of colon carcinogenesis. Am J Pathol. 2005; 167:233-242

**Burnstock G, Di Virgilio F.** Purinergic signalling and cancer. Purinergic Signal. 2013; 9:491-540

**Büsselberg D, Florea AM.** Targeting Intracellular Calcium Signaling ([Ca(2+)](i)) to Overcome Acquired Multidrug Resistance of Cancer Cells: A Mini-Overview. Cancers (Basel). 2017; 9;9

**Carozzi VA, Canta A, Chiorazzi A.** Chemotherapy-induced peripheral neuropathy: What do we know about mechanisms? Neurosci Lett. 2015; 596:90-107

**Cavaletti G, Ceresa C, Nicolini G, Marmiroli P**. Neuronal drug transporters in platinum drugs-induced peripheral neurotoxicity. Anticancer Res. 2014; 34:483-486

**Cedar H, Bergman Y**. Linking DNA methylation and histone modification: patterns and paradigms. Nat Rev Genet. 2009; 10:295-304

**Cereghetti GM, Stangherlin A, Martins de Brito O, Chang CR, Blackstone C, Bernardi P, Scorrano L.** Dephosphorylation by calcineurin regulates translocation of Drp1 to mitochondria. Proc Natl Acad Sci U S A. 2008; 105:15803-15808

**Cerri S, Piccolini VM, Santin G, Bottone MG, De Pascali SA, Migoni D, Iadarola P, Fanizzi FP, Bernocchi G**. The developmental neurotoxicity study of platinum compounds. Effects of cisplatin versus a novel Pt(II) complex on rat cerebellum. Neurotoxicol Teratol. 2011; 33:273-281

**Chai J, Du C, Wu JW, Kyin S, Wang X, Shi Y.** Structural and biochemical basis of apoptotic activation by Smac/DIABLO. Nature. 2000; 406:855-862

**Chan FK, Chun HJ, Zheng L, Siegel RM, Bui KL, Lenardo MJ**. A domain in TNF receptors that mediates ligand-independent receptor assembly and signaling. Science. 2000; 288:2351-2354

**Chen HH, Yan JJ, Chen WC, Kuo MT, Lai YH, Lai WW, Liu HS, Su WC.** Predictive and prognostic value of human copper transporter 1 (hCtr1) in patients with stage III non-small-cell lung cancer receiving first-line platinum-based doublet chemotherapy. Lung Cancer. 2012; 75:228-234

**Chen N, Debnath J.** Autophagy and tumorigenesis. S Lett. 2010; 584:1427-1435

**Chen YF, Chen YT, Chiu WT, Shen MR.** Remodeling of calcium signaling in tumor progression. J Biomed Sci. 2013; 20:23

**Chinnaiyan AM, O'Rourke K, Tewari M, Dixit VM.** FADD, a novel death domain-containing protein, interacts with the death domain of Fas and initiates apoptosis. Cell. 1995; 81:505-512

**Chirino YI, Pedraza-Chaverri J.** Role of oxidative and nitrosative stress in cisplatin-induced nephrotoxicity. Exp Toxicol Pathol. 2009; 61:223-242

**Cho YS, Challa S, Moquin D, Genga R, Ray TD, Guildford M, Chan FK.** Phosphorylation-driven assembly of the RIP1-RIP3 complex regulates programmed necrosis and virus-induced inflammation. Cell. 2009; 137:1112-1123

**Choe WT, Chinosornvatana N, Chang KW.** Prevention of cisplatin ototoxicity using transtympanic N-acetylcysteine and lactate. Otol. Neurotol. 2004; 25:910-915

**Choudhari SK, Chaudhary M, Bagde S, Gadbail AR, Joshi V.** Nitric oxide and cancer: a review. World J Surg Oncol. 2013; 11:118

**Christakos S, Liu Y.** Biological actions and mechanism of action of calbindin in the process of apoptosis. J Steroid Biochem Mol Biol. 2004;89-90:401-404

**Clapham DE.** Calcium signaling. Cell. 2007; 31:1047-1058

**Cohen I, Poręba E, Kamieniarz K, Schneider R.** Histone modifiers in cancer: friends or foes? Genes Cancer. 2011; 2:631-647

**Coradini, PP, Cigana L, Selistre SG, Rosito LS, Brunetto AL.** Ototoxicity from cisplatin therapy in childhood cancer. J. Pediatr. Hematol. Oncol. 2007; 29:355-360

**Cribbs JT, Strack S.** Reversible phosphorylation of Drp1 by cyclic AMP-dependent protein kinase and calcineurin regulates mitochondrial fission and cell death. EMBO Rep. 2007; 8:939-944

**Csordás G, Renken C, Várnai P, Walter L, Weaver D, Buttle KF, Balla T, Mannella CA, Hajnóczky G.** Structural and functional features and significance of the physical linkage between ER and mitochondria. J Cell Biol. 2006; 174:915-921

**Czabotar PE, Lessene G, Strasser A, Adams JM.** Control of apoptosis by the BCL-2 protein family: implications for physiology and therapy. Nat Rev Mol Cell Biol. 2014; 15:49-63

**Dasari S, Tchounwou PB.** Cisplatin in cancer therapy: molecular mechanisms of action. Eur J Pharmacol. 2014; 740:364-378

**Davidovich P, Kearney CJ, Martin SJ**. Inflammatory outcomes of apoptosis, necrosis and necroptosis. Biol Chem. 2014; 395:1163-1171

**De Pinto VD, Palmieri F.** Transmembrane arrangement of mitochondrial porin or voltage-dependent anion channel (VDAC). J Bioenerg Biomembr. 1992; 24:21-26

**Deretic V.** Multiple regulatory and effector roles of autophagy in immunity. Curr Opin Immunol. 2009; 21:53-62

**Dickey, DT, Muldoon, LL, Doolittle ND, Peterson DR, Kraemer DF, Neuwelt, EA.** Effect of N-acetylcysteine route of administration on chemoprotection against cisplatin-induced toxicity in rat models. Cancer Chemother. Pharmacol. 2008; 62:235-241

**Dielschneider RF, Henson ES, Gibson SB.** Lysosomes as Oxidative Targets for Cancer Therapy. Oxid Med Cell Longev. 2017; 2017:3749157

**Dietrich J, Han R, Yang Y, Mayer-Pröschel M, Noble M.** CNS progenitor cells and oligodendrocytes are targets of chemotherapeutic agents in vitro and in vivo. J Biol. 2006; 5:22

**Di Leva F, Domi T, Fedrizzi L, Lim D, Carafoli E.** The plasma membrane Ca2+ ATPase of animal cells: structure, function and regulation. Arch Biochem Biophys. 2008; 476:65-74

**Di Lisa F, Bernardi P.** A CaPful of mechanisms regulating the mitochondrial permeability transition. J Mol Cell Cardiol. 2009; 46:775-780

**Du C, Fang M, Li Y, Li L, Wang X.** Smac, a mitochondrial protein that promotes cytochrome c-dependent caspase activation by eliminating IAP inhibition. Cell. 2000; 102:33-42

**Eckelman BP, Salvesen GS, Scott FL.** Human inhibitor of apoptosis proteins: why XIAP is the black sheep of the family. EMBO Rep. 2006; 7:988-994

**Eggermont A, Robert C, Soria JC, Zitvogel L.** Harnessing the immune system to provide long-term survival in patients with melanoma and other solid tumors. Oncoimmunology. 2014; 3:e27560

**Elmore S.** Apoptosis: a review of programmed cell death. Toxicol Pathol. 2007; 35:495-516

**Enari M, Sakahira H, Yokoyama H, Okawa K, Iwamatsu A, Nagata S.** A caspase-activated DNase that degrades DNA during apoptosis, and its inhibitor ICAD. Nature. 1998; 391:43-50. Erratum in: Nature 1998; 28; 393:396

**Eno CO, Zhao G, Venkatanarayan A, Wang B, Flores ER, Li C**. Noxa couples lysosomal membrane permeabilization and apoptosis during oxidative stress. Free Radic Biol Med. 2013; 65:26-37

**Esposti MD.** The roles of Bid. Apoptosis. 2002; 7:433-440

**Feng S, Yang Y, Mei Y, Ma L, Zhu DE, Hoti N, Castanares M, Wu M.** Cleavage of RIP3 inactivates its caspase-independent apoptosis pathway by removal of kinase domain. Cell Signal. 2007; 19:2056-2067

**Fenoglio C, Albicini F, De Pascali SA, Milanesi G, Fumagalli M, Migoni D, Fanizzi FP, Bernocchi G.** Renal fibrogenesis and platinum compounds in a rat model: a novel Pt (II) complex vs. cisplatin. Anticancer Res. 2015; 35:739-751

**Filipski KK, Loos WJ, Verweij J, Sparreboom A**. Interaction of Cisplatin with the human organic cation transporter 2. Clin Cancer Res. 2008; 14:3875-3880

**Filipski KK, Mathijssen RH, Mikkelsen TS, Schinkel AH, Sparreboom A.** Contribution of organic cation transporter 2 (OCT2) to cisplatin-induced nephrotoxicity. Clin Pharmacol Ther. 2009; 86:396-402

**Fischer U, Jänicke RU, Schulze-Osthoff K.** Many cuts to ruin: a comprehensive update of caspase substrates. Cell Death Differ. 2003; 10:76-100

**Florea AM, Dopp E, Büsselberg D**. Elevated Ca2+(i) transients induced by trimethyltin chloride in HeLa cells: types and levels of response. Cell Calcium. 2005; 37:251-258

**Florea AM, Büsselberg D.** Anti-cancer drugs interfere with intracellular calcium signaling. Neurotoxicology. 2009; 30:803-810

**Florea AM, Büsselberg D.** Cisplatin as an anti-tumor drug: cellular mechanisms of activity, drug resistance and induced side effects. Cancers (Basel). 2011; 3:1351-1371

**Foskett JK, White C, Cheung KH, Mak DO.** Inositol trisphosphate receptor Ca2+ release channels. Physiol Rev. 2007; 87:593-658

**Foyouzi-Youssefi R, Arnaudeau S, Borner C, Kelley WL, Tschopp J, Lew DP, Demaurex N, Krause KH.** Bcl-2 decreases the free Ca2+ concentration within the endoplasmic reticulum. Proc Natl Acad Sci U S A. 2000; 97:5723-5728

**Fraga MF, Ballestar E, Villar-Garea A, Boix-Chornet M, Espada J, Schotta G, Bonaldi T, Haydon C, Ropero S, Petrie K, Iyer NG, Pérez-Rosado A, Calvo E, Lopez JA, Cano A, et al**. Loss of acetylation at Lys16 and trimethylation at Lys20 of histone H4 is a common hallmark of human cancer. Nat Genet. 2005; 37:391-400

**Frank S, Gaume B, Bergmann-Leitner ES, Leitner WW, Robert EG, Catez F, Smith CL, Youle RJ.** The role of dynamin-related protein 1, a mediator of mitochondrial fission, in apoptosis. Dev Cell. 2001; 1:515-525

**Frezza C, Cipolat S, Martins de Brito O, Micaroni M, Beznoussenko GV, Rudka T, Bartoli D, Polishuck RS, Danial NN, De Strooper B, Scorrano L**. OPA1 controls apoptotic cristae remodeling independently from mitochondrial fusion. Cell. 2006; 126:177-189

**Fridman WH, Zitvogel L, Sautès-Fridman C, Kroemer G.** The immune contexture in cancer prognosis and treatment. Nat Rev Clin Oncol. 2017; 14:717-734

**Friedberg EC, Meira LB.** Database of mouse strains carrying targeted mutations in genes affecting biological responses to DNA damage Version 7. DNA Repair (Amst). 2006; 5:189-209

**Fu Q, Fu TM, Cruz AC, Sengupta P, Thomas SK, Wang S, Siegel RM, Wu H, Chou JJ.** Structural basis and functional role of intramembrane trimerization of the Fas/CD95 death receptor. Mol Cell. 2016; 61:602-613

**Fulda S, Debatin KM.** Extrinsic versus intrinsic apoptosis pathways in anticancer chemotherapy. Oncogene. 2006; 25:4798-4811

**Füllgrabe J, Kavanagh E, Joseph B.** Histone onco-modifications. Oncogene. 2011; 30:3391-3403

**Gabrilovich DI.** The mechanisms and functional significance of tumour-induced dendritic-cell defects. Nat Rev Immunol. 2004; 4:941-952

**Gabrilovich DI, Ostrand-Rosenberg S, Bronte V.** Coordinated regulation of myeloid cells by tumours. Nat Rev Immunol. 2012; 12:253-268

**Galluzzi L, Maiuri MC, Vitale I, Zischka H, Castedo M, Zitvogel L, Kroemer G**. Cell death modalities: classification and pathophysiological implications. Cell Death Differ. 2007; 14:1237-1243

**Galluzzi L, Vitale I, Michels J, Brenner C, Szabadkai G, Harel-Bellan A, Castedo M, Kroemer G.** Systems biology of cisplatin resistance: past, present and future. Cell Death Dis. 2014; 5:e1257

**Galluzzi L, Kepp O, Kroemer G.** Mitochondrial regulation of cell death: a phylogenetically conserved control. Microb Cell. 2016; 3:101-108

**Galluzzi L, Baehrecke EH, Ballabio A, Boya P, Bravo-San Pedro JM, Cecconi F, Choi AM, Chu CT, Codogno P, Colombo MI, Cuervo AM, Debnath J, Deretic V, Dikic I, Eskelinen EL, et al.** Molecular definitions of autophagy and related processes. EMBO J. 2017; 36:1811-1836

**Galluzzi L, Vitale I, Aaronson SA, Abrams JM, Adam D, Agostinis P, Alnemri ES, Altucci L, Amelio I, Andrews DW, Annicchiarico-Petruzzelli M, Anto AV, Arama E, Baehrecke EH, Barlev NA, et al.** Molecular mechanisms of cell death: recommendations of the Nomenclature Committee on Cell Death 2018. Cell Death Differ. 2018; 25:486-541

**Gander JC, Bustos-Castillo M, Stüber D, Hunziker W, Celio M, Schwaller B.** The calcium-binding protein calretinin 22k, an alternative splicing product of the calretinin gene is expressed in several colon adeno carcinoma cell lines. Cell Calcium. 1996; 20:63-72

**Garcia-Garcia A, Rodriguez-Rocha H, Madayiputhiya N, Pappa A, Panayiotidis MI, Franco R.** Biomarkers of protein oxidation in human disease. Curr Mol Med. 2012; 12:681-97

**Gill JS, Windebank AJ.** Cisplatin-induced apoptosis in rat dorsal root ganglion neurons is associated with attempted entry into the cell cycle. J Clin Invest. 1998; 101:2842-2850

**Glick D, Barth S, Macleod KF.** Autophagy: cellular and molecular mechanisms. J Pathol. 2010; 221:3-12

**Green DR, Kroemer G**. The pathophysiology of mitochondrial cell death. Science. 2004; 305:626-629

**Gluba A, Banach M, Hannam S, Mikhailidis DP, Sakowicz A, Rysz J.** The role ofToll-like receptors in renal diseases. Nat Rev Nephrol. 2010; 6:224-235

**Goodsell DS.** The molecular perspective: Cisplatin. Stem Cells. 2006; 24:514-515

**Grimaldi M, Santin G, Insolia V, Dal Bo V, Piccolini VM, Veneroni P, Barni S, Verri M, De Pascali SA, Fanizzi FP, Bernocchi G, Bottone MG.** [Pt(O,O'-acac)(γ-acac)(DMS)] versus cisplatin: apoptotic effects in B50 neuroblastoma cells. Histochem Cell Biol. 2016; 145:587-601

**Guo Q, Christakos S, Robinson N, Mattson MP**. Calbindin D28k blocks the proapoptotic actions of mutant presenilin 1: reduced oxidative stress and preserved mitochondrial function. Proc Natl Acad Sci U S A. 1998; 95:3227-3232

**Gupta RK, Patel AK, Shah N, Chaudhary AK, Jha UK, Yadav UC, Gupta PK, Pakuwal U.** Oxidative stress and antioxidants in disease and cancer: a review. Asian Pac J Cancer Prev. 2014; 15:4405-4409

**Gutierrez T, Simmen T.** Endoplasmic reticulum chaperones and oxidoreductases: critical regulators of tumor cell survival and immunorecognition. Front Oncol. 2014; 4, 291

**Gutierrez T, Simmen T**. Endoplasmic reticulum chaperones tweak the mitochondrial calcium rheostat to control metabolism and cell death. Cell Calcium. 2017; 70, 64-75

**Halliwell B.** Biochemistry of oxidative stress. Biochem Soc Trans. 2007; 35:1147-1150

**Hanahan D, Weinberg RA.** Hallmarks of cancer: the next generation. Cell. 2011; 144:646-674

**Handra-Luca A, Hernandez J, Mountzios G, Taranchon E, Lacau-St-Guily J, Soria JC, Fouret P.** Excision repair cross complementation group 1 immunohistochemical expression predicts objective response and cancer-specific survival in patients treated by Cisplatin-based induction chemotherapy for locally advanced head and neck squamous cell carcinoma. Clin Cancer Res. 2007; 13:3855-3859

**Haouzi D, Cohen I, Vieira HL, Poncet D, Boya P, Castedo M, Vadrot N, Belzacq AS, Fau D, Brenner C, Feldmann G, Kroemer G.** Mitochondrial permeability transition as a novel principle of hepatorenal toxicity in vivo. Apoptosis. 2002; 7:395-405

**Hara T, Nakamura K, Matsui M, Yamamoto A, Nakahara Y, Suzuki-Migishima R, Yokoyama M, Mishima K, Saito I, Okano H, Mizushima N.** Suppression of basal autophagy in neural cells causes neurodegenerative disease in mice. Nature. 2006; 441:885-889

**Hardwick JM, Soane L.** Multiple functions of BCL-2 family proteins. Cold Spring Harb Perspect Biol. 2013; 5

**Hartmann J, Verkhratsky A**. Relations between intracellular Ca2+ stores and store-operated Ca2+ entry in primary cultured human glioblastoma cells. J Physiol. 1998; 513:411-424

**He S, Wang L, Miao L, Wang T, Du F, Zhao L, Wang X.** Receptor interacting protein kinase-3 determines cellular necrotic response to TNF-alpha. Cell. 2009; 137:1100-1111

**Ho GY, Woodward N, Coward JI.** Cisplatin versus carboplatin: comparative review of therapeutic management in solid malignancies. Crit Rev Oncol Hematol. 2016; 102:37-46

**Holzer AK, Manorek GH, Howell SB.** Contribution of the major copper influx transporter CTR1 to the cellular accumulation of cisplatin, carboplatin, and oxaliplatin. Mol Pharmacol. 2006; 70:1390-1394

**Huang K, Zhang J, O'Neill KL, Gurumurthy CB, Quadros RM, Tu Y, Luo X.** Cleavage by Caspase 8 and Mitochondrial Membrane Association Activate the BH3-only Protein Bid during TRAIL-induced Apoptosis. J Biol Chem. 2016; 291:11843-11851

**Hughes MA, Powley IR, Jukes-Jones R, Horn S, Feoktistova M, Fairall L, Schwabe JW, Leverkus M, Cain K, MacFarlane M.** Co-operative and hierarchical binding of c-FLIP and Caspase-8: a unified model defines how c-FLIP isoforms differentially control cell fate. Mol Cell. 2016; 61:834-49

**Ishida R, Takaoka Y, Yamamoto S, Miyazaki T, Otaka M, Watanabe S, Komatsuda A, Wakui H, Sawada K, Kubota H, Itoh H.** Cisplatin differently affects amino terminal and carboxyl terminal domains of HSP90. S Lett. 2008; 582:3879-3883

**Ivanova H, Kerkhofs M, La Rovere RM, Bultynck G.** Endoplasmic reticulum-mitochondrial Ca(2+) fluxes underlying cancer cell survival. Front Oncol. 2017; 7:70

**Izzo A, Schneider R.** Chatting histone modifications in mammals. Brief Funct Genomics. 2010; 9:429-443

**Julien O, Wells JA.** Caspases and their substrates. Cell Death Differ. 2017; 24:1380-1389

**Kalayda GV, Wagner CH, Buss I, Reedijk J, Jaehde U.** Altered localisation of the copper efflux transporters ATP7A and ATP7B associated with cisplatin resistance in human ovarian carcinoma cells. BMC Cancer. 2008; 8:175

**Kang KP, Kim DH, Jung YJ, Lee AS, Lee S, Lee SY, Jang KY, Sung MJ, Park SK, Kim W.** Alpha-lipoic acid attenuates cisplatin-induced acute kidney injury in mice by suppressing renal inflammation. Nephrol Dial Transplant. 2009; 24:3012-3020

**Kanwal R, Gupta S.** Epigenetic modifications in cancer. Clin Genet. 2012; 81:303-311

**Katano K, Safaei R, Samimi G, Holzer A, Rochdi M, Howell SB.** The copper export pump ATP7B modulates the cellular pharmacology of carboplatin in ovarian carcinoma cells. Mol Pharmacol. 2003; 64:466-473

**Kavuri SM, Geserick P, Berg D, Dimitrova DP, Feoktistova M, Siegmund D, Gollnick H, Neumann M, Wajant H, Leverkus M.** Cellular FLICE-inhibitory protein (cFLIP) isoforms block CD95- and TRAIL death receptor-induced gene induction irrespective of processing of caspase-8 or cFLIP in the death-inducing signaling complex. J Biol Chem. 2011; 286:16631-16646

**Kerkar SP, Restifo NP.** Cellular constituents of immune escape within the tumor microenvironment. Cancer Res. 2012; 72:3125-3130

**Kerkhofs M, Bittremieux M, Morciano G, Giorgi C, Pinton P, Parys JB, Bultynck G.** Emerging molecular mechanisms in chemotherapy: Ca(2+) signaling at the mitochondria-associated endoplasmic reticulum membranes. Cell Death Dis. 2018; 9:334

**Kim MK, Cho KJ, Kwon GY, Park SI, Kim YH, Kim JH, Song HY, Shin JH, Jung HY, Lee GH, Choi KD, Kim SB.** Patients with ERCC1-negative locally advanced esophageal cancers benefit from preoperative chemoradiotherapy. Clin Cancer Res. 2008; 14:4225-4231

**Kim JS, Lee JH, Jeong WW, Choi DH, Cha HJ, Kim DH, Kwon JK, Park SE, Park JH, Cho HR, Lee SH, Park SK, Lee BJ, Min YJ, Park JW.** Reactive oxygen species-dependent EndoG release mediates cisplatin-induced caspase-independent apoptosis in human head and neck squamous carcinoma cells. Int J Cancer. 2008; 122:672-80

**Kischkel FC, Lawrence DA, Chuntharapai A, Schow P, Kim KJ, Ashkenazi A.** Apo2L/TRAIL-dependent recruitment of endogenous FADD and caspase-8 to death receptors 4 and 5. Immunity. 2000; 12:611-620

**Knight, KR, Kraemer DF, Neuwelt EA**. Ototoxicity in children receiving platinum chemotherapy: underestimating a commonly occurring toxicity that influence academic and social development. J. Clin. Oncol. 2005; 23:8588-8596

**Köberle B, Tomicic MT, Usanova S, Kaina B.** Cisplatin resistance: preclinical findings and clinical implications. Biochim Biophys Acta. 2010; 1806:172-182

**Korita PV, Wakai T, Shirai Y, Matsuda Y, Sakata J, Takamura M, Yano M, Sanpei A, Aoyagi Y, Hatakeyama K, Ajioka Y.** Multidrug resistance-associated protein 2 determines the efficacy of cisplatin in patients with hepatocellular carcinoma. Oncol Rep. 2010; 23:965-972

**Kothakota S, Azuma T, Reinhard C, Klippel A, Tang J, Chu K, McGarry TJ, Kirschner MW, Koths K, Kwiatkowski DJ, Williams LT**. Caspase-3-generated fragment of gelsolin: effector of morphological change in apoptosis. Science. 1997; 278:294-298

**Kouzarides T.** Chromatin modifications and their function. Cell. 2007; 128:693-705

**Kreuz S, Fischle W.** Oxidative stress signaling to chromatin in health and disease. Epigenomics. 2016; 8:843-862

**Kroemer G, Martin SJ.** Caspase-independent cell death. Nat Med. 2005; 11:725-730

**Kroemer G, Petit P, Zamzami N, Vayssière JL, Mignotte B.** The biochemistry of programmed cell death. FASEB J. 1995; 9:1277-1287

**Kudryavtseva AV, Krasnov GS, Dmitriev AA, Alekseev BY, Kardymon OL, Sadritdi a AF, Fedorova MS, Pokrovsky AV, Melnikova NV, K in AD, Moskalev AA, Snezhkina AV.** Mitochondrial dysfunction and oxidative stress in aging and cancer. Oncotarget. 2016; 7:44879-44905

**Kurosaka K, Takahashi M, Watanabe N, Kobayashi Y.** Silent cleanup of very early apoptotic cells by macrophages. J Immunol. 2003; 171:4672-4679

**Kushner BH, Budnick A, Kramer K, Modak S, Cheung NK.** Ototoxicity from high-dose use of platinum compounds in patients with neuroblastoma. Cancer. 2006; 107: 417-422

**Kwon MJ, Kim SS, Choi YL, Jung HS, Balch C, Kim SH, Song YS, Marquez VE, Nephew KP, Shin YK.** Derepression of CLDN3 and CLDN4 during ovarian tumorigenesis is associated with loss of repressive histone modifications. Carcinogenesis. 2010; 31:974-983

**Lajer H, Kristensen M, Hansen HH, Nielsen S, Frøkiaer J, Ostergaard LF, Christensen S, Daugaard G, Jonassen TE.** Magnesium depletion enhances cisplatin-induced nephrotoxicity. Cancer Chemother Pharmacol. 2005; 56:535-542

**Levy JMM, Towers CG, Thorburn A.** Targeting autophagy in cancer. Nat Rev Cancer. 2017; 17:528-542

**Lewit-Bentley A, Réty S.** EF-hand calcium-binding proteins. Curr Opin Struct Biol. 2000; 10:637-643

**Li B, Carey M, Workman JL.** The role of chromatin during transcription. Cell. 2007; 128:707-719

**Li P, Nijhawan D, Budihardjo I, Srinivasula SM, Ahmad M, Alnemri ES, Wang X.** Cytochrome c and dATP-dependent formation of Apaf-1/caspase-9 complex initiates an apoptotic protease cascade. Cell. 1997; 91:479-489

**Lim SD, Sun C, Lambeth JD, Marshall F, Amin M, Chung L, Petros JA, Arnold RS.** Increased Nox1 and hydrogen peroxide in prostate cancer. Prostate. 2005; 62:200-207

**Lin A, Schildknecht A, Nguyen LT, Ohashi PS**. Dendritic cells integrate signals from the tumor microenvironment to modulate immunity and tumor growth. Immunol Lett. 2010; 127:77-84

**Lodola F, Laforenza U, Bonetti E, Lim D, Dragoni S, Bottino C, Ong HL, Guerra G, Ganini C, Massa M, Manzoni M, Ambudkar IS, Genazzani AA, Rosti V, Pedrazzoli P, et al.** Store-operated Ca2+ entry is remodelled and controls in vitro angiogenesis in endothelial progenitor cells isolated from tumoral patients. PLoS One. 2012; 7:e42541

**Lodola F, Laforenza U, Cattaneo F, Ruffinatti FA, Poletto V, Massa M, Tancredi R, Zuccolo E, Khdar DA, Riccardi A, Biggiogera M, Rosti V, Guerra G, Moccia F.** VEGF-induced intracellular Ca(2+) oscillations are down-regulated and do not stimulate angiogenesis in breast cancer-derived endothelial colony forming cells. Oncotarget. 2017; 8:95223-95246

**Los M, Mozoluk M, Ferrari D, Stepczynska A, Stroh C, Renz A, Herceg Z, Wang ZQ, Schulze-Osthoff K**. Activation and caspase-mediated inhibition of PARP: a molecular switch between fibroblast necrosis and apoptosis in death receptor signaling. Mol Biol Cell. 2002; 13:978-988

**Machaca K.** Ca(2+) signaling, genes and the cell cycle. Cell Calcium. 2010; 48:243-250

**Maleszewska M, Kaminska B**. Deregulation of histone-modifying enzymes and chromatin structure modifiers contributes to glioma development. Future Oncol. 2015; 11:2587-2601

**Mandalà M, Ferretti G, Barni S.** Oxaliplatin in colon cancer. N Engl J Med. 2004; 351:1691-1692; author reply 1691-1692

**Mani SA, Guo W, Liao MJ, Eaton EN, Ayyanan A, Zhou AY, Brooks M, Reinhard F, Zhang CC, Shipitsin M, Campbell LL, Polyak K, Brisken C, Yang J, Weinberg RA.** The epithelial-mesenchymal transition generates cells with properties of stem cells. Cell. 2008; 133:704-715

**Manohar S, Leung N.** Cisplatin nephrotoxicity: a review of the literature. J Nephrol. 2018; 31:15-25

**Mantovani A, Sica A.** Macrophages, innate immunity and cancer: balance, tolerance, and diversity. Curr Opin Immunol. 2010; 22:231-237

**Marchi S, Pinton P.** Alterations of calcium homeostasis in cancer cells. Curr Opin Pharmacol. 2016; 29:1-6

**Mariño G, Madeo F, Kroemer G.** Autophagy for tissue homeostasis and neuroprotection. Curr Opin Cell Biol. 2011; 23:198-206

**Martines de Brito, Scorrano L**. Mitofusin 2 tethers endoplasmic reticulum to mitochondria. Nature. 2008; 456:605-610

**Martinou JC, Youle RJ.** Which came first, the cytochrome c release or the mitochondrial fission? Cell Death Differ. 2006; 13:1291-1295

**Masri FA, Comhair SA, Koeck T, Xu W, Janocha A, Ghosh S, Dweik RA, Golish J, Kinter M, Stuehr DJ, Erzurum SC, Aulak KS.** Abnormalities in nitric oxide and its derivatives in lung cancer. Am J Respir Crit Care Med. 2005; 172:597-605

**McDonald ES, Randon KR, Knight A, Windebank AJ.** Cisplatin preferentially binds to DNA in dorsal root ganglion neurons in vitro and in vivo: a potential mechanism for neurotoxicity. Neurobiol Dis. 2005; 18:305-313

**McWhinney SR, Goldberg RM, McLeod HL.** Platinum neurotoxicity pharmacogenetics. Mol Cancer Ther. 2009; 8:10-6

**Michaud WA, Nichols AC, Mroz EA, Faquin WC, Clark JR, Begum S, Westra WH, Wada H, Busse PM, Ellisen LW, Rocco JW**. Bcl-2 blocks cisplatin-induced apoptosis and predicts poor outcome following chemoradiation treatment in advanced oropharyngeal squamous cell carcinoma. Clin Cancer Res. 2009; 15:1645-1654

**Michels J, Vitale I, Galluzzi L, Adam J, Olaussen KA, Kepp O, Senovilla L, Talhaoui I, Guegan J, Enot DP, Talbot M, Robin A, Girard P, Oréar C, Lissa D, et al.** Cisplatin resistance associated with PARP hyperactivation. Cancer Res. 2013; 73:2271-2280

**Michels J, Adam J, Goubar A, Obrist F, Damotte D, Robin A, Alifano M, Vitale I, Olaussen KA, Girard P, Cremer I, Castedo M, Soria JC, Kroemer G.** Negative prognostic value of high levels of intracellular poly(ADP-ribose) in non-small cell lung cancer. Ann Oncol. 2015; 26:2470-2477

**Moldoveanu T, Follis AV, Kriwacki RW, Green DR.** Many players in BCL-2 family affairs. Trends Biochem Sci. 2014; 39:101-111

**Montell C.** The TRP superfamily of cation channels. Sci STKE. 2005; 2005:re3

**Morciano G, Giorgi C, Bonora M, Punzetti S, Pavasini R, Wieckowski MR, Campo G, Pinton P.** Molecular identity of the mitochondrial permeability transition pore and its role in ischemia-reperfusion injury. J Mol Cell Cardiol. 2015; 78:142-153

**Morciano G, Marchi S, Morganti C, Sbano L, Bittremieux M, Kerkhofs M, Corricelli M, Danese A, Karkucinska-Wieckowska A, Wieckowski MR, Bultynck G, Giorgi C, Pinton P**. Role of mitochondria-associated ER membranes in calcium regulation in cancer-specific settings. Neoplasia. 2018; 20:510-523

**Moreno-Smith M, Halder JB, Meltzer PS, Gonda TA, Mangala LS, Rupaimoole R, Lu C, Nagaraja AS, Gharpure KM, Kang Y, Rodriguez- Aguayo C, Vivas-Mejia PE, Zand B, Schmandt R, Wang H, et al.** ATP11B mediates platinum resistance in ovarian cancer. J Clin Invest. 2013; 123:2119-2130

**Mukherjea, D, Jajoo S, Kaur T, Sheehan K E, Ramku V, Rybak LP.** Transtympanic administration of short interfering (si)RNA for the NOX3 isoform of NADPH oxidase protects against cisplatin-induced hearing loss in the rat. Antioxid. Redox Signal. 2010; 13:589–598

**Murdoch C, Muthana M, Coffelt SB, Lewis CE.** The role of myeloid cells in the promotion of tumour angiogenesis. Nat Rev Cancer. 2008; 8:618-631

**Muscella A, Calabriso N, De Pascali SA, Urso L, Ciccarese A, Fanizzi FP, Migoni D, Marsigliante S.** New platinum(II) complexes containing both an O,O'-chelated acetylacetonate ligand and a sulfur ligand in the platinum coordination sphere induce apoptosis in HeLa cervical carcinoma cells. Biochem Pharmacol. 2007; 74:28-40

**Muscella A, Calabriso N, Fanizzi FP, De Pascali SA, Urso L, Ciccarese A, Migoni D, Marsigliante S.** [Pt(O,O'-acac)(gamma-acac)(DMS)], a new Pt compound exerting fast cytotoxicity in MCF-7 breast cancer cells via the mitochondrial apoptotic pathway. Br J Pharmacol. 2008; 153:34-49. Erratum in: Br J Pharmacol. 2008; 153:175

**Muscella A, Calabriso N, Vetrugno C, Urso L, Fanizzi FP, De Pascali SA, Marsigliante S.** Sublethal concentrations of the platinum(II) complex [Pt(O,O'-acac)(gamma-acac)(DMS)] alter the motility and induce anoikis in MCF-7 cells. Br J Pharmacol. 2010; 60:1362-1377

**Muscella A, Calabriso N, Vetrugno C, Fanizzi FP, De Pascali SA, Storelli C, Marsigliante S.** The platinum (II) complex [Pt(O,O'-acac)(γ-acac)(DMS)] alters the intracellular calcium homeostasis in MCF-7 breast cancer cells. Biochem Pharmacol. 2011; 81:91-103

**Muscella A, Vetrugno C, Migoni D, Biagioni F, Fanizzi FP, Fornai F, De Pascali SA, Marsigliante S.** Antitumor activity of [Pt(O,O'-acac)(γ-acac)(DMS)] in mouse xenograft model of breast cancer. Cell Death Dis. 2014; 5:e1014

**Muscella A, Vetrugno C, Biagioni F, Calabriso N, Calierno MT, Fornai F, De Pascali SA, Marsigliante S, Fanizzi FP.** Antitumour and antiangiogenic activities of [Pt(O,O'-acac)(γ-acac)(DMS)] in a xenograft model of human renal cell carcinoma. Br J Pharmacol. 2016; 173:2633-2644

**Muscella A, Vetrugno C, Cossa LG, Antonaci G, De Nuccio F, De Pascali SA, Fanizzi FP, Marsigliante S.** *In vitro* and *in vivo* antitumor activity of [Pt(O,O'-acac)(γ-acac)(DMS)] in malignant pleural mesothelioma. PLoS One. 2016; 11:e0165154

**Muscella A, Vetrugno C, Cossa LG, Antonaci G, Barca A, De Pascali SA, Fanizzi FP, Marsigliante S.** Apoptosis by [Pt(O,O'-acac)(γ-acac)(DMS)] requires PKC-δ mediated p53 activation in malignant pleural mesothelioma. PLoS One. 2017; 12:e0181114

**Nakamura Y, Yasuoka H, Tsujimoto M, Yoshidome K, Nakahara M, Nakao K, Nakamura M, Kakudo K.** Nitric oxide in breast cancer: induction of vascular endothelial growth factor-C and correlation with metastasis and poor prognosis. Clin Cancer Res. 2006; 12:1201-1207

**Nakayama K, Kanzaki A, Terada K, Mutoh M, Ogawa K, Sugiyama T, Takenoshita S, Itoh K, Yaegashi N, Miyazaki K, Neamati N, Takebayashi Y.** Prognostic value of the Cu-transporting ATPase in ovarian carcinoma patients receiving cisplatin-based chemotherapy. Clin Cancer Res. 2004; 10:2804-2811

**Nguyen CT, Weisenberger DJ, Velicescu M, Gonzales FA, Lin JC, Liang G, Jones PA.** Histone H3-lysine 9 methylation is associated with aberrant gene silencing in cancer cells and is rapidly reversed by 5-aza-2'-deoxycytidine. Cancer Res. 2002; 62:6456-6461

**Nicholls DG**. Mitochondrial calcium function and dysfunction in the central nervous system. Biochim Biophys Acta. 2009; 1787:1416-1424

**O'Neill KL, Huang K, Zhang J, Chen Y, Luo X.** Inactivation of prosurvival Bcl-2 proteins activates Bax/Bak through the outer mitochondrial membrane. Genes Dev. 2016; 30:973-988

**O'Rourke B.** Pathophysiological and protective roles of mitochondrial ion channels. J Physiol. 2000; 529 Pt 1:23-36

**Oakes SA, Scorrano L, Opferman JT, Bassik MC, Nishino M, Pozzan T, Korsmeyer SJ.** Proapoptotic BAX and BAK regulate the type 1 inositol trisphosphate receptor and calcium leak from the endoplasmic reticulum. Proc Natl Acad Sci U S A. 2005; 102:105-110

**Oberoi HS, Nukolova NV, Kabanov AV, Bronich TK.** Nanocarriers for delivery of platinum anticancer drugs. Adv Drug Deliv Rev. 2013; 65:1667-1685

**Ohsumi Y.** Historical landmarks of autophagy research. Cell Res. 2014; 24:9-23

**Okon IS, Zou MH.** Mitochondrial ROS and cancer drug resistance: Implications for therapy. Pharmacol Res. 2015; 100:170-174

**Olaussen KA, Dunant A, Fouret P, Brambilla E, André F, Haddad V, Taranchon E, Filipits M, Pirker R, Popper HH, Stahel R, Sabatier L, Pignon JP, Tursz T, Le Chevalier et al**. DNA repair by ERCC1 in non-small-cell lung cancer and cisplatin-based adjuvant chemotherapy. N Engl J Med. 2006; 355:983-991

**Ostrand-Rosenberg S, Sinha P.** Myeloid-derived suppressor cells: linking inflammation and cancer. J Immunol. 2009; 182:4499-4506

**Pacher P, Beckman JS, Liaudet L.** Nitric oxide and peroxynitrite in health and disease. Physiol Rev. 2007; 87:315-424

**Padányi R, Pászty K, Hegedűs L, Varga K, Papp B, Penniston JT, Enyedi Á.** Multifaceted plasma membrane Ca(2+) pumps: From structure to intracellular Ca(2+) handling and cancer. Biochim Biophys Acta. 2016; 1863:1351-1363

**Palmer AE, Jin C, Reed JC, Tsien RY.** Bcl-2-mediated alterations in endoplasmic reticulum Ca2+ analyzed with an improved genetically encoded fluorescent sensor. Proc Natl Acad Sci U S A. 2004; 101:17404-17409

**Pan MR, Hsu MC, Chen LT, Hung WC.** Orchestration of H3K27 methylation: mechanisms and therapeutic implication. Cell Mol Life Sci. 2018; 75:209-223

**Parkash J, Asotra K**. Calcium wave signaling in cancer cells. Life Sci. 2010; 87:587-595

**Pászty K, Antalffy G, Hegedüs L, Padányi R, Penheiter AR, Filoteo AG, Penniston JT, Enyedi A.** Cleavage of the plasma membrane Ca+ATPase during apoptosis. Ann N Y Acad Sci. 2007; 1099:440-450

**Piccolini VM, Bottone MG, Bottiroli G, De Pascali SA, Fanizzi FP, Bernocchi G.** Platinum drugs and neurotoxicity: effects on intracellular calcium homeostasis. Cell Biol Toxicol. 2013; 29:339-353

**Piccolini VM, Esposito A, Dal Bo V, Insolia V, Bottone MG, De Pascali SA, Fanizzi FP, Bernocchi G.** Cerebellum neurotransmission during postata development: [Pt(O,O'-acac)(γ-acac)(DMS)] vs cisplatin and neurotoxicity. Int J Dev Neurosci. 2015; 40:24-34

**Pihán P, Carreras-Sureda A, Hetz C.** BCL-2 family: integrating stress responses at the ER to control cell demise. Cell Death Differ. 2017; 24:1478-1487

**Pinton P, Ferrari D, Magalhães P, Schulze-Osthoff K, Di Virgilio F, Pozzan T, Rizzuto R.** Reduced loading of intracellular Ca(2+) stores and downregulation of capacitative Ca(2+) influx in Bcl-2-overexpressing cells. J Cell Biol. 2000; 148:857-862

**Pinton P, Ferrari D, Rapizzi E, Di Virgilio F, Pozzan T, Rizzuto R.** The Ca2+ concentration of the endoplasmic reticulum is a key determinant of ceramide-induced apoptosis: significance for the molecular mechanism of Bcl-2action. EMBO J. 2001; 20:2690-2701

**Pivovarova NB, Andrews SB.** Calcium-dependent mitochondrial function and dysfunction in neurons. S J. 2010; 277:3622-3636

**Podratz JL, Lee H, Knorr P, Koehler S, Forsythe S, Lambrecht K, Arias S, Schmidt K, Steinhoff G, Yudintsev G, Yang A, Trushina E, Windebank A.** Cisplatin induces mitochondrial deficits in Drosophila larval segmental nerve. Neurobiol Dis. 2017; 97:60-69

**Polster BM, Basanez G, Etxebarria A, Hardwick JM, Nicholls DG.** Calpain I induces cleavage and release of apoptosis-inducing factor from isolated mitochondria. J Biol Chem. 2005; 280:6447-6454

**Portela A, Esteller M.** Epigenetic modifications and human disease. Nat Biotechnol. 2010; 28:1057-1068

**Prokai L, Yan LJ, Vera-Serrano JL, Stevens SM Jr, Forster MJ.** Mass spectrometry-based survey of age-associated protein carbonylation in rat brain mitochondria. J Mass Spectrom. 2007; 42:1583-1589

**Qian BZ, Pollard JW.** Macrophage diversity enhances tumor progression and metastasis. Cell. 2010; 141:39-51

**Ramesh G, Reeves WB**. TNF-alpha mediates chemokine and cytokine expression and renal injury in cisplatin nephrotoxicity. J Clin Invest. 2002; 110:835-842

**Rao RS, Møller IM.** Pattern of occurrence and occupancy of carbonylation sites in proteins. Proteomics. 2011; 11:4166-73

**Rasola A, Bernardi P.** Mitochondrial permeability transition in Ca(2+)-dependent apoptosis and necrosis. Cell Calcium. 2011; 50:222-233

**Rasola A, Bernardi P.** The mitochondrial permeability transition pore and its adaptive responses in tumor cells. Cell Calcium. 2014; 56:437-445

**Ray Chaudhuri A, Nussenzweig A.** The multifaceted roles of PARP1 in DNA repair and chromatin remodelling. Nat Rev Mol Cell Biol. 2017; 18:610-621

**Reed E**. Platinum-DNA adduct, nucleotide excision repair and platinum based anti-cancer chemotherapy. Cancer Treat Rev. 1998; 24:331-344

**Reers M, Smiley ST, Mottola-Hartshorn C, Chen A, Lin M, Chen LB.** Mitochondrial membrane potential monitored by JC-1 dye. Methods Enzymol. 1995; 260:406-417

**Reisner PD, Brandt PC, Vanaman TC.** Analysis of plasma membrane Ca(2+)-ATPase expression in control and SV40-transformed human fibroblasts. Cell Calcium. 1997; 21:53-62

**Ren A, Yan G, You B, Sun J.** Down-regulation of mammalian sterile 20-like kinase 1 by heat shock protein 70 mediates cisplatin resistance in prostate cancer cells. Cancer Res. 2008; 68:2266-2274

**Ren D, Tu HC, Kim H, Wang GX, Bean GR, Takeuchi O, Jeffers JR, Zambetti GP, Hsieh JJ, Cheng EH.** BID, BIM, and PUMA are essential for activation of the BAX- and BAK-dependent cell death program. Science. 2010; 330:1390-1393

**Rizzuto R, Pozzan T.** When calcium goes wrong: genetic alterations of a ubiquitous signaling route. Nat Genet. 2003; 34:135-341

**Rizzuto R, De Stefani D, Raffaello A, Mammucari C.** Mitochondria as sensors and regulators of calcium signalling. Nat Rev Mol Cell Biol. 2012; 13:566-578

**Roberts NB, Wadajkar AS, Winkles JA, Davila E, Kim AJ, Woodworth GF.** Repurposing platinum-based chemotherapies for multi-modal treatment of glioblastoma. Oncoimmunology. 2016; 5:e1208876

**Roos WP, Thomas AD, Kaina B.** DNA damage and the balance between survival and death in cancer biology. Nat Rev Cancer. 2016; 16:20-33

**Rosenberg B, Vancamp L, Krigas T**. Inhibition of cell division in escherichia coli by electrolysis products from a platinum electrode. Nature. 1965; 205:698-699

**Ruggiero A, Trombatore G, Triarico S, Arena R, Ferrara P, Scalzone M, Pierri F, Riccardi R.** Platinum compounds in children with cancer: toxicity and clinical management. Anti-Cancer Drugs. 2013; 24:1007-1019

**Rybak, LP, Husain K, Morris C, Whitworth C, Somani S.** Effect of protective agents against cisplatin ototoxicity. Am. J. Otol. 2000; 21:513-520

**Saito K, Uzawa K, Endo Y, Kato Y, Nakashima D, Ogawara K, Shiba M, Bukawa H, Yokoe H, Tanzawa H.** Plasma membrane Ca2+ ATPase isoform 1 down-regulated in human oral cancer. Oncol Rep. 2006; 15:49-55

**Sakahira H, Enari M, Nagata S**. Cleavage of CAD inhibitor in CAD activation and DNA degradation during apoptosis. Nature. 2015; 526:728

**Sakamoto M, Kondo A, Kawasaki K, Goto T, Sakamoto H, Miyake K, Koyamatsu Y, Akiya T, Iwabuchi H, Muroya T, Ochiai K, Tanaka T, Kikuchi Y, Tenjin Y.** Analysis of gene expression profiles associated with cisplatin resistance in human ovarian cancer cell lines and tissues using cDNA microarray. Hum Cell. 2001; 14:305-315

**Samimi G, Safaei R, Katano K, Holzer AK, Rochdi M, Tomioka M, Goodman M, Howell SB.** Increased expression of the copper efflux transporter ATP7A mediates resistance to cisplatin, carboplatin, and oxaliplatin in ovarian cancer cells. Clin Cancer Res. 2004; 10:4661-4669

**Sassano ML, van Vliet AR, Agostinis P.** Mitochondria-associated membranes as networking platforms and regulators of cancer cell fate. Front Oncol 2017; 7:174

**Satheesh NJ and Büsselberg D.** The role of intracellular calcium for the development and treatment of neuroblastoma. Cancers. 2015; 7:823-848

**Savill J, Fadok V.** Corpse clearance defines the meaning of cell death. Nature. 2000; 407:784-788

**Schiewer MJ, Knudsen KE.** Transcriptional roles of PARP1 in cancer. Mol Cancer Res. 2014; 12:1069-1080

**Schreiber RD, Old LJ, Smyth MJ.** Cancer immunoediting: integrating immunity's roles in cancer suppression and promotion. Science. 2011; 331:1565-1570

**Schwab BL, Guerini D, Didszun C, Bano D, Ferrando- E, Fava E, Tam J, Xu D, Xanthoudakis S, Nicholson DW, Carafoli E, Nicotera P.** Cleavage of plasma membrane calcium pumps by caspases: a link between apoptosis and necrosis. Cell Death Differ. 2002; 9:818-831

**Schwaller B.** Cytosolic Ca2+ buffers. Cold Spring Harb Perspect Biol. 2010; 2:a004051

**Scorrano L, Oakes SA, Opferman JT, Cheng EH, Sorcinelli MD, Pozzan T, Korsmeyer SJ.** BAX and BAK regulation of endoplasmic reticulum Ca2+: a control point for apoptosis. Science. 2003; 300:135-139

**Scott FL, Stec B, Pop C, Dobaczewska MK, Lee JJ, Monosov E, Robinson H, Salvesen GS, Schwarzenbacher R, Riedl SJ.** The Fas-FADD death domain complex structure unravels signalling by receptor clustering. Nature. 2009; 457:1019-1022

**Seo JH, Ahn Y, Lee SR, Yeol Yeo C, Chung Hur K.** The major target of the endogenously generated reactive oxygen species in response to insulin stimulation is phosphatase and tensin homolog and not phosphoinositide-3 kinase (PI-3 kinase) in the PI-3 kinase/Akt pathway. Mol Biol Cell. 2005; 16:348-357

**Shalini S, Dorstyn L, Dawar S, Ku S**. Old, new and emerging functions of caspases. Cell Death Differ. 2015; 22:526-539

**Shamas-Din A, Kale J, Leber B, Andrews DW.** Mechanisms of action of Bcl-2 family proteins. Cold Spring Harb Perspect Biol. 2013; 5:a008714

**Sheth S, Mukherjea D, Rybak LP, Ramkumar V**. Mechanisms of Cisplatin-Induced Ototoxicity and Otoprotection. Front Cell Neurosci. 2017; 11:338

**Shojaei F, Ferrara N.** Refractoriness to antivascular endothelial growth factor treatment: role of myeloid cells. Cancer Res. 2008; 68:5501-5504

**Sica A, Bronte V.** Altered macrophage differentiation and immune dysfunction in tumor development. J Clin Invest. 2007; 117:1155-1166

**Singh P, Ravanan P, Talwar P.** Death Associated Protein Kinase 1 (DAPK1): A Regulator of Apoptosis and Autophagy. Front Mol Neurosci. 2016; 9:46

**Socco S, Bovee RC, Palczewski MB, Hickok JR, Thomas DD.** Epigenetics: The third pillar of nitric oxide signaling. Pharmacol Res. 2017; 121:52-58

**Sosa V, Moliné T, Somoza R, Paciucci R, Kondoh H, LLeonart ME.** Oxidative stress and cancer: an overview. Ageing Res Rev. 2013; 12:376-390

**Sprauten M, Darrah TH, Peterson DR, Campbell ME, Hannigan RE, Cvancarova M, Beard C, Haugnes HS, Fosså SD, Oldenburg J, Travis LB.** Impact of long-term serum platinum concentrations on neuro- and ototoxicity in Cisplatin-treated survivors of testicular cancer. J Clin Oncol. 2012; 30:300-307

**Stadtman ER.** Protein oxidation in aging and age-related diseases. Ann N Y Acad Sci. 2001; 928:22-38

**Stathopulos PB, Schindl R, Fahrner M, Zheng L, Gasmi-Seabrook GM, Muik M, Romanin C, Ikura M.** STIM1/Orai1 coiled-coil interplay in the regulation of store-operated calcium entry. Nat Commun. 2013; 4:2963

**Stewart TA, Yapa KT, Monteith GR.** Altered calcium signaling in cancer cells. Biochim Biophys Acta. 2015; 1848:2502-2511

**Sun L, Wang H, Wang Z, He S, Chen S, Liao D, Wang L, Yan J, Liu W, Lei X, Wang X.** Mixed lineage kinase domain-like protein mediates necrosis signalling downstream of RIP3 kinase. Cell. 2012; 148:213-227

**Sun S, Li F, Gao X, Zhu Y, Chen J, Zhu X, Yuan H, Gao D**. Calbindin-D28K inhibits apoptosis in dopaminergic neurons by activation of the PI3-kinase-Akt signaling pathway. Neuroscience. 2011; 199:359-367

**Susin SA, Lorenzo HK, Zamzami N, Marzo I, Snow BE, Brothers GM, Mangion J, Jacotot E, Costantini P, Loeffler M, Larochette N, Goodlett DR, Aebersold R, Siderovski DP, Penninger JM, et al.** Molecular characterization of mitochondrial apoptosis-inducing factor. Nature. 1999; 397:441-446

**Syntichaki P, Tavernarakis N.** The biochemistry of neuronal necrosis: rogue biology? Nat Rev Neurosci. 2003; 4:672-684

**Szabadkai G, Bianchi K, Várnai P, De Stefani D, Wieckowski MR, Cavagna D, Nagy AI, Balla T, Rizzuto R**. Chaperone-mediated coupling of endoplasmic reticulum and mitochondrial Ca2+ channels. J Cell Biol. 2006; 175:901-911

**Tait SW, Green DR**. Mitochondria and cell death: outer membrane permeabilization and beyond. Nat Rev Mol Cell Biol. 2010; 11:621-632

**Tajeddine N, Galluzzi L, Kepp O, Hangen E, Morselli E, Se illa L, Araujo N, Pinna G, Larochette N, Zamzami N, Modjtahedi N, Harel-Bellan A, Kroemer G.** Hierarchical involvement of Bak, VDAC1 and Bax in cisplatin-induced cell death. Oncogene. 2008; 27:4221-4232

**Taliano RJ, Lu S, Singh K, Mangray S, Tavares R, Noble L, Resnick MB, Yakirevich E.** Calretinin expression in high-grade invasive ductal carcinoma of the breast is associated with basal-like subtype and unfavorable prognosis. Hum Pathol. 2013; 44:2743-2750

**Tallis M, Morra R, Barkauskaite E, Ahel I.** Poly(ADP-ribosyl)ation in regulation of chromatin structure and the DNA damage response. Chromosoma. 2014; 123:79-90

**Tattersall MN**. Ovarian cancer chemotherapy: carboplatin as standard. Lancet. 2002; 360:500-501

**Thomas DD, Heinecke JL, Ridnour LA, Cheng RY, Kesarwala AH, Switzer CH, McVicar DW, Roberts DD, Glynn S, Fukuto JM, Wink DA, Miranda KM.** Signaling and stress: The redox landscape in NOS2 biology. Free Radic Biol Med. 2015; 87:204-22

**Timerbaev AR, Hartinger CG, Aleksenko SS, Keppler BK.** Interactions of antitumor metallodrugs with serum proteins: advances in characterization using modern analytical methodology. Chem Rev. 2006; 106:2224-2248

**Tobiume K, Matsuzawa A, Takahashi T, Nishitoh H, Morita K, Takeda K, Minowa O, Miyazono K, Noda T, Ichijo H.** ASK1 is required for sustained activations of JNK/p38 MAP kinases and apoptosis. EMBO Rep. 2001; 2:222-228

**Tojo T, Ushio-Fukai M, Yamaoka-Tojo M, Ikeda S, Patrushev N, Alexander RW.** Role of gp91phox (Nox2)-containing NAD(P)H oxidase in angiogenesis in response to hindlimb ischemia. Circulation. 2005; 111:2347-2355

**Tulub AA, Stefanov** VE. Cisplatin stops tubulin assembly into microtubules. A new insight into the mechanism of antitumor activity of platinum complexes. Int J Biol Macromol. 2001; 28:191-198

**Ushio-Fukai M, Nakamura Y**. Reactive oxygen species and angiogenesis: NADPH oxidase as target for cancer therapy. Cancer Lett. 2008; 266:37-52

**van Kempen LC, Ruiter DJ, van Muijen GN, Coussens LM.** The tumor microenvironment: a critical determinant of neoplastic evolution. Eur J Cell Biol. 2003; 82:539-548

**Vance JE.** Phospholipid synthesis and transport in mammalian cells. Traffic. 2015; 16:1-18

**Vanden Berghe T, Linkermann A, Jouan-Lanhouet S, Walczak H, Vandenabeele P.** Regulated necrosis: the expanding network of non-apoptotic cell death pathways. Nat Rev Mol Cell Biol. 2014; 15:135-1347

**Vandenabeele P, Galluzzi L, Vanden Berghe T, Kroemer G.** Molecular mechanisms of necroptosis: an ordered cellular explosion. Nat Rev Mol Cell Biol. 2010; 11:700-714

**Vannini F, Kashfi K, Nath N.** The dual role of iNOS in cancer. Redox Biol. 2015; 6:334-343

**Verhagen AM, Ekert PG, Pakusch M, Silke J, Connolly LM, Reid GE, Moritz RL, Simpson RJ, Vaux DL.** Identification of DIABLO, a mammalian protein that promotes apoptosis by binding to and antagonizing IAP proteins. Cell. 2000; 102:43-53

**Veskoukis AS, Tsatsakis AM, Kouretas D.** Dietary oxidative stress and antioxidant defense with an emphasis on plant extract administration. Cell Stress Chaperones. 2012; 17:11-21

**Vetrugno C, Muscella A, Fanizzi FP, Cossa LG, Migoni D, De Pascali SA, Marsigliante S.** Different apoptotic effects of [Pt(O,O'-acac)(γ-acac)(DMS)] and cisplatin on normal and cancerous human epithelial breast cells in primary culture. Br J Pharmacol. 2014; 171:5139-5153

**Vetter SW, Leclerc E.** Novel aspects of calmodulin target recognition and activation; Eu. J. of Biochem. 2003; 270:404-414

**Vitale I, Manic G, De Maria R, Kroemer G, Galluzzi L**. DNA damage in stem cells. Mol Cell. 2017; 66:306-319

**von Karstedt S, Montinaro A, Walczak H.** Exploring the TRAILs less travelled: TRAIL in cancer biology and therapy. Nat Rev Cancer. 2017; 17:352-366

**Waissbluth S, Chuang A, Del Valle Á, Cordova M.** Long term platinum-induced ototoxicity in pediatric patients. Int J Pediatr Otorhinolaryngol. 2018; 107:75-79

**Wajant H.** The Fas signaling pathway: more than a paradigm. Science. 2002; 296:1635-1636

**Wang D, Lippard SJ.** Cellular processing of platinum anticancer drugs. Nat Rev Drug Discov. 2005; 4:307-320

**Wang L, Liang C, Li F, Guan D, Wu X, Fu X, Lu A, Zhang G.** PARP1 in Carcinomas and PARP1 Inhibitors as Antineoplastic Drugs. Int J Mol Sci. 2017; 18

**Wang YY, Zhao R, Zhe H**. The emerging role of CaMKII in cancer. Oncotarget. 2015; 6:11725-11734

**White E.** The role for autophagy in cancer. J Clin Invest. 2015; 125:42-46

**Williams J, Lucas PC, Griffith KA, Choi M, Fogoros S, Hu YY, Liu JR.** Expression of Bcl-xL in ovarian carcinoma is associated with chemoresistance and recurrent disease. Gynecol Oncol. 2005; 96:287-295

**Wimmer C, Mees K, Stumpf P, Welsch U, Reichel O, Suckfull M.** Round window application of D-methionine, sodium thiosulfate, brainderived neurotrophic factor, and fibroblast growth factor-2 in cisplatin-induced ototoxicity. Otol. Neurotol. 2004; 25:33-40

**Winter C, Albers P.** Testicular germ cell tumors: pathogenesis, diagnosis and treatment. Nat Rev Endocrinol. 2011; 7:43-53

**Xu XY, Gou WF, Yang X, Wang GL, Takahashi H, Yu M, Mao XY, Takano Y, Zheng HC.** Aberrant SERCA3 expression is closely linked to pathogenesis, invasion, metastasis, and prognosis of gastric carcinomas. Tumour Biol. 2012; 33:1845-1854

**Xu Y, Wang C, Su J, Xie Q, Ma L, Zeng L, Yu Y, Liu S, Li S, Li Z, Sun L.** Tolerance to endoplasmic reticulum stress mediates cisplatin resistance in human ovarian cancer cells by maintaining endoplasmic reticulum and mitochondrial homeostasis. Oncol Rep. 2015; 34:3051-3060

**Yamaguchi S, Sakurada S, Nagumo M.** Role of intracellular SOD in protecting human leukemic and cancer cells against superoxide and radiation. Free Radic Biol Med. 1994; 17:389-395

**Yamamoto K, Okamoto A, Isonishi S, Ochiai K, Ohtake Y**. Heat shock protein 27 was up-regulated in cisplatin resistant human ovarian tumor cell line and associated with the cisplatin resistance. Cancer Lett. 2001; 168:173-181

**Yamasaki M, Makino T, Masuzawa T, Kurokawa Y, Miyata H, Takiguchi S, Nakajima K, Fujiwara Y, Matsuura N, Mori M, Doki Y**. Role of multidrug resistance protein 2 (MRP2) in chemoresistance and clinical outcome in oesophageal squamous cell carcinoma. Br J Cancer. 2011; 104:707-713

**Yan F, Liu JJ, Ip V, Jamieson SM, McKeage MJ.** Role of platinum DNA damage-induced transcriptional inhibition in chemotherapy-induced neuronal atrophy and peripheral neurotoxicity. J Neurochem. 2015; 135:1099-1112

**Yokoyama Y, Hieda M, Nishioka Y, Matsumoto A, Higashi S, Kimura H, Yamamoto H, Mori M, Matsuura S, Matsuura N.** Cancer-associated upregulation of histone H3 lysine 9 trimethylation promotes cell motility in vitro and drives tumor formation in vivo. Cancer Sci. 2013; 104:889-895

**You Y, Cheng AC, Wang MS, Jia RY, Sun KF, Yang Q, Wu Y, Zhu D, Chen S, Liu MF, Zhao XX, Chen XY.** The suppression of apoptosis by α-herpesvirus. Cell Death Dis. 2017; 8:e2749

**Youle RJ, Strasser A.** The BCL-2 protein family: opposing activities that mediate cell death. Nat Rev Mol Cell Biol. 2008; 9:47-59

**Yu H, Su J, Xu Y, Kang J, Li H, Zhang L, Yi H, Xiang X, Liu F, Sun L.** p62/SQSTM1 involved in cisplatin resistance in human ovarian cancer cells by clearing ubiquitinated proteins. Eur J Cancer. 2011; 47:1585-1594

**Yu SW, Wang H, Poitras MF, Coombs C, Bowers WJ, Federoff HJ, Poirier GG, Dawson TM, Dawson VL.** Mediation of poly(ADP-ribose) polymerase-1-dependent cell death by apoptosis-inducing factor. Science. 2002; 297:259-263

**Zaidi A.** Plasma membrane Ca-ATPases: Targets of oxidative stress in brain aging and neurodegeneration. World J Biol Chem. 2010; 1:271-280

**Zhang DW, Shao J, Lin J, Zhang N, Lu BJ, Lin SC, Dong MQ, Han J.** RIP3, an energy metabolism regulator that switches TNF-induced cell death from apoptosis to necrosis. Science. 2009; 325:332-336

**Zhang T, Cooper S, Brockdorff N.** The interplay of histone modifications - writers that read. EMBO Rep. 2015; 16:1467-1481

**Zhivotovsky B, Orrenius S.** Calcium and cell death mechanisms: a perspective from the cell death community. Cell Calcium. 2011; 50:211-221

**Zitvogel L, Galluzzi L, Kepp O, Smyth MJ, Kroemer G.** Type I interferons in anticancer immunity. Nat Rev Immunol. 2015; 15:405-414

**Zuccolo E, Bottino C, Diofano F, Poletto V, Codazzi AC, Mannarino S, Campanelli R, Fois G, Marseglia GL, Guerra G, Montagna D, Laforenza U, Rosti V, Massa M, Moccia F.** Constitutive Store-Operated Ca(2+) Entry Leads to Enhanced Nitric Oxide Production and Proliferation in Infantile Hemangioma-Derived Endothelial Colony-Forming Cells. Stem Cells Dev. 2016; 25:301-319

# List  of
# Original Manuscripts

SOURCE DATA    TRANSPARENT PROCESS

THE **EMBO** JOURNAL

# Metabolic vulnerability of cisplatin-resistant cancers

Florine Obrist[1,2,3,4,5,6], Judith Michels[1,2,3,4,5,6,7], Sylvere Durand[2,3,4,5,6], Alexis Chery[2,3,4,5,6], Jonathan Pol[2,3,4,5,6] [iD], Sarah Levesque[1,2,3,4,5,6], Adrien Joseph[2,3,4,5,6], Valentina Astesana[2,3,4,5,6,8], Federico Pietrocola[2,3,4,5,6], Gen Sheng Wu[9], Maria Castedo[2,3,4,5,6,*,†] [iD] & Guido Kroemer[2,3,4,5,6,10,11,**,†] [iD]

## Abstract

Cisplatin is the most widely used chemotherapeutic agent, and resistance of neoplastic cells against this cytoxicant poses a major problem in clinical oncology. Here, we explored potential metabolic vulnerabilities of cisplatin-resistant non-small human cell lung cancer and ovarian cancer cell lines. Cisplatin-resistant clones were more sensitive to killing by nutrient deprivation *in vitro* and *in vivo* than their parental cisplatin-sensitive controls. The susceptibility of cisplatin-resistant cells to starvation could be explained by a particularly strong dependence on glutamine. Glutamine depletion was sufficient to restore cisplatin responses of initially cisplatin-resistant clones, and glutamine supplementation rescued cisplatin-resistant clones from starvation-induced death. Mass spectrometric metabolomics and specific interventions on glutamine metabolism revealed that, in cisplatin-resistant cells, glutamine is mostly required for nucleotide biosynthesis rather than for anaplerotic, bioenergetic or redox reactions. As a result, cisplatin-resistant cancers became exquisitely sensitive to treatment with antimetabolites that target nucleoside metabolism.

See also: **N Guidi & VD Longo**

## Introduction

The platinum derivative cis-diamminedichloroplatinum(II) (CDDP), best known as cisplatin, is used for the antineoplastic treatment of patients affected by bladder, head and neck, lung, ovarian, uterine, cervical and germ cell cancers (Kelland, 2007). Intravenous injection of CDDP is associated with high rates of clinical responses. However, with the notable exception of germ cell tumors (Winter & Albers, 2011), neoplastic cells exposed to CDDP ineluctably acquire resistance to the cytostatic and cytotoxic effects of the drug, and eventually resume proliferation, thus causing fatal relapse (Galluzzi *et al*, 2014). Hence, chemoresistance (be it intrinsic or acquired) constitutes the most prominent obstacle against the clinical use of CDDP.

As a result of the reduced cytoplasmic concentration of chloride (as opposed to sodium) ions, intracellular CDDP is rapidly "aquated", hence acquiring electrophilic reactivity. Aquated CDDP binds with high affinity to nuclear DNA, in particular to nucleophilic N7 sites on purines, thereby activating the DNA damage response (Wang & Lippard, 2005). Originally, the anticancer effects of CDDP were fully explained by its capacity to induce unrepairable DNA lesions, thereby either triggering an irreversible proliferative arrest known as cellular senescence (which causes cytostasis) or igniting the mitochondrial pathway of apoptosis (which leads to cytotoxicity; Galluzzi *et al*, 2012a). However, CDDP also physically interacts with cytoplasmic nucleophiles, including mitochondrial DNA (mtDNA) and multiple proteins, thereby (i) stimulating oxidative and reticular stress responses (Martins *et al*, 2011); (ii) igniting a lethal signaling pathway that involves the pro-apoptotic BCL-2 family members BAK1 and BAX, as well as the mitochondrion-sessile

1 Faculty of Medicine, University of Paris Sud, Kremlin-Bicêtre, France
2 Metabolomics and Cell Biology Platforms, Gustave Roussy Cancer Campus, Villejuif, France
3 Centre de Recherche des Cordeliers, Equipe 11 labellisée Ligue Nationale Contre le cancer, Paris, France
4 Institut National de la Santé et de la Recherche Médicale, U1138, Equipe labellisée Ligue Nationale Contre le Cancer, Villejuif, France
5 Université Paris Descartes, Sorbonne Paris Cité, Paris, France
6 Université Pierre et Marie Curie, Paris, France
7 Department of Medical Oncology, Gustave Roussy Comprehensive Cancer Center, Villejuif Paris-Sud University, Villejuif, France
8 Department of Biology and Biotechnology L. Spallanzani, University of Pavia, Pavia, Italy
9 Departments of Oncology and Pathology, Molecular Therapeutics Program, Karmanos Cancer Institute, Wayne State University School of Medicine, Detroit, MI, USA
10 Pôle de Biologie, Hôpital Européen Georges Pompidou, AP-HP, Paris, France
11 Department of Women's and Children's Health, Karolinska University Hospital, Stockholm, Sweden
  *Corresponding author. Tel: +33 1 44 27 76 61; E-mail: marie.castedo-delrieu@gustaveroussy.fr
  **Corresponding author. Tel: +33 6 77 06 79 43; E-mail: kroemer@orange.fr
  †These authors contributed equally to this work

voltage-dependent anion channel 1 (VDAC1; Tajeddine *et al*, 2008); and (iii) activating the cytoplasmic pool of the tumor suppressor protein TP53 (Erster *et al*, 2004). The relative contribution of these cytoplasmic and nuclear pathways may be context-dependent.

Cells selected by CDDP-based chemotherapies *in vivo* or by constant exposure to low CDDP concentrations *in vitro* activate a variety of resistance mechanisms. Such alterations can (i) affect steps preceding the binding of CDDP to DNA (pre-target resistance; Hall *et al*, 2008; Ishida *et al*, 2010; Karekla *et al*, 2017), (ii) be directly related to DNA-CDDP adducts and their repair (on-target resistance; Ray Chaudhuri *et al*, 2016; Sourisseau *et al*, 2016), (iii) invalidate the lethal signaling pathway(s) ignited by CDDP-induced DNA damage (post-target resistance; Li *et al*, 2016), or (iv) affect molecular circuitries that are not directly linked to CDDP-elicited signals (off-target resistance; Huang *et al*, 2016; Leung *et al*, 2016). In addition, CDDP-resistant cells undergo a major rewiring in their metabolism, as revealed by changes in the ratio between the enzymes that generate active vitamin B6, pyridoxine kinase (PDXK), or destroy vitamin B6, pyridoxine phosphatase (PDXP; Galluzzi *et al*, 2012b) and an overactivation of the enzymatic activity of poly (ADP-ribose; PAR) polymerase (PARP; Galluzzi *et al*, 2014; Michels *et al*, 2013). Decreased PDXK expression and high PARP activation are not uniformly associated with CDDP resistance (meaning that they do not occur in all resistant clones), yet constitute clinically useful biomarkers that predict poor prognosis in non-small cell lung cancer (NSCLC; Galluzzi *et al*, 2012b; Michels *et al*, 2015).

The exact mechanisms that account for metabolic rewiring in CDDP resistance have not been elucidated. However, driven by the notion that such a reprogramming process occurs, we decided to explore the metabolic vulnerabilities of CDDP-resistant cells in a systematic fashion. Here, we reveal the fact that CDDP-resistant cells are particularly vulnerable to starvation-induced cell death, due to their particular dependency on glutamine. In CDDP-resistant cells, glutamine is mostly required for nucleoside biosynthesis rather than for bioenergetic metabolism. As a result, CDDP-resistant cancer cells become sensitive to chemotherapeutic antimetabolites that poison nucleotide metabolism. Hence, CDDP-resistant cancers become exquisitely susceptible to treatment by periodic fasting or specific antimetabolites.

## Results

### Cisplatin-resistant cancer cells are sensitive to starvation

To identify potential metabolic vulnerabilities linked to cisplatin (CDDP) resistance, we comparatively assessed cell death induction (indicated by a $DiOC_6(3)$-detectable loss of the mitochondrial transmembrane potential, $\Delta\Psi m$, alone or accompanied by a propidium iodide [PI]-detectable loss of plasma membrane integrity) in human A549 non-small cell lung cancer (NSCLC) cells that were either wild type (WT; i.e., parental) or CDDP-resistant (clones R2 and R4). These CDDP-resistant cells had been derived from WT cells by continuous culture in CDDP for several months (Michels *et al*, 2013). WT, R2 and R4 cells were exposed to a variety of microtubule and metabolic inhibitors. The largest differential susceptibility was observed when the cells were cultured in nutrient-free conditions (NF), that is, Earle's balanced salt solution (EBSS), which contains no nutrients with the exception of a minimal glucose level of 5.6 mM (Fig 1A). CDDP-resistant cells died in EBSS much more than CDDP-sensitive counterparts did (Fig 1A and B). Moreover, CDDP-resistant cells were more susceptible to cell death induction by microtubule inhibitors (paclitaxel, nocodazole, rotenone), caloric restriction mimetics (C646, spermidine, salicylate), the absence of glucose (or the inhibition of glucose phosphorylation by 2-deoxyglucose), and lipid-lowering medication (by means of lipid synthesis inhibitor 5-(tetradecyloxy)-2-furoic acid (TOFA) or the statin simvastatin; Fig 1A). No differences were found for inhibitors of oxidative phosphorylation (antimycin A, metformin, oligomycin), suggesting that the selective susceptibility to rotenone was related to its capacity to inhibit microtubule assembly rather than its inhibitory effects on respiratory chain complex 1 (Meisner & Sorensen, 1966). The susceptibility of cancer cells to starvation-induced cell death correlated with the accumulation of the PARP product PAR. Thus, CDDP-resistant clones with high PAR levels (R2, R3, R4, R5) were particularly sensitive to culture in EBSS, while the clone with low PAR level (R1) and parental WT cells were relatively resistant (Fig 1C and D). Inhibition of the enzymatic activity of PARP with three distinct agents (PJ-34, BMN-673 and ABT-888; Penning *et al*, 2009; Shen *et al*, 2013), leading to a strong reduction in intracellular PAR levels (Fig EV1A), failed to reverse the killing of R2 and R4 cells by culture in EBSS (Fig EV1B–D). This excludes the possibility that the hyperactivation of PARP would directly cause the selective vulnerability of such cells to starvation-induced death. Of note, knockdown of pro-apoptotic proteins from the BCL2 family (BAK, BAX, PUMA) reduced killing of R2 and R4 cells by EBSS, while knockdown of MCL1, which is anti-apoptotic (Kozopas *et al*, 1993; Michels *et al*, 2014b), accelerated killing by EBSS (Fig EV1E and F). These results suggest the involvement of the mitochondrial cell death pathway in starvation-induced cell death of CDDP-resistant cancer cells.

Importantly, the selective susceptibility of CDDP-resistant cells to EBSS was observed for other pairs of sensitive versus resistant human NSCLC lines such as H460, H1650 and mouse lung cancer line TC-1 (Fig 1E–G). We also evaluated the possibility to combine CDDP treatment with nutrient depletion. This combination exhibited an additive cell-killing potential, when applied to CDDP-sensitive A549 cells, yet failed to yield such effects on CDDP-resistant cells. Such cells succumbed to nutrient depletion alone, and this starvation-induced killing was not further enhanced by CDDP (Fig EV2A and B).

Considering the effect of nutrient depletion on CDDP-resistant cells *in vitro*, we tested whether the selective susceptibility of CDDP-resistant cells to nutrient depletion could be observed *in vivo* as well. Indeed, A549 R4 tumors developing in immuno-deficient mice reduced their growth in response to periodic starvation (24 h of fasting twice per week), while parental A549 tumors were not affected by this regimen (Fig 2A and B). Accordingly, periodic starvation was able to prolong the survival of mice bearing xenografted CDDP-resistant but not parental NSCLC (Fig 2C and D).

### Glutamine dependency of cisplatin-resistant cancer cells

Next, we attempted to determine which specific nutrients might rescue CDDP-resistant cancer cells from death occurring in EBSS.
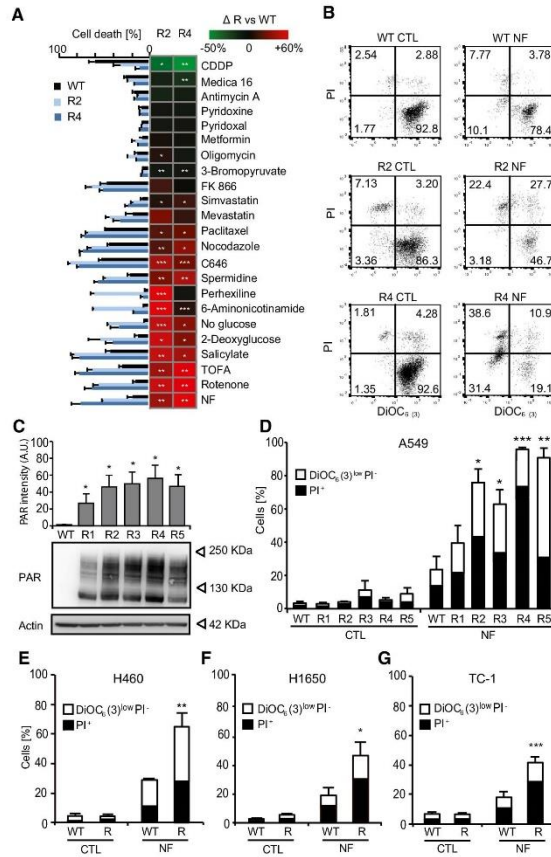
**Figure 1.  Starvation preferentially kills CDDP-resistant human A549 cancer cells.**

A, B   Parental A549 cells (WT) and two CDDP-resistant derivatives (R2 and R4) were maintained in control condition (CTL) or treated with CDDP (30 μM), MEDICA 16 (200 μM), antimycin A (100 μM), pyridoxine (2 mM), pyridoxal (2 mM), metformin (10 mM), oligomycin (10 μM), 3-bromopyruvate (200 μM), FK866 (500 nM), simvastatin (50 μM), mevastatin (20 μM), nocodazole (200 nM), paclitaxel (100 nM), C646 (50 μM), spermidine (1 mM), perhexiline (10 μM), 6-aminonicotinamide (100 μM), 2-deoxyglucose (80 μM), salicylate (20 mM), TOFA (80 μM), rotenone (1 μM) or cultured in glucose-free or EBSS media (nutrient-free, NF) for 24–48 h. Thereafter, the cells were subjected to the flow cytometry-assisted measurement of cell death parameters upon co-staining with the vital dye propidium iodide (PI) and the mitochondrial membrane potential (Δψm)-sensing dye $DiOC_6(3)$ (mean ± SEM; three independent experiments). *$P < 0.05$, **$P < 0.01$, ***$P < 0.001$ (Student's $t$-test), in comparison with equally treated WT cells. Representative dot plots of cells cultured in nutrient-free (NF) conditions are shown in (B) (numbers refer to the percentage of cells found in each quadrant).

C   Parental WT A549 cell line and five CDDP-resistant (R1–R5) derivatives were cultured in normal growth medium and processed for the immunoblotting-based assessment of PAR-containing proteins. Actin levels were monitored to ensure equal loading of lanes. The densitometric analysis of PARylated proteins/actin ratio (upper panel; mean ± SEM, $n = 3$) and a representative immunoblot (lower panel) are shown. *$P < 0.05$ (Student's $t$-test), as compared to WT cells.

D–G   A549 (D), H460 (E), H1650 (F), and TC-1 (G) WT and R cells were cultured in normal growth medium (CTL) or nutrient-free medium (NF) for 24 h (D) or for 36 h (E, F). Thereafter, the cells were subjected to the flow cytometry-assisted measurement of cell death parameters upon co-staining with the vital dye propidium iodide (PI) and the mitochondrial membrane potential (Δψm)-sensing dye $DiOC_6(3)$. Data represent mean ± SEM of $n$ independent experiments ($n = 3$ in D, 4 in E, 5 in F, and 4 in G). *$P < 0.05$, **$P < 0.01$, ***$P < 0.001$ (Student's $t$-test), as compared to equally treated WT cells.

Source data are available online for this figure.
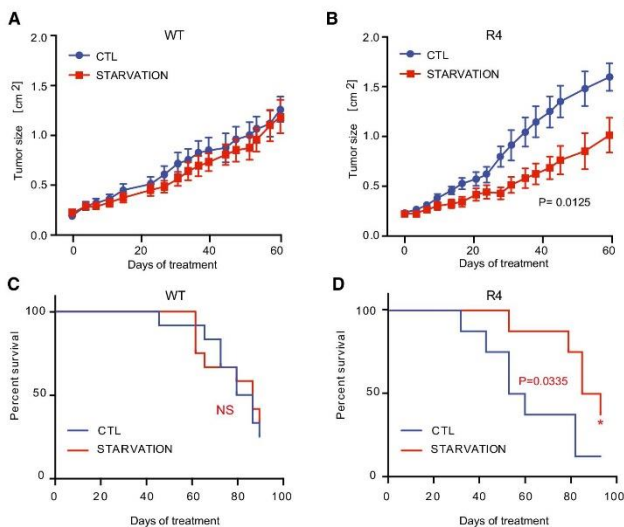
**Figure 2. Therapeutic effects of starvation on CDDP-resistant xenografts *in vivo*.**

A, B   WT A549 cell line (A) and its CDDP-resistant derivative R4 (B) were subcutaneously xenografted into athymic nu/nu mice (12 mice in WT CTL, 11 mice in WT NF, 8 mice in R4 CTL and R4 NF). When tumors became palpable, mice were fed *ad libitum* or underwent cycles of starvation (24 h, two times a week). Tumor growth was routinely monitored with a standard caliper and is reported as means ± SEM. *$P < 0.05$ (Wald test, type 2 ANOVA), as compared to mice fed *ad libitum*.

C, D   Kaplan–Meier survival curves of nude mice xenografted with A549 WT or CDDP-resistant R4 cells, and fed *ad libitum* or starved 24 h, two times a week (12 mice in WT CTL, 11 mice in WT NF, 8 mice in R4 CTL, and 8 mice in R4 NF). Starvation significantly prolongs survival of mice xenografted with CDDP-resistant R4 A549 cancer cells (log-rank test).

Glutamine (GLN) turned out to be the most effective agent to close-to fully suppress the death of R2 or R4 cells in EBSS (Fig 3A and B). Glutamate (GLU) had a smaller but still significant effect, while the cell-permeable α-ketoglutarate precursor, dimethyl α-ketoglutarate, exhibited rather partial effects. In contrast, glucose, amino acids, the cell-permeable pyruvate derivative, 3-methyl pyruvate, polyamines and glutathione-replenishing agents (glutathione ester or *N*-acetylcysteine) failed to reverse the lethal effects of EBSS (Fig 3A). The effects of GLN were obtained at relatively low doses (20 μM) at which GLU had no effects (Fig 3C). The rescue by GLN was observed in multiple CDDP-resistant human and mouse cancer cell lines (Fig 3C–F). These results underline the key role of glutamine in cell survival in the context of nutrient depletion. Of note, fasting of mice for 24 h (which reduced the growth of CDDP-resistant tumors, see above, Fig 2A and B) also led to a reduction in plasma GLN levels (Fig EV3A).

In the subsequent step, we determined whether GLN withdrawal from the medium would be sufficient to kill CDDP-resistant cells. While this was not the case, GLN depletion was sufficient to reestablish CDDP-induced killing of *a priori* CDDP-resistant cells. Thus, A549 R2 and R4 clones, as well as other CDDP-resistant cells (such as the NSCLC H460 R cell line, the NSCLC H1650 R cell line and the ovarian carcinoma TOV 112D R cell line), became susceptible to

CDDP-induced cell death when they were cultured in the absence of GLN (Figs 4A–J, and EV3B and C). In conclusion, it appears that the abundance of GLN has a major impact on the cytotoxicity of CDDP, in particular in cells that have been selected for CDDP resistance.

**Glutamine-fueled nucleoside synthesis in cisplatin resistance**

To understand the mechanism through which GLN rescues CDDP-resistant cells from starvation-induced death, we resorted to mass spectrometric metabolomics. We compared the levels of metabolites detectable in EBSS (i.e., in conditions of starvation, also referred as nutrient-free condition, NF) with those found in complete medium (control, CTL) or in EBSS supplemented with 2 mM GLN (NF + GLN). As expected (Zhang *et al*, 2017), GLN was particularly efficient in replenishing its amino acid derivatives alanine, asparagine and GLU, the GLU metabolite α-ketoglutarate, some intermediates of the Krebs cycle (fumarate, malate) and glutathione (written in red in Fig 5A). Of note, in normal culture conditions, resistant clones were characterized by a relative depletion of Krebs cycle intermediates (α-ketoglutarate, fumarate, malate, citrate/isocitrate, oxaloacetate/pyruvate) when compared to parental A549 cells (Figs 5B and EV4A). Driven by these observations, we explored the mechanisms through which GLN rescues
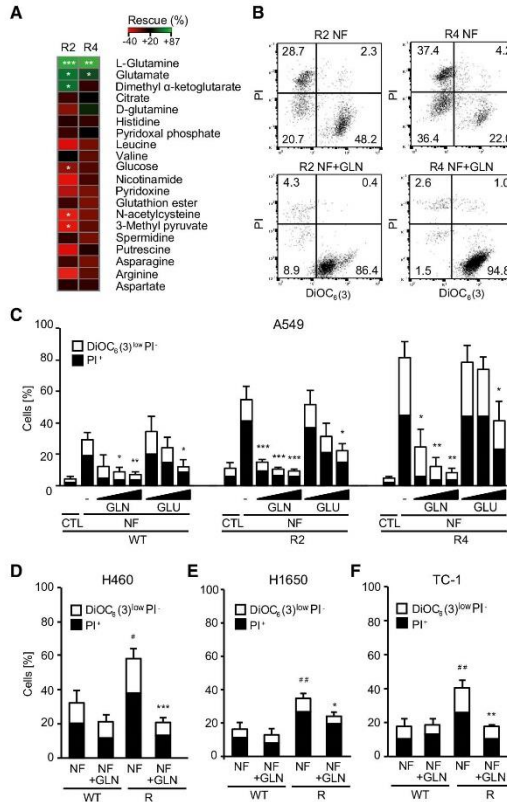
**Figure 3. Glutamine and glutamate sustain the survival of CDDP-resistant cells during starvation.**

A, B   CDDP-resistant A549 R2 and R4 cells were cultured for 24 h in EBSS in the absence or presence of the indicated nutrients (ʟ-glutamine (2 mM), glutamate (2 mM), dimethyl α-ketoglutarate (1 mM), citrate (1 mM), ᴅ-glutamine (2 mM), histidine (0.15 mM), pyridoxal phosphate (2 mM), leucine (0.1 mM), valine (0.45 mM), glucose (5.56 mM), nicotinamide (100 mM), pyridoxine (2 mM), glutathion ester (5 mM), N-acetylcysteine (10 mM), spermidine (30 µM), putrescine (100 uM), asparagine (0.05 mM), arginine (0.7 mM), aspartate (0.5 mM)), then processed for the cytofluorometric determination of cell death-related parameters. *P < 0.05, **P < 0.01, ***P < 0.001 (Student's t-test; n = 3), compared with cells of the same type exposed to EBSS alone. Rescue = (% of cells death in EBSS − % of cell death in EBSS supplemented with nutrient)/(% of cells death in EBSS) × 100. Representative dot plots of cells cultured in EBSS medium (nutrient-free, NF) in the absence or in the presence of 2 mM glutamine (GLN) are shown in (B). Numbers refer to the percentage of cells found in each quadrant.

C   A549 WT and R cells were cultured in normal growth medium (CTL) or EBSS medium (NF) and exposed to increasing concentrations (0.02, 0.2, and 2 mM) of glutamine (GLN) or glutamate (GLU) before the evaluation of the cell death-associated parameters. White and black columns depict the percentage of dying and dead cells, respectively (mean ± SEM; n = 3). *P < 0.05, **P < 0.01, ***P < 0.001 (Student's t-test), in comparison with cells of the same type in EBSS alone.

D–F   H460 (D), H1650 (E), and TC-1 (F) WT and R cells were cultured in EBSS alone or in combination to 2 mM glutamine (GLN) for 36 h. PI⁻ = dead cells; DiOC6(3)^low PI⁻ = dying cells. Data represent mean ± SEM of n independent experiments (n = 5 in D, n = 4 in E, and n = 3 in F). *P < 0.05, **P < 0.01, ***P < 0.001 (Student's t-test), as compared to cells of the same type exposed to EBSS alone. #P < 0.05, ##P < 0.01 (Student's t-test), as compared to equally treated WT cells.

CDDP-resistant cells. To fuel the Krebs cycle, intracellular GLN must be converted to GLU (which is the precursor of the anaplerotic substrate α-ketoglutarate). This amidohydrolase reaction is catalyzed by glutaminase (GLS; Fig 5C). We therefore expected that GLS inhibition by bis-2-(5-phenylacetamido-1,3,4-thiadiazol-2-yl)ethyl sulfide (BPTES) would abolish the rescue
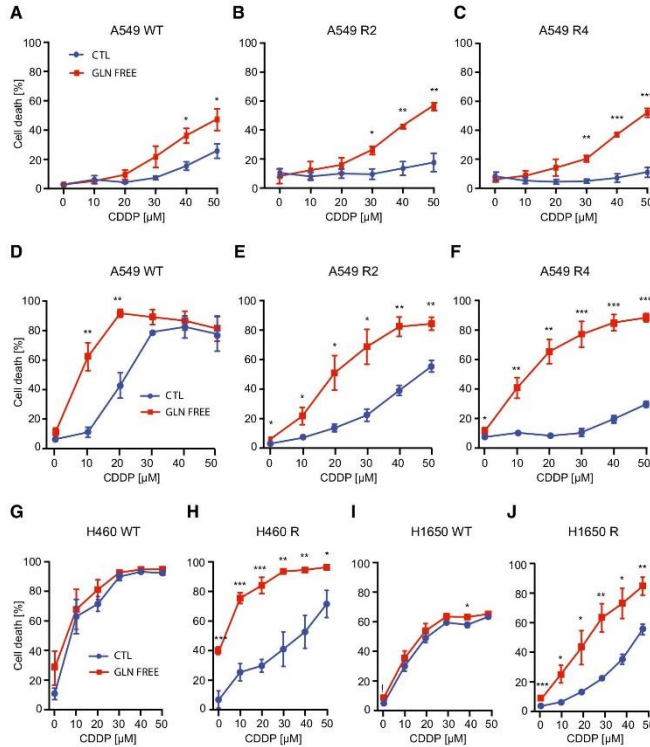
Figure 4. Glutamine starvation sensitizes human cancer cells to CDDP.

A–J   A549 (A–F), H460 (G, H), and H1650 (I, J) WT and R cells were cultured in complete medium (CTL) or glutamine (GLN)-free medium, and exposed for 24 h (A–C) or 48 h (D–J) to the indicated concentrations of CDDP. Thereafter, cells were subjected to flow cytometry-assisted measurement of cell death parameters. Values represent the percentage of dying $DiOC_6(3)^{low}PI^-$ plus dead $PI^+$ cells. Data represent mean ± SEM of three independent experiments except for (E) (*n* = 4).
*$P$ < 0.05, **$P$ < 0.01, ***$P$ < 0.001 (Student's *t*-test), as compared to cells of the same type in CTL medium.

effect of GLN. In stark contrast, however, BPTES failed to counteract the pro-survival action of GLN on CDDP-resistant cells cultured in EBSS. Rather, BPTES reduced the mortality of R2 and R4 cells in EBSS as it reduced the intracellular GLU concentrations (in WT, R2 and R4 cells), while it tended to augment GLN (in WT cells; Fig 5D and E). Similarly, another pharmacological GLS inhibitor compound 968 (C968) reduced the killing of R2 and R4 cells by starvation (Fig EV4B). Finally, knockdown of GLS with two distinct, non-overlapping siRNAs (Fig EV4C) partially rescued R2 and R4 cells from the cytotoxic consequences of starvation (Figs 5F and EV4D).

Based on the aforementioned results, we speculated that GLN-fueled nucleoside biosynthesis (which does not require the action of GLS and actually would be favored by GLS inhibition, Fig 5C) might account for its rescue effect on starved CDDP-resistant cells. Indeed, GLN was able to normalize the intracellular concentration of succinyl adenosine (a precursor of AMP), adenosine monophosphate (AMP), adenosine diphosphate (ADP) and adenosine triphosphate (ATP) in CDDP-resistant cells cultured in nutrient-free conditions (Fig 6A–D). Similarly, GLS inhibition by BPTES resulted in a significant elevation of AMP and uridine monophosphate (UMP) in R2 and R4 cells (Fig EV4E). Direct addition of nucleosides (and in particular a mixture of all four ribonucleosides: adenosine, guanosine, uridine and cytidine [AGUC]) rescued all tested CDDP-resistant NSCLC lines from starvation-induced killing. Ribonucleosides were more

efficient than their desoxyribonucleoside derivatives (Fig 6E and F).

Altogether, these results suggest that GLN rescues CDDP-resistant cells from starvation-induced death by elevating the intracellular concentrations of nucleosides rather than by fueling anaplerotic reactions.

**Selective susceptibility of cisplatin-resistant cells to antimetabolites targeting nucleotide biosynthesis**

We next explored the possibility that CDDP-resistant cells might be particularly vulnerable to chemotherapeutic agents that target nucleotide-related pathways such as 5-fluorouracil (5-FU, an inhibitor of thymidylate synthase; Chon *et al*, 2017), clofarabine and gemcitabine (CLO and GCB, two inhibitors of ribonucleotide reductase; Aye *et al*, 2015). Upon short-term exposure (24 h), such antimetabolites failed to kill A549 R2 and R4 cells on their own, yet counteracted the rescue effect of GLN on starved cells (Fig 7A and B). Upon long-term exposure (48 h), 5-FU, CLO, cytarabine (CTB) and cladribine (2CdA), two other antimetabolites antagonizing nucleotide metabolism, killed R2 and R4 cells more efficiently than their parental equivalent (Figs 7C and D, and EV5A and B). Similarly, 5-FU killed other CDDP-resistant NSCLC cell lines (H1650, H460) more efficiently than their CDDP-susceptible precursors (Fig EV5C and D). Moreover, CDDP-resistant A549 tumors significantly reduced their growth upon treatment with 5-FU *in vivo*, in immunodeficient mice, contrasting with wild-type tumors that barely responded to this chemotherapeutic regimen (Fig 7E and F). Accordingly, 5-FU was able to prolong survival of mice bearing xenografted CDDP-resistant but not parental NSCLC (Fig 7G and H). In conclusion, it appears that CDDP-resistant tumors are endowed with an exquisite sensitivity to antimetabolites targeting nucleotide biosynthesis.

## Discussion

In spite of the surge of targeted anticancer treatments and immunotherapies, CDDP is still the most widely used anticancer agent and CDDP resistance continues to pose a major problem in the clinical management of malignant diseases. Here, we investigated the metabolic vulnerabilities of CDDP-resistant NSCLC and ovarian cancers. We found that CDDP-resistant cells became sensitive to nutrient depletion, meaning that they died *in vitro* upon culture in nutrient-free medium. Moreover, CDDP-resistant cancers drastically reduced their growth in mice that were subjected to repeated fasting cycles, contrasting with their CDDP-sensitive parental cancers that were not affected by fasting. Although the biochemical consequences of starvation of cells *in vitro* (by removal of multiple or individual nutrients from the medium) and starvation of mice *in vivo* (by removal of the food supply) admittedly could be quite distinct, the selective susceptibility of CDDP-resistant cells to both types of starvations (*in vitro* and *in vivo*) appears coherent in its pattern. Notably, it has been previously shown that fasting cycles can sensitize cancer cells to chemotherapy (Lee *et al*, 2012), but our data demonstrate for the first time the specific vulnerability of CDDP-resistant tumors to fasting cycles. This could have promising applications in clinical settings, as fasting cycles could be proposed to patients, after CDDP treatment, to target emerging CDDP-resistant cells. Stimulated by this encouraging result, we investigated the particular metabolic needs of CDDP-resistant cells and identified glutamine as a factor that can suppress starvation-induced cell death and whose depletion alone would be sufficient to re-sensitize normally CDDP-resistant cells to CDDP.

Previous studies have dealt with changes in energy metabolism that are coupled to CDDP resistance. Thus, it has been reported for different CDDP-resistant cell lines that they increase glycolysis (Qian *et al*, 2017), switch to oxidative phosphorylation (Galluzzi *et al*, 2014; Matassa *et al*, 2016; Wangpaichitr *et al*, 2017), and/or increase GLN metabolism by upregulating the GLN transporter ASCT2 and GLS (Hudson *et al*, 2016; Wangpaichitr *et al*, 2017). According to one study, the critical target explaining glutamine metabolism-linked CDDP resistance was GLS, meaning that knocking down GLS was sufficient to re-sensitize CDDP-resistant ovarian cancers to CDDP, while its transgenic overexpression in CDDP-sensitive cells could confer CDDP resistance (Hudson *et al*, 2016). However, we found that genetic or pharmacologic GLS inhibition did not reverse the capacity of GLN to rescue CDDP-resistant cells from starvation-induced death. Rather, GLS inhibition had a rescue effect on its own, perhaps because it prevented the conversion of

---

**Figure 5.  Inhibition of glutaminase (GLS) extends the survival of nutrient-starved CDDP-resistant cancer cells.**

A   WT, R2, and R4 A549 cells were cultured for 10 h in complete medium (CTL) or nutrient-deprived medium (NF), in the absence or presence of 2 mM glutamine (NF + GLN). Heatmap represents the amount of each metabolite (log2 scale) in nutrient-deprived medium (NF), shown as a black (high) and white (low) gradient. Metabolite differences between CTL and NF, or NF + GLN and NF are shown as a color gradient (log2 scale). Five replicates per condition. Both metabolites (rows) and conditions (columns) were clustered by means of the Ward method on the Euclidean distance matrix.

B   Heatmap indicates the level of Krebs cycle-related intermediates in WT, R2, and R4 A549 cells maintained in complete medium. For all metabolites, except for fumarate, differences between parental (WT), and CDDP-resistant (R2 and R4) cells were significant ($P < 0.001$, Student's *t*-test). These data were extracted from Fig EV4A.

C   Schematic representation of the main pathways of glutamine (GLN) metabolism.

D   WT, R2, and R4 A549 cells were cultured in complete medium (CTL) or EBSS in the absence or presence of the GLS inhibitor BPTES (5 μM) for 24 h and then assayed for cell death parameters. DiOC$_6$(3)$^{low}$ PI$^-$ = dying cells, PI$^+$ = dead cells (mean ± SEM; $n = 3$). *$P < 0.05$ (Student's *t*-test) as compared to cells of the same type cultured in the same medium, but in the absence of BPTES.

E   Levels of GLU and GLN in parental WT and the two CDDP-resistant R2 and R4 cancer cells cultured for 10 h in EBSS supplemented or not with 5 μM BPTES. Data are shown as area of the metabolite peak, normalized to the metabolite peak of WT cells cultured without BPTES. Means ± SEM of five replicates. *$P < 0.05$, **$P < 0.01$, ***$P < 0.001$ (Student's *t*-test), as compared to cells of the same type cultured in the absence of BPTES.

F   Parental (WT) and CDDP-resistant (R) A549 cells were transfected with control siRNA (siUNR) or with siRNAs specific for glutaminase (siGLSA) for 48 h. Thereafter, cells were cultured for 24 h either in the complete medium (CTL) or in EBSS prior to the cytofluorometric assessment of apoptosis-related variables. DiOC$_6$(3)$^{low}$ PI$^-$ = dying cells, PI$^+$ = dead cells (mean ± SEM; $n = 3$ independent experiments). *$P < 0.05$, **$P < 0.01$ (Student's *t*-test), as compared to cells of the same type transfected with siUNR.

---
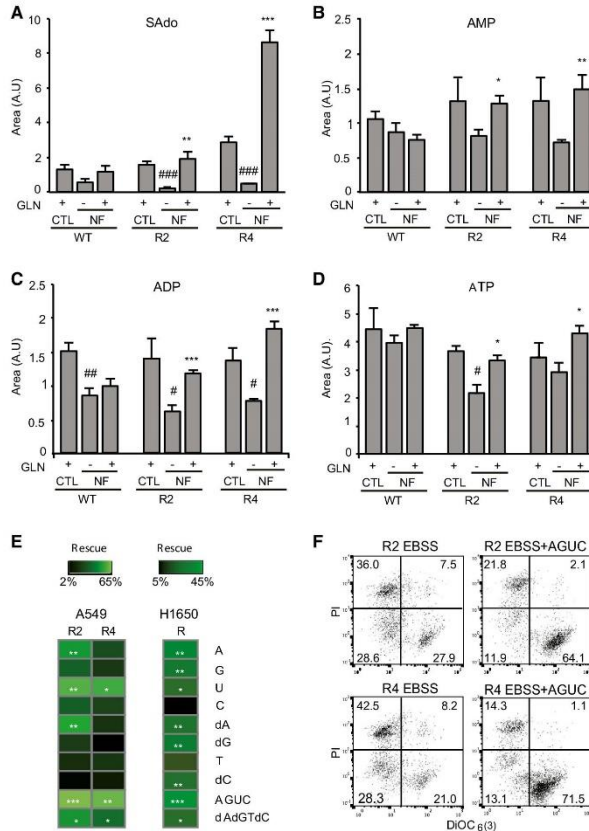
Figure 5.

**Figure 6. Glutamine promotes nucleotide synthesis in starved CDDP-resistant cells.**

A–D  Levels of succinyl adenosine (A), AMP (B), ADP (C), and ATP (D) in parental WT and CDDP-resistant R2 and R4 cancer cells cultured for 10 h in complete medium (CTL) or in EBSS medium (nutrient-free: NF) supplemented or not with 2 mM GLN (five replicates per condition). Data are shown as area of the metabolite peak. Means ± SEM of five replicates. $^{\#}P < 0.05$, $^{\#\#}P < 0.01$, $^{\#\#\#}P < 0.001$ (Student's $t$-test), as cells in EBSS compared to cells of the same type in complete medium; $^{*}P < 0.05$, $^{**}P < 0.01$, $^{***}P < 0.001$ (Student's $t$-test), as compared to cells of the same type cultured in EBSS alone.

E, F  CDDP-resistant cells were incubated in EBSS with or without adenosine (A), guanosine (G), uridine (U), cytidine (C), deoxyadenosine (dA), deoxyguanosine (dG), thymidine (dT), deoxycytidine (dT) each at 0.1 mM or in combination during 24 h (A549 cells) or 36 h (H1650 cells), then processed for the cytofluorometric determination of cell death-related parameters upon co-staining with the vital dye propidium iodide (PI) and the mitochondrial membrane potential ($\Delta\psi$m)-sensing dye $DiOC_6(3)$. Heatmaps in (E) represent the percentage of cell rescue by nucleosides. Rescue = (% of cells death in EBSS − % of cell death in EBSS supplemented with nucleosides)/(% of cells death in EBSS) × 100. $^{*}P < 0.05$, $^{**}P < 0.01$, $^{***}P < 0.001$ (Student's $t$-test; $n = 3$), as compared to cell death in the absence of nucleosides. Representative dot plots of A549 cells are shown in (F). Numbers refer to the percentage of cells found in each quadrant.

dwindling sources of intracellular GLN to GLU, hence maintaining GLN at a level compatible with fueling nucleotide biosynthesis. In accord with this analysis, cell-permeable dimethyl α-ketoglutarate, a precursor of α-ketoglutarate that readily penetrates into A549 cells (Marino *et al*, 2014), was unable to replace GLN and hence to rescue CDDP-resistant A549 cells from starvation-induced death.
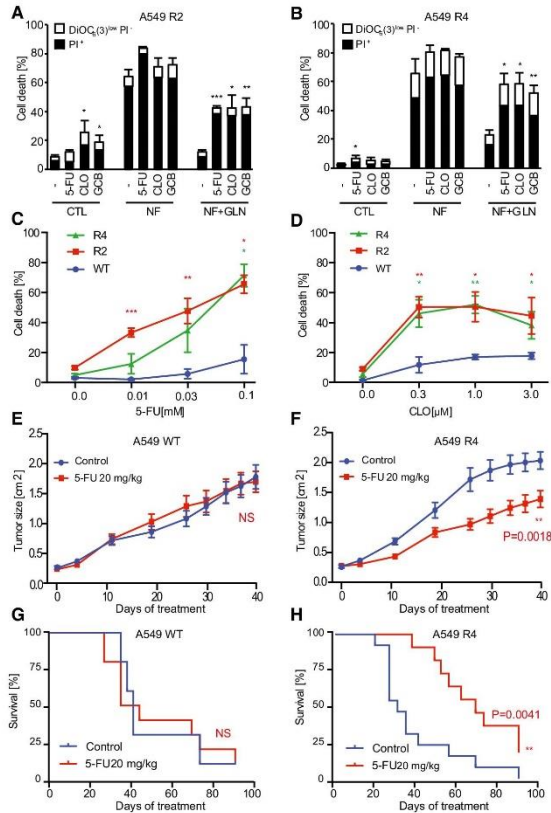
**Figure 7.  Inhibition of nucleotide biosynthesis preferentially kills CDDP-resistant cancer cells.**

A, B   Cytofluorometric assessment of cell death in A549 CDDP-resistant R2 (A) and R4 (B) cancer cells cultured in complete medium (CTL), EBSS (NF), or EBSS containing 0.02 mM glutamine (NF + GLN), in the absence or in the presence of 5-fluorouracil (5-FU; 60 μM), clofarabine (CLO; 2 μM), or gemcitabine (GCB; 2 μM) for 24 h. $DiOC_6(3)^{low} PI^-$ = dying cells, $PI^+$ = dead cells (mean ± SEM; $n$ = 3). *$P$ < 0.05, **$P$ < 0.01, ***$P$ < 0.001 (Student's $t$-test), as compared to cells in the same culture medium in the absence of nucleotide antagonists.

C, D   A549 parental (WT) and CDDP-resistant (R2 and R4) cancer cells were cultured in complete medium, either untreated or exposed to the indicated concentrations of 5-fluorouracil (5-FU; in C) or clofarabine (CLO; in D). After 48 h of incubation, the cells were subjected to the flow cytometry-assisted measurement of cell death parameters. Values represent the percentage of dying $DiOC_6(3)^{low} PI^-$ plus dead $PI^+$ cells (mean ± SEM; $n$ = 4 in C and 3 in D). *$P$ < 0.05, **$P$ < 0.01, ***$P$ < 0.001 (Student's $t$-test), as compared to equally treated WT cells.

E, F   WT cell line (E) and its CDDP-resistant R4 derivative (F) were subcutaneously xenografted into athymic nu/nu mice. When tumors became palpable, animals were randomized and treated with 5-fluorouracil (5-FU; i.p. injection) or an equivalent volume of vehicle (CTL), three times per week for 12 weeks. Tumor growth is reported as means ± SEM (WT CTL and WT 5-FU, 10 mice; R4 CTL, 13 mice; R4 5-FU, 11 mice). **$P$ < 0.01 (Wald test, type 2 ANOVA), as compared to CTL

G, H   Kaplan–Meier survival curves of nude mice xenografted with A549 WT (G) or CDDP-resistant R4 cancer cells (H), and treated with 5-FU or an equivalent volume of vehicle (CTL). Treatment with 5-FU significantly prolongs survival of mice xenografted with CDDP-resistant R4 A549 cancer cells (log-rank test).

Moreover, high doses of the glutathione precursors glutathione ethyl ester or *N*-acetyl cysteine also were unable to replace GLN in this rescue assay. Altogether, these results indicate that anaplerotic, Krebs cycle-related, and redox reactions were not important for the GLN-mediated rescue effect. In line with this idea, even rather small doses of GLN (in the range of 50 μM) were

sufficient to rescue CDDP-resistant A549 cells from death, underscoring the notion that subtle effects (such as nucleotide biosynthesis) rather than bioenergetically relevant reactions (that would involve the conversion of GLN into GLU and then into the anaplerotic substrate α-ketoglutarate) requiring high GLN concentrations are involved in the rescue effect. In line with this notion, Tardito *et al* have shown that GLN-starved glioblastoma cells were not rescued by TCA cycle replenishment (Tardito *et al*, 2015). Here, we report that supplementation with ribonucleosides could effectively suppress starvation-induced cell death in CDDP-resistant NSCLC cells. Of note, Brown *et al* (2017) have recently shown that genotoxic chemotherapeutic agents (including cisplatin) can induce an elevation of nucleotide synthesis, which is necessary for cell survival. It is tempting to speculate that such an adaptation in nucleotide metabolism occurs in response to DNA repair during CDDP treatment and then persists in CDDP-resistant cells after CDDP removal thereby inducing metabolic vulnerabilities. Of note, our work does not clarify whether such metabolic rewiring is responsible for cisplatin resistance. Rather, it reveals a specific characteristic of cisplatin-resistant cells that be taken advantage of to kill them.

More importantly from the therapeutic point of view, we observed that CDDP-resistant cells acquired an exquisite susceptibility to several chemotherapeutic agents that inhibit nucleotide metabolism such as 5-fluorouracil (5-FU, an inhibitor of thymidylate synthase; Chon *et al*, 2017) or clofarabine (CLO, an inhibitor of ribonucleotide reductase; Aye *et al*, 2015). Interestingly, a recent siRNA-based genetic screen also revealed that knockdown of ribonucleoside-diphosphate reductase subunit M2 B can sensitize cancer cells to CDDP as well (Leung *et al*, 2016), pleading in favor of the specificity of the effects. Moreover, several combination chemotherapy trials have established the superiority of CDDP combined with the aforementioned chemotherapeutic antimetabolites over monotherapies (Decker *et al*, 1983; Heinemann *et al*, 2006; Comella *et al*, 2007). The present data may provide a rational explanation for this combination effect. In line with this notion, the combination of CDDP and raltitrexed, a chemotherapeutic agent that is a folic acid antagonist inhibiting the synthesis of nucleotides precursors, improves overall survival compared with CDDP alone in patients with malignant pleural mesothelioma (van Meerbeeck *et al*, 2005). Of note, the pretreatment with pemetrexed (Alimta®), another folate antimetabolite, re-established *in vitro* CDDP-induced killing of a CDDP-resistant NSCLC cell population (Tieche *et al*, 2016).

Previous studies revealed that hematopoietic stem cells only undergo erythroid differentiation upon supplementation of extra GLN or nucleosides, exemplifying a physiological case of "GLN addiction" (Oburoglu *et al*, 2014). In the context of cancer, activation of the oncogenic transcription factor MYC is well known to induce GLN addiction (Yuneva *et al*, 2007, 2012; Altman *et al*, 2016). Moreover, autophagy-deficient KRAS-induced lung cancers reportedly rely on extra supply of GLN or nucleosides (Guo *et al*, 2016). Although MYC can cause CDDP resistance (Sklar & Prochownik, 1991), we found no signs of autophagy deficiency in the CDDP-selected NSCLC cell lines characterized here (Michels *et al*, 2014a). Hence, the exact relationship between transcriptional effects and metabolic reprogramming with respect to GLN metabolism remains to be investigated.

In synthesis, CDDP resistance is coupled to major shifts in cellular metabolism that, in several NSCLC and ovarian cancer models, causes a relative GLN dependency. Metabolomic, genetic, and pharmacological studies indicate that GLN must fuel a nucleotide biosynthesis pathway in the context of CDDP resistance. Consequently, CDDP-resistant cells become exclusively sensitive to fasting as well as to antimetabolites that target nucleotide synthesis.

## Materials and Methods

### Cell lines, culture conditions, and chemicals

Culture media and cell culture supplements were purchased from Life Technologies (Carlsbad, CA, USA) unless otherwise specifically mentioned. Non-small cell lung cancer (NSCLC) cells and both parental (also known as wild type (WT)) and their CDDP-resistant counterparts were maintained at 37°C under 5% $CO_2$, in the following culture media: Glutamax-containing Dulbecco's modified Eagle's medium/F12 medium supplemented with 10% fetal bovine serum (FBS), 10 mM HEPES buffer, 100 units/ml penicillin G sodium, and 100 mg/ml streptomycin sulfate for human NSCLC A549 cells; RPMI-1640 medium supplemented as above for human NSCLC H460 and H1650 cells; A 1:1 mixture of MCDB 105/M199 medium (Sigma-Aldrich, St Louis, MO, USA) supplemented as above and with 0.75 g/l sodium bicarbonate in addition, for TOV-112D cells; RPMI-1640 medium supplemented as above, and with non-essential amino acids in addition, for murine TC1 cells. WT cells were purchased from American Type Culture Collection, and their CDDP-resistant counterparts were obtained *in vitro* by prolonged culture of parental WT cells with sublethal CDDP concentrations as previously described (Michels *et al*, 2013). The following chemicals were purchased from Sigma-Aldrich: acetic acid, acetonitrile, adenosine, 6-aminonicotinamide, antimycin A, arginine, asparagine, aspartate, BPTES, 3-bromopyruvate, C646, CDDP, chloroform, citrate, cladribine, cytidine, 2-deoxyglucose, deoxyadenosine, deoxycytidine deoxyguanosine, dibutylamine acetate concentrate (DBAA), dimethyl α-ketoglutarate, EBSS, FK866, 5-fluorouracil, gemcitabine, glucose, glutamate, D-glutamine, L-glutamine, glutathione reduced ethyl ester, guanosine, histidine, leucine, MEDICA 16, methanol, methoxyamine, mevastatin, *N*-acetyl-L-cysteine, necrostatin-1, nicotinamide, *N*-methyl-*N*-(trimethylsilyl)trifluoroacetamide (MSTFA), nocodazole, N-tert-butyldimethylsilyl-N-methyltrifluoroacetamid    (MSTBFA), O-ethylhydroxylamine hydrochloride, oligomycin, paclitaxel, perhexiline, putrescine, pydoxine, pyridoxal-5-phosphate, rotenone, salicylate, simvastatin, spermidine, thymidine, TOFA, uridine, and valine. 3-methylpyruvate was purchased from FLUKA. Veliparib (ABT-888), BMN 673, and clofarabine were purchased from Selleckchem. Compound 968 (C968) was purchased from Calbiochem-Merck. Z-val-ala-asp(Ome)-fluoromethylketone (Z-VAD-fmk) was purchased from BACHEM.

### RNA interference

The siRNA heteroduplexes specific for Bak (sense 5′-CCGACGCUAU GACUCAGAGdTdT), Bax (sense 5′-GGUGCCGGAACUGAUCAGA dTdT), Mcl-1 (sense 5′-GUGCCUUUGUGGCCUAAACAdTdT), p53 (sense 5′-GCAUGAACCGGAGGCCCAU dTdT-3′; Martinez *et al*,

2002), PUMA (sense 5′-GGAUGGCGGACGACCUCAAdTdT), Glutaminase (siGLS; sense 5′-CUGAAUAUGUGCAUCGAUAdTdT), and one nontargeting siRNA (UNR, sense 5′-GCCGGUAUGCCGGUUAAG UdTdT-3′) were purchased from Sigma-Proligo. A second siRNA specific for GLS (GLSB) was purchased from Qiagen (SI04243148 FlexiTubegen solution, Qiagen). A549 cells pre-seeded in 12-well plates at 20,000 cells per well were transfected with siRNAs after 30 h using Hiperfect transfecting agent (Qiagen). Cells were treated with EBSS 36 h after transfection, during 24 h.

### Cytofluorometry

To measure apoptotic features, adherent and non-adherent cells were collected and co-stained for 30 min at 37°C with 40 nM 3,3′ dihexiloxalocarbocyanine iodide ($DiOC_6(3)$), Molecular Probes-Invitrogen), a mitochondrial transmembrane potential-sensitive dye, and 1 µg/ml propidium iodide (PI), which only accumulates in dead cells exhibiting plasma membrane rupture. Cytofluorometric acquisitions were carried out on a Milteny cytofluorometer (MACSQuant® Analyzer 10), and statistical analyses were performed by using the FlowJo software (LLC, Oregon, USA) upon gating on events exhibiting normal forward scatter (FSC) and side scatter (SSC) parameters.

### Immunoblotting

Cells were trypsinized, collected, washed twice with cold PBS, and lysed in a buffer containing 50 mM Tris–HCl pH 6.8, glycerol 10%, 2% SDS, 10 mM DTT, and 0.005% bromophenol blue. Subsequently, protein extracts (30 µg/lane) were separated on precast 4–12% SDS–PAGE gels (Invitrogen) followed by electrotransfer to nitrocellulose membranes (Biorad) and immunoblotting with primary antibodies targeting PAR (Clone 10H, mAb to Poly(ADP-ribose Abcam, 1:1,000) or glutaminase (GLS; SAB2105954, Sigma-Aldrich, 1:1,000). An antibody, which recognizes actin (mAb to beta actin, ab 49900, Abcam, 1:5,000), was used to monitor equal lane loading. Thereafter, membranes were incubated with appropriate horseradish peroxides-conjugated secondary antibodies (Southern Biotech), followed by chemiluminescence detection with the ECLTM Prime Western Blotting Detection Reagent (GE Healthcare), before being revealed by the ImageQuantTM LAS 4000 Biomolecular Imager (GE Healthcare Life Sciences). Finally, protein expression was quantified by ImageJ software (NIH, USA).

### Mouse housing and experiments

Mice were maintained in specific pathogen-free conditions, at 25°C, with 12-h light/12-h dark cycles. All animals were used under an approved protocol by the local Ethics Committee (C2EA 26 no E-94-076-11, protocol no 1113 and C2EA 05 no B-75-06-12, protocol no 7810) under conditions in accordance with the EU Directive 63/2010. Eight-week-old female nude athymic (nu/nu) mice were purchased from Envigo France. Sample sizes were calculated to detect a statistically significant effect. For tumor growth experiments, $5 \times 10^6$ WT and CDDP-resistant R4 A549 cells were injected subcutaneously. The estimation of the tumor surface (longest dimension × perpendicular dimension) was measured using a common caliper. When the tumor surface reached 30–40 mm², mice were randomized into the different groups to be treated (by

starvation or drugs). The investigator was blinded during the tumor size measurement.

### Starvation regimen *in vivo*

After randomization, 8-week-old female nude athymic (nu/nu) mice were either kept in standard conditions (food and water *ad libitum*), or left for 24 h in the absence of nutrients (though with *ad libitum* access to drinking water) two times a week. Mice weight was routinely monitored, and nutrients absence was stopped if weight loss was superior to 20%.

### Drug treatment *in vivo*

After randomization, mice were treated intraperitoneally either with 20 or 30 mg/kg 5-fluorouracil (5-FU) in a mix of 200 µl PBS containing 3% DMSO, or with 200 µl PBS containing 3% DMSO alone. Mice were sacrificed when tumor reached 2 cm².

### Sample preparation for metabolome analysis

WT, R2, and R4 A549 cells were seeded in 6-well plates and cultured for 48 h in complete medium. Ten hours before extraction, medium was changed and cells were cultured either in complete medium (CTL) or nutrient-deprived medium (NF), in the absence or presence of 2 mM glutamine (NF + GLN). Five replicates per condition. Subsequently, cells were washed six times with cold PBS and then scraped in 500 µl of methanol (90%)-water (10%). After a centrifugation (10,000 g, 10 min, 4°C), 100 µl chloroform was added, and a second centrifugation was performed (10,000 g, 10 min, 4°C). The whole supernatant was evaporated at 40°C to obtain dried extracts. 300 µl of methanol was added on dried extract and split in two 150 µl fractions for GC-MS and LC-MS analyses, respectively. For GC-MS assay, methanol solubilized aliquots were transferred to glass tubes and solvent was evaporated. 50 µl of methoxyamine (20 mg/ml in pyridine) was added on dried extracts and then stored at room temperature in dark, during 16 h. The day after, 80 µl of MSTFA was added and final derivatization occurred during 30 min at 40°C. Samples were then transferred to vials and directly injected into GC-MS. After a second evaporation round, LC-MS dried extracts were solubilized with 300 µl of MilliQ water, centrifuged (10 min at 15,000 g, 4°C), and aliquoted in three microcentrifuge tubes (100 µl). Aliquots were transferred in UHPLC vials and injected into the UHPLC/MS or kept at −80°C until injection.

### Plasma preparation for metabolome analysis

A volume of 50 µl of plasma was mixed with 500 µl of a cold solvent mixture (MeOH/Water/Chloroform, 9/1/1, −20°C) and then vortexed and centrifuged (10 min at 15,000 g, 4°C). Then upper phase of the supernatant was split in two parts: 220 µl for the GC/MS experiment and 200 µl for the UHPLC/MS experimentations. Concerning the GC-MS aliquots, 30 µl from each sample was pooled in a QC vial, and then, 150 µl of samples was transferred in vial injection and evaporated. 50 µl of methoxyamine (20 mg/ml in pyridine) was added on dried extracts and then stored at room temperature in dark, during 16 h. The day after,

80 μl of MSTFA was added and final derivatization occurred at 40°C during 30 min. Samples were then directly injected into GC-MS. Concerning the LC-MS aliquots, the collected supernatant was evaporated at 40°C in a pneumatically assisted concentrator (Techne DB3, Staffordshire, UK). The LC-MS dried extracts were solubilized with 450 μl of MilliQ water. After picked up 60 μl from each microtubes to create pool of QC, samples were aliquoted (100 μl) for LC methods and backup. Biological samples and QC aliquots were kept at −80°C until injection or transferred in vials for direct analysis by UHPLC/MS.

### Untargeted analysis of intracellular metabolites by ultra-high-performance liquid chromatography (UHPLC) coupled to a quadrupole–time of flight (QTOF) mass spectrometer

Profiling of intracellular metabolites was performed on a Liquid Chromatography (LC) 1260 System (Agilent Technologies, Waldbronn, Germany) coupled to a QTOF 6520 (Agilent Technologies) equipped with an electrospray source operating in both positive and negative mode and full scan mode from 50 to 1,000 Da. The gas temperature was set to 350°C with a gas flow of 12 l/min. The capillary voltage was set to 3.5 kV and the fragmentor at 120 V. Two reference masses were used to maintain the mass accuracy during analysis: m/z 121.050873 and m/z 922.009798 in positive mode and m/z 112.985587 and m/z 980.016375 in negative mode. 10 μl of sample was injected on a SB-Aq column (100 × 2.1 mm particle size 1.8 μm) from Agilent Technologies, protected by a guard column XDB-C18 (5 × 2.1 mm particle size 1.8 μm), and heated at 40°C. The gradient mobile phase consisted of water with 0.2% of acetic acid (A) and acetonitrile (B). The flow rate was set to 0.3 ml/min. Initial condition is 98% phase A and 2% phase B. Molecules were then eluted using a gradient from 2 to 95% phase B in 7 min. The column was washed using 95% mobile phase B for 3 min and equilibrated using 2% mobile phase B for 3 min. The autosampler was kept at 4°C. Data processing was performed using in-house script to align molecular features found by the Agilent MassHunter qualitative software (B.07.00).

### Targeted analysis of intracellular metabolites by ultra-high-performance liquid chromatography (UHPLC) coupled to a triple quadrupole (QQQ) mass spectrometer

Targeted analysis was performed on a LC 1260 System (Agilent Technologies, Waldbronn, Germany) coupled to a Triple Quadrupole 6410 (Agilent Technologies) equipped with an electrospray source operating in positive mode. The gas temperature was set to 350°C with a gas flow of 12 l/min. The capillary voltage was set to 3.5 kV. 10 μl of sample were injected on a Zorbax Eclipse Plus C18 column (100 × 2.1 mm particle size 1.8 μm) from Agilent technologies, protected by a guard column XDB-C18 (5 × 2.1 mm particle size 1.8 μm), and heated at 40°C. The gradient mobile phase consisted of 2 mM of dibutylamine ammonium acetate (DBAA) in water (A) and acetonitrile (B). The flow rate was set to 0.2 ml/min, with the gradient as follows: initial condition was 90% phase A and 10% phase B, maintained during 4 min, from 10 to 95% phase B over 3 min, 95% mobile phase B for 3 min, and finally 10% mobile phase B for 3 min. The autosampler was kept at 4°C. Peak detection and integration were performed using the Agilent MassHunter quantitative software (B.07.01).

### Targeted analysis of intracellular metabolites gas chromatography (GC) coupled to a triple quadrupole (QQQ) mass spectrometer

The GC-MS/MS method was performed on a 7890A gas chromatography (Agilent Technologies, Waldbronn, Germany) coupled to a triple quadrupole 7000C (Agilent Technologies, Waldbronn, Germany) equipped with an electronic impact source (EI) operating in positive mode. The injection was performed in splitless mode with a front inlet temperature set to 250°C. The transfer line and the ion-source temperature were, respectively, at 250 and 230°C. The septum purge flow was fixed at 3 ml/min. The purge flow set to split vent and operated at 80 ml/min during 1 min. Gas saver mode was set to 15 ml/min after 5 min. The helium gas flowed at 1 ml/min through the column (J&WScientificHP-5MS, 30 m × 0.25 mm, i.d. 0.25 mm, d.f., Agilent Technologies Inc.). Column temperature was held at 60°C for 1 min, then raised to 210°C (10°C/min), followed by a step to 230°C (5°C/min), and reached 325°C (15°C/min), and be held at this temperature for 5 min. The collision gas was nitrogen. Peak detection and integration were performed using the Agilent MassHunter software (B.07.01). Data were presented in hitmaps generated with Gene E software, Broad Institute, Cambridge, USA.

### Statistical procedures of *in vitro* experiments

Unless otherwise specified, all experiments were conducted in duplicate and independently repeated at least three times, yielding comparable results. No statistical methods were used to predetermine sample size. For *in vitro* studies, data were analyzed with Microsoft Excel (Microsoft Co.) and statistical significance was assessed by means of unpaired Student's *t*-test except for Fig EV3A (paired). *P*-values were considered significant when lower than 0.05. In the experiments in which the effect meets the criterion for significance in either direction, a two-sided *t*-test was used (Figs 1A, 3A, 5E, 6A–D, and EV3A). In all other experiments, as we expected the effect to be in a given direction, one-sided *t*-tests were applied.

### Statistical procedures of *in vivo* experiments

Longitudinal analyses of tumor growth data were carried out by linear mixed-effect modeling on tumor sizes. Wald tests were used to compute *P*-values by testing jointly that both tumor growth slopes and intercepts were the same between treatment groups of interest. For graphing, tumor growth data are represented in group-averaged tumor size alongside its SEM at each time point. Survival data are represented in Kaplan–Meier survival curves. Log-rank test was used to compute *P*-values.

### Data availability

Raw data from metabolomic experiments were deposited on figshare (https://figshare.com/s/3994153f2df6e8a7f7f0).

**Expanded View** for this article is available online.

## Author contributions

FO, MC, SL, AJ, and VA performed the experiments. SD and AC performed mass spectrometry and data analysis. GSW provided TOV-112D cell lines; FO, SD, and MC analyzed and interpreted the data; JM, JP, and FP reviewed and edited the initial draft; FO, MC and GK designed the study and wrote the paper.

## Conflict of interest

The authors declare that they have no conflict of interest.

# References

Altman BJ, Stine ZE, Dang CV (2016) From Krebs to clinic: glutamine metabolism to cancer therapy. *Nat Rev Cancer* 16: 619–634

Aye Y, Li M, Long MJ, Weiss RS (2015) Ribonucleotide reductase and cancer: biological mechanisms and targeted therapies. *Oncogene* 34: 2011–2021

Brown KK, Spinelli JB, Asara JM, Toker A (2017) Adaptive reprogramming of de novo pyrimidine synthesis is a metabolic vulnerability in triple-negative breast cancer. *Cancer Discov* 7: 391–399

Chon J, Stover PJ, Field MS (2017) Targeting nuclear thymidylate biosynthesis. *Mol Aspects Med* 53: 48–56

Comella P, Filippelli G, De Cataldis G, Massidda B, Frasci G, Maiorino L, Putzu C, Mancarella S, Palmeri S, Cioffi R, Roselli M, Buzzi F, Milia V, Gambardella A, Natale D, Bianco M, Ghiani M, Masullo P, Southern Italy Cooperative Oncology Group (2007) Efficacy of the combination of cisplatin with either gemcitabine and vinorelbine or gemcitabine and paclitaxel in the treatment of locally advanced or metastatic non-small-cell lung cancer: a phase III randomised trial of the Southern Italy Cooperative Oncology Group (SICOG 0101). *Ann Oncol* 18: 324–330

Decker DA, Drelichman A, Jacobs J, Hoschner J, Kinzie J, Loh JJ, Weaver A, Al-Sarraf M (1983) Adjuvant chemotherapy with cis-diamminodichloroplatinum II and 120-hour infusion 5-fluorouracil in Stage III and IV squamous cell carcinoma of the head and neck. *Cancer* 51: 1353–1355

Erster S, Mihara M, Kim RH, Petrenko O, Moll UM (2004) In vivo mitochondrial p53 translocation triggers a rapid first wave of cell death in response to DNA damage that can precede p53 target gene activation. *Mol Cell Biol* 24: 6728–6741

Galluzzi L, Senovilla L, Vitale I, Michels J, Martins I, Kepp O, Castedo M, Kroemer G (2012a) Molecular mechanisms of cisplatin resistance. *Oncogene* 31: 1869–1883

Galluzzi L, Vitale I, Senovilla L, Olaussen KA, Pinna G, Eisenberg T, Goubar A, Martins I, Michels J, Kratassiouk G, Carmona-Gutierrez D, Scoazec M, Vacchelli E, Schlemmer F, Kepp O, Shen S, Tailler M, Niso-Santano M, Morselli E, Criollo A et al (2012b) Prognostic impact of vitamin B6 metabolism in lung cancer. *Cell Rep* 2: 257–269

Galluzzi L, Vitale I, Michels J, Brenner C, Szabadkai G, Harel-Bellan A, Castedo M, Kroemer G (2014) Systems biology of cisplatin resistance: past, present and future. *Cell Death Dis* 5: e1257

Guo JY, Teng X, Laddha SV, Ma S, Van Nostrand SC, Yang Y, Khor S, Chan CS, Rabinowitz JD, White E (2016) Autophagy provides metabolic substrates to maintain energy charge and nucleotide pools in Ras-driven lung cancer cells. *Genes Dev* 30: 1704–1717

Hall MD, Okabe M, Shen DW, Liang XJ, Gottesman MM (2008) The role of cellular accumulation in determining sensitivity to platinum-based chemotherapy. *Annu Rev Pharmacol Toxicol* 48: 495–535

Heinemann V, Quietzsch D, Gieseler F, Gonnermann M, Schonekas H, Rost A, Neuhaus H, Haag C, Clemens M, Heinrich B, Vehling-Kaiser U, Fuchs M, Fleckenstein D, Gesierich W, Uthgenannt D, Einsele H, Holstege A, Hinke A, Schalhorn A, Wilkowski R (2006) Randomized phase III trial of gemcitabine plus cisplatin compared with gemcitabine alone in advanced pancreatic cancer. *J Clin Oncol* 24: 3946–3952

Huang D, Duan H, Huang H, Tong X, Han Y, Ru G, Qu L, Shou C, Zhao Z (2016) Cisplatin resistance in gastric cancer cells is associated with HER2 upregulation-induced epithelial-mesenchymal transition. *Sci Rep* 6: 20502

Hudson CD, Savadelis A, Nagaraj AB, Joseph P, Avril S, DiFeo A, Avril N (2016) Altered glutamine metabolism in platinum resistant ovarian cancer. *Oncotarget* 7: 41637–41649

Ishida S, McCormick F, Smith-McCune K, Hanahan D (2010) Enhancing tumor-specific uptake of the anticancer drug cisplatin with a copper chelator. *Cancer Cell* 17: 574–583

Karekla E, Liao WJ, Sharp B, Pugh J, Reid H, Quesne JL, Moore D, Pritchard C, MacFarlane M, Pringle JH (2017) Ex vivo explant cultures of non-small cell lung carcinoma enable evaluation of primary tumor responses to anticancer therapy. *Cancer Res* 77: 2029–2039

Kelland L (2007) The resurgence of platinum-based cancer chemotherapy. *Nat Rev Cancer* 7: 573–584

Kozopas KM, Yang T, Buchan HL, Zhou P, Craig RW (1993) MCL1, a gene expressed in programmed myeloid cell differentiation, has sequence similarity to BCL2. *Proc Natl Acad Sci USA* 90: 3516–3520

Lee C, Raffaghello L, Brandhorst S, Safdie FM, Bianchi G, Martin-Montalvo A, Pistoia V, Wei M, Hwang S, Merlino A, Emionite L, de Cabo R, Longo VD (2012) Fasting cycles retard growth of tumors and sensitize a range of cancer cell types to chemotherapy. *Sci Transl Med* 4: 124ra27

Leung AW, Hung SS, Backstrom I, Ricaurte D, Kwok B, Poon S, McKinney S, Segovia R, Rawji J, Qadir MA, Aparicio S, Stirling PC, Steidl C, Bally MB (2016) Combined use of gene expression modeling and siRNA screening identifies genes and pathways which enhance the activity of cisplatin when added at no effect levels to non-small cell lung cancer cells in vitro. *PLoS One* 11: e0150675

Li Q, Zhan M, Chen W, Zhao B, Yang K, Yang J, Yi J, Huang Q, Mohan M, Hou Z, Wang J (2016) Phenylethyl isothiocyanate reverses cisplatin resistance in biliary tract cancer cells via glutathionylation-dependent degradation of Mcl-1. *Oncotarget* 7: 10271–10282

Marino G, Pietrocola F, Eisenberg T, Kong Y, Malik SA, Andryushkova A, Schroeder S, Pendl T, Harger A, Niso-Santano M, Zamzami N, Scoazec M, Durand S, Enot DP, Fernandez AF, Martins I, Kepp O, Senovilla L, Bauvy C, Morselli E et al (2014) Regulation of autophagy by cytosolic acetyl-coenzyme A. *Mol Cell* 53: 710–725

Martinez LA, Naguibneva I, Lehrmann H, Vervisch A, Tchenio T, Lozano G, Harel-Bellan A (2002) Synthetic small inhibiting RNAs: efficient tools to inactivate oncogenic mutations and restore p53 pathways. *Proc Natl Acad Sci USA* 99: 14849 – 14854

Martins I, Kepp O, Schlemmer F, Adjemian S, Tailler M, Shen S, Michaud M, Menger L, Gdoura A, Tajeddine N, Tesniere A, Zitvogel L, Kroemer G (2011) Restoration of the immunogenicity of cisplatin-induced cancer cell death by endoplasmic reticulum stress. *Oncogene* 30: 1147 – 1158

Matassa DS, Amoroso MR, Lu H, Avolio R, Arzeni D, Procaccini C, Faiccia D, Maddalena F, Simeon V, Agliarulo I, Zanini E, Mazzoccoli C, Recchi C, Stronach E, Marone G, Gabra H, Matarese G, Landriscina M, Esposito F (2016) Oxidative metabolism drives inflammation-induced platinum resistance in human ovarian cancer. *Cell Death Differ* 23: 1542 – 1554

van Meerbeeck JP, Gaafar R, Manegold C, Van Klaveren RJ, Van Marck EA, Vincent M, Legrand C, Bottomley A, Debruyne C, Giaccone G, European Organisation for Research and Treatment of Cancer Lung Cancer Group, National Cancer Institute of Canada (2005) Randomized phase III study of cisplatin with or without raltitrexed in patients with malignant pleural mesothelioma: an intergroup study of the European Organisation for Research and Treatment of Cancer Lung Cancer Group and the National Cancer Institute of Canada. *J Clin Oncol* 23: 6881 – 6889

Meisner HM, Sorensen L (1966) Metaphase arrest of Chinese hamster cells with rotenone. *Exp Cell Res* 42: 291 – 295

Michels J, Vitale I, Galluzzi L, Adam J, Olaussen KA, Kepp O, Senovilla L, Talhaoui I, Guegan J, Enot DP, Talbot M, Robin A, Girard P, Orear C, Lissa D, Sukkurwala AQ, Garcia P, Behnam-Motlagh P, Kohno K, Wu GS *et al* (2013) Cisplatin resistance associated with PARP hyperactivation. *Cancer Res* 73: 2271 – 2280

Michels J, Obrist F, Castedo M, Vitale I, Kroemer G (2014a) PARP and other prospective targets for poisoning cancer cell metabolism. *Biochem Pharmacol* 92: 164 – 171

Michels J, Obrist F, Vitale I, Lissa D, Garcia P, Behnam-Motlagh P, Kohno K, Wu GS, Brenner C, Castedo M, Kroemer G (2014b) MCL-1 dependency of cisplatin-resistant cancer cells. *Biochem Pharmacol* 92: 55 – 61

Michels J, Adam J, Goubar A, Obrist F, Damotte D, Robin A, Alifano M, Vitale I, Olaussen KA, Girard P, Cremer I, Castedo M, Soria JC, Kroemer G (2015) Negative prognostic value of high levels of intracellular poly(ADP-ribose) in non-small cell lung cancer. *Ann Oncol* 26: 2470 – 2477

Oburoglu L, Tardito S, Fritz V, de Barros SC, Merida P, Craveiro M, Mamede J, Cretenet G, Mongellaz C, An X, Klysz D, Touhami J, Boyer-Clavel M, Battini JL, Dardalhon V, Zimmermann VS, Mohandas N, Gottlieb E, Sitbon M, Kinet S *et al* (2014) Glucose and glutamine metabolism regulate human hematopoietic stem cell lineage specification. *Cell Stem Cell* 15: 169 – 184

Penning TD, Zhu GD, Gandhi VB, Gong J, Liu X, Shi Y, Klinghofer V, Johnson EF, Donawho CK, Frost DJ, Bontcheva-Diaz V, Bouska JJ, Osterling DJ, Olson AM, Marsh KC, Luo Y, Giranda VL (2009) Discovery of the Poly(ADP-ribose) polymerase (PARP) inhibitor 2-[(R)-2-methylpyrrolidin-2-yl]-1H-benzimidazole-4-carboxamide (ABT-888) for the treatment of cancer. *J Med Chem* 52: 514 – 523

Qian X, Xu W, Xu J, Shi Q, Li J, Weng Y, Jiang Z, Feng L, Wang X, Zhou J, Jin H (2017) Enolase 1 stimulates glycolysis to promote chemoresistance in gastric cancer. *Oncotarget* 18: 47691 – 47708

Ray Chaudhuri A, Callen E, Ding X, Gogola E, Duarte AA, Lee JE, Wong N, Lafarga V, Calvo JA, Panzarino NJ, John S, Day A, Crespo AV, Shen B, Starnes LM, de Ruiter JR, Daniel JA, Konstantinopoulos PA, Cortez D, Cantor SB *et al* (2016) Replication fork stability confers chemoresistance in BRCA-deficient cells. *Nature* 535: 382 – 387

Shen Y, Rehman FL, Feng Y, Boshuizen J, Bajrami I, Elliott R, Wang B, Lord CJ, Post LE, Ashworth A (2013) BMN 673, a novel and highly potent PARP1/2 inhibitor for the treatment of human cancers with DNA repair deficiency. *Clin Cancer Res* 19: 5003 – 5015

Sklar MD, Prochownik EV (1991) Modulation of cis-platinum resistance in Friend erythroleukemia cells by c-myc. *Cancer Res* 51: 2118 – 2123

Sourisseau T, Helissey C, Lefebvre C, Ponsonnailles F, Malka-Mahieu H, Olaussen KA, Andre F, Vagner S, Soria JC (2016) Translational regulation of the mRNA encoding the ubiquitin peptidase USP1 involved in the DNA damage response as a determinant of Cisplatin resistance. *Cell Cycle* 15: 295 – 302

Tajeddine N, Galluzzi L, Kepp O, Hangen E, Morselli E, Senovilla L, Araujo N, Pinna G, Larochette N, Zamzami N, Modjtahedi N, Harel-Bellan A, Kroemer G (2008) Hierarchical involvement of Bak, VDAC1 and Bax in cisplatin-induced cell death. *Oncogene* 27: 4221 – 4232

Tardito S, Oudin A, Ahmed SU, Fack F, Keunen O, Zheng L, Miletic H, Sakariassen PO, Weinstock A, Wagner A, Lindsay SL, Hock AK, Barnett SC, Ruppin E, Morkve SH, Lund-Johansen M, Chalmers AJ, Bjerkvig R, Niclou SP, Gottlieb E (2015) Glutamine synthetase activity fuels nucleotide biosynthesis and supports growth of glutamine-restricted glioblastoma. *Nat Cell Biol* 17: 1556 – 1568

Tieche CC, Peng RW, Dorn P, Froment L, Schmid RA, Marti TM (2016) Prolonged pemetrexed pretreatment augments persistence of cisplatin-induced DNA damage and eliminates resistant lung cancer stem-like cells associated with EMT. *BMC Cancer* 16: 125

Wang D, Lippard SJ (2005) Cellular processing of platinum anticancer drugs. *Nat Rev Drug Discov* 4: 307 – 320

Wangpaichitr M, Wu C, Li YY, Nguyen DJM, Kandemir H, Shah S, Chen S, Feun LG, Prince JS, Kuo MT, Savaraj N (2017) Exploiting ROS and metabolic differences to kill cisplatin resistant lung cancer. *Oncotarget* 8: 49275 – 49292

Winter C, Albers P (2011) Testicular germ cell tumors: pathogenesis, diagnosis and treatment. *Nat Rev Endocrinol* 7: 43 – 53

Yuneva M, Zamboni N, Oefner P, Sachidanandam R, Lazebnik Y (2007) Deficiency in glutamine but not glucose induces MYC-dependent apoptosis in human cells. *J Cell Biol* 178: 93 – 105

Yuneva MO, Fan TW, Allen TD, Higashi RM, Ferraris DV, Tsukamoto T, Mates JM, Alonso FJ, Wang C, Seo Y, Chen X, Bishop JM (2012) The metabolic profile of tumors depends on both the responsible genetic lesion and tissue type. *Cell Metab* 15: 157 – 170

Zhang J, Pavlova NN, Thompson CB (2017) Cancer cell metabolism: the essential role of the nonessential amino acid, glutamine. *EMBO J* 36: 1302 – 1315

ELSEVIER

# A new platinum-based prodrug candidate: Its anticancer effects in B50 neuroblastoma rat cells

Beatrice Rangone[a,1], Beatrice Ferrari[b,1], Valentina Astesana[b], Irene Masiello[b], Paola Veneroni[b], Ilaria Zanellato[a], Domenico Osella[a], Maria Grazia Bottone[b,*]

[a] Dipartimento di Scienze e Innovazione Tecnologica, Università del Piemonte Orientale "A. Avogadro", viale Teresa Michel 11, 15121 Alessandria, Italy
[b] Dipartimento di Biologia e Biotecnologie "L. Spallanzani", Università di Pavia, via Ferrata 9, 27100 Pavia, Italy

## ARTICLE INFO

*Keywords:*
B50
Neuroblastoma cells
Cisplatin
Cell death
Immunocytochemistry

## ABSTRACT

*Aims:* Neuroblastoma is a rare cancer that affects children, mostly under the age of 5. This type of cancer starts in very early forms of immature nerve cells or developing cells found in embryo or fetus. To date cisplatin represents one of the most potent antitumor agent known, however, the onset of systemic side effects and the induction of drug resistance limit its use in the clinic for long-term treatment. In the present study we have analysed the effects of a new compound of platinum(IV) conjugates, named Pt(IV)Ac-POA, which is able to generate a synergistic antineoplastic action when released along with cisplatin upon intracellular Pt(IV) → Pt(II) reduction.
*Main methods:* To assess the growth inhibition of the compounds under investigation, a cell viability test, i.e. the resazurin reduction assay was used on the B50 neuroblastoma rat cells. Further analysis on the cell cycle and metabolic alterations were carried out through flow cytometry. Morphological changes and activation of different cell death pathways after treatment, were observed at transmission electron microscope and by immunocytochemistry at fluorescence microscopy. Protein expression was examined by western blot analysis.
*Key findings:* This compound bearing bioactive axial ligand, such as the active histone deacetylase inhibitor (HDACi) (2-propynyl)octanoic acid (POA), induced cell death through different pathways at a concentration ten times lower than cisplatin.
*Significance:* The results showed that Pt(IV)Ac-POA could represent a promising improvement of Pt-based chemotherapy against neuroblastoma.

## 1. Introduction

One of the most active agents used in the systemic treatment of cancer is cisplatin. This metal-drug and its analogues (carboplatin and oxaliplatin) represent the standard therapy for a wide range of childhood and adult tumours, including some nervous system cancers, such as neuroblastoma [10]. This type of cancer is the most common extracranial tumour in children. It represents 8–10% of all childhood cancers and could start in embryonic or fetal life [12]. The benefit of cisplatin is hampered by severe side effects, including neurotoxicity, such as some studies conducted on rats treated with this drug have demonstrated [19,37]. Damages against the Peripheral Nervous System (PNS) are well-known [13] and some morpho-functional alterations were detected both during development [3] and in adult Central Nervous System (CNS) ([48]; Kelly et al. [30]).

A goal of biomedical research is the synthesis of new antitumor agents, having the same therapeutic effect of the reference drug, but with less systemic toxicity. In this context, the class of platinum(IV) derivatives, Pt(IV), is gaining increasing attention. It is generally accepted that Pt(IV) complexes act as prodrugs, i.e. they are reduced to cytotoxic Pt(II) analogues within the hypoxic tumour cells [24,27,50] (Scheme 1).

The two axial ligands, released along with the Pt(II) metabolite, can be synergistic or adjuvant agents, giving rise to multi-action Pt(IV) drugs [20,23,31]. In particular, Pt(IV) complexes bearing histone deacetylase inhibitors (HDACi) would benefit of the widely-described synergistic effect that these molecules exert on DNA-damaging agents as cisplatin. Indeed, HDAC inhibition increases histone acetylation, decreasing histone-DNA interactions and allowing for chemo-sensitization versus DNA-damaging agents [6,35]. Members of medium chain fatty
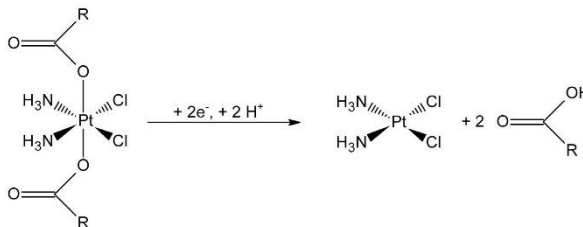
**Scheme 1.** Activation by reduction mechanism of a generic cisplatin-based Pt(IV) compound. R = alkyl or aryl substituent.

acid (MCFA) family as valproate (VPA) and phenyl-butyrate (PhB), have proved themselves as HDACi, and have been abundantly discussed in literature ([39,40,43]; Witt et al. 2017).

Here we report on a new Pt(IV) complex, based on cisplatin containing a different MCFA-HDACi, namely 2-(2-propynyl)octanoate (POA), along with an inert acetate (Ac) as axial ligands. POA has been reported to be more active than VPA inducing histone hyperacetylation in cerebellar granule cells [34], and showing antiproliferative activity on neuroblastoma cancer cells (neuritogenesis and differentiation) [5]. The resulting complex (OC-6-44)-acetatodiamminedichlorido(2-(2-propynyl)octanoato)platinum(IV), named Pt(IV)Ac-POA (Scheme 2), has showed a promising antitumor activity both in vitro and in vivo on several human cancer cell lines [21] with less side effects than cisplatin, as generally Pt(IV) derivatives do.

On these bases, the aim of our study is to evaluate the effects on the B50 neuroblastoma rat cells induced by exposure to Pt(IV)Ac-POA, to understand the activation of cell death pathways and the morphological and functional changes.

## 2. Materials and methods

### 2.1. Cell culture and treatments

B50 neuroblastoma rat cells (Istituto Zooprofilattico Sperimentale della Lombardia e dell'Emilia Romagna, catalogue no. BS TCL 115), were cultured in Dulbecco's Modified Eagle Medium (DMEM) supplemented with L-glutamine (2 mM), penicillin 100 IU ml$^{-1}$, streptomycin (100 mg l$^{-1}$) and 10% fetal bovine serum (FBS). Cell culture was carried out at 37 °C in a 5% $CO_2$ humidified chamber. Cells were challenged with Pt(IV)Ac-POA or free POA or free cisplatin for 48 h continuous treatment, CT, then viability assay, flow cytometry,

immunocytochemistry and molecular analysis were performed.

The cells were incubated with 40 μM cisplatin (Teva Pharma, Milan, Italy) for 48 h at 37 °C. This concentration was chosen considering in vivo experiments experimental design (i.e., a single injection of 5 μg/g b.w.) in the normal development nervous system [7] and corresponds to the dose most commonly used in the chemotherapy [4,17]. B50 cells were chosen since they offer several advantages for studying CNS neurons in culture [42]. Moreover these cells were previously used to investigate the mechanisms of cisplatin-induced cytotoxicity.

### 2.2. Antiproliferative activity and combination index

To assess the growth inhibition of the compounds under investigation, a cell viability test, i.e. the resazurin reduction assay was used. Briefly, cells were seeded in black sterile tissue-culture treated 96-well plates. At the end of treatment (48 h), viability was assayed by 100 μg mL$^{-1}$ resazurin (Acros Chemicals, France) in fresh medium for 1 h at 37 °C, and the amount of the reduced product, i.e. resorufin, was measured by means of fluorescence (excitation 535 nm, emission 595 nm) with a Tecan Infinite F200Pro plate reader (Tecan Austria). In each experiment, cells were exposed to the drugs at different concentrations and the final data were calculated from at least three replicates of the same experiment performed in triplicate. The fluorescence of 8 wells containing medium without cells were used as blank. Fluorescence data were normalized to 100% cell viability for non-treated cells.

Half inhibitory concentration (IC$_{50}$), defined as the concentration of the drug reducing cell viability by 50%, was obtained from the dose-response curve fitting using Origin Pro (version 8, Microcal Software, Inc., Northampton, MA, USA).

In the combination index (CI) analysis [15], Pt(IV)Ac-POA
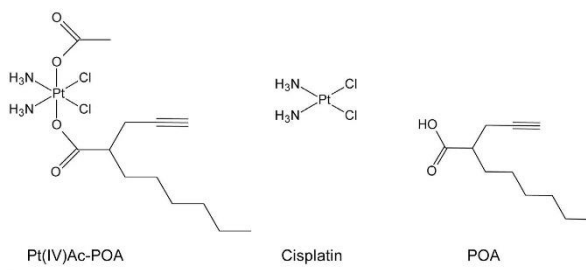


**Scheme 2.** Sketch of cisplatin, 2-(2-propynyl)octanoic acid, POA, and its Pt(IV) mixed derivative (OC-6-44)-acetatodiamminedichlorido(2-(2-propynyl)octanoato) platinum(IV), Pt(IV)Ac-POA.

conjugate was viewed as a combination of cisplatin and POA at fixed 1:1 dose ratio [53], according to its stoichiometry. The residual viability was compared to those obtained with free cisplatin or free POA as single treatments, by means of the simple formula:

$$CI = \frac{C1_m}{C1_a} + \frac{C2_m}{C2_a}$$

where C1 and C2 are the drug concentrations of metabolites cisplatin and POA in Pt(IV)Ac-POA (C1m and C2m) or when administrated as single treatment (C1a and C2a) to obtain the same level of residual viability. The value of CI allows evaluating drug interaction: $CI \cong 1$ indicates an additive effect, $CI < 1$ and a $CI > 1$ indicate synergism and antagonism, respectively.

### 2.3. Cell uptake

Cell uptake was measured according to already published procedure (Ravera et al.) [44]. Briefly, cells were seeded in T25 flasks and continuously treated for 4 h with 1 and 10 μM concentrations of Pt(IV)Ac-POA or free cisplatin, respectively. At the end of the exposure, cells were washed, detached from the flasks and harvested in fresh complete medium. An automatic cell counting device (Countess®, Life Technologies), was used to measure the cell number and the mean diameter from every cell count. About $5 \times 10^6$ cells were transferred into a glass tube, centrifuged, and the supernatant was carefully removed by aspiration. Cellular pellets were stored at −20 °C until mineralization. After defrosting, cells were mineralized with HNO$_3$ in an ultrasonic bath. Platinum determination was performed by inductively coupled plasma-mass spectrometry (ICP-MS, Thermo Optek X Series 2). The level of Pt found in cells after the treatment was normalized upon the cell number and the cellular volume, in order to obtain the intracellular Pt concentration. The ratio between the intracellular and the extracellular (in the culture medium) Pt concentration is defined accumulation ratio, AR [20].

### 2.4. Flow cytometry

B50 cells were treated in 75 cm² plastic flasks with different concentrations of Pt(IV)Ac-POA for 48 h at 37 °C (continued exposure to 1, 4 and 10 μM). After treatments, cells were detached by mild trypsinization (0.25% in phosphate-buffered saline, PBS, with 0.05% EDTA) to obtain single-cell suspensions to be processed for flow cytometry with a Partec PAS III flow cytometer (Münster, Germany), equipped with argon laser excitation (power 200 mW) at 488 nm. Data were analysed with the built-in software (Flowmax, Partec).

### 2.5. Cell cycle analysis and identification of apoptotic cells

Cells were washed in PBS, permeabilized in 70% ethanol for 10 min, treated with RNase A 100 U mL$^{-1}$ and then stained for 10 min at room temperature with Propidium Iodide (PI) 50 μg mL$^{-1}$ (Sigma-Aldrich, Milan, Italy) 1 h before flow cytometric analysis. PI red fluorescence was detected with a 610-nm long-pass emission filter. At least 20,000 cells *per* sample were measured to obtain the distribution among the different phases of the cell cycle and the percentage of apoptotic cells.

### 2.6. Analysis of cell death with Annexin V assay

Single-cell suspensions, obtained as described above, were incubated with Annexin V-FITC (Annexin V-FITC Apoptosis Detection Kit, Abcam, Italy) for 10 min in the dark. Propidium Iodide was used as a counterstain to discriminate necrotic/dead cells from apoptotic cells. Fluorescence was revealed by means flow cytometry at 488 nm excitation and with 530/30 (FITC) and 585/42 (PI) band-pass emission filters.

### 2.7. Transmission electron microscopy (TEM)

B50 cells treated with different concentrations of Pt(IV)Ac-POA (1, 4 and 10 μM) were harvested by mild trypsinization (0.25% trypsin in PBS containing 0.05% EDTA) and collected by centrifugation at 800 rpm for 5 min in fresh tubes. The samples were immediately fixed with 2.5% glutaraldehyde in culture medium (2 h at room temperature), centrifuged at 2000 rpm for 10 min and washed several times with PBS. Then, samples were post-fixed in 1% OsO$_4$ for 2 h at room temperature and washed in water. The cell pellets were pre-embedded in 2% agar, dehydrated with increasing concentrations of acetone (30, 50, 70, 90 and 100%, respectively). Finally, the pellets were embedded in EPON resin and polymerized at 60 °C for 48 h. Ultrathin sections were obtained with ultramicrotome Rechter, then placed on nickel grids and stained with uranyl acetate and lead citrate. Sections were observed under a Zeiss EM 900 transmission electron microscope operating at 80 kV. The plates, after being developed, have been computerized through Epson Perfection 4990 Photo scanner at a resolution of 600 dpi and then processed using the Epson Scan software.

### 2.8. Measurement of mitochondrial membrane potential with JC-1

Changes in mitochondrial membrane potential were monitored using the JC-1 dye (namely, 5,5′,6,6′-tetrachloro-1,1′,3,3′-tetraethylbenzimidazolylcarbocyanine iodide, Molecular Probes, Invitrogen, Italy). B50 cells, harvested as described above, were incubated in culture medium with 2 μM JC-1 for 20 min at 37 °C in the dark. After two washes with PBS at 37 °C, the suspension was analysed at 488 nm excitation and with 530/30 and 585/42 nm band-pass emission filters.

### 2.9. Immunocytochemical reactions at fluorescence microscope

B50 cells were grown on coverslips and treated with the compound under investigation Pt(IV)Ac-POA at the concentration of 4 μM. After 48 h, the cells were fixed with 4% formalin for 20 min and post-fixed with 70% ethanol at −20 °C for at least 24 h. Samples were rehydrated for 10 min in PBS and then immunolabeled with primary antibodies for 60 min at room temperature in a dark moist chamber. After some washes in PBS, coverslips were incubated with secondary antibodies for 45 min. After that, sections were counterstained for DNA with 0.1 μg mL$^{-1}$ Hoechst 33258 (Sigma-Aldrich, Milano, Italy), washed with PBS, and mounted in a drop of Mowiol (Calbiochem, Inalco, Italy), for fluorescence microscopy analysis. An Olympus BX51 microscope equipped with a 100-W mercury lamp was used under the following conditions: 330–385 nm excitation filter (excf), 400 nm dichroic mirror (dm) and 420 nm barrier filter (bf) for Hoechst 33258; 450–480 nm excf, 500 nm dm and 515 nm bf for the fluorescence of Alexa 488; 540 nm excf, 580 nm dm and 620 nm bf for Alexa 594. Images were recorded with an Olympus MagniFire camera system and processed with the Olympus Cell F software. The percentage of caspase-positive cells was obtained by counting the cells on coverslips.

Primary and secondary antibodies used for immunocytochemical reactions at fluorescence microscope are reported in Table 1.

### 2.10. Western blotting

After treatments with cisplatin and Pt(IV)Ac-POA cells were washed twice with PBS and lysed in RIPA buffer (Tris HCl 1 M pH 7.6, EDTA 0.5 M pH 8, NaCl 5 M, NP40 Nonidet 100%, with the addition of proteases and phosphatases inhibitors) at 4 °C for 30 min. Proteins were quantified using the Bradford reagent (Sigma Aldrich, Italy). Samples were electrophoresed in a 15% SDS-PAGE minigel and transferred onto a nitrocellulose membrane (Bio-Rad, Hercules, CA) by a semidry blotting for 1.30 h under a constant current of 60 mA. The membranes were saturated for 30 min with PBS containing 0.2% Tween-20 and 5% skim milk, and incubated *overnight* with monoclonal mouse anti-PCNA

**Table 1**
Primary and secondary antibodies used for immunocytochemical reactions at fluorescence microscope.

| Primary antibody | | Dilution | Secondary antibody | Dilution |
|---|---|---|---|---|
| Caspase-9 | Polyclonal rabbit anti-caspase-9 (Cell Signaling Technology, Danvers, USA) | 1:200 in PBS | Alexa 594-conjugated anti-rabbit antibody (Molecular Probes, Invitrogen) | 1:200 in PBS |
| Caspase-3 | Monoclonal rabbit anti-caspase-3 (Cell Signaling Technology, Danvers, USA) | 1:200 in PBS | Alexa 594-conjugated anti-rabbit antibody (Molecular Probes, Invitrogen) | 1:200 in PBS |
| PARP-1 | Monoclonal rabbit anti-PARP1 (Cell Signaling Technology, Danvers, USA) | 1:200 in PBS | Alexa 594-conjugated anti-rabbit antibody (Molecular Probes, Invitrogen) | 1:200 in PBS |
| Caspase-8 | Monoclonal rabbit anti-caspase-8 (Cell Signaling Technology, Danvers, USA) | 1:100 in PBS | Alexa 594-conjugated anti-rabbit antibody (Molecular Probes, Invitrogen) | 1:200 in PBS |
| RIP1 | Polyclonal rabbit anti-RIP1 (Santa Cruz Biotechnology) | 1:200 in PBS | Alexa 594-conjugated anti-rabbit antibody (Molecular Probes, Invitrogen) | 1:200 in PBS |
| Golgi | Human autoimmune serum recognizing proteins of Golgi Apparatus[a] | 1:200 in PBS | Alexa 594-conjugated anti-human antibody (Molecular Probes, Invitrogen) | 1:200 in PBS |
| Mitochondria | Human autoimmune serum recognizing the 70 kDa E2 subunit of the pyruvate dehydrogenase complex[a] | 1:200 in PBS | Alexa 594-conjugated anti-human antibody (Molecular Probes, Invitrogen) | 1:200 in PBS |
| LC3B | Polyclonal rabbit anti-LC3B (Cell Signaling Technology, Danvers, USA) | 1:400 in PBS | Alexa 594-conjugated anti-rabbit antibody (Molecular Probes, Invitrogen) | 1:200 in PBS |
| Lysosomes | Human autoimmune serum recognizing lysosomal proteins[a] | 1:400 in PBS | Alexa 488-conjugated anti-human antibody (Molecular Probes, Invitrogen) | 1:200 in PBS |
| α-Tubulin | Monoclonal mouse anti-α-tubulin (Invitrogen) | 1:100 in PBS | Alexa 488-conjugated anti-mouse antibody (Molecular Probes, Invitrogen) | 1:200 in PBS |
| PCNA | Monoclonal mouse anti-PCNA (Abcam, Cambridge, USA) | 1:200 in PBS | Alexa 594-conjugated anti-mouse antibody (Molecular Probes, Invitrogen) | 1:200 in PBS |
| Actin | Alexa 488-Phalloidin (Molecular Probes, Invitrogen) | 1:40 in PBS | | |

[a] Buttone et al. [9]

antibody (1:5000, Abcam, Cambridge, USA). After several washes with PBS-Tween, the membranes were incubated for 30 min with the proper secondary antibody conjugated with horseradish peroxidase (1:2000, Dako, Italy). Immunoreactive bands were detected with the reagent Luminata ™ Crescendo (Merck Millipore, Billerica, MA), according to the appropriate instructions, and revealed on Amersham HyperfilmTM ECL (GE Healthcare, Little Chalfont, UK) slabs. The density of the protein bands were normalized with the respective actin and subsequently with the loading control using Image J software.

### 2.11. Statistical analysis

Every experiment was performed with three independent replicates and the obtained scores were expressed as the mean ± SD (standard deviation) or SEM (standard error of mean). Data differences were analysed for statistical significance by means of a Student's t-test.

## 3. Results

### 3.1. Antiproliferative activity, combination index and cellular accumulation

Pt(IV)Ac-POA was tested on the B50 neuroblastoma rat cell line along with free cisplatin and free POA as reference compounds. Noteworthy, Pt(IV)Ac-POA exhibited an $IC_{50}$ value one orders of magnitude lower (higher potency) than the prototypal metal-drug cisplatin (Table 2 and Fig. 1A). Fig. 1A shows that the preformed Pt(IV)Ac-POA was by far more active than both drugs when administered alone.

In order to further verify if POA enhances the antitumor effect of cisplatin, a combination index was computed. Pt(IV)Ac-POA conjugate was viewed as a combination of cisplatin and POA at fixed 1:1 dose ratio, according to its stoichiometry (see Materials and Methods). At every level of residual viability, CI analysis showed a strong synergistic effect (CI around 0.01) (Fig. 1B).

A key parameter of the mechanisms of action of a drug is its cellular accumulation [36]. Accordingly, when B50 cells were challenged with Pt(IV)Ac-POA, CT 4 h (Table 2), the Pt accumulation ratio (AR) resulted around 12 times higher than that of free cisplatin, in tune with its higher potency (Table 2).

A further investigation on the antiproliferative propensity of Pt(IV)Ac-POA was carried out. The level of the proliferation marker PCNA (Proliferating Cell Nuclear Antigen), correlated in the literature with the degree of glioma malignancy [26] or the efficiency of antitumor treatment [32], was evaluated by western blotting. Fig. 2 shows the PCNA expression in cells after CT with 40 μM cisplatin or 4 μM Pt(IV)Ac-POA.

Data indicated a reduction (compared to control) in PCNA expression in cells after all treatments, in particular after exposition to Pt(IV)Ac-POA, thus indicating a synergistic inhibition of PCNA by the combo compound (Fig. 2).

### 3.2. Cell cycle distribution

The first graph of Fig. 3A represents the distribution of DNA in B50 cells. Decreasing Pt(IV)Ac-POA concentrations (namely 10, 4 and 1 μM)

**Table 2**
Antiproliferative activity ($IC_{50}$) obtained after 48 h CT and accumulation ratio (AR) obtained after 4 h CT. All data are means ± SEM of at least three independent replicates.

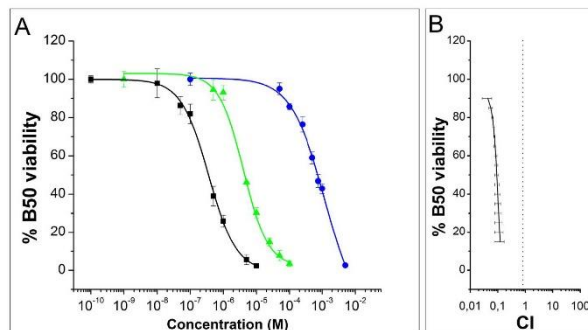| Compound | B50 | |
|---|---|---|
| | $IC_{50}$(μM) | AR |
| POA | 750 ± 120 | – |
| Cisplatin | 3.8 ± 0.6 | 2.3 ± 0.5 |
| Pt(IV)Ac-POA | 0.37 ± 0.05 | 26.9 ± 0.1 |

**Fig. 1.** (A) B50 cells were treated for 48 h with cisplatin (green triangles), POA (blue dots), or the 1:1 the combo molecule Pt(IV)Ac-POA (black squares). Data are means ± standard deviation of a representative experiment. Residual viability was assessed by means of the resazurin reduction assay and data were fitted with a four-parameter function (green, blue, and black lines, respectively). Residual viability data were compared to obtain the Combination index (CI) value. (CI < 1: synergism; CI around 1 additive effect; CI > 1 antagonism). (B) CI plot (black line) for the 1:1 the combo molecule Pt(IV)Ac-POA. (For interpretation of the references to colour in this figure legend, the reader is referred to the web version of this article.)
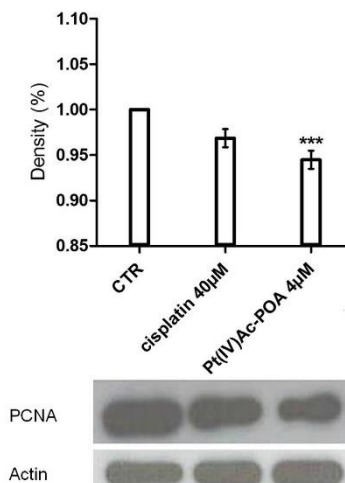


**Fig. 2.** Western blotting of PCNA following 48 h CT with 40 μM cisplatin or 4 μM Pt(IV)Ac-POA. The density of the bands was normalized over actin and over the untreated control (CTR). Data are means ± SEM. Statistical analysis: number of observations per control and treated samples: 3; $*p < 0.05$; $**p < 0.01$; $***p < 0.001$.

were used for 48 h CT. Untreated cells (CTR) were distributed among the cell phases ($G_1$, S, $G_2$), the intensity of S phase indicated that the cells were proliferating. Conversely, the treatment with 10 μM CT deeply modified the histogram distribution. We observed a massive number of cells in sub-$G_1$ phase (dead cells), while peaks $G_1$, S and $G_2$ were almost absent. After 4 μM CT the sub-$G_1$ peak was still evident, while the presence of $G_1$ and S peaks and the absence of $G_2$ peak indicated arrested proliferation. After 1 μM CT, the cells were still distributed in the different phases of cell cycle, along with a small sub-$G_1$ peak.

### 3.3. Ultrastructural analysis

In control, (Fig. 3B.a) the sample cell was characterized by the presence of a nucleus in peripheral position, a decondensed chromatin and a large nucleolus. Reticulum endoplasmic and Golgi Apparatus were present in perinuclear zone and there were small-to-medium size mitochondria in cytoplasm and sporadic lysosomes. In Fig. 3B.b cell after 10 μM CT exhibited typical necrosis morphology. Indeed, an evident subcellular disorganization and disaggregation of organelles and cytoskeletal components were observed. Moreover, the fragmentation of the nucleus and highly condensed chromatin (karyorrhexis) were also detectable.

Treatments with 1 μM (Fig. 3B.c) and, even more, with 4 μM (Fig. 3B.d) seem to induce autophagy. A reduction of nucleus volume (pyknosis) and an increase of lysosomes and autophagic vacuole number were observed. Some vacuoles contained membranous cytoplasmic residues in the degradation phase, which can be attributable to autophagosomes. In addition, elongated mitochondria were observed, a characteristic of a cell that tries to survive [46].

One cell in apoptosis and another in necroptosis were evidenced in Fig. 3B.e and B.f, several types of cell death were detectable in the sample treated at 4 μM.

### 3.4. Flow cytometric analysis after staining with Annexin V and PI

To assess the induction of apoptosis after 4 and 10 μM CT with Pt(IV)Ac-POA, a test with Annexin V/PI staining was performed. Fig. 3C shows that in the control almost all cells are living, while after treatments the number of viable cells tended to decrease drastically. In particular, at 4 μM an increase of late apoptotic cells (Q3, yellow bars) compared to control (62.6 ± 0.8 vs 2.1 ± 0.2) was observed. At 10 μM CT necrotic cells (Q2, red bars) increased compared to 4 μM CT (45.79 ± 0.32 vs 10.88 ± 0.44).

For this reason, the concentration of 4 μM of Pt(IV)Ac-POA was chosen hereafter for the standard 48 h CT.

### 3.5. Activation of apoptotic pathways

The intrinsic pathway is activated by several stimuli making permeable the mitochondrial membrane. The results obtained with JC-1 assay in cytofluorometric analysis demonstrated a perturbation of the mitochondrial membrane potential (MMP). In treated cells, the fluorescence changed from orange (JC-1 aggregates, Q3), observed in the control, to green fluorescent (monomeric JC-1, Q4), indicating a significant depolarization of MMP [1] (Fig. 4A and B).
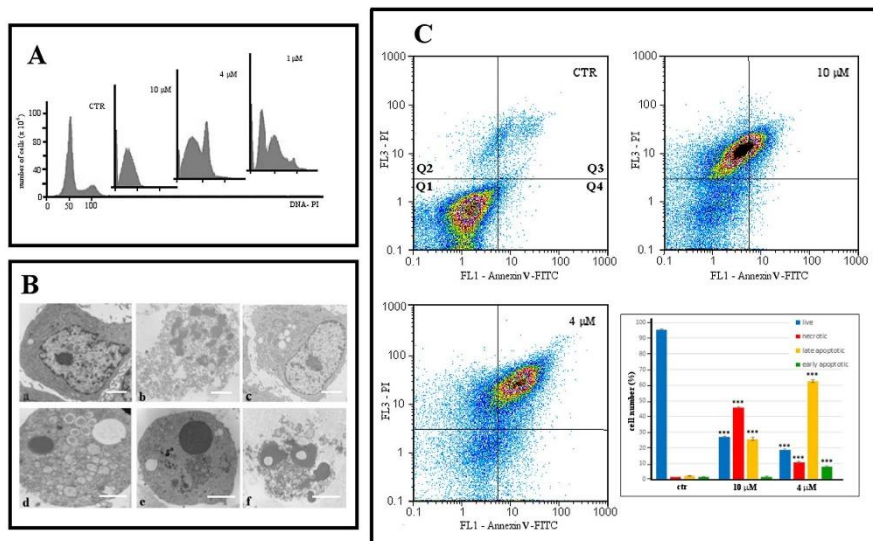
**Fig. 3.** (A) Histograms of DNA content in Flow cytometry after PI staining in B50 control cells (CTR) and treated for 48 h with Pt(IV)Ac-POA at different concentrations (10, 4 and 1 μM). (B) Electron microscopy. a) B50 cell in control condition. B) B50 cell after treatment with Pt(IV)Ac-POA at 10 μM for 48 h. c) B50 cell after treatment with Pt(IV)Ac-POA at 1 μM for 48 h. d), e), f) B50 cells after treatment with Pt(IV)Ac-POA at 4 μM for 48 h. Pictures d–f show examples of cell death for d) autophagy, e) apoptosis, and f) necroptosis. Bars: 1.5 μm. (C) Dual parameter cytograms of FITC-labelled Annexin V (FL1) versus PI staining (FL3) of the control (CTR, upper left plot) and of cells treated with Pt(IV)Ac-POA at 10 (upper right plot) and 4 μM (lower left plot) concentrations, respectively. The histogram represents the average of three independent experiments, shows the values percentage of Annexin V/PI positive cells; in quadrant Q1 (viable cells), Q2 (necrotic), Q3 (late apoptotic) and Q4 (early apoptotic). Statistical analysis: number of observations per control and treated samples: 5; *p < 0.05; **p < 0.01; ***p < 0.001.

Furthermore, to evaluate the activation of apoptotic pathway, immunocytochemical detection for active caspase -9,-3 and for PARP-1 was performed.

In the intrinsic apoptotic pathway, the executive caspase-3 was activated by caspase-9: in control condition, cells were not immunopositive to caspase-3, as testified by the presence of only proliferative viable cells (mitosis is visible in the lower-left box of Fig. 5B). In this condition, actin cytoskeletal was well organized in filaments within all cytoplasm. After treatment, the cells underwent apoptosis: the immunopositivity of both caspase-9 and caspase-3 (red fluorescence) was increased. In this condition, cell morphology was altered: the cells had a round shape and their nucleus appeared fragmented (visible in the lower left panel of Fig. 5B). The actin cytoskeleton collapsed, with inhomogeneous distribution localized around the nucleus.

The percentage of caspase-3 positive cells was 3 ± 0.5% in the control and 52 ± 2% in the samples after CT.

Poly [ADP-ribose] polymerase 1, PARP-1, is an enzyme involved in repair processes of DNA. Its proteolytic cleavage fragments, i.e. "cleaved PARP-1" are one of the hallmark of apoptosis, since PARP-1 is a preferential substrate for caspase-3. The longer fragment is released from the nucleus to the cytosol, due to its lower DNA-binding affinity [14]. Accordingly, PARP-1 (red fluorescence) was found colocalized in nuclei in control and in early apoptotic cells (Fig. 5C), while it moved to the cytoplasm in late apoptotic cells, where nuclei resulted clearly fragmented. The cytoskeletal tubulin showed alterations and formed aggregates, so the cells lost their tapered shape.

Caspase-8 is involved in the extrinsic apoptotic pathway; and its activation is induced by the death receptors Fas, tumour necrosis factor receptor-1 and death receptor-3. In Fig. 5D, a high increase in caspase-8 cytoplasmic immunopositivity (red fluorescence) was observed in cells treated only.

To confirm the activation of the extrinsic apoptotic pathway, an immunocytochemical detection of RIP1 (receptor-interacting protein kinase 1), which is a caspase-8 substrate, was performed. In control cells (Fig. 5E), RIP1 was expressed in the cytoplasm with a homogeneous distribution, but the treatment caused a redistribution of RIP1 from the cytoplasm to a perinuclear zone, indicating that active RIP1 translocated from the cytoplasm, which was totally destroyed in tardive apoptosis.

### 3.6. Evaluation of autophagy

LC3 is an ubiquitin-like protein that is cleaved at its C-terminal to form LC3B-I (14 kDa). LC3B-I is then conjugated to phosphatidylethanolamine in the autophagosome membrane to form LC3B-II (16 kDa) [28]. In control cells, LC3B was detected both in the nucleus and in the cytoplasm and did not colocalize with lysosomes in the cytoplasm. On the contrary after CT, LC3B moved mostly into the cytoplasm of apoptotic cells (Fig. 5F). In particular, in early apoptosis LC3B colocalized with lysosomes in the cytoplasm (represented in the box), whereas in late apoptosis there was no colocalization and lysosomes decreased.
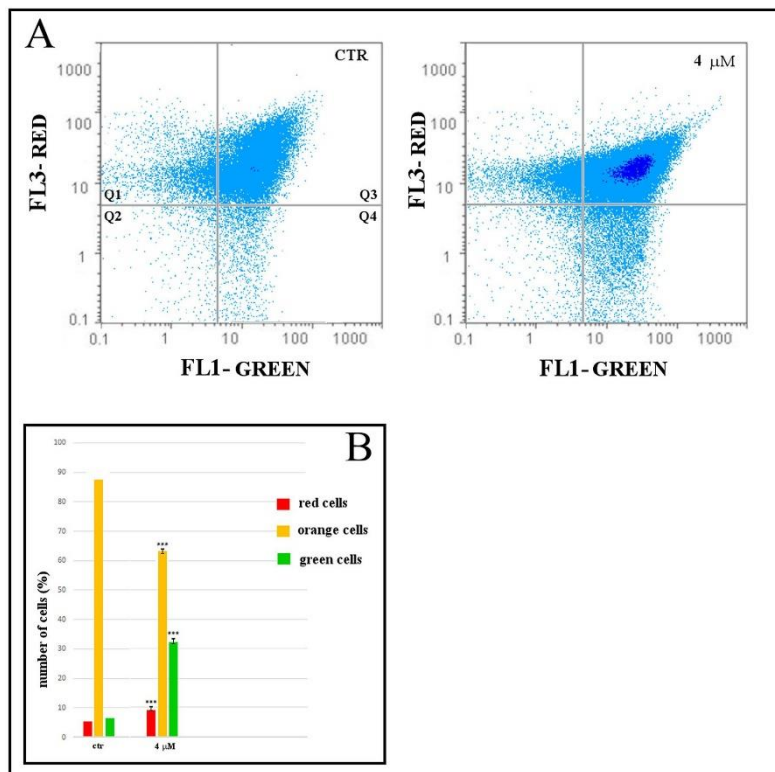
**Fig. 4.** Effect of Pt(IV)Ac-POA treatment on mitochondrial potential of B50 cells. (A) Cytometric analysis of green-versus-red fluorescence of JC-1 showing cell falling into the red fraction (Q1), the orange fraction (Q3) and green fraction (Q4). Representative plots of the control (CTR, upper left plot) and 4 μM Pt(IV)Ac-POA (upper right plot) treated samples. (B) Histograms with percentage of JC-1 positive cells: green, red and orange cells bar chart. Statistical analysis: number of observations per control and treated samples: 3; $^*p < 0.05$; $^{**}p < 0.01$; $^{***}p < 0.001$. (For interpretation of the references to colour in this figure legend, the reader is referred to the web version of this article.)

### 3.7. Effects of Pt(IV)Ac-POA on intracellular organelles

We evaluated also the effects of Pt(IV)Ac-POA on cytoplasmic organelles, such as Golgi Apparatus and mitochondria. In control cells (Fig. 6A), immunofluorescence for Golgi apparatus (red fluorescence) appeared homogeneous with a perinuclear localization while the actin cytoskeleton maintained its organization. After CT, cells underwent to death showing evident alterations. In this condition, the nucleus was fragmented and the actin cytoskeleton collapsed around it; Golgi Apparatus lost its tubular connections and resulted distributed in the cytoplasm.

In control, mitochondria (red fluorescence) with a spotted-like shape, localized in cytoplasm and near the nucleus, were observed (Fig. 6B). Compared to control, treated cells showed mitochondria with morphological alterations, in particular the immunofluorescence for mitochondria appeared homogeneous and these organelles clustered

and formed dense masses around the nucleus.

### 4. Discussion and conclusions

Cisplatin has been used for almost half a century in the chemotherapeutic treatment of different types of cancer [29]. Many side effects, including nephrotoxicity, neurotoxicity, ototoxicity, etc., limit its clinical application [49].

In recent years, many attempts have been made to obtain molecules that can overcome these problems [51]. Particularly, new platinum(II)-based compounds, which have as the cellular targets the amino acid residues of protein, have been synthesized [16,38] and were used compared to cisplatin treatment, showing a lower cytotoxicity in vivo studies on development of rat cerebellum and hippocampus [8]. In addition, in vitro studies, these new platinum(II)-based compounds have been shown to induced, similarly to cisplatin, apoptotic cell death
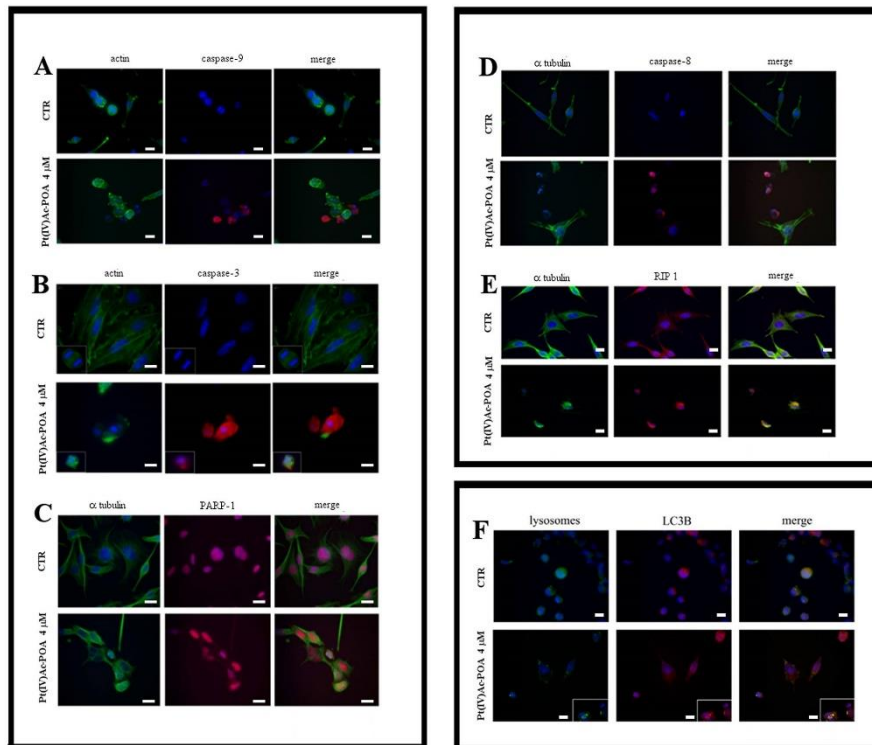
**Fig. 5.** Double immunocytochemical detection in control (CTR) and 48 h Pt(IV)Ac-POA at 4 μM treated cells: (A) caspase-9 (red fluorescence) and actin (green fluorescence); (B) caspase-3 (red fluorescence) and actin (green fluorescence); (C) PARP-1 (red fluorescence) and α tubulin (green fluorescence); (D) caspase-8 (red fluorescence) and actin (green fluorescence); (E) RIP1 (red fluorescence) and α tubulin (green fluorescence); (F) LC3B (red fluorescence) and lysosomes (green fluorescence). DNA was counterstained with Hoechst 33258 (blue fluorescence). Bars: 20 μm. (For interpretation of the references to colour in this figure legend, the reader is referred to the web version of this article.)

in B50 neuroblastoma rat cells at concentration 4 times lower than cisplatin [25].

Nowadays, platinum(IV) prodrugs are actively investigated [23]. In particular, a new prodrug, namely Pt(IV)Ac-POA, has been recently synthesized [21]. This complex is a new multi-action prodrug candidate, designed as a cisplatin/POA "combo" molecule. This considerable advantage is due to its ability to deliver at the same time huge amounts of cisplatin and POA in cells. This enhancement of cellular uptake is mainly due to the lipophilicity of the Pt(IV)Ac-POA assembly with respect to the hydrophilic cisplatin and the amphiphilic POA (in anionic form at physiologic pH) precursors, enhancement referred as "*synergistic cellular accumulation*" [21].

The action of POA as an HDAC inhibitor represents a promising strategy specifically for neuroblastoma chemotherapy [41,52]. In particular, HDAC8 inhibition enhances the effects of DNA-damaging drugs, as cisplatin, inducing overall chemosensitization and decreasing chemoresistance [52]. Furthermore, POA has showed a strong

antiproliferative activity associated with morphological changes in neuroblastoma cells (neuritogenesis and differentiation) [5]. The limit of HDACi is the need of high dosages, giving rise to considerable side effects [41]. Pt(IV)Ac-POA could bypass the problem because Pt(IV)-based complexes are stable in the bloodstream [18] and enter tumour cells to higher extent than free POA [27]. In aggregate, Pt(IV)Ac-POA could offer the advantages of cisplatin (DNA-damaging activity) and of POA (HDAC inhibition) without the limiting toxicities of both agents when administered individually on neuroblastoma.

Viability assays showed that this prodrug has a higher antiproliferative activity than cisplatin on B50 cell line, since its half-maximal inhibitory concentration (IC$_{50}$) after 48 h CT was 0.37 compared to 3.8 μM for cisplatin. The higher activity of Pt(IV)Ac-POA has been further confirmed by the decreased PCNA expression and by the different cell cycle distribution.

Pt(IV)Ac-POA exhibited a strong synergistic effect in respect to the free drugs, taking advantage of an exceptional increase of cellular
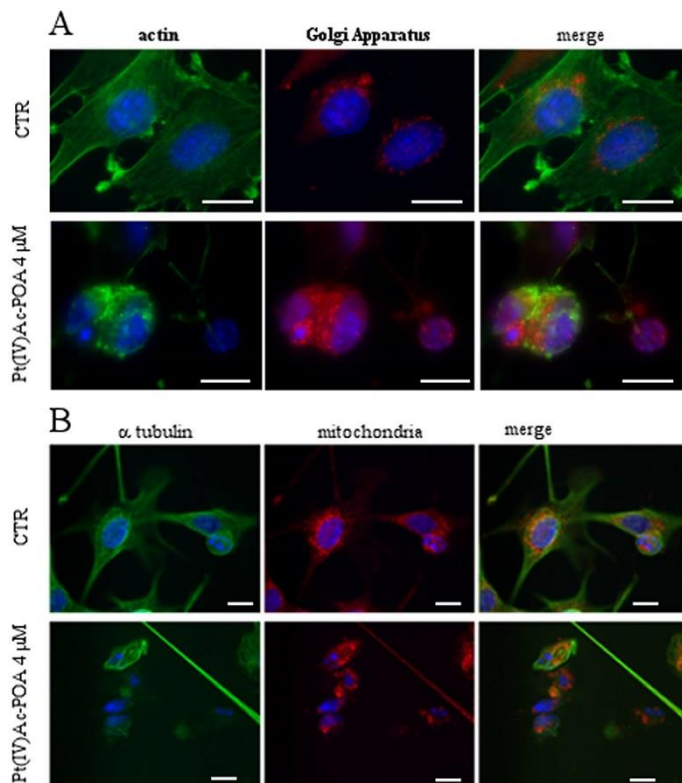
**Fig. 6.** (A) Golgi apparatus (red fluorescence) and actin (green fluorescence) in control and 48 h Pt(IV)Ac-POA at 4 μM treated cells. (B) Double immunocytochemical detection of mitochondria (red fluorescence) and α tubulin (green fluorescence) in control and 48 h Pt(IV)Ac-POA at 4 μM treated cells. DNA was counterstained with Hoechst 33258 (blue fluorescence). Bars: 20 μm. (For interpretation of the references to colour in this figure legend, the reader is referred to the web version of this article.)

uptake, often referred as "*synergistic cellular accumulation*" (e.g. [21]).

Results obtained by Santin et al. proved that cisplatin induced 22% of caspase-3 positive apoptotic cells in B50 cell line [45], while Pt (IV)Ac-POA, used at a concentration ten time less than cisplatin, causes a higher apoptotic effect (52%).

Electron microscopy analysis demonstrated that after 10 μM CT, cells exhibited necrotic morphology, while after 4 μM CT, cells showed apoptotic morphology. In addition, cells with autophagic characteristics were also detectable, as the activation of autophagy which may concur in type II cell death. An immunocytochemical staining of different markers confirmed the activation of different pathways. The treated samples were immunopositive to cleaved PARP-1 and caspases-9, -3, -8 and RIP1 demonstrating the activation of both the intrinsic and extrinsic apoptotic pathways. Since RIP1 is also involved in a preliminary step of the necroptotic pathway, we could not exclude its activation as some cells showed the typical necroptotic morphology [2,22]. The

colocalization of the staining for LC3B and lysosomes suggested the activation of the autophagic pathway [47].

JC-1 staining showed a drop of the mitochondrial membrane potential, a further indication that Pt(IV)Ac-POA is able to induce apoptosis. Indeed, this dye is a valuable indicator of the health and functional state of the cells [33]. Like cisplatin [3], the new prodrug also targets cytoplasmic organelles: after fluorescent immunolabelling mitochondria appeared small and rounded and often organized in clusters in dying cells. In control cells, Golgi apparatus had flattened perinuclear tanks, while after treatment it was observed as round bodies in cytoplasm. The actinic and tubulinic cytoskeleton disassembled and reorganized, assuming a more homogeneous appearance.

Considering that Pt(IV)Ac-POA prodrug acts on B50 neuroblastoma rat cells at concentration ten times lower respect to cisplatin and induced different patterns of cell death, it could represent a potential alternative to cisplatin.

## Conflict of interest

The authors declare no conflict of interest.

## Author contributions

All authors had full access to all experimental data and assume responsibility for the integrity and accuracy of data and analysis.

MG Bottone: study concept and design, analysis and interpretation of data, writing and finalizing the manuscript and supervision; B Rangone: analysis and interpretation of data, writing the manuscript; B Ferrari: analysis and interpretation of data, writing the manuscript; V Astesana: analysis and interpretation of data, writing the manuscript; I Masiello: Acquisition, analysis and interpretation of data; P Veneroni technical assistance for cell culture; I Zanellato: analysis and interpretation of data, writing the manuscript; D Osella: analysis and interpretation of data, writing and finalizing the manuscript.

Beatrice Rangone and Beatrice Ferrari: both authors contributed equally to this work.

## Acknowledgements

## References

[1] E. Bedner, X. Li, W. Gorczyca, M.R. Melamed, Z. Darzynkiewicz, Analysis of apoptosis by laser scanning cytometry, Cytometry 35 (1999) 181–195.

[2] J. Belizário, L. Vieira-Cordeiro, S. Enns, Necroptotic cell death signaling and execution pathway: lessons from knockout mice, Mediat. Inflamm. 2015 (2015) 128076, https://doi.org/10.1155/2015/128076.

[3] G. Bernocchi, M.G. Bottone, V.M. Piccolini, V. Dal Bo, G. Santin, S.A. De Pascali, D. Migoni, P.F. Fanizzi, Developing central nervous system and vulnerability to platinum compounds, Chemother. Res. Pract. 2011 (2011) 315418, https://doi.org/10.1155/2011/315418.

[4] D.L. Bodenner, P.C. Dedon, P.C. Keng, J.C. Katz, R.F. Borch, Selective protection against cis-diamminedichloroplatinum (II)-induced toxicity in kidney, gut, and bone marrow by diethyldithiocarbamate, Cancer Res. 46 (1986) 2751–2755.

[5] U. Bojic, K. Ehlers, U. Ellerbeck, C.L. Bacon, E. O'Driscoll, C. O'Connell, V. Berezin, A. Kawa, E. Lepekhin, E. Bock, C.M. Regan, H. Nau, Studies on the teratogen pharmacophore of valproic acid analogues: evidence of interactions at a hydrophobic centre, Eur. J. Pharmacol. 354 (2–3) (1998) 289–299, https://doi.org/10.1016/S0014-2999(98)00462-2.

[6] J.E. Bolden, M.J. Peart, R.W. Johnstone, Anticancer activities of histone deacetylase inhibitors, Nat. Rev. Drug Discov. 5 (2006) 769–784, https://doi.org/10.1038/nrd2133.

[7] M.G. Bottone, C. Soldani, P. Veneroni, D. Avella, M.B. Pisu, G. Bernocchi, Cell proliferation, apoptosis and mitochondrial damage in rat B50 neuronal cells after cisplatin treatment, Cell Prolif. 41 (2008) 506–520, https://doi.org/10.1111/j.1365-2184.2008.00530.x.

[8] M.G. Bottone, G. Santin, V.M. Piccolini, V. Dal Bo, G. Bernocchi, Cisplatin neurotoxicity induces cell death in vivo and in vitro, Cisplatin: Pharmacology, Clinical Uses and Adverse Effects, Nova Science Publishers, 2011, https://www.novapublishers.com/catalog/product_info.php?products_id=37177.

[9] M.G. Bottone, G. Santin, C. Soldani, P. Veneroni, A.I. Scovassi, C. Alpini, Intracellular distribution of Tankyrases as detected by multicolor immunofluorescence techniques, Eur. J. Histochem. 56 (2012) e4, https://doi.org/10.4081/ejh.2012.e4.

[10] T. Boulikas, A. Pantos, E. Bellis, P. Christofis, Designing platinum compounds in cancer: structures and mechanism, J. Cancer Ther. 5 (2007) 537–583.

[11] G.M. Brodeur, M.D. Hogarty, Y.P. Mossé, J.M. Maris, Neuroblastoma, in: P.A. Pizzo, D.G. Poplack (Eds.), Principle and Practice of Pediatric Oncology, 6th ed., Lippincott, Williams and Wilkins, Philadelphia (PA), USA, 2011, pp. 886–922.

[13] G. Cavaletti, B. Frigeni, F. Lanzani, L. Mattavelli, E. Susani, P. Alberti, D. Cortinovis, P. Bidoli, Chemotherapy-induced peripheral neurotoxicity assessment: a critical revision of the currently available tools, Eur. J. Cancer 46 (2010) 479–494, https://doi.org/10.1016/j.ejca.2009.12.008.

[14] G.V. Chaitanya, J.S. Alexander, P.P. Babu, PARP-1 cleavage fragments: signatures of cell-death proteases in neurodegeneration, Cell Commun. Signal 8 (2010) 31, https://doi.org/10.1186/1478-811X-8-31.

[15] T.C. Chou, P. Talalay, Quantitative analysis of dose-effect relationships: the combined effects of multiple drugs or enzyme inhibitors, Adv. Enzym. Regul. 22 (1984) 27–55, https://doi.org/10.1016/0065-2571(84)90007-4.

[16] S.A. De Pascali, P. Papadia, A. Ciccarese, C. Pacifico, F.P. Fanizzi, First examples of βdiketonate platinum II complexes with sulfoxide ligands, Eur. J. Inorg. Chem. 5 (2005) 788–796, https://doi.org/10.1002/ejic.200400665.

[17] J. Dietrich, R. Han, Y. Yang, M. Mayer-Pröschel, M. Noble, CNS progenitor cells and oligodendrocytes are target of chemotherapeutic agents in vitro and in vivo, J. Biol. 5 (2006) 22–34, https://doi.org/10.1186/jbiol50.

[18] R.C. Dolman, G.B. Deacon, T.W. Hambley, Studies of the binding of a series of platinum(IV) complexes to plasma proteins, J. Inorg. Biochem. 88 (3–4) (2002) 260–267, https://doi.org/10.1016/S0162-0134(01)00360-9.

[19] C. Fenoglio, C.A. Boicelli, M. Ottone, C. Addario, P. Chiari, M. Viale, Protective effect of procaine hydrochloride on cisplatin-induced alterations in rat kidney, Anti-Cancer Drugs 13 (10) (2002) 1043–1054, https://doi.org/10.1097/00001813-200211000-00008.

[20] E. Gabano, M. Ravera, D. Osella, Pros and cons of bifunctional platinum(IV) antitumor prodrugs: two are (not always) better than one, Dalton Trans. 43 (2014) 98213–99820, https://doi.org/10.1039/c4dt00911h.

[21] E. Gabano, M. Ravera, I. Zanellato, S. Tinello, A. Gallina, B. Rangone, V. Gandin, C. Marzano, M.G. Bottone, D. Osella, An unsymmetric cisplatin-based Pt(IV) derivative containing 2-(2-propynyl)octanoate: a very efficient multi-action antitumor prodrug candidate, Dalton Trans. 46 (2017) 14174–14185, https://doi.org/10.1039/c7dt02928d.

[22] L. Galluzzi, O. Kepp, G. Kroemer, Mitochondrial regulation of cell death: a phylogenetically conserved control, Microb. Cell Fact. 3 (2016) 101–108, https://doi.org/10.15698/mic2016.03.483.

[23] D. Gibson, Platinum(IV) anticancer prodrugs - hypotheses and facts, Dalton Trans. 45 (33) (2016) 12983–12991, https://doi.org/10.1039/c6dt01414c.

[24] N. Graf, S.J. Lippard, Redox activation of metal-based prodrugs as a strategy for drug delivery, Adv. Drug Deliv. Rev. 64 (2012) 993–1004, https://doi.org/10.1016/j.addr.2012.01.007.

[25] M. Grimaldi, G. Santin, V. Insolia, V. Dal Bo, V.M. Piccolini, P. Veneroni, S. Barni, M. De Pascali S.A. Verri, F.P. Fanizzi, M.G. Bottone, [Pt(O,O'-acac)(γ-acac)(DMS)] versus cisplatin: apoptotic effects in B50 neuroblastoma cells, Histochem. Cell Biol. 145 (5) (2016) 587–601, https://doi.org/10.1007/s00418-015-1396-1.

[26] K. Guzińska-Ustymowicz, A. Pryczynicz, A. Kemona, J. Czyżewska, Correlation between proliferation markers: PCNA, Ki-67, MCM-2 and antiapoptotic protein Bcl-2 in colorectal cancer, Anticancer Res. 29 (8) (2009) 3049–3052.

[27] T.C. Johnstone, K. Suntharalingam, S.J. Lippard, The next generation of platinum drugs: targeted Pt(II) agents, nanoparticle delivery, and Pt(IV) prodrugs, Chem. Rev. 116 (2016) 3436–3486, https://doi.org/10.1021/acs.chemrev.5b00597.

[28] Y. Kabeya, N. Mizushima, T. Uero, A. Yamamoto, T. Kirisako, T. Noda, E. Kominami, Y. Ohsumi, T. Yoshimori, LC3, a mammalian homologue of yeast Apg8p, is localized in autophagosome membranes after processing, EMBO J. 19 (2000) 5720–5728, https://doi.org/10.1093/emboj/19.21.5720.

[29] L. Kelland, The resurgence of platinum-based cancer chemotherapy, Nat. Rev. Cancer 7 (2007) 573–584, https://doi.org/10.1038/nrc2167.

[30] M.R. Kelley, Y. Jiang, C. Guo, A. Reed, H. Meng, M.R. Vasko, Role of the DNA base excision repair protein, APE1 in cisplatin, oxaliplatin, or carboplatin induced sensory neuropathy, PLoS One 9 (2014) e106485, https://doi.org/10.1371/journal.pone.0106485.

[31] R.G. Kenny, S.W. Chuah, A. Crawford, C.J. Marmion, Platinum(IV) Prodrugs – a step closer to Ehrlich's vision? Eur. J. Inorg. Chem. 2017 (2017) 1596–1612, https://doi.org/10.1002/ejic.201601278.

[32] M. Kutwin, E. Sawosz, S. Jaworski, M. Wierzbicki, B. Strojny, M. Grodzik, A. Chwalibog, Assessment of the proliferation status of glioblastoma cell and tumour tissue after nanoplatinum treatment, PLoS One (2017) 12(5), https://doi.org/10.1371/journal.pone.0178277.

[33] A.V. Kuznetsov, R. Margreiter, A. Amberger, V. Saks, M. Grimm, Changes in mitochondrial redox state, membrane potential and calcium precede mitochondrial dysfunction in doxorubicin-induced cell death, Biochim. Biophys. Acta 1813 (6) (2011) 1144–1152, https://doi.org/10.1016/j.bbamcr.2011.03.002.

[34] Y. Leng, Z. Marinova, M.A. Reis-Fernandes, H. Nau, D.M. Chuang, Potent neuroprotective effects of novel structural derivatives of valproic acid: potential roles of HDAC inhibition and HSP70 induction, Neurosci. Lett. 476 (2010) 127–132, https://doi.org/10.1016/j.neulet.2010.04.013.

[35] Y. Li, E. Seto, HDACs and HDAC inhibitors in cancer development and therapy, Cold Spring Harb. Perspect. Med. 6 (10) (2016), https://doi.org/10.1101/cshperspect.a026831.

[36] E. Lindauer, E. Holler, Cellular distribution and cellular reactivity of platinum(II) complexes, Biochem. Pharmacol. 52 (1996) 7–14, https://doi.org/10.1016/0006-2952(96)00106-2.

[37] M. Liu, C.C. Chien, M. Burne-Taney, R.R. Molls, L.C. Racusen, R.B. Colvin, H. Rabb, A pathophysiologic role for T lymphocytes in murine acute cisplatin nephrotoxicity, J. Am. Soc. Nephrol. 17 (2006) 765–774, https://doi.org/10.1681/ASN.2005010102.

[38] A. Muscella, N. Calabrisio, C. Vetrugno, F.P. Fanizzi, S.A. De Pascali, C. Storelli, S. Marsigliante, The platinum (II) complex [Pt(O,O'-acac)(γ-acac)(DMS)] alters the intracellular calcium homeostasis in MCF-7 breast cancer cells, Biochem. Pharmacol. 81 (2011) 91–103, https://doi.org/10.1016/j.bcp.2010.09.012.

[39] V. Novohradsky, L. Zerzankova, J. Stepankova, O. Vrana, R. Raveendran, D. Gibson,

J. Kasparkova, V. Brabec, New insights into the molecular and epigenetic effects of antitumor Pt(IV)-valproic acid conjugates in human ovarian cancer cells, Biochem. Pharmacol. 95 (2015) 133–144, https://doi.org/10.1016/j.bcp.2015.04.003.

[40] V. Novohradsky, I. Zanellato, C. Marzano, J. Pracharova, J. Kasparkova, D. Gibson, V. Gandin, D. Osella, V. Brabec, Epigenetic and antitumor effects of platinum(IV)-octanoato conjugates, Sci. Rep. 7 (1) (2017) 3751, https://doi.org/10.1038/s41598-017-03864-w.

[41] I. Oehme, H.E. Deubzer, M. Lodrini, T. Milde, O. Witt, Targeting of HDAC8 and investigational inhibitors in neuroblastoma, Expert Opin. Investig. Drugs 18 (11) (2009) 1605–1617, https://doi.org/10.1517/14728220903241658.

[42] C.A. Otey, M. Boukhelifa, P. Maness, B35 neuroblastoma cells: an easily transfected, cultured cell model of central nervous system neurons, Methods Cell Biol. 71 (2003) 287–304.

[43] R. Raveendran, J.P. Braude, E. Wexselblatt, V. Novohradsky, O. Stuchlikova, V. Brabec, V. Gandin, D. Gibson, Pt(IV) derivatives of cisplatin and oxaliplatin with phenylbutyrate axial ligands are potent cytotoxic agents that act by several mechanisms of action, Chem. Sci. 7 (2016) 2381–2391, https://doi.org/10.1039/C5SC04205D.

[44] M. Ravera, E. Gabano, I. Zanellato, A. Gallina, E. Perin, A. Arrais, S. Cantamessa, D. Osella, Cisplatin and valproate released from the bifunctional [Pt (IV)Cl₂(NH₃)₂(valproate)₂] antitumor prodrug or from liposome formulations: who does what? Dalton Trans. 46 (2017) 1559–1566, https://doi.org/10.1039/c6dt03749f.

[45] G. Santin, V.M. Piccolini, P. Veneroni, S. Barni, G. Bernocchi, M.G. Bottone, Different patterns of apoptosis in response to cisplatin in B50 neuroblastoma rat cells, Histol. Histopathol. 26 (7) (2011) 831–842, https://doi.org/10.14670/HH-26.831.

[46] G. Santin, V.M. Piccolini, S. Barni, P. Veneroni, V. Giansanti, V. Dal Bo, G. Bernocchi, M.G. Bottone, Mitochondrial fusion: a mechanism of cisplatin-induced resistance in neuroblastoma cells? Neurotoxicology 34 (2013) 51–60, https://doi.org/10.1016/j.neuro.2012.10.011.

[47] I. Tanida, T. Ueno, E. Kominami, LC3 and autophagy, Methods Mol. Biol. 445 (2008) 77–88, https://doi.org/10.1007/978-1-59745-157-4_4.

[48] L. Troy, K. McFarland, S. Littman-Power, B.J. Kelly, E.T. Walpole, D. Wyld, D. Thomson, Cisplatin-based therapy: a neurological and neuropsychological review, Psychooncology 9 (2000) 29–39, https://doi.org/10.1002/(SICI)1099-1611(200001/02)9:1<29::AID-PON428>3.0.CO;2-Z.

[49] D. Wang, S.J. Lippard, Cellular processing of platinum anticancer drugs, Nat. Rev. Drug Discov. 4 (2005) 307–320, https://doi.org/10.1038/nrd1691.

[50] E. Wexselblatt, D. Gibson, What do we know about the reduction of Pt(IV) prodrugs? J. Inorg. Biochem. 117 (2012) 220–229, https://doi.org/10.1016/j.jinorgbio.2012.06.013.

[51] N.J. Wheate, S. Walker, G.E. Craig, R. Oun, The status of platinum anticancer drug in the clinic and in clinical trials, Dalton Trans. 39 (2010) 8113–8127, https://doi.org/10.1039/c0dt00292e.

[52] O. Witt, H.E. Deubzer, M. Lodrini, T. Milde, I. Oehme, Targeting histone deacetylases in neuroblastoma, Curr. Pharm. Des. 15 (4) (2009) 436–447, https://doi.org/10.2174/138161209787315774.

[53] I. Zanellato, C.D. Boidi, G. Lingua, P.G. Betta, S. Orecchia, E. Monti, D. Osella, In vitro anti-mesothelioma activity of cisplatin–gemcitabine combinations: evidence for sequence-dependent effects, Cancer Chemother. Pharmacol. 67 (2) (2010) 265–273, https://doi.org/10.1007/s00280-010-1314-0.